A Versatile Nanobody-Based Toolkit to Analyze Retrograde Transport from the Cell Surface

Inauguraldissertation

zur

Erlangung der Würde eines Doktors der Philosophie

vorgelegt der

Philosophisch-Naturwissenschaftlichen Fakultät

der Universität Basel

von

Dominik Pascal Buser

aus Zunzgen (BL)

Basel, 2018

Genehmigt von der Philosophisch-Naturwissenschaftlichen Fakultät
auf Antrag von

Prof. Dr. Martin Spiess
Prof. Dr. Anne Spang

Basel, den 19. September 2017

Prof. Dr. Martin Spiess
Dekan der Phil.-Nat. Fakultät

Acknowledgments

This work was performed in the group of Prof. Dr. Martin Spiess in the Focal Area Growth & Development at the Biozentrum of the University of Basel (Switzerland). I would like to express my heartfelt gratitude to the following people:

- First and foremost, I would like to thank **Prof. Dr. Martin Spiess** for giving me the opportunity to do a PhD in his research lab, his scientific expertise, helpful inputs, confidence, and support in writing a manuscript to be published in the near future. His offered freedom in project choice and progression gave me the independence and creativity to develop my own ideas and scientific skills. Apart from being my PhD thesis supervisor, it was always nice to chat or discuss problems with him so frankly and easily. Also his offer to contribute to other publications was appreciated. Thank you very much, Martin.

- Likewise, I would like to give many thanks to my PhD advisory committee members **Prof. Dr. Anne Spang** and **Prof. Dr. Jean Pieters** for their advice, directness, and critical comments. Even though I initially considered the committee meetings just a 'mandatory duty' of the PhD, it really acted as 'prosthetic cofactor' for setting my research focus. Also, I would like to thank **Prof. Dr. Markus Affolter** for being chair of my PhD exam.

- I am very grateful to **Nicole Beuret** for professional technical assistance, helpful advices, keeping the lab in excellent shape, and her presence over all this time since I have joined the Spiess Lab. She always had an open ear for discussing both scientific and non-scientific topics. Moreover, apart from acting as one of the 'pillars' of the Spiess lab, it was an appreciated gesture of her to offer precedence in finishing other publications.

- I am also very thankful to **Cristina Baschong** and **Kai Schleicher** for data contribution and analysis. Working in a collaborative and productive interface was a new experience for me that I do not want to miss in future experimental endeavors that I cannot handle on my own.

- Particularly, I would like to express my gratitude to the current members of the Spiess Lab, among them **Dr. Valentina Millarte**, **Dr. Daniela Stadel**, **Erhan Demirci**, **Marco Janoschke**, **Mirjam Pennauer**, **Jennifer Reck**, **Anna Brunauer**, **Simon Schlienger** and **Tina Junne Bieri**, as well as former lab members, including **Dr. Sonja Huser Studer**, **Dr. Simone Kälin**, **Dr. David Hirschmann**, **Dr. Deyan Mihov**, **Dr. Eva Raja**, **Dr. Barry Shortt**, **Franziska Hasler, Christine Käser** and **Mirjam Zimmermann**. They created an enjoyable and familiar working atmosphere. I appreciated their cordiality, helpfulness and respect a lot. Particular thanks are addressed to Dr. Simone Kälin to be involved in the revision process of her publication.

- I am also thankful to **Maja Güntensperger-Heckel** and **Brigitte Olufsen** for their professional administrative assistance and all their help, in particular to Maja to discuss topics even beyond the scope of science.

- Furthermore, I would like to thank **Dr. Paul Jenö** and **Suzette Moes** for excellent mass spectrometric analysis and discussions, even though no data have been included in the present study.

- A great thank-you is also given to the **Imaging Core Facility (IMCF)** and **FACS Core Facility (FCF)** for their support and service, in particular to **Janine Bögli** for cell sorting.

- An enormously particular gratitude is expressed to the great **fifth floor** of the Biozentrum and Pharmazentrum, mostly to the fifth floor of the Biozentrum, including the **Hall Lab**, **Pieters Lab** and **Spang Lab** for material supply and helpful discussions. Interaction with a number of people from the floor was responsible for the progress of my scientific work, either because of advice or just simply because of their physical presence. Many people from the floor became much more than just floor colleagues, they turned to be lovely friends whose attendance at every occasion I highly appreciate. In this regard, special thanks are addressed to **Dr. Asier Gonzalez Sevine**, **Dr. Mitsugu Shimobayashi**, **Dr. Dirk Mossmann**, **Dr. Sravanth Kumar Hindupur**, **Dr. Sunil Shetty**, **Coralie Etter**, **Diana Weissenberger**, **Ekaterina Voronova** and **Benjamin Sellner**.

- A big thank-you is also directed to all floor managers who have kept the fifth floor running all the time, among them **Andrea Löschmann-Hage**, **Marina Kuhn Rüfenacht**, **Leo Faletti**, **Markus Meier** and **Daniel Michel**.

- A special gratitude is also addressed to the kitchen ladies of the fifth floor, **Isabelle Lanz** and **Elisabete Leite dos Reis**, for their superb, professional service, and for fulfilling many of my little special wishes.

- A special thank-you is also directed to the Fellowships for Excellence (FFE) program for supporting me the first three years of my PhD. I highly appreciated the efforts made by **Angie Klarer**, **Prof. Dr. Christoph Handschin**, **Prof. Dr. Joachim Seelig** and **Dr. Anna Seelig-Löffler** to set up the FFE program, organize FFE dinners, the FFE selection week, and the yearly trips to amazing destinations, among them Munich, Nuremberg, China (Shanghai and Beijing), and Berlin. Apart from that, I will be always very thankful for the opportunity that I was given to be part of the program and for all of the wonderful people I have gotten to know.

- I would like to thank the **Biozentrum** as institution for providing great infrastructure and for employing helpful and nice staff. Definitely, I am one of the biggest 'Biozentrum groupies'.

- Last but not least, I would like to thank my friends besides science and most importantly to **my family**, above all to my parents for emotional and financial support throughout all my life. Without my parents, I would not be there where I am now. Thus, the biggest thank-you I can spend is dedicated to them.

Summary

Retrograde transport of membranes and proteins from the cell surface is essential to maintain homeostasis and compartment identity. Following internalization via clathrin-dependent or -independent endocytosis, lipid and protein cargoes first populate early endosomes from where they are further redirected either along the endo-lysosomal system, recycled to the plasma membrane, or targeted to the trans-Golgi network (TGN) compartment. A number of distinct sorting machineries have been implicated in retrograde transport from endosomes to the TGN, among them the AP-1/clathrin machinery. Apart from an involvement in retrograde transport, AP-1/clathrin carriers have a well-established function in cargo export from the TGN. Even though the concept of bidirectional traffic at the TGN-to-endosome interface is commonly accepted, there is still uncertainty about the precise contribution of AP-1 to retrograde transport, since the conclusions of most studies were based on altered receptor steady-state distribution or mislocalization analysis upon knockdown or knockout of AP-1. Their readouts may be misleading, because the observed phenotype may be an indirect consequence of long-term AP-1 depletion, the result of upregulation of alternative pathways to compensate for the reduced or missing protein, thereby potentially masking the true AP-1 phenotype.

To elucidate the involvement of AP-1 in endosome-to-TGN traffic, we set up a more generic approach allowing us to follow cargo molecules during their retrograde transport from the plasma membrane. To this end, we established a versatile nanobody-based approach conferring recombinant protein cargo to be tracked from the cell surface biochemically, by live cell imaging, and by electron microscopy. We engineered and bacterially expressed functionalized anti-GFP nanobodies fused to a sulfation consensus motif, to fluorophores, or to a peroxidase reporter. These functionalized nanobodies are specifically captured by EGFP-modified receptor proteins at the cell surface and transported piggyback to the receptor's homing compartments. Using the sulfatable nanobody, we could biochemically determine the kinetics of bonafide sorting receptors, the MPRs, from the cell surface to the TGN. In combination with the knocksideways approach to look at the immediate and direct consequences of AP-1 inactivation, we could also show the role of AP-1/clathrin carriers in retrograde transport of MPRs from endosomes to the TGN. At the same time, however, we also evidenced that an AP-1 knockdown and knockout produced conflicting results when compared to acute inactivation strategies.

Collectively, the present study describes a versatile nanobody-based approach to analyze retrograde transport of cargo proteins from the cell surface, and moreover provides insights into the role of the AP-1/clathrin machinery in retrograde transport.

Table of Contents

I Introduction

1 Introduction

1.1 Endocytic Pathways from the Cell Surface

The secretory and endocytic pathway of eukaryotic cells consists of a series of tightly interconnected membrane compartments that are collectively referred to as the endomembrane system or network. Among this elaborate endomembrane network, the endoplasmic reticulum (ER), the ER-Golgi intermediate compartment (ERGIC), the Golgi complex, the trans-Golgi network (TGN) as well as a variety of endosomal and lysosomal compartments serve as the major protagonists in partitioning protein and lipid cargo either for export, import, recycling or degradation.

In order to mediate selective transport of cargo throughout the endomembrane compartments, membrane-enclosed carriers are required that ferry biomolecules from one organelle to the other. In the biosynthetic (secretory) pathway, where cargo is moved in an anterograde manner from the ER to the endo-lysosomal system or to the cell surface via the Golgi complex, the repertoire of involved transport-mediating carriers, their formation, regulation as well as sorting information for efficient transport have been studied in depth.

To maintain cellular homeostasis and membrane compartment identity, it is also crucial that anterograde traffic is accompanied and counterbalanced by retrograde transport at each level of the secretory route. Particularly, knowledge about retrograde traffic from the cell surface to the TGN and even beyond has become of significant interest. This route is not only hijacked by bacterial and plant toxins to harness the host cell machineries, but is also increasingly utilized for targeted drug delivery to reach the interior of cells. Thus, understanding the basic molecular mechanisms and involved sorting machineries in retrograde transport of a variety of distinct cargo molecules from the cell surface to intracellular compartments is of undeniable importance.

In the following, we are giving an overview of the two main endocytic pathways that deliver cargo proteins from the plasma membrane to the interior of the cell.

1.1.1 Clathrin-Dependent Endocytosis

Clathrin-dependent or -mediated endocytosis (CDE or CME) represents the major pathway of uptake (**Fig. 1.1**) and refers to the selective internalization of cargo receptors or molecules into the cell using clathrin-coated carriers (Kirchhausen et al., 2014; McMahon and Boucrot, 2011; Traub and Bonifacino, 2013). Indeed, it has been previously shown that clathrin-independent pathways do not significantly contribute (~ 5%) to the endocytic flux (Bitsikas et al., 2014), confirming the crucial role of clathrin in endocytosis. Clathrin is a membrane-distal heterohexameric protein coat that has recently celebrated its anniversary of forty years after its initial discovery by Barbara Pearse (Pearse, 1975; Pearse, 1976; Robinson, 2015). Clathrin as a coat does not directly bind to the membrane or to cargo receptors and molecules, but interacts instead with membrane-associated adaptor complexes, cargo-specific adaptor proteins, and accessory factors at the site of internalization. Over the recent years, it has become clear

that unlike to intracellular membrane sites, where adaptor coat recruitment is initiated by members of the ADP-ribosylation factor (ARF) family, clathrin-coated carrier formation at the plasma membrane is regulated in a different manner.

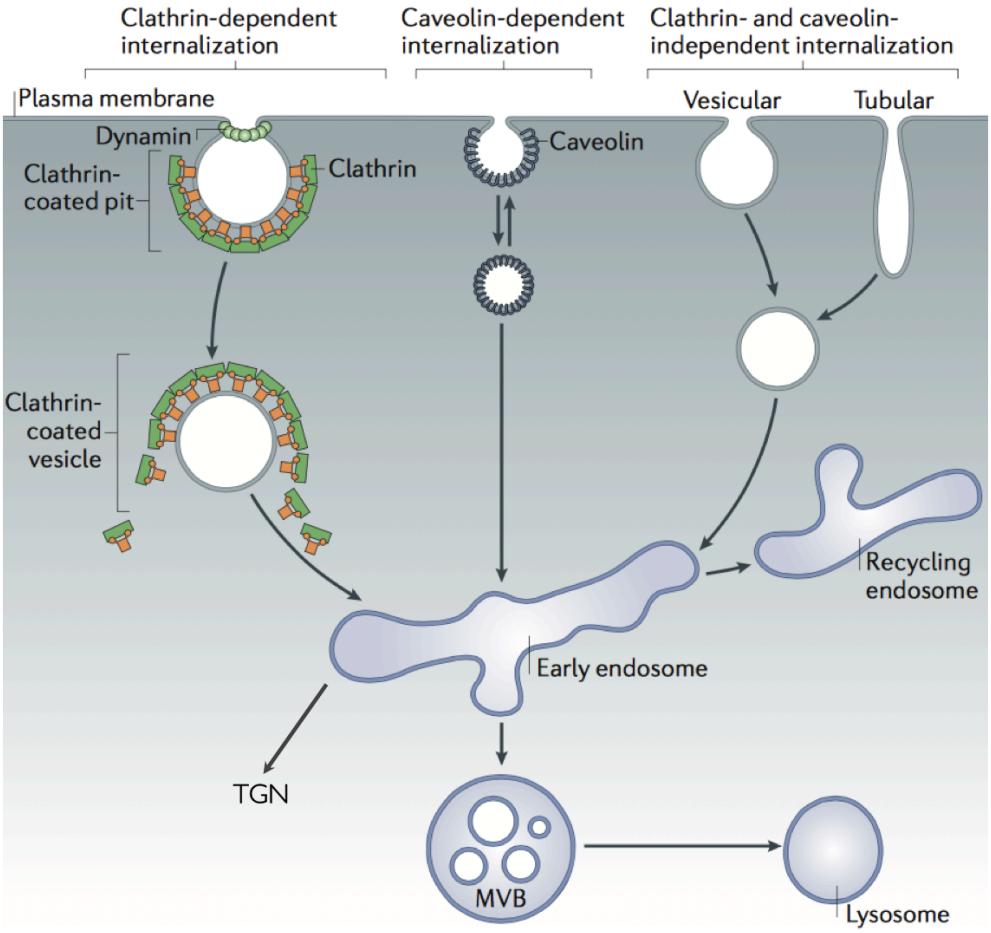

Figure 1.1: Clathrin-dependent and -independent internalization pathways. There are multiple endocytic pathways into the cells, including clathrin-dependent, caveolin-dependent, and clathrin- and caveolin-independent vesicular as well as tubular internalization routes (we refer to as clathrin-independent endocytosis for the two latter ones). Internalized cargo is transported to early endosomes, from where it is recycled to the cell surface, to other compartments of the endo-lysosomal system, including recycling endosomes, MVBs and lysosomes, or to the TGN. Figure modified from McMahon and Boucrot, 2011.

Biochemical and ultrastructural observations have defined five stages (**Fig. 1.2**, step 1-5) of clathrin-coated carrier formation, including nucleation, cargo selection, coat assembly, scission and uncoating (McMahon and Boucrot, 2011).

In the stage of nucleation (**Fig. 1.2**, step 1), a membrane invagination called a clathrin-coated pit (CCP) is formed. Which proteins actually initiate nucleation still remains a matter of debate. While a study from Kirchhausen and colleagues supports carrier formation to initially begin with two molecules of AP-2 and one clathrin triskelion as demonstrated by single molecule TIRF imaging (Cocucci et al., 2012), others propose the requirement of a nucleation module that defines plasma membrane sites where then AP-2 and clathrin will be recruited (Henne et al., 2010; Stimpson et al., 2009). This nucleation module is thought to selectively assemble at the plasma membrane and includes FCH domain-only (FCHO) proteins,

EGFR pathway substrate 15 (EPS15) and intersectins (Henne et al., 2010; Reider et al., 2009; Stimpson et al., 2009). Depletion of either FCHO proteins or EPS15 and intersectins has been reported to prevent clathrin coat recruitment. Recently published studies (Hollopeter et al., 2014; Ma et al., 2016; Merrifield, 2012; Umasankar et al., 2014), however, favor nucleation to be started by AP-2 and clathrin, and suggest that proteins from the above-mentioned 'nucleation module' regulate the conformational state of AP-2 rather than recruiting it to the site of endocytosis.

After the site of carrier formation and internalization has been marked, AP-2 adaptors selectively interact with cytoplasmic tails of transmembrane receptor molecules for cargo selection (**Fig. 1.2**, step 2). Apart from clathrin, AP-2 is the most abundant component of clathrin-coated carriers. There are an estimated three quarters of a million AP-2 adaptors present in every cell (Hirst et al., 2012b). In addition to AP-2, other accessory adaptors specific for endocytosis modulate and expand the cargo spectrum of AP-2. For instance, ARH and Dab2 are specific for LDL receptors (Garcia et al., 2001; Keyel et al., 2004; Mettlen et al., 2010; Mishra et al., 2002), β-arrestins bind to G-protein coupled receptors (GPCRs) (Ferguson et al., 1996; Smith and Rajagopal, 2016; Yu et al., 2007), HRB interacts with SNAREs (Luzio et al., 2010; Pryor et al., 2008), and additional ones bind to their cargo in distinct cell types to confer tissue specificity. All these accessory adaptors bind directly to the AP-2 adaptor appendage domains and hence do not impair direct cargo binding. In addition to conferring cargo specificity, the existence of diverse cargo adaptors ensures, when one receptor is present in high levels on the cell surface, that this does not disable the internalization of cargo whose receptor only has minor membrane representation.

Once cargo receptors are selected and sequestered by AP-2 or accessory adaptors, the clathrin coat starts to assemble (**Fig. 1.2**, step 3). Thereby, clathrin triskelia are recruited from the cytosol to sites with high adaptor concentration on the membrane to facilitate carrier formation. The subsequent polymerization of clathrin is thought to stabilize membrane curvature, but is not inducing membrane bending and deformation (McMahon and Boucrot, 2011). Membrane bending and sculpting is instead mediated by curvature effectors that ensure curvature generation regardless of which cargo is selected.

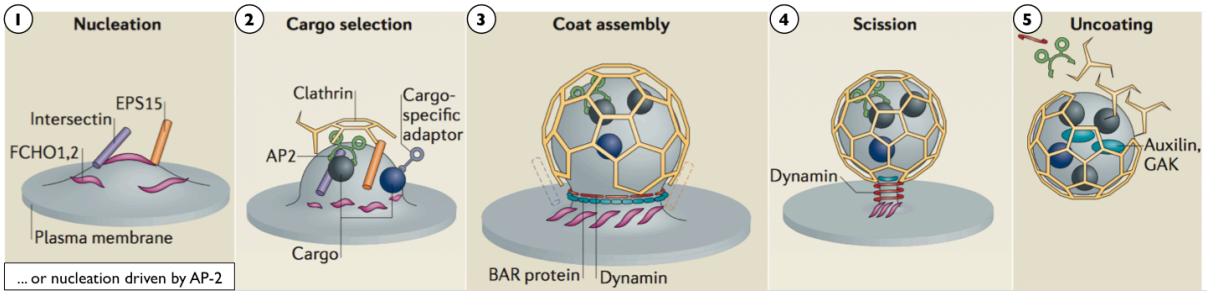

Figure 1.2: The five steps of clathrin-coated carrier formation. Clathrin-coated pit formation is either initiated by the nucleation module composed of FCHO proteins, EPS15 and intersectins, or by the AP-2 adaptor (1). AP-2 with possible cooperation with cargo-specific adaptors interact with cytoplasmic tails of cargo proteins and other coat components (2). Clathrin coat polymerization leads to carrier assembly and recruitment of BAR domain-containing curvature effectors to the neck of the nascent carrier (3). After coat assembly, dynamin pinches off the formed clathrin-coated membrane (4). In the last step, clathrin polymers are uncoated by the sequential action of auxilin and the ATPase Hsc70 (here named GAK). Figure modified from McMahon and Boucrot, 2011.

Clathrin coat formation at the membrane is followed by scission (**Fig. 1.2**, step 4), a process, which is exerted by the mechanochemical enzyme dynamin (Antonny et al., 2016; Daumke et al., 2014). Dynamin is recruited by BAR (Bin/Amphiphysin/Rvs) domain-containing proteins, including amphiphysins, endophilins or SNX9, which have a preference for the curvature at the neck of the coated pit and are likely to be involved in forming the membrane neck (Bendris and Schmid, 2017; Ferguson et al., 2009; Sundborger et al., 2011; Wigge et al., 1997). Interestingly, these curvature effectors are not only localizing to clathrin-coated invaginations at the plasma membrane, but also to intracellular membranes such as the TGN or endosomes (Huser et al., 2012). This favors these proteins to be involved more generally in the process of clathrin-coated carrier formation at membranes, rather than only at endocytic sites. Recruited dynamin polymerizes and wraps helically around the forming carrier membrane and finally undergoes a GTP hydrolysis-dependent conformational change to pinch off the carrier from its parental membrane (Bashkirov et al., 2008; Hinshaw and Schmid, 1995; Roux et al., 2006; Stowell et al., 1999; Sweitzer and Hinshaw, 1998).

To recycle clathrin machinery components for additional rounds of carrier formation and budding, the detached membrane has to loose its coat (**Fig. 1.2**, step 5). Since, after scission, the clathrin cage is incomplete at the zone where the neck was attached to the parental membrane (McMahon and Boucrot, 2011), auxilin can bind at this position to clathrin and recruits the ATPase Hsc70 (GAK) that catalyzes the disassembly of the clathrin shell (Fotin et al., 2004; Massol et al., 2006; Rapoport et al., 2008; Scheele et al., 2001; Taylor et al., 2011; Ungewickell et al., 1995; Xing et al., 2010). Subsequent changes in the phosphoinositide composition, for instance by the phosphatase synaptojanin (Cremona, 2001; Cremona et al., 1999), are also required to terminate the uncoating process and to liberate the coat components. However, whether this occurs already before or after auxilin recruitment is not clear.

1.1.2 Clathrin-Independent Endocytosis

Since endocytic uptake is not entirely blocked in the absence of clathrin, it has become clear that clathrin-dependent endocytosis does not represent the exclusive pathway to internalize cargo from the cell surface. We refer to all of these non-clathrin internalization pathways as clathrin-independent endocytosis (CIE). Compared to clathrin-driven endocytosis, detailed understanding of CIE pathways has lagged behind, mainly because (i) wealth of attention has been addressed to CME only, (ii) the fact that CIE pathways are typically not constitutive and only activated upon specific stimuli, (iii) the repertoire of molecular players are mostly lacking, (iv) and some CIE events might be too slow or too fast to be recorded by classical methods applied to investigate endocytosis (Watanabe and Boucrot, 2017).

Among CIE pathways themselves, even internalization mechanisms with distinct features exist, including whether uptake is of small-scale or large-scale nature (Doherty and McMahon, 2009; Johannes et al., 2015; Mayor and Pagano, 2007; Mayor et al., 2014). Large-scale CIE pathways include macropinocytosis and phagocytosis **(Fig. 1.3)**, two endocytic processes with membrane dimensions in the large micrometer-scale. Small-scale CIE pathways can be neatly classified whether they require dynamin (dynamin-dependent) or not (dynamin-independent). Another relevant classification criterion is the presence or absence of a morphological coat that marks the internalized patch of the membrane, and in those

that lack a defined coat, it is a small GTPase that regulates productive CIE (Mayor et al., 2014). In the following, we are giving a short overview of the reported small-scale CIE pathways that mediate uptake of distinct cargo proteins.

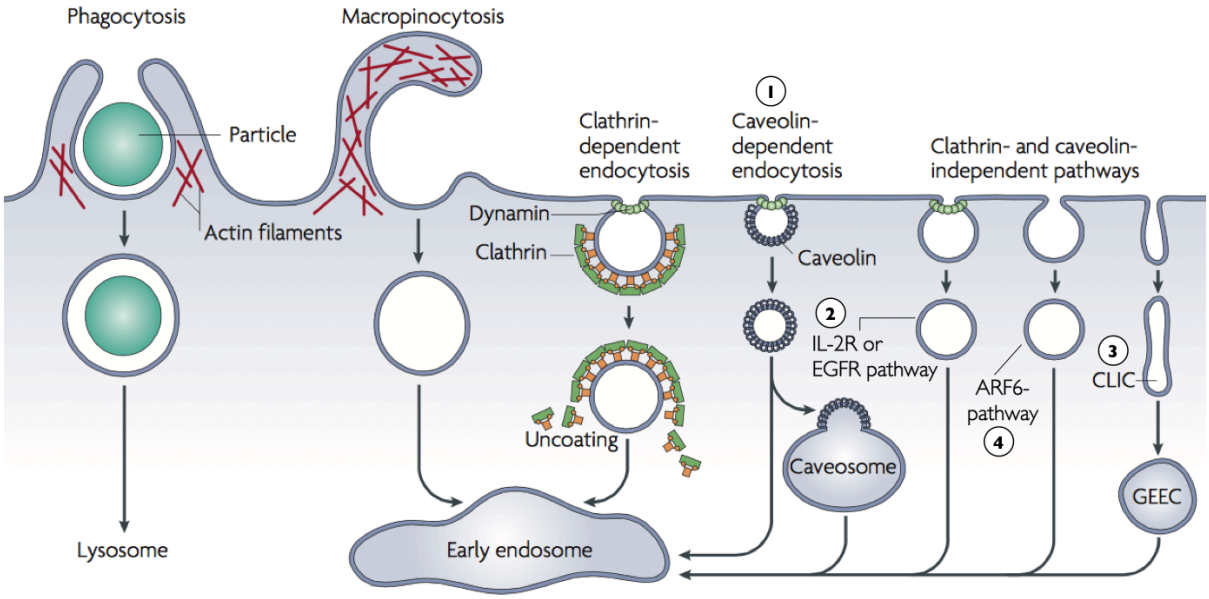

Figure 1.3: Pathways of clathrin-independent endocytosis. Large-scale particles can be taken up by phagocytosis, whereas fluid uptake occurs by macropinocytosis. Both processes are thought to be clathrin-independent. In comparison with other CIE endocytic pathways (1-4), the size of the carriers formed by phagocytosis and macropinocytosis is much larger. Small-scale CIE pathways are mainly characterized by the features whether internalization is dynamin-dependent and whether they have a morphologically characterized coat. Figure modified from Mayor and Pagano, 2007.

The best-studied CIE internalization route is the dynamin-dependent caveloar endocytic pathway (**Fig. 1.3**, 1). Caveolae are 50-80 nm flask-shaped plasma membrane invaginations and are characterized by ~ 140 copies of the oligomeric transmembrane protein caveolin-1 (CAV1), 30-70 molecules of caveolin-2 (CAV2), and a peripheral protein coat complex composed of cavins (Cheng and Nichols, 2016; Hansen and Nichols, 2010; Hayer et al., 2010; Parton and del Pozo, 2013). Even though unclear for a long time, it has become evident that caveolae are not immobile structures that just decorate the plasma membrane, but can dynamically detach from membrane sites to form endocytic caveloar carriers (Boucrot et al., 2011; Hill et al., 2008; Moren et al., 2012; Stoeber et al., 2012). The precise physiological importance and function of caveloae, and the spectrum of transported cargo are not yet that well established as for CME (Mayor and Pagano, 2007; Mayor et al., 2014). However, recent reports suggested caveolae to play a role in membrane stretching (Ariotti et al., 2015b; Lo et al., 2016; Lo et al., 2015).

Other dynamin-dependent CIE routes are the interleukin-2 receptor (IL-2R) and the epidermal growth factor receptor (EGFR) endocytic pathway (**Fig. 1.3**, 2). The former internalization pathway is dependent on the small GTPase RhoA and on lipid raft microdomains (Gesbert et al., 2004; Lamaze et al., 2001). Ultrastructural studies showed that IL-2 receptors as well as other cytokine receptors are concentrated and then internalized via small non-coated invaginations. Thus, both the specific concentra-

tion of the receptors and the uniform size of the endocytic carrier implicate a putative machinery involved in pit formation (Mayor et al., 2014). Interestingly, the amyloid precursor protein (APP) also seems to use this pathway to some extent under certain physiological conditions (Saavedra et al., 2007).

While EGFR is directed to CME pathways at low doses of its ligand (EGF), it appears that the receptor uses a distinct CIE pathway (**Fig. 1.3**, 2) at high doses (Sigismund et al., 2013; Sigismund et al., 2008; Sigismund et al., 2005). Then, enhanced ligand-dependent receptor ubiquitination has been proposed to operate as a regulatory pathway switch that detours EGFR towards a clathrin-independent endocytic route, possibly involving an ubiquitin adaptor (Sigismund et al., 2013). Recent evidence, however, suggested that IL-2R and EGFR internalization actually belongs to the same clathrin-independent endocytic pathway (Watanabe and Boucrot, 2017). This pathway is proposed to be mediated by the protein endophilin that induces the formation of endocytic carriers quickly upon certain stimuli. Due to the fast mode of action, this recently described CIE pathway is named fast endophilin-mediated endocytosis, or just shortly FEME (Boucrot et al., 2015; Renard et al., 2015). The FEME pathway is also taken by bacterial toxins to enter host cells (Renard et al., 2015). The precise mechanisms by which endophilin primes membranes for CIE remain to be further investigated.

Among the coat- and dynamin-independent CIE pathways, there is the CLIC/GEEC pathway (**Fig. 1.3**, 3) and the ARF6-associated pathway (**Fig. 1.3**, 4). The former is involved in the uptake of lipid-anchored proteins, such as glycosylphosphatidylinositol-anchored proteins (GPI-AP), into distinct early endosomal compartments that also accommodate a major fraction of internalized fluid phase (Kirkham and Parton, 2005; Sabharanjak et al., 2002). Due to the nature of high local GPI-AP concentrations, these endosomes are referred to as GEECs (GPI-AP enriched endocytic compartments), and they result from fusion of primary uncoated tubulovesicular carriers called CLICs (clathrin-independent carriers), which are directly derived from the plasma membrane (Kirkham and Parton, 2005; Mayor et al., 2014; Mayor and Riezman, 2004). Controversially, the molecular machinery of the CLIC/GEEC pathway was reported to depend on ARF1 (Gupta et al., 2009; Kumari and Mayor, 2008), a protein that usually only localizes to intracellular membranes.

Another mode of CIE (**Fig. 1.3**, 4) that does not have any visible coat and that is also dynamin-independent is the mentioned ARF6-associated pathway (Grant and Donaldson, 2009; Radhakrishna and Donaldson, 1997). In steady-state, ARF6 localizes to the cell surface and in many cells also to endosomes that contain CIE cargo protein. The ARF6-associated pathway resembles the CLIC/GEEC pathway in that it also internalizes GPI-APs (Eyster et al., 2009; Howes et al., 2010a; Howes et al., 2010b). It is not certain whether they represent the same or a distinct mode of internalization. Apart from these two pathways, another dynamin-independent endocytic pathway internalizes GPI-APs. This pathway depends on proteins termed flotilins (Glebov et al., 2006), whose precise function in CIE remains to be determined.

Though mechanistically, structurally and functionally completely different, CME and CIE have both in common that their cargo finally reaches early endosomes.

1.2 Endo-Lysosomal Pathways along Endocytic Compartments

The endocytic compartments of the endo-lysosomal system can be temporally, morphologically and biochemically subdivided into early endosomes, late endosomes and lysosomes (**Fig 1.4**), temporally based on the sequential order in which endocytosed cargo reaches these compartments, morphologically based on their degree in tubular-vacuolar appearance with or without intraluminal vesicles (ILVs), and biochemically based on recruited Rab marker proteins and membrane lipid identity. Among them, early endosomes represent a major hub of bifurcated traffic, since internalized protein and lipid cargo is shuttled either further along the endo-lysosomal system, recycled to the plasma membrane, delivered to the TGN, or also receives material from the biosynthetic route.

1.2.1 Early Endosomes

The term 'early endosomes' actually describes two distinct endosomal organelles, that are sorting and recycling endosomes (Maxfield and McGraw, 2004). Depending on the literature and authors, however, the terminology 'early endosomes' and 'sorting endosomes' are used synonymously.

Sorting Endosomes

Sorting endosomes represent the first endocytic compartments that accept protein and lipid cargo internalized from the plasma membrane. It is thought that endocytic carriers derived from CME or CIE, respectively, fuse with each other to give rise to a primary early sorting endosome. These initial structures in turn undergo homotypic fusion and by this start to grow (Huotari and Helenius, 2011; Mills et al., 1999; Scott et al., 2014). Sorting endosomes are heterogeneous in terms of localization, composition, morphology and function (Lakadamyali et al., 2006; Miaczynska et al., 2004; van Meel and Klumperman, 2008). The overall distribution of sorting endosomes is cell type-dependent. Most of them localize to the periphery of the cell in close vicinity to the plasma membrane, but also to the perinuclear region. Sorting endosomes typically have a slightly acidic lumen with a pH of around 6. Individual sorting endosomes have a complex structure and morphology with tubular and vacuolar domains. Most of the membrane surface area is part of the tubular elements, and much of the volume is in the globular part (Gruenberg, 2001; Huotari and Helenius, 2011). While the globular part matures into late endosomes, the tubular extensions give rise to early recycling endosomes (Mellman, 1996). Recycling receptors, such as the transferrin receptor (TfR), which constitutively capture ligands from the extracellular environment to deliver them into the cell, can either migrate back to the cell surface directly via sorting endosomes (fast recycling) or indirectly via recycling endosomes (slow recycling) (Hao and Maxfield, 2000; van Dam et al., 2002). The other main function of sorting endosomes is to target cargo either further along the endo-lysosomal system or to transport them to the TGN.

A major criterion to define sorting endosomes is by the presence membrane-associated markers (**Fig 1.4**). Sorting endosomes are positive for Rab5 and its cognate downstream effectors, such as the early endosomal antigen 1 (EEA1) or rabaptin5, for instance (Stenmark, 2009; Stenmark et al., 1995;

Wandinger-Ness and Zerial, 2014; Zerial and McBride, 2001; Zhen and Stenmark, 2015). In addition, Rab4 also localizes to sorting endosomes (van der Sluijs et al., 1992), but likewise to Rab11-positive recycling endosomes (Trischler et al., 1999). While recycling endosomes deliver their material back to the plasma membrane, sorting endosomes mature to late endosomes, which are also called multivesicular bodies (MVBs). So far, it was believed that Rab5 triggers initial effector recruitment to mature a sorting to a late endosome. Recent evidence, however, contradicted this notion and suggested Rab4 rather than Rab5 to initiate endosome conversion (Kalin et al., 2016; Kalin et al., 2015).

Apart from morphology, pH and recruited cytosolic factors, organelles are also defined by their lipid content. Sorting endosomes are typically characterized by the presence of phosphatidylinositol-3-phosphate (PI(3)P) (Behnia and Munro, 2005). Recently, even more 'exotic' and different (sorting) endosomes have been described that are delivering a subset of selected cargo to the nuclear envelope (Chaumet et al., 2015). Due to their close association with the nucleus, these endosomes were termed nuclear envelope-associated endosomes (NAE).

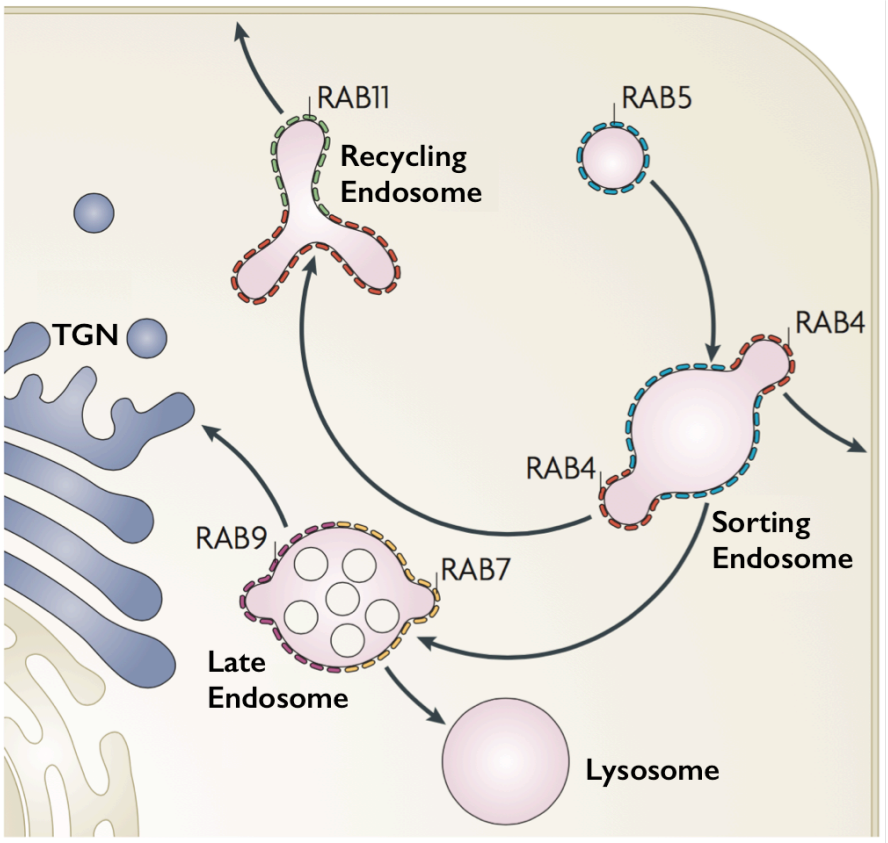

Figure 1.4: Sorting along the endo-lysosomal system. The primary endocytic CME or CIE carriers deliver their contents and their membranes to sorting endosomes in the periphery of the cell. Depending on the cargo's function, it is either recycled, further transported along the endo-lysosomal pathway or trafficked to the TGN. Recycling can occur from sorting endosomes in a Rab4-dependent manner (fast recycling) or from recycling endosomes in a Rab11-dependent manner (slow recycling). Maturation from a sorting to a late endosome is initiated by a Rab5-to-Rab7 conversion. Apart from the Rab7-positive vacuolar domain, late endosomes also contain Rab9-positive tubular elements that confer recycling/retrieval of MPRs to the TGN. Late endosomes also acquire intraluminal vesicles (ILVs) to facilitate degradation of selected transmembrane proteins. Fusion of a late endosome with a lysosome forms a hybrid organelle, the endolysosome, in which active degradation takes place. The endolysosome in turn is converted into a classical dense storage lysosome. Figure modified from Stenmark, 2009.

Recycling Endosomes

As mentioned earlier, recycling endosomes are derived from tubular extensions of sorting endosomes. Recycling from these tubular elements to the cell surface is termed slow recycling since cargo receptors apparently take a longer route than they would do from sorting endosomes. Recycling endosomes are characterized by a pH of ~ 6.5, slightly less acidic than sorting endosomes (Taguchi, 2013), and by the presence of Rab11 (Trischler et al., 1999). Many ligand receptors seem to use the slow Rab11-dependent recycling pathway in addition to the fast Rab4-dependent recycling route, including TfR, LDLR and the asialoglycoprotein receptor (ASGPR) subunit H1 (Maxfield and McGraw, 2004; Pagano et al., 2004). Apart from cargo molecules that have to recycle back to the cell surface to exert their function as ligand receptors, there is also evidence that some other cargo commute via recycling endosomes to reach the TGN, including bacterial toxins and a subset of endogenous proteins, among them TGN38 (Matsudaira et al., 2013; McKenzie et al., 2012; Taguchi, 2013; Uchida et al., 2011).

1.2.2 Late Endosomes

Late endosomes are derived from the vacuolar domains of sorting endosomes by maturation. Maturation is initiated by a Rab5-to-Rab7 conversion, which in turn remodels the identity of the endosomal membrane by recruitment of additional Rab effectors with concomitant loss of others (Poteryaev et al., 2010; Rink et al., 2005). Mature late endosomes typically localize to the perinuclear region and have a pH in the range of 5-6 (Maxfield and Yamashiro, 1987). Late endosomes are not only positive for Rab7, but also for Rab9 (Kucera et al., 2016a; Lombardi et al., 1993). As for sorting endosomes, late endosomes to some extent also have a vacuolar and tubular domain. Rab7 and Rab9 use different machineries for their recruitment to late endosomes and this possibly explains why Rab7 preferentially associates with the vacuolar domain and Rab9 with the tubular elements. The greatest distinction, however, between these two late endosomal Rab proteins is that Rab9 has been predominantly reported in the retrieval of the mannose-6-phosphate receptors (MPRs) to the TGN, and not directly involved in the process of endosome maturation. Recent evidence has shown that Rab9 enters the endosomal pathway at the Rab5-to-Rab7 transition (Kucera et al., 2016a; Kucera et al., 2016b).

Late endosomes are typically also characterized by the high lipid content for $PI(3,5)P_2$ and already contain some lysosomal hydrolases. Proteins destined for degradation follow their route by further maturation of the vacuolar domain, while proteins selected for retrieval enter the Rab9-positive tubular domains of late endosomes (Huotari and Helenius, 2011).

Another striking morphological feature of late endosomes is that they contain numerous intraluminal vesicles. A subset of transmembrane proteins and lipids are directed into these vesicles for facilitated degradation by active lysosomal hydrolases. The machinery involved in intraluminal vesicle formation is called ESCRT complex (endosomal sorting complex required for transport) that is composed of ESCRT-0, ESCRT-I, ESCRT-II and ESCRT-III complexes as well as a number of additional accessory factors (Henne et al., 2013; Hurley and Emr, 2006; Schoneberg et al., 2017).

1.2.3 Lysosomes

Lysosomes are organelles of heterogeneous size and represent the main sites for intracellular digestion of macromolecules in the endomembrane system (Sorkin and von Zastrow, 2009; Staudt et al., 2016; Wartosch et al., 2015). Whether lysosomal biogenesis occurs by maturation of late endosomes/MVBs or whether prelysosomal compartments fuse in a homo- or heterotypic manner with each other to give rise to lysosomes is not fully clear (Bright et al., 2005; Luzio et al., 2007; Mullins and Bonifacino, 2001). Lysosomes typically have a luminal pH of 4.5-5, perinuclear localization and are positive for the integral membrane protein LAMP-1 (lysosome-associated membrane protein-1). Other proteins found in lysosomes to exert their dedicated function are a number of acid hydrolases and other integral lysosomal membrane proteins (LMPs). Among them, LAMP-1 represents the most well characterized protein among the LMPs. To degrade biomolecules, lysosomes contain about 50 types of acid hydrolases including proteases, nucleases, glycosidases, lipases, phospholipases, phosphatases and sulfatases (Kroemer and Jaattela, 2005). Newly synthesized acid hydrolases are selectively shuttled to lysosomes by the MPRs. While the lysosomal hydrolases reside in the lumen of lysosomes, LMPs are embedded in the lysosomal limiting membrane. The mammalian lysosome comprises around 25 heavily glycosylated LMPs with diverse functions, including lysosomal acidification, protein import from the cytosol, transporters to release digested products into the cytosol as well as constituents mediating fusion events (Saftig and Klumperman, 2009).

As in other fields of membrane traffic, the idea how things are operating is often questioned, reconceptualized or newly interpreted, as it is true for lysosomes with regard to degradation. A recent model suggests not lysosomes to be the compartment of degradation, but rather a hybrid compartment termed 'endolysosome' that is the result of the fusion of a late endosome with a storage lysosome. It is thought that the terminal endocytic compartment is composed of acid hydrolase-active, acidic endolysosomes and acid hydrolase-inactive, non-acidic, terminal storage lysosomes, which are linked and function in a lysosome regeneration cycle (Bright et al., 2016).

In this subchapter (subchapter 1.2), we have had a glimpse at unidirectional transport events along the endo-lysosomal route. However, as already mentioned, other pathways can branch off along these endo-lysosomal compartments. In the following subchapter (subchapter 1.3), we are focusing on retrograde sorting pathways conferring transport from endosomes to the TGN.

1.3 Retrograde Transport from Endosomes to the TGN

The TGN is a major traffic hub of the cell, as it regulates protein sorting from the biosynthetic pathway as well as it receives cargo molecules by retrograde transport from endocytic compartments. Retrograde transport from endosomes to the TGN is important for recycling of membrane proteins which regulate a number of cellular and developmental functions. In the following, we will discuss how retrograde transport was 'discovered', stress its function and transported cargo, as well as outline the protein sorting machineries involved in endosome-to-TGN transport.

1.3.1 Overview and Discovery of Retrograde Transport

The initial discovery of cargo undergoing retrograde traffic to intracellular compartments and subsequent advances using a set of biochemical and imaging approaches have led to the identification of retrograde transport pathways. But which landmark discoveries have paved the way for our current understanding of retrograde transport from the cell surface to the TGN and even beyond?

Investigating how the plant toxin ricin enters the cell to exert its cytotoxicity led to the discovery of retrograde transport. In 1972, Olsnes and Pihl (Olsnes and Pihl, 1972) have presented evidence that ricin inhibits protein biosynthesis by modifying ribosomal RNA of infected cells (Montanaro et al., 1973). Using ricin-horseradish peroxidase (HRP) as reporter, Avrameas and colleagues (Gonatas et al., 1975) subsequently detected ricin in the Golgi complex of target cells, probably because endocytic uptake was mediated by host cell factors.

The idea that host cell surface proteins might shuttle toxins into cells was inspiring these days and has stimulated the search for endogenous proteins undergoing themselves retrograde transport. Snider and Rogers in turn were the first in 1985 who described a cellular protein, TfR, to traffic from the plasma membrane to the Golgi (Snider and Rogers, 1985). Several other reports followed soon using approaches based on Golgi-specific modifications. Of these, the findings by Duncan and Kornfeld on MPRs came to light (Duncan and Kornfeld, 1988). Duncan and Kornfeld provided direct evidence for a model in which trafficking between endosomes and the TGN is part of the functional cycle of MPRs. MPR's function is to ferry lysosomal enzymes from the TGN to endosomes, from where the empty cargo receptor then returns to the TGN for a new transport cycle.

Following the discovery of endogenous proteins to traffic from endosomes to the TGN, the next step to look at intracellular organelles beyond the Golgi was envisaged using a toxin as model tool. Sandvig and collaborators showed in 1992 for the first time that bacterial Shiga toxin could even reach the ER by retrograde transport with transit through the Golgi (Sandvig et al., 1992).

Next, we would like to briefly outline the importance and significance of endosome-to-TGN transport by listing a number of essential cellular functions it regulates.

1.3.2 Function and Importance of Retrograde Transport

As secretory cargo is exported from the TGN, anterograde cargo receptors (e.g. MPRs) and vesicle targeting and fusion factors (e.g. SNAREs) are depleted from the donor compartment and must be replenished to maintain TGN function. It is thus crucial that anterograde transport from the TGN is accompanied and counterbalanced by retrograde traffic from endosomes. This is not only essential for transport from endosomes, as illustrated here, but at each section of the secretory route. Retrograde transport is also important to retrieve resident proteins that have escaped from their compartments of function. A system lacking any retrieval mechanisms based on retrograde transport carriers would not only result in loss of compartment identity, but would affect also whole cell homeostasis.

Understanding the mechanisms and machineries involved in retrograde transport represents a field of high significance and interest. Retrograde transport does not only have pivotal housekeeping, physiological, and developmental functions, their dysregulation is also associated with disease, and the route is exploited as entry portal into the cell by a number of bacterial and plant toxins. We first consider the function and importance of retrograde transport by means of two examples.

A first example for the physiological function of retrograde transport is the maintenance of insulin-regulated trafficking. In skeletal muscle and adipocytes, insulin signaling results in the recruitment and translocation of the major insulin-responsive glucose transporter, GLUT4, to the plasma membrane. There, GLUT4 facilitates the cellular uptake of glucose and thus regulates blood glucose levels (Burd, 2011; Leto and Saltiel, 2012; Stockli et al., 2011). In the state with basal glucose levels, GLUT4 and a number of additional proteins are sequestered in special organelles termed 'GLUT4 storage compartments (GSC)' where they await stimuli for exocytosis. GSCs are produced from the TGN (Bryant et al., 2002), highlighting that a number of compartment components undergo retrograde transport to the TGN. The sorting receptor sortilin was shown to be an abundant component of GSCs and also to be essential for their formation (Jedrychowski et al., 2010; Shi and Kandror, 2005). After insulin-stimulated translocation to the cell surface, GSC proteins are internalized from the cell surface and then shuttled via the retrograde pathway to endosomes and the TGN where GSCs are then reassembled de novo (Bogan and Kandror, 2010). Efficient retrograde sorting is hence essential for glucose homeostasis through its role in reassembling GSCs for other rounds of GLUT4 exocytosis.

A second example illustrating the physiological importance of retrograde transport is synaptic plasticity generation at neurons for learning and memory formation. Synapse formation, remodeling and activity strongly depend on a broad spectrum of transmembrane proteins including adhesion proteins and receptor molecules. Receptors mediating synaptic plasticity include the NMDA and AMPA receptors. Synaptic plasticity describes the ability of pre- and postsynaptic terminals to strengthen or weaken over time in response to neuronal cues. Thus, the repertoire of NMDA and AMPA receptors at the cell surface, their orchestrated action and activity determines the extent of plasticity and memory formation (Chater and Goda, 2014; Derkach et al., 2007; Henley and Wilkinson, 2013; Henley and Wilkinson, 2016). Modulation of synaptic plasticity might be accomplished by exocytosis or by retrieval or downregulation of these receptors by retrograde transport to the TGN.

Retrograde transport is also important during development where intercellular communication is vital to give rise to a multicellular organism out of single cells. The Wnt proteins represent a family of conserved signaling molecules that are involved in establishing positional cues and cell fate decision during development (Burd, 2011). After biosynthesis at the ER, Wnts undergo palmitoylation, and probably because of this posttranslational modification (PTM), secretion of Wnts requires the receptor Wntless (WLS) as escort factor. At steady-state, WLS localizes to the ER, Golgi and plasma membrane, suggesting that it traffics along all these compartments (Yu et al., 2014). In cells with deficient retrograde sorting machineries, Wnt molecules are still produced, but fail to be efficiently secreted due to impairment of WLS cycling. Thus, retrograde transport of WLS to the ER is required to escort newly synthesized Wnts to the plasma membrane to ensure proper development (Harterink and Korswagen, 2012; Herr et al., 2012; Port et al., 2008).

Apart from the cellular function of retrograde transport in physiology and development, dysregulation of sorting machineries mediating endosome-to-TGN traffic or toxin invasion have been associated with a variety of diseases. A study of Teasdale and colleagues (Follett et al., 2016) has shown that when the retromer complex sorting machinery, a transport pathway that will be discussed later on more extensively, is blocked, there was an accumulation of α-synuclein-positive aggregates. Such aggregates containing α-synuclein are hallmark features of Parkinson's disease (Chua and Tang, 2006). Another neurological disorder is Alzheimer's disease, a disease that is characterized by the deposition of β-amyloid plaques in the brain. The β-amyloid peptides are derived from the amyloid precursor protein (APP) that traffics in post-Golgi compartments. Current data suggest that perturbations to the endosomal sorting pathway promote production of β-amyloid out of APP. Thereby, APP processing is mainly dependent on its residence time in the individual endosomal compartments, on additional APP escort proteins such as SorLA, as well as on the localization of APP cleaving enzymes in the endosomal network.

1.3.3 Cargo Proteins in Retrograde Transport

In the subchapter above, we discussed the importance of retrograde transport in regulating cell function and homeostasis and thereby also depicted some illustrative examples. In the following, we are having a brief look at cargo proteins undergoing retrograde transport from the cell surface. Retrograde transport cargoes vary considerably in their function and structure, but they can be basically classified into five distinct groups, including cargo receptors, SNARE proteins, integral membrane proteases, nutrient transporters, and other transmembrane proteins. In addition to these, bacterial and plant toxins as well as viral proteins can also be considered retrograde transport proteins, however, they constitute a class of exogenous rather than of endogenous cargoes (see also **Tab. 1.1**).

Table 1.1: Retrograde transport cargo proteins. Retrograde transport cargo proteins can be classified into different categories, including cargo receptors, SNAREs, integral membrane proteases, nutrient transporters, other endogenous transmembrane proteins as well as exogenous proteins. The depicted list of retrograde cargo molecules is incomplete, a selected number of proteins has been taken for illustration purposes. Abbreviations: CD/CIMPR, cation-dependent/-independent mannose-6-phosphate receptor; SorLA, sortilin-related receptor with LDLR class A repeats; WLS, Wntless; vti1a/b, vesicle transport through interaction with t-SNARE homolog 1a/b; BACE1/2, β site APP cleavage enzyme 1/2; GLUT4, glucose transporter 4; DMT1, divalent metal ion transporter 1; TGN protein, trans-Golgi network integral membrane protein; APP, amyloid precursor protein; ANK, progressive ankylosis protein.

Cargo Class	Retrograde Cargo Protein	Cellular Function
Cargo receptors		
	MPRs (CDMPR and CIMPR)	Hydrolase cargo receptor
	Sortilin	Biogenesis of GSCs
	SorLA	Escorting other cargo (e.g. APP)
	WLS	Wnt cargo receptor
SNAREs		
	vti1a	Membrane targeting and fusion
	vti1b	Membrane targeting and fusion
	Syntaxins	Membrane targeting and fusion
Integral membrane proteases		
	Furin	Proenzyme maturation
	Carboxypeptidase D	Proenzyme maturation
	BACE1/2	Processing of APP
Nutrient transporters		
	GLUT4	Glucose transporter
	Menkes protein (ATP7A/B)	Copper transporter
	DMT1	Iron transporter
Other transmembrane proteins		
	TGN38/46/48/51	Unknown function
	APP	Unknown function
	ANK	Unknown, PP_i transporter
Exogenous cargo		
	Shiga toxin	Inhibition of translation
	Cholera toxin	Regulation of adenylyl cyclase
	Ricin	Inhibition of translation
	Abrin	Inhibition of translation

Cargo Receptors

One of the best characterized and most abundant retrograde transport cargo proteins (**Tab. 1.1**) in mammalian cells represent the mannose-6-phosphate receptors (MPRs) (Ghosh et al., 2003a). To undergo additional rounds of cargo delivery, MPRs need to be retrieved from post-Golgi compartments. Even though different in cargo recognition, yeast also has an analogous MPR-like receptor, Vps10p, which

shuttles proteins destined for vacuoles. Mammalian MPRs have type I transmembrane topology and exist in two different isoforms, a short variant known as cation-dependent MPR (CDMPR) of ~ 46 kDa, and a long variant termed cation-independent MPR (CIMPR) of ~ 300 kDa. As their names indicate, MPRs bind cargo decorated with a M6P-tag on glycans, and hence it is not surprising that both receptor isoforms have at least one M6P-binding site in their extracytoplasmic domain (Garmroudi et al., 1996; Hancock et al., 2002; Marron-Terada et al., 2000; Schmidt et al., 1995). The cytoplasmic tail of both receptors contains numerous determinants, some of which are modified by palmitoylation and phosphorylation (Meresse et al., 1990; Rosorius et al., 1993; Schweizer et al., 1996; Schweizer et al., 1997). The CDMPR is predomi-nantly present as a non-covalent homodimer, while CIMPR seems to be a dimer in the membrane, too, even though it behaves as a monomer in detergent solutions under most circumstances. Both isoforms have a similar intracellular distribution, with the receptor to be present in the TGN, early endosomes, late endosomes as well as in the plasma membrane. The trafficking between these membranes is directed by a number of diverse sorting signals present the cytoplasmic tail. These sorting determinants interact with transport machineries that facilitate efficient anterograde and retrograde transport. The involved machineries mediating retrograde transport of MPRs are described in subchapter 1.3.4.

Apart from MPRs, other cargo receptors travel along the retrograde transport route, among them WLS, sortilin and SorLA (Johannes and Popoff, 2008). As discussed above in subchapter 1.3.2, WLS undergoes retrograde transport to the TGN and then subsequently to the ER to escort newly synthesized Wnt ligands for secretion (Yu et al., 2014). Up to the collaborative study of Bard and Virshup (Yu et al., 2014), it was generally believed that retrograde transport of WLS to the TGN was sufficient to mediate Wnt secretion. This notion was based on experiments with C-terminally tagged WLS that predominantly localized to the Golgi complex in steady-state. Native and untagged WLS, in contrast, localizes mainly to the ER. The discrepancy between these two different steady-state localizations could be resolved by the finding that C-terminal tagging masked an ER retrieval motif and prevented WLS interaction with the COPI machinery.

Sortilin is a sorting receptor that has been implicated in escorting and trafficking of diverse proteins, inlcuding other transmembrane proteins, hydrolases or sphingolipid activator proteins (SAPs) (Canuel et al., 2008; Hermey, 2009; Lefrancois et al., 2003; Pallesen and Vaegter, 2012). Since the cytoplasmic tails of MPR and sortilin exhibit functional and sequence homology, it is hypothesized that both receptors share a conserved sorting and trafficking mechanism (Nielsen et al., 2001). As mentioned before (subchapter 1.3.2), sortilin has been shown to convey GLUT4 into GSCs for their de novo assembly (Leto and Saltiel, 2012).

Similar to sortilin, the SorLA receptor is also involved in trafficking of a broader spectrum of lumenal and transmembrane cargo (Schmidt et al., 2017). Recently, additional interest has been addressed to SorLA, mainly because it has been associated with Alzheimer's disease. The receptor has emerged as a central regulator of trafficking and processing of APP. SorLA has interaction with a number of cytosolic adaptors for anterograde and retrograde movement of APP between the TGN and early endosomes, and thereby is supposed to restrict delivery of the precursor to compartments that favor amyloidogenic

processing. Any impairment with SorLA trafficking and its interacting adaptors resulted in transport defects and enhanced amyloid processing of APP, the major risk factor to promote Alzheimer's disease (Willnow and Andersen, 2013).

For completeness sake, it should be mentioned that the TfR was the first endogenous cargo proposed to undergo retrograde transport based on resialylation (Snider and Rogers, 1985). This transport was, however, characterized by relatively slow kinetics. Subsequently, no further indication of retrograde traffic was found anymore.

SNAREs

SNARE proteins (soluble N-ethylmaleimide-sensitive fusion factor attachment receptors) constitute a large protein superfamily with more than 60 members in mammals (see also **Tab 1.1**) (Hong, 2005; Sudhof and Rizo, 2011). From the structural point of view, SNAREs are transmembrane proteins that are characterized by a C-terminal hydrophobic region that functions as membrane anchor, so that the protein is mainly oriented towards the cytoplasm. The function of SNAREs is to mediate membrane fusion. In the basic model of SNARE function, transport carriers that bud from the TGN carry specific vesicle-SNAREs (v-SNAREs) that interact with endosomal target-SNAREs (t-SNAREs) to mediate membrane fusion. After disassembly of the v-/t-SNARE complex, the v-SNARE must be reshuttled to the TGN for reuse. Depending on which retrograde sorting carrier is used, different SNAREs are required to mediate endosome-to-TGN transport. For example, efficient endosome-to-TGN traffic of MPRs requires syntaxin 16 and vti1a (Amessou et al., 2007; Medigeshi and Schu, 2003; Saint-Pol et al., 2004), while the bacterial Shiga toxin requires another set of SNAREs for retrograde transport. Other SNAREs, such as vti1b, mediate membrane fusion events at other membranes (Hong, 2005).

Integral Membrane Proteases

Integral membrane proteases include proprotein convertases that cycle between the TGN and the endo-lysosomal system. These enzymes typically have a type I membrane topology with an N-terminal lumenal protease domain that processes proprotein precursor domains of immature proteins, a transmembrane domain, and a cytoplasmic tail containing sorting determinants for targeted transport (Burd, 2011). Furin and carboxypeptidase D belong to this category of retrograde transport cargo (Chia et al., 2011; Varlamov and Fricker, 1998). Although these enzymes predominantly localize to the TGN, they also migrate to endosomes for not yet fully understood reasons. It might be that cycling allows these convertases to function on numerous substrates that traverse the TGN and endosomes, similar to the APP processing enzymes. It is not known, however, whether these enzymes are actively sorted into TGN-derived carriers, as it is the case for MPRs at the TGN, or whether they simply leak out and need to be actively retrieved.

Nutrient Transporters

The localization of nutrient transporters is mainly regulated by metabolic cues. This regulation optimizes the capacity of nutrient uptake, sustains intracellular nutrient homeostasis and also protects the cell from

toxic amounts of nutrients (Burd, 2011). Retrograde transport cargo proteins belonging to this class are for instance GLUT4, Menkes proteins and DMT1 (**Tab 1.1**).

As discussed above (subchapter 1.3.2), the GLUT4 transporter is translocated to the cell surface in insulin-responsive cells where the protein facilitates glucose uptake. Decreasing levels of glucose and thus of insulin triggers the nutrient transporter to undergo retrograde transport and storage in GSCs to await the next stimuli. While GLUT4 trafficking for glucose uptake is governed by the levels of insulin, Menkes proteins (also known as ATP7A/B) are part of the mammalian copper transport pathway where they continuously cycle between the Golgi complex and the plasma membrane (La Fontaine and Mercer, 2007; Polishchuk and Lutsenko, 2013). In cells sensing low extracellular copper concentrations, exit of the transporter from the TGN is slower than retrograde retrieval from the cell surface. Menkes copper transporters thus localize to the TGN in steady-state. When, however, the copper concentrations are increased, the rate of Menkes protein exocytosis increases as well, and leads to transporter redistribution to the plasma membrane. Increased cell surface expression of the transporter probably increases the efficiency of copper removal from cells (Petris and Mercer, 1999).

DMT1 is another member of the family of nutrient transporters. It is a divalent metal ion transporter that mediates the transport of divalent metal ions, inlcuding iron, from the lumen of compartments into the cytosol (Garrick et al., 2003; Tabuchi et al., 2002). Even though TfR and DMT1 functionally cooperate in iron uptake, they have distinct retrograde sorting itineraries. While TfR is recycled to the cell surface from early endosomes, DMT1 undergoes first export to the TGN and is then delivered back to the plasma membrane (Tabuchi et al., 2010). Different sorting itineraries of cooperating TfR and DMT1 might provide a mechanism to dose the amount of iron in the cytosol to avoid toxicity. Thus, retrograde transport is very important to regulate nutrient homeostasis.

Other Transmembrane Proteins

This category includes all kind of integral membrane proteins that cannot be classified as hydrolase or hydrolase-like cargo receptors, SNARE proteins, integral membrane proteases or as nutrient transporters (**Tab 1.1**). Among these are the trans-Golgi network integral membrane protein TGN46 and its isoforms (TGN38, TGN48 and TGN51), and APP. Recently, a novel retrograde transport cargo, ANK, with unknown, but predicted PP_i transport function, has been described (Seifert et al., 2016).

In steady-state, TGN46 and its isoforms exclusively localize to the TGN, suggesting these cargoes to be TGN-resident proteins. Previous studies, however, could report that TGN46 and isoforms are also present at the cell surface from where they can be retrieved again (Banting et al., 1998; Banting and Ponnambalam, 1997; Ponnambalam et al., 1996; Ponnambalam et al., 1994; Rajasekaran et al., 1994). Recently, also the TGN-derived carriers involved in anterograde transport of TGN46 and isoforms have been described (Wakana et al., 2012), as well as the sorting machinery mediating their retrograde traffic from endosomes (Lieu et al., 2007; Lieu and Gleeson, 2010; Saint-Pol et al., 2004). TGN46 and isoforms are type I single-spanning transmembrane proteins with yet unknown function.

APP also has type I topology and is a well-characterized cargo molecule, probably mainly due to its association with Alzheimer's disease. The functional role and importance of APP in the cell is unknown

and remains to be determined (Agostinho et al., 2015; Grimm et al., 2017), however, its absence or its processing by enzymes may have fatal consequences. Since some of APP's processing is reported to occur in the TGN (Choy et al., 2012), retrograde transport from endosomes to this compartment is required. As discussed above (subchapter 1.3.2), the sortilin-related receptor SorLA has been described to escort APP along distinct post-Golgi compartments. In this regard, APP could also be considered a cargo of SorLA.

Exogenous Cargo Proteins

Apart from endogenous cargo, a subgroup of toxins and viral proteins also enter cells by retrograde transport from the cell surface (Bonifacino and Rojas, 2006; Johannes and Popoff, 2008). Protein toxins include such that are secreted by bacteria (e.g. Shiga and cholera toxin) and plants (e.g. ricin and abrin). Most of these toxins have a modular organization, a ligand moiety that confers binding to cell surface glycoproteins or glycosphingolipids, and an enzymatically active domain that inhibits host cell reactions in the cytosol. After binding to the cell surface, the toxins are internalized into endosomes either by CME or CIE. Toxins then traverse the TGN and the Golgi complex to reach the ER, where the ligand and enzymatic domain then separate from each other. The enzymatic moiety in turn gains access to the cytosol by retrotranslocation where it exerts its toxicity (Johannes and Goud, 1998; Johannes and Goud, 2000; Sandvig and van Deurs, 1994; Sandvig and van Deurs, 1996; Sandvig and van Deurs, 2002; Sandvig and van Deurs, 2005).

However, not all toxins undergo passage through the TGN. It was recently shown that the toxin 'Pseudomonas exotoxin (PE) A' undergoes a novel endosomal route via NAEs to reach the host nucleoplasm (Chaumet et al., 2015). It remains to be investigated to which extent this pathway contributes to toxin delivery in general.

1.3.4 Sorting Machineries Involved in Retrograde Transport

After internalization by CME or CIE, early endosomes are populated before cargo is subsequently segregated for recycling, sorted further along the endo-lysosomal pathway or transported to the TGN. Endosome-to-TGN transport is not only occurring from early endosomes, but can also occur from late endosomes. As for other intracellular pathways, retrograde transport between these endocytic compartments and the TGN requires the formation of membrane-enclosed transport carriers. Therefore, molecular components needed for the formation of selective transport carriers must be recruited from the cytosol to specific domains of the endosomal membrane to confer retrograde transport. A number of distinct sorting pathways have been described, among them the AP-1-, epsinR-, retromer complex- and Rab9/TIP47-dependent pathway (**Fig. 1.5**). In the following, these retrograde endosome-to-TGN sorting machineries will be discussed.

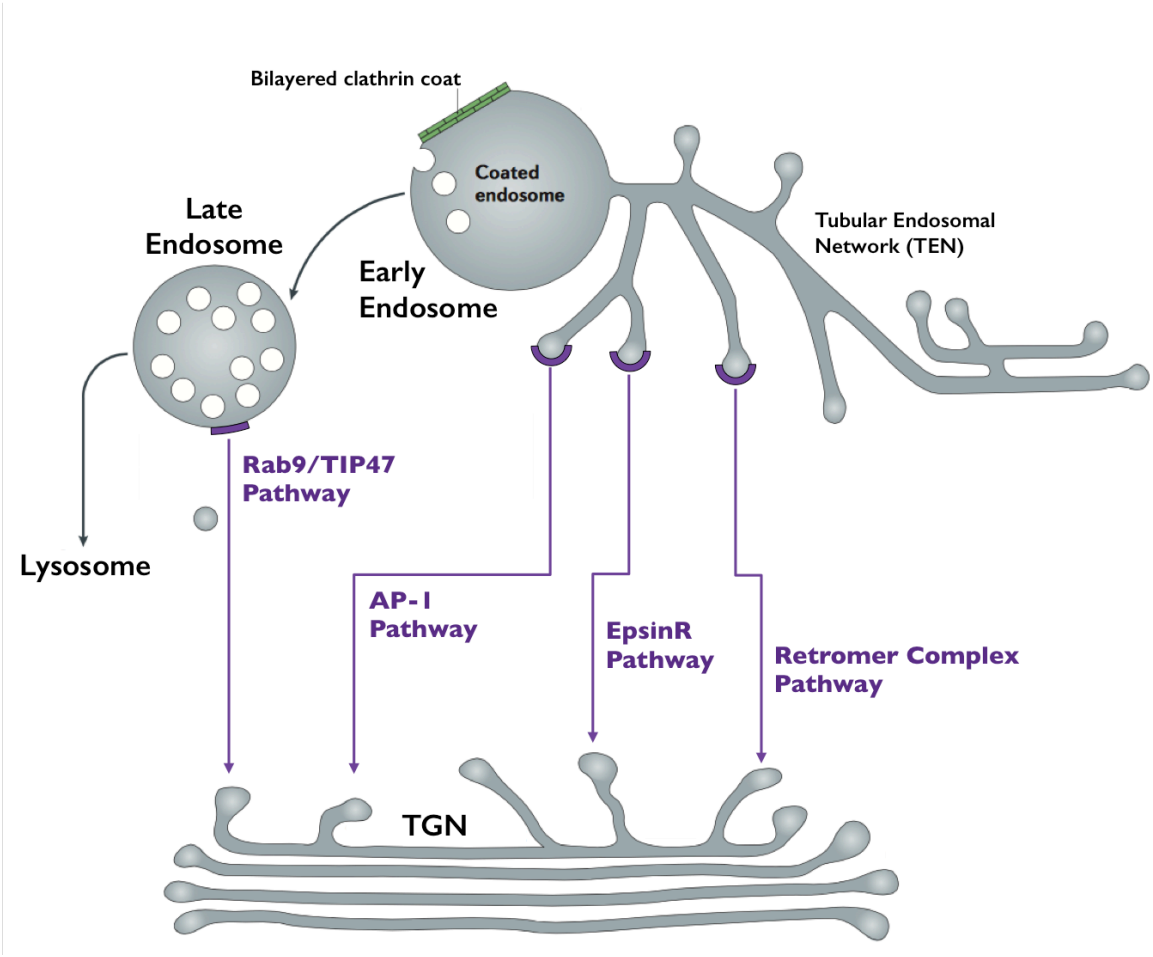

Figure 1.5: Pathways that mediate retrograde transport from endosomes to the TGN. Following internalization by CME or CIE, several pathways exist that sort cargo to the TGN. Cargo sorting can either occur from early or late endosomes. Retrograde endosome-derived transport carriers have been described to bud from the tubular rather than the vacuolar domains. Due to the network-forming character of these tubular elements, the name 'tubular endosomal network (TEN)' has been coined. It is the TEN from where transport machineries, including AP-1, epsinR and retromer complex, operate to deliver cargo to the TGN. Similar tubular elements arise from late endosomes to give rise to Rab9/TIP47-dependent carriers. Figure modified from Bonifacino and Rojas, 2006.

AP-1 Pathway

Like AP-2, AP-1 is a member of the heterotetrameric cargo adaptor protein (AP) complex family, a family that also comprises AP-3, AP-4 and AP-5. Each of these five AP complexes localize to distinct intracellular compartments and have specific, but in part also overlapping cargo recognition function (Hirst et al., 2012b). In their role as cargo adaptors, they are recruited to their target membranes to mediate formation of specific transport carriers containing selected cargo proteins. The evolutionary tree of APs shows AP-5 diverging first, followed by AP-3 and AP-4, while AP-1 and AP-2 are most closely related (Dacks and Robinson, 2017; Hirst et al., 2014).

Each of the AP complexes is composed of two distinct large subunits (~ 100-130 kDa) termed β(1-5)-adaptin and γ-,α-,δ-,ε- or ζ-adaptin, a medium μ(1-5)-subunit (~ 50 kDa), as well as of a small σ(1-5)-subunit (~ 20 kDa) existing in different isoforms (**Fig. 1.6**). In the case of AP-1, the complex is made up of a β1-, γ-, μ1-, and σ1-adaptin subunit. The presence of individual AP-1 adaptin isoforms is cell type-

specific. In polarized cells, for instance, there are two different μ1 subunits, μ1A and μ1B, with overlapping, but also separate functions (Bonifacino, 2014; Gravotta et al., 2012a; Zizioli et al., 2010). Recently, a second γ-subunit has been more thoroughly characterized, thereby giving rise to a γ1- and γ2-isoform-containing AP-1 complex (Zizioli et al., 2017). While the AP-1/γ1 complex is expressed in all eukaryotes, AP-1/γ2 expression only occurs in vertebrates and plants. They both have different functions in development and traffic and do not functionally compensate for each other (Zizioli et al., 2017). To avoid any confusion when talking about the γ-subunit of AP-1, we always refer to the ubiquitous γ1 and not to the other isoform (Lewin et al., 1998; Takatsu et al., 1998; Zizioli et al., 2017; Zizioli et al., 1999). Regarding structure, the two large subunits (γ and β1) can be subdivided into a C-terminal ear-like appendage domain connected to the N-terminal core domain via a flexible and unstructured linker sequence (Canagarajah et al., 2013; Kirchhausen, 1999; Owen et al., 2004; Robinson, 2004).

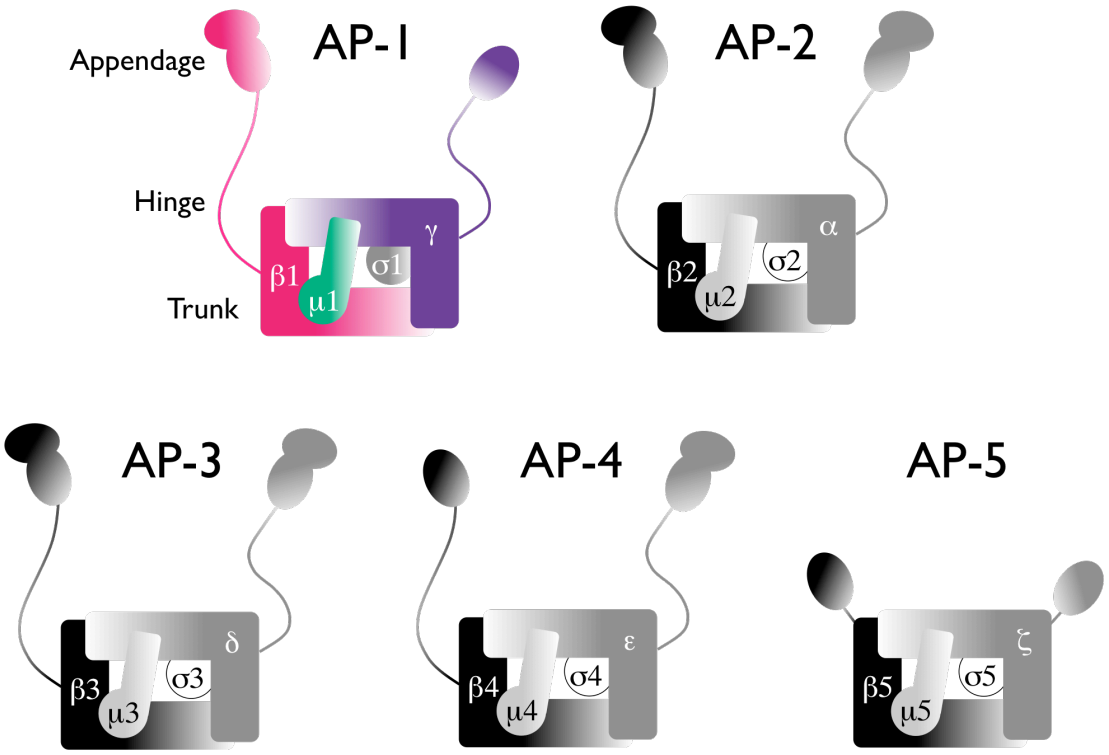

Figure 1.6: Structural organization of the five adaptor protein (AP) complexes. The AP complexes are heterotetrameric protein complexes composed of two large subunits (β(1-5)-adaptin and γ-,α-,δ-,ε- or ζ-adaptin), a medium μ(1-5)-subunit and a σ(1-5)-subunit. Some adaptins exist in different isoforms that are in part expressed in a tissue-specific manner. AP complexes are structurally organized into a C-terminal appendage domain, and an N-terminal trunk domain that are linked via a flexible hinge. Since AP-1 is of importance later on, it is highlighted in different colors than the other APs. Figure in the style derived from Canagarajah et al., 2013.

AP-1 mainly localizes to the TGN and to tubular early endosomes, indicating a dual distribution pattern and the involvement in distinct sorting pathways. Membrane recruitment of AP-1 is dependent on activated ARF GTPases, where the adaptor binds tyrosine- or dileucine-based sorting signals on cargo proteins via the μ1 subunit or the γ/σ1-hemicomplex (Doray et al., 2007; Ohno et al., 1995; Owen and

Evans, 1998). While AP-1 and AP-2 functionally cooperate with clathrin and are thus bonafide components of clathrin-coated carriers (CCVs), this is less clear for AP-3, AP-4 and AP-5 (Hirst et al., 2012b; Robinson, 2004). After AP-2, AP-1 is the second most abundant cargo adaptor with a copy number of about 370'000 per cell (Hirst et al., 2012b).

After the brief and incomplete structural excursion on AP-1, we would like to focus now more on its functional role in cargo traffic. What is the cargo adaptor precisely doing in retrograde traffic from early endosomes? Apart from the well-established involvement in anterograde TGN-to-endosome transport (Ghosh et al., 2003b; Hinners and Tooze, 2003; Puertollano et al., 2001; Puertollano et al., 2003), AP-1 was also described in retrieval of cargo receptors to the TGN, in particular of the MPRs. Schu and colleagues reported that the steady-state distribution of both CDMPR and CIMPR in μ1A subunit-deficient fibroblasts derived from knockout mouse embryos was shifted to early endosomes at the expense of the TGN (Meyer et al., 2000). If AP-1 exclusively mediated anterograde transport from the TGN to endosomes, one would expect that in AP-1 knockouts both MPRs would accumulate in the TGN. MPRs, however, do exit the TGN in the absence of AP-1, reach the cell surface and are re-endocytosed from there, but accumulate to some extent in EEA1-positive compartments. Schu and colleagues also provided biochemical evidence for defective MPR retrieval from endosomes to the TGN using a resialylation assay (Meyer et al., 2000).

In an additional study of Schu (Medigeshi and Schu, 2003), it was further demonstrated that membranes isolated from AP-1-deficient cells have a reduced transport competence in an in vitro retrograde endosome-to-TGN transport assay. These observations from Schu and coworkers supported a potential role of AP-1 in retrograde endosome-to-TGN traffic.

Another readout for AP-1 dysfunction is the general observation that the lysosomal hydrolase precursor cathepsin D is preferentially missorted into the medium rather than being delivered to lysosomes (Hirst et al., 2005; Hirst et al., 2003; Mardones et al., 2007; Meyer et al., 2000). If M6P-mediated lysosomal hydrolase delivery were really dependent on MPRs for TGN exit, then also these cargo proteins should accumulate in the TGN, however, they do not. Lysosomal hydrolases exit the TGN independently of AP-1 and MPR localization.

Apart from sorting of MPRs in the retrograde direction, other endocytosed cargo (e.g. cholera toxin) has been described to require AP-1 to reach the TGN (Matsudaira et al., 2015). AP-1-dependent transport from endosomes is not only restricted to deliver cargo proteins along the retrograde route, but has been implicated also in receptor recycling to the plasma membrane in polarized MDCK cells (Pagano et al., 2004).

Due to the ambivalent character of AP-1, acting anterogradely and retrogradely, the concept of bidirectional traffic has emerged, that is AP-1 to mediate both TGN-to-endosome transport and vice versa. However, most of what we know about the involvement of AP-1 in bidirectional traffic at the TGN-to-endosome interface is based on knockdown and knockout studies, and clearly, these studies influenced our understanding how the cargo adaptor operates. A major disadvantage of gradual or long-term protein depletion strategies is that compensatory or indirect effects may occur, either due to

cellular adaptation or altered steady-state distribution of involved factors. In particular, in the case of a cargo adaptor like AP-1 that permanently shuttles proteins between two intracellular compartments, the question about directionality is more challenging to tackle, since the observed phenotype might not be a direct consequence of AP-1 dysfunction.

Using a novel strategy for rapid protein inactivation termed 'knocksideways (KS)' (see also subchapter 1.4), Robinson and coworkers readdressed the function of AP-1 in bidirectional traffic at the TGN-to-endosome interface (Robinson et al., 2010). Using such a technique that eliminates possible compensatory or indirect effects, Robinson and colleagues could not only confirm AP-1 to function in endosome-to-TGN retrieval of MPRs, but also highlighted that gradual depletion (knockdown) and rapid depletion (knocksideways) can result in different readouts. While the protein levels of CIMPR present in clathrin-coated vesicles (CCVs) were substantially reduced in the knocksideways condition, almost no reduction was found in the knockdown condition (Robinson et al., 2010). It seems that other transport carriers fractionating with CCVs compensate for AP-1 loss during the period of a knockdown, but they do not appear in the knocksideways situation since upregulatory changes would take longer than minutes to eventuate.

The concept of AP-1 to be involved in bidirectional transport was further corroborated in a follow-up study by Robinson and coworkers (Hirst et al., 2012a) using quantitative proteomics. The study demonstrated that AP-1 in cooperation with GGA2, a monomeric adaptor at the TGN, facilitates cargo sorting of lysosomal proteins with their receptors for anterograde transport, while AP-1 alone operates in the selective retrieval of the empty cargo receptors in the retrograde direction (Hirst et al., 2012a). The idea of the orchestrated action of AP-1 and GGA adaptors at the TGN has been already suggested by Kornfeld and colleagues (Doray et al., 2002), however, quantitative data for this concept have been lacking. Also very interesting is the fact that not only cargo receptors and well-established AP-1 binding partners were depleted from the isolated CCV fraction, but also endosomally associated proteins such as Rab4 and rabaptin5 (Hirst et al., 2012a). This again points to AP-1 carriers budding from early endosomes.

The knocksideways approach (see also subchapter 1.4), in particular for AP-1, is thus an extremely powerful tool since acute depletion can provide unprecedented insights into protein function that are not apparent when proteins are depleted gradually.

EpsinR Pathway

Another clathrin adaptor operating at early endosomes apart from AP-1 is epsinR (derived from epsin-related). EpsinR, also termed CLINT1, epsin4 or enthoprotin, is a monomeric adaptor protein of ~ 70 kDa with an epsin N-terminal homology (ENTH) domain, a structural domain that is present in epsins operating in CME (Bonifacino and Traub, 2003).

EpsinR was originally discovered in a pull-down screen for proteins interacting with the appendage domain of the γ-subunit of AP-1 (Hirst et al., 2003). Since epsinR interacts with AP-1 in vitro and in vivo, it was not surprising that they have a nearly identical intracellular distribution pattern. Association of epsinR with membranes, however, is independent of AP-1, since epsinR localizes normally in AP-1-deficient cells. The same argument holds true for the opposite case. RNAi-mediated depletion of epsinR

also does not affect the subcellular localization of AP-1. Like AP-1, epsinR is recruited to the TGN and early endosomal membranes by members of the ARF GTPase family and the phosphoinositide PI(4)P (Hirst et al., 2003).

What is the function of epsinR in retrograde transport? The first cargo that was found to bind epsinR in a yeast two-hybrid screen was the SNARE protein vti1b (Chidambaram et al., 2004), an interaction that was subsequently corroborated in vivo (Hirst et al., 2004). It was shown that depletion of epsinR altered the steady-state distribution of vti1b as well as of vti1a, a SNARE which is 33% identical to vti1b, from a perinuclear to a more scattered peripheral labeling pattern. Thus, these SNARE proteins were proposed to be most likely involved in membrane targeting and fusion events at the TGN-to-endosome interface. Since vti1b, but not vti1a, was also strongly reduced in CCV fractions isolated from epsinR-depleted cells, epsinR was characterized as a SNARE-specific cargo adaptor that most likely operates in endosome-to-TGN retrieval of vti1b.

That epsinR/clathrin is not exclusively acting as SNARE-specific adaptor, but functioning in endosome-to-TGN cargo transport more generally was demonstrated by a study of Johannes and colleagues (Saint-Pol et al., 2004). Using a sulfation assay, they showed that cells depleted of epsinR had deficits in delivering Shiga toxin, CIMPR as well as TGN38/46 from TfR-positive compartments to the TGN (Saint-Pol et al., 2004).

Recently, Robinson and colleagues established an epsinR knocksideways cell line to analyze the immediate consequences of epsinR inactivation on clathrin-mediated intracellular traffic (Hirst et al., 2015). Similar to their former study (Hirst et al., 2012a), they isolated CCVs from cells where epsinR was rapidly inactivated, followed by quantitative CCV proteome analysis. Surprisingly, it was found that the epsinR knocksideways had a more global effect on intracellular CCV cargoes, similar to the effect of an AP-1 knocksideways. Top hits of depleted proteins were not only epsinR itself and predicted cargo proteins (e.g. vti1b), but also other coat components such as GGA2, AP-1 and clathrin, suggesting that, like AP-1, epsinR acts as a linchpin factor in the formation of an entire CCV population (Hirst et al., 2015). Interestingly, several cargo proteins that depend on AP-1 and/or GGAs (e.g. hydrolase receptors) were depleted even more strongly from CCVs isolated from epsinR KS than from AP-1 KS cells.

The observation that epsinR concomitantly depletes AP-1 from CCVs and vice versa suggests that they might operate cooperatively in intracellular CCV formation. It thus might be that epsinR and AP-1 belong to the same transport pathway, apart from their independent cellular function.

Retromer Complex Pathway

The retromer complex is an evolutionary conserved multimeric protein coat that is considered a master conductor in the orchestration of multiple cargo sorting events within the tubular endosomal network (TEN) (Bonifacino and Hurley, 2008; Cullen and Korswagen, 2011; Gallon and Cullen, 2015; Mukadam and Seaman, 2015; Seaman, 2012). Unlike to classical coats such as COPI or COPII as well as clathrin, the retromer complex does not form a visible electron dense layer on membranes by electron microscopy (Arighi et al., 2004; Popoff et al., 2007a; Seaman, 2004). Even though the terminology 'retro'-mer complex suggests its exclusive role in retrograde transport, it actually facilitates also endosomal cargo recycling to

the plasma membrane. Though conserved between kingdoms, the retromer complex in mammalian cells features some subtle functional and structural particularities that yeast do not have.

The retromer complex was initially identified almost 20 years ago in Saccharomyces cerevisiae to be required for endosome-to-TGN retrieval of the carboxypeptidase Y (CPY) receptor Vps10p, 'yeast's MPR'. In yeast, the retromer complex is made up of two different subcomplexes, a heterotrimer of Vps26p, Vps29p, Vps35p, and a heterodimer of Vps5p and Vps17p (Horazdovsky et al., 1997; Seaman et al., 1997; Seaman et al., 1998). In mammalian cells, genes encoding Vps5p and Vps17p have diversified such that the sorting nexin 1 and sorting nexin 2 (SNX1 and SNX2) are the mammalian homologues of Vps5p, while SNX5, SNX6 and most likely also SNX32 are the counterparts of Vps17p. Any combination of SNX1 or SNX2 with SNX5 or SNX6 can assemble to the heterodimeric subcomplex (Rojas et al., 2007b; Wassmer et al., 2007).

A particular feature of these SNXs is that they comprise a C-terminal Bin/Amphiphysin/Rvs (BAR) domain, and hence are termed SNX-BARs (Carlton et al., 2004). These BAR domains enable SNX-BARs to form specific homo- and heterodimers and, in this structural arrangement, can sense, model and drive membrane curvature for the formation of tubular-vesicular carriers (Frost et al., 2008; Frost et al., 2009; van Weering et al., 2012; Zimmerberg and McLaughlin, 2004). In addition, SNX-BARs of the retromer subcomplex also comprise a phagocytic oxidase (phox) homology (PX) domain (Teasdale and Collins, 2012), a domain specifically binding to PI(3)P-enriched membranes. As a result of coincidence detection of PI(3)P and curvature, SNX-BARs preferentially associate with tubular-vacuolar membranes of early endosomes. The heterodimeric subcomplex in its organization and function is often referred to as the SNX-BAR subcomplex or the 'tubulation complex' (Gallon and Cullen, 2015; Trousdale and Kim, 2015).

Discrimination of the retromer complex into two distinct subcomplexes is necessary. Then even though the SNX-BAR subcomplex interacts strongly with the heterotrimeric subcomplex in yeast, this interaction appears to be less robust in mammalian cells. It thus seems that the two subcomplexes in mammals only transiently interact with each other, similar to AP complexes with clathrin on the respective membranes during carrier formation. Since the heterotrimeric Vps26-Vps29-Vps35 subcomplex together with various other factors select cargo for transport, it is often referred to as 'cargo selective complex (CSC)', 'cargo recognition complex (CRC)' or 'retromer'. We will use the terminology retromer and, hence, the retromer subcomplex and the SNX-BAR subcomplex form together the '(SNX-BAR-) retromer complex'.

Similar to other cargo coats such as the AP complexes, retromer complex selectively recognizes short linear amino acid stretches in the cytoplasmic tail of transmembrane proteins. Vps35 is thought to select cargo, specifically CIMPR and sortilin, by association with a [FW]L[MV] motif (Seaman, 2007). Similarly, Vps26 binds the sequence FANSHY in the cytoplasmic tail of SorLA (Fjorback et al., 2012). Recently, several lines of evidence suggested that SNX components might also be involved in cargo recognition (Harterink et al., 2011; Steinberg et al., 2013; Strochlic et al., 2007; Temkin et al., 2011; Zhang et al., 2011). However, generic amino acid motifs as cargo sorting determinants are unknown and remain to be determined. The few reports of interactions with cargo do not explain the number of processes in which retromer complex is implicated to be involved. Other accessory factors downstream of retromer

complex recruitment might cooperate in cargo selection and facilitate binding of a broader repertoire of transmembrane proteins with distinct sorting motifs (Gallon and Cullen, 2015).

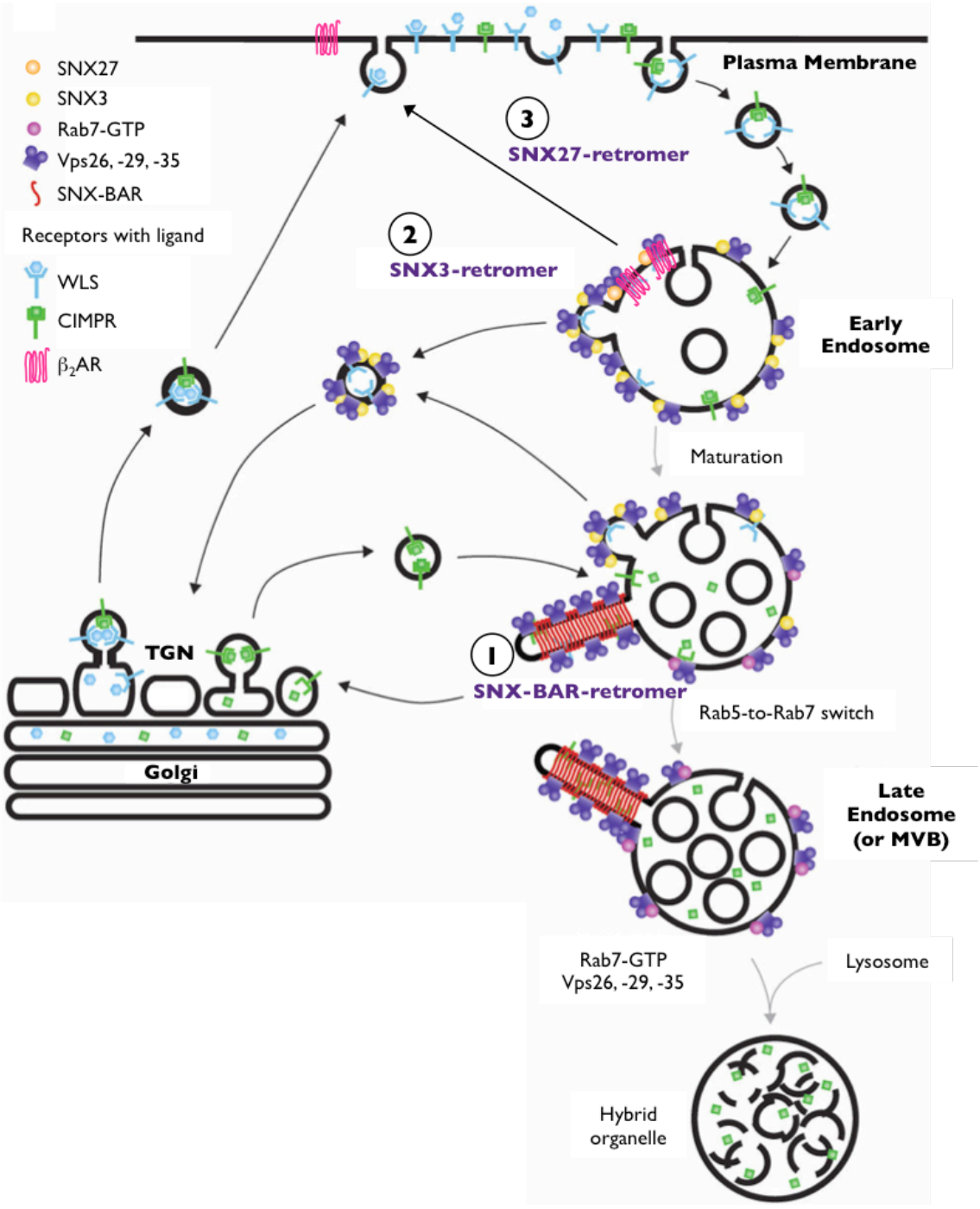

Figure 1.7: Distinct retromer complexes involved in endosome-to-TGN transport and recycling to the plasma membrane. The mammalian retromer complex mediates at least three distinct pathways from endosomes. The 'canonical' SNX-BAR-retromer complex (1), comprising the core retromer trimer (Vps26-Vps29-Vps35) and the SNX-BAR subcomplex, mediates retrograde transport of cargo such as CIMPR to the TGN. The SNX3-retromer complex (2), comprising the core retromer trimer and SNX3, shuttles cargo such as WLS from endosomes to the TGN. The SNX27-retromer complex, comprising the core retromer trimer and SNX27 (3), traffics cargo such as the β_2 adrenergic receptor from endosomes to the plasma membrane. Figure modified from Cullen and Korswagen, 2011.

The retromer complex as such cannot bind to PI(3)P-enriched early endosomes on its own since it lacks a lipid-binding domain. Instead, retromer requires Rab7a for membrane recruitment, most probably via Vps35 (Nakada-Tsukui et al., 2005; Rojas et al., 2008; Seaman et al., 2009). As commented elsewhere (Johannes and Wunder, 2011), this finding was found rather puzzling since Rab7 is associated with late rather than early endosomes. It is thus believed that cargo sorting by retromer complex is a progressive process that is part of endosomal maturation during the Rab5-to-Rab7 switch (Rojas et al., 2008). Along with Rab7a, SNX3 has also been implicated in the recruitment of retromer (Harterink et al., 2011). Unlike the SNX-BARs, SNX3 belongs to the SNX-PX subfamily of SNXs since it only has a PX, but not a BAR domain (Gallon and Cullen, 2015; Yu and Lemmon, 2001). Unlike the 'canonical retromer complex', the SNX3-retromer complex represents a heterotetrameric and not a heteropentameric assembly complex, which has been reported in the selective transport of WLS.

After the brief and by far incomplete excursion on retromer complex biology, we would like to focus now more on its functional role in cargo traffic. The characterization and involvement of SNX family proteins and additional factors allowed defining at least three distinct exit routes from endosomes (**Fig. 1.7**), including the canonical SNX-BAR-retromer complex (**Fig. 1.7**, 1) that mediates transport to the TGN from tubular regions of endosomes, the SNX3-retromer complex (**Fig. 1.7**, 2) that facilitates endosome-to-TGN transport of WLS, and last but not least, the SNX27-retromer complex (**Fig. 1.7**, 3) that traffics cargoes from endosomes to the plasma membrane (Gallon and Cullen, 2015). We are only interested in the pathways mediated by the SNX-BAR-retromer and SNX3-retromer complex (**Fig. 1.5** and **Fig. 1.7**) since they are delivering cargo destined to the TGN.

Compared to retrograde transport mediated by AP-1, epsinR and other machineries, retromer complex-driven sorting is probably the most thoroughly characterized retrograde endosome-to-TGN pathway. Therefore, it is not a surprise that myriads of cargo proteins have been described that are sorted by the retromer complex. Most of the proteins listed in **Table 1.1** have been reported to be recognized and sorted by the retromer complex. Probably the best-characterized cargo of the SNX-BAR retromer complex is CIMPR. In the study by Seaman (Seaman, 2004), it was investigated whether the mammalian retromer complex fulfills the same function as in yeast regarding endosome-to-TGN retrieval of the mammalian homologue of Vps10p, CIMPR. Using cells derived from transgenic mice deleted for mammalian Vps26 and through the application of RNAi to knockdown expression of Vps26, it was found that the absence of the retromer subunit resulted in a range of phenotypes consistent with a defect in endosome-to-Golgi retrieval. Similar to a knockdown or knockout of AP-1 (Hirst et al., 2005; Meyer et al., 2000), Vps26 depletion caused CIMPR redistribution to EEA1-positive endosomes and defects in cathepsin D maturation (Seaman, 2004). Parallel to the study of Seaman, Bonifacino and colleagues reported similar phenotypes for cells depleted of Vps35 (Arighi et al., 2004). It thus seems that ligand-free CIMPR, or MPRs in general, is dependent on more than just one retrograde sorting machinery. Whether for instance the AP-1/clathrin and retromer complex are separate or cooperative sorting machineries will be discussed further below.

Apart from MPRs, the other two listed cargo receptors (**Tab 1.1**), sortilin and SorLA, are also trafficked from endosomes to the TGN in an SNX-BAR-retromer-dependent manner (Fjorback et al., 2012; Nielsen et al., 2007; Seaman, 2004).

Other endosome-to-TGN cargoes sorted by retromer complex are DMT1, TGN38 and WLS (Bai and Grant, 2015; Belenkaya et al., 2008; Tabuchi et al., 2010). However, unlike MPR and MPR-like cargo receptors, DMT1, TGN38 and WLS transport is mediated by the SNX3-retromer complex. Also here, it has to be mentioned that TGN38 is trafficked to the TGN by an alternative route, namely by the epsinR pathway (Saint-Pol et al., 2004).

Endosome-to-PM recycling by retromer complex has been reported for the β_2 adrenergic receptor (β_2AR) and TfR. Direct recycling of β_2AR to the cell surface involves the SNX27-retromer complex and Rab4, while TfR recycling was proposed to be indirect via recycling endosomes but to require SNX3 (Chen et al., 2013b; Temkin et al., 2011). Even though there are more cargo proteins relying on retromer complex for correct localization, these few examples illustrate the importance of the complex in endosomal sorting.

As briefly touched above, some cargoes (e.g. MPRs or TGN38 and isoforms) seem to use more than just one transport route for correct membrane localization. Together with the fact that retromer complex has been appreciated not only as cargo coat but also as 'recruiting hub' for multiple factors, the idea has raised that retromer complex is linked to clathrin coat formation on endosomes (Burd and Cullen, 2014; Gallon and Cullen, 2015; Seaman, 2012). Clathrin-coated structures on endosomes in close vicinity to retromer complex have been indeed reported, and proteomics-based studies have identified retromer complex subunits to be present in semi-pure preparations of CCVs (Borner et al., 2006; Popoff et al., 2009; Popoff et al., 2007a; Shi et al., 2009). In contrast to these observations, however, a finding from Robinson and colleagues was that clathrin and retromer complex subunits are present on distinct transport intermediates (Borner et al., 2012). In addition to that, there are currently no reports of any direct interactions between clathrin and retromer or the SNX subunits (McGough and Cullen, 2011; McGough and Cullen, 2013). Thus, whether clathrin and retromer complex operate together in endosomal protein sorting requires further investigation. Retromer complex has also been linked to the ESCRT machinery since SNX1 binds to Hrs-1, an ESCRT-0 component. But as for the clathrin machinery, more evidence is needed to link retromer complex to the ESCRT machinery.

Rab9/TIP47 Pathway

The first discovered pathway that mediates retrograde transport from an endocytic compartment to the TGN was the Rab9/TIP47 pathway (Pfeffer, 2009). The GTPase Rab9 has been initially shown by Pfeffer and colleagues to localize to tubular late endosomes and to be required for efficient transport of MPRs to the TGN (Lombardi et al., 1993; Soldati et al., 1993). With the subsequent search for additional factors using a yeast two-hybrid screen, Diaz and Pfeffer identified a protein of 47 kDa, that they named tail-interacting protein, or briefly TIP47 (Diaz and Pfeffer, 1998). In follow-up studies after the discovery of TIP47, it was then shown that Rab9 and TIP47 are operating in an intertwined process where active Rab9

acts as crucial hub to recruit downstream effectors, including TIP47, to mediate late endosome-to-TGN transport (Carroll et al., 2001).

Further characterization by Pfeffer and colleagues demonstrated that depletion of TIP47 using antisense oligonucleotides or siRNA strongly destabilized MPRs in living cells (Diaz and Pfeffer, 1998; Ganley et al., 2004), and antibody depletion of TIP47 from cytosol led to a partial loss of cytosol activity in terms of its ability to support in vitro transport of MPRs from endosomes to the TGN (Diaz et al., 1997). The association of TIP47 with purified endosome-enriched membranes was impaired by antibodies binding to the cytoplasmic domain of MPRs, implicating TIP47 to specifically recognize MPRs (Krise et al., 2000; Orsel et al., 2000). Also, binding of TIP47 to CIMPR was reported to be somewhat stronger than to CDMPR, suggesting minute trafficking differences between the two receptors in retrieval (Krise et al., 2000). TIP47 expression was also shown to stimulate MPR transport from late endosomes to the TGN, and the presence of Rab9 even increased the affinity with which TIP47 bound MPR tails (Sincock et al., 2003). The importance of TIP47 in Rab9 function was further highlighted by the striking observation that depletion of TIP47 destabilized the GTPase (Ganley et al., 2004). Although the total levels of Rab9 did not change, the rates of turnover and new synthesis did.

Taking together all these findings, Pfeffer and coworkers proposed the Rab9-recruited protein TIP47 to act as a cargo selection device for MPRs in late endosome-to-TGN transport (Pfeffer, 2009). Apart from TIP47, other Rab9 effectors are required for efficient MPR retrieval from late endosomes, including p40 and GCC185 (Derby et al., 2007; Diaz et al., 1997). While p40's function in transport is unclear, GCC185 has been shown to be a tether for vesicle docking and fusion at the TGN.

While AP-1, epsinR and retromer complex seem to cover a spectrum of cargo, including MPRs, for retrograde transport from early endosomes, TIP47 seems to specifically traffic only MPRs from late endosomes. Despite the considerable body of evidence, the role and function of TIP47 in cargo traffic from late endosomes has been recently challenged. In particular because TIP47 has also been reported in lipid droplet biosynthesis (Wolins et al., 2001). In addition to that, other groups argue against the involvement of TIP47 in retrograde transport of MPRs from late endosomes (Bulankina et al., 2009). Höning and colleagues failed to reproduce some of the initially described functions of Rab9 and TIP47. They showed that TIP47 does not colocalize with MPRs, Rab9 and other marker proteins of the secretory and endocytic pathways. Also, depletion of TIP47 did not affect the steady-state distribution of MPRs, as it does during interference with the retromer complex or the AP-1 machinery.

Along with the fact that TIP47 does not have any obvious adaptor coat organization, like AP-2 or AP-1, or any corresponding membrane-distal coat, such as clathrin, the function of TIP47 as selective cargo device remains in question. Clearly, further attempts are required to resolve the discrepancy of TIP47 function in lipid droplet biogenesis and retrograde transport from late endosomes. At least, the name TIP47 has become scarce, instead the name perlipin-3 (PLIN3) has gained acceptance. Perlipin-3 belongs to the perlipin protein family and shares significant homology to other proteins of this family, such as adipophilin, a well-characterized protein of lipid droplets (Itabe et al., 2017; Pol et al., 2014; Wilfling et al., 2014).

Adaptor protein localization to endosomes may suggest a function in cargo recycling to the plasma membrane or retrieval to the TGN. Other cargo adaptor molecules reported to be present on endosomes are the Golgi-localized, γ-ear-containing, ADP ribosylation factor (ARF)-binding proteins, briefly GGAs (Bonifacino, 2004). In the study of Walter and coworkers (Wahle et al., 2005), it was shown that GGA1, one out of three GGAs (GGA1-3), is involved in retrograde transport of the processing enzyme BACE1 from early endosomes to the TGN. Some other lines of evidence confirming GGA localization and function on endosomes were reported by Casanova and colleagues (D'Souza et al., 2014). They showed that GGA3 localizes onto dynamic Rab4-enriched tubular domains of early endosomes. It has to be stressed, however, that GGAs are mainly known to operate in anterograde cargo traffic from the TGN. In particular, GGA proteins were described as adaptor proteins cooperating with AP-1 to package MPRs with bound lysosomal hydrolases into AP-1-containing coated carriers (see also 'AP-1 pathway') (Doray et al., 2002; Ghosh and Kornfeld, 2004; Hirst et al., 2012a). The significance of GGAs in retrograde transport from early endosomes to the TGN is due to only a few number of studies hard to assess.

We have seen that multiple trafficking routes exist that confer transport from endosomal compartments to the TGN. Most of the studies dominating today's conception of each transport route were based on steady-state localization readouts after interference with the respective sorting machineries. Ideally, kinetics of transport to the TGN rather than misdistribution analysis of cargo reporters in the TGN/endosomal network are potentially of more meaningful value since we can track proteins in action. In addition, RNAi-mediated depletion or knockout strategies entail a number of drawbacks that can make it very challenging to interpret the observed data. During the period of gradual protein depletion for instance, it is difficult to see whether the observed phenotype is a direct result of protein loss, or whether mislocalization of other factors, that are dependent on the depleted protein, are responsible. In case of the latter, we speak about indirect or secondary effects. To study PM-to-TGN retrograde transport kinetics more precisely and reliably, tools are required allowing rapid inactivation of sorting machineries.

1.4 Rapid Protein Inactivation by Knocksideways

Knocksideways (KS) describes the rapid inactivation of proteins by trapping them onto mitochondria. Unlike other methods to inactivate proteins, including knockdown with interference on the mRNA level or knockout by CRISPR/Cas9-mediated editing on the genomic level, knocksideways occurs on the protein level. The knocksideways approach has been pioneered by Margaret Robinson and colleagues (Robinson and Hirst, 2013; Robinson et al., 2010), but has in the meantime found increasing application by a number of other laboratories (Birnbaum et al., 2017; Cheeseman et al., 2013; Garay et al., 2015; Giorgino and De Fabritiis, 2011; Hughes and Waters, 2017; Renard et al., 2015; Willett et al., 2014; Willox and Royle, 2012). The system can be principally used on any protein of interest that is either cytosolic or transiently membrane-associated. Since knocksideways is considerably faster (typically within minutes) than a knockdown or knockout (Robinson and Hirst, 2013), one can look at the immediate consequences of inactivating a protein of interest. This has the benefit of more clear-cut results than those obtained with a knockdown or knockout, since there is much less time for indirect and/or compensatory events to come into play. Above all in the case of sorting machineries that regulate protein traffic between two intracellular organelles, fast inactivation can provide more significant readouts since gradual or long-term depletion might just reflect the accumulation of indirect effects.

But how is the knocksideways approach working? The approach is based on the ability of rapamycin or rapalogs to form non-covalent heterodimers between proteins modified with a FKBP or FRB domain (**Fig. 1.8**). One of the domains, for instance FRB, is anchored in the outer mitochondrial membrane, while the FKBP domain is attached to the protein to be inactivated. In such a setup, knocksideways thus mediates the rapid sequestration and thus immobilization of FKBP-modified target prey proteins onto mitochondria by rapamycin/rapalog-induced heterodimerization with the FRB-tagged outer mitochondrial bait protein. Since the mitochondrial protein acts as trap for the cytosolic FKBP-modified preys, it is referred to as Mitotrap (Robinson and Hirst, 2013). Since the dissociation time of $t_{1/2}$ ~ 17.5 hr for rapamycin and its analogues is extremely slow (Hosoi et al., 1999), one can consider mitochondrial rerouting as irreversible.

Apart from FKBP and FRB domains, other protein modules conferring ligand-triggered heterodimerization can be essentially used. Although not yet published for KS approaches, prey and bait proteins tagged with a SNAP-tag or Halo-tag can be introduced to achieve crosslinking using the recently described heterodivalent compound HaXS and in its variants (Erhart et al., 2013; Zimmermann et al., 2014).

Apart from introducing recombinant prey and baits into the system, it is also a requirement to deplete the endogenous counterpart of the prey protein without affecting the recombinant one. This is normally achieved by making the prey construct RNAi-resistant. Thus, to start the actual knocksideways procedure, it is necessary to deplete the endogenous counterpart of the protein of interest (POI) first. Most importantly, the recombinant FKBP-tagged prey construct thereby has to functionally compensate for the role of the endogenous protein. Alternatively, the recombinant prey construct can be rendered single guide (sg) RNA-resistant so that subsequent CRISPR/Cas9-mediated gene editing will abolish endo-

genous expression. Gene editing could be principally also used to knock in the FKBP domain into the target locus, retaining essentially endogenous expression levels.

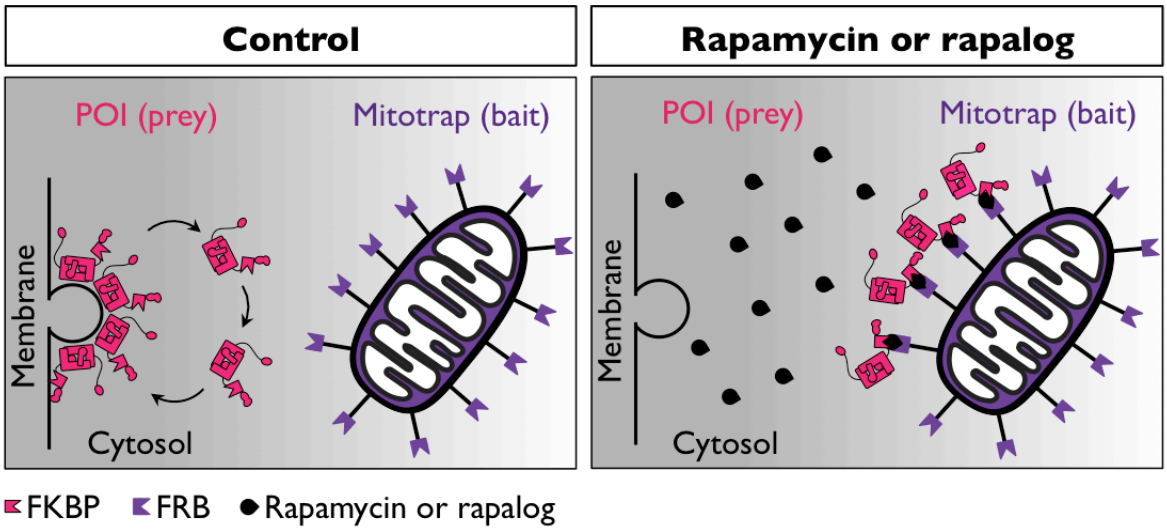

Figure 1.8: Schematic diagram of the knocksideways approach. The prey (pink) and bait proteins (violet) have FKBP and FRB domains that can bind a small molecule, such as rapamycin and analogs, for non-covalent heterodimerization. Preys are typically modified with a FKBP domain, baits with a FRB domain. Apart from the FRB domain, the bait is modified so that it localizes to the outer mitochondrial membrane. The prey is the protein of interest (POI) to be inactivated, and that cycles between the cytosol and a membrane or other cellular structures. Administration of the small molecule causes the prey to be immobilized on mitochondria where it cannot perform its function anymore. Figure in the style derived from Robinson and Hirst, 2013.

Even though KD and KS can culminate in identical readouts, as shown for AP-1 with regard to the accumulation of CIMPR in early endosomes in anti-CIMPR antibody uptake experiments (Meyer et al., 2000; Robinson et al., 2010), there is also a body of evidence that the two inactivation strategies result in different readouts. In the same study by Robinson (Robinson et al., 2010), it was shown that isolated CCVs from AP-1 KS cells had a strong depletion of CIMPR, while this was not the case in AP-1 KD cells. This observation suggested that during the period of a gradual knockdown, CIMPR was presumably trafficked by other transport intermediates to find its way to its target compartment (see also 'AP-1 pathway' subchapter). The same CCV isolation experiment further showed that there is more α-adaptin associated with vesicles prepared from AP-1 KD cells, whereas levels in AP-1 KS cells were unaltered. This observation is thought to reflect an attempt by the cells to compensate for the loss of AP-1 (Robinson et al., 2010).

A more striking difference between KS and KD readouts was shown in a follow-up study by Robinson and colleagues (Hirst et al., 2012a). With the aim to tease apart the interrelationship between AP-1 and GGA2 in cargo packaging at the TGN, Hirst and coauthors isolated CCVs from AP-1 KS and GGA2 KS cells. Interestingly, while GGA2 copurified with CCVs isolated from AP-1 KD cells in control cells, it is strongly depleted from CCVs prepared from AP-1 KS cells. It thus seems that during the period of a knockdown, something happens that allows the cell to nevertheless recruit GGA2 onto CCVs. In addition, in a recent study of Robinson and coworkers (Navarro Negredo et al., 2017), proteomics profiling of CCVs isolated from AP-1 KS and AP-1 KO cells demonstrated that ARF1 was lost from the

vesicles when AP-1 was acutely inactivated, while the GTPase was barely affected from the membrane fraction when isolated from AP-1 KO cells. The phenomena of such different readouts between KS and KD or KO are difficult to interpret, since it can be hardly predicted how cells react if they face gradual AP-1 depletion. For the experimenter, hence, 'unforeseen' signaling events might occur during the typical time of ~ 72-96 h of a knockdown, thereby enabling the cell to compensate and/or adapt. Only by combining the knocksideways technique with CCV profiling, it was possible to show that AP-1 may act as a linchpin in the formation of intracellular CCVs, and that if AP-1 is rapidly lost, no such carriers can form.

A similar importance in intracellular CCV formation could be assigned to the epsinR adaptor (see also 'EpsinR pathway'). EpsinR knocksideways did not only affect its cargo protein vti1b, but more globally a broad range of cargo (Hirst et al., 2015). This observation was mainly possible due to the rapidity of the knocksideways approach. A second protein that Hirst and coauthors investigated in the respective study was gadkin. Gadkin is a CCV component that provides a connection between AP-1 and the cytoskeleton. Knocksideways of gadkin also resulted in phenotypes different from knockdowns or knockouts (Laulagnier et al., 2011; Maritzen et al., 2012). Clearly, the manner and time of inactivation can produce different readouts. If one has to believe in one of the two experimental out-comes, i.e. 'knocksideways' versus 'knockdown/knockout', then it is plausible to trust the KS readout more since it is free of any indirect or compensatory effects, at least specifically with regard to AP-1, while other KDs/KOs should not be discredited from the beginning.

Which other proteins have been studied with the knocksideways technique apart from AP-1, GGA2, epsinR and gadkin? Willox and Royle used FKBP-modified stonin2, an endocytic adaptor specific to neurons, and clathrin to look at synaptic vesicle retrieval (Willox and Royle, 2012). Rapid rerouting of stonin2 and clathrin allowed the authors to switch endocytically competent synapses to a blocked state on the timescale of minutes.

In another study of Royle and coworkers (Cheeseman et al., 2013), the protein TACC3 was investigated. TACC3 was reported to be an essential non-motor protein that associates with the microtubule polymerase ch-TOG and brings it to spindle fibers during mitosis. It was proposed that TACC3-ch-TOG complexes are crucial for promoting spindle assembly, a process that is also dependent on clathrin. To specifically remove TACC3-ch-TOG-clathrin complexes from mitotic spindles after normal spindle assembly, an FKBP-tagged TACC3 fusion was used. Using the knocksideways technique, it was possible to remove TACC3-ch-TOG-clathrin at different stages of mitosis. The use of RNAi to study the function of spindle proteins is complicated because the cell may have undergone a number of cell cycles with gradual reduction of the proteins. During this time, the cell might adapt and/or upregulate alternative pathways to compensate for the depleted protein.

Other studies using the knocksideways approach came from Lupashin and colleagues who studied the mobility of the conserved oligomeric Golgi (COG) complex (Willett et al., 2014), a complex that orchestrates tethering and fusion of intra-Golgi carriers with Golgi membranes. Using the knocksideways approach, the authors found that the COG complex is tightly associated with Golgi membranes since it is not significantly relocated onto mitochondria in the presence of rapamycin within 24 h.

In the study of Renard and colleagues, rapid rerouting of endophilin-A2 was performed to study its function in membrane scission during CIE (Renard et al., 2015). It is now clear that endophilin-A2 is part of a separate CIE pathway termed FEME. We briefly discussed this CIE pathway in subchapter 1.1.

Antonescu and colleagues (Garay et al., 2015) used the knocksideways approach to perturb clathrin function and to monitor its consequences on EGF-stimulated Akt phosphorylation. It was shown that clathrin rerouting resulted in inhibition of EGF-stimulated Akt phosphorylation. Antonescu and coworkers could not only show that clathrin is required for EGFR signaling finally resulting in Akt phosphorylation, but also that the requirement for clathrin is functionally independent from its role in EGFR endocytosis.

Knocksideways has not only been applied on cultured cells, but also on other model systems, such as on Plasmodium falciparum (Birnbaum et al., 2017; Hughes and Waters, 2017). The protozoan Plasmodium falciparum, a parasite leading to the most severe form of malaria, was used to selectively knock in FKBP into loci of its essential genes. Inactivating these proteins allowed the authors to get insights into their in vivo function in the progression of malaria disease.

Knocksideways has a number of advantages in comparison to a knockdown and/or knockout, that are its versatility, its rapidity, and the reduced risk of indirect or compensatory effects. In particular in order to study protein traffic, it is favorable to have acute inactivation strategies to immediately interfere with the sorting machinery without indirect effects to prevail.

Membrane traffic between two compartments can be investigated best when we label reporter proteins in the donor compartment, acutely inactivate the sorting machinery by knocksideways, and then look at arrival in the acceptor membrane. In order to elucidate the role of AP-1 in coated vesicle biogenesis at the TGN and early endosomes, Robinson and colleagues (Hirst et al., 2012a; Robinson et al., 2010) combined CCV isolation with quantitative proteomics in cells where AP-1 was acutely lost. An alternative approach to CCV isolation to study anterograde traffic from the TGN is sulfation, a modification restricted to this compartment. Likewise, to assess transport from the cell surface to the TGN, sulfation can be used as arrival indicator. This alternative approach would require specific cell surface modification of proteins to render them sulfatable. Furthermore, in comparison to CCV isolation, sulfation has the benefit to make statements about directionality.

1.5 Protein Binders as Tool to Analyze Retrograde Transport

1.5.1 Overview of Protein Binders

Studying retrograde traffic from the cell surface requires specific surface labeling of proteins of interest. An approach to label proteins in vivo and in vitro in general is the use of protein binders, proteins that bind to a specific target. Such protein binders not only function to study protein-protein interactions, but also to modulate or inhibit their activity as well as to visualize dynamic changes of cellular localization in living cells.

Apart from the most established protein binders, the conventional antibodies, new approaches have been developed to generate additional highly specific binders. As a result, a number of small protein scaffolds were adapted or engineered, leading to the establishment of scFVs, nanobodies, DARPins, and more. In the following, an overview of each of these protein binder scaffolds is given. It has to be mentioned that this subchapter of the PhD thesis only provides a very short glimpse at protein binders. For a more detailed picture of protein binders, a number of excellent reviews have been published over the last three years (Bieli et al., 2016; De Meyer et al., 2014; Helma et al., 2015; Kaiser et al., 2014; Pluckthun, 2015). In addition, it has to be emphasized already here that the use of such protein binders has a great potential as tool in basic research, including in the field of protein and membrane traffic within the secretory and endocytic pathways.

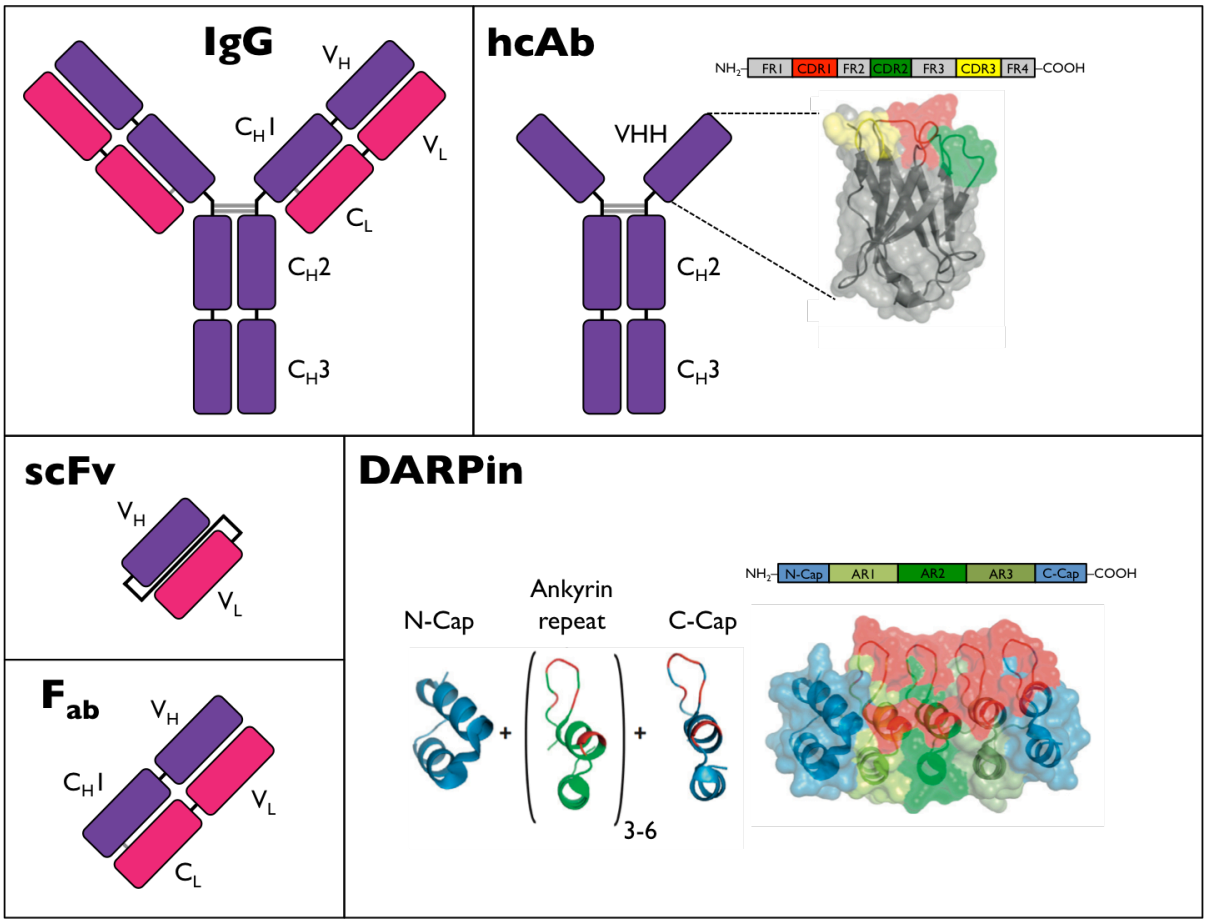

Figure 1.9 (see previous page): Schematic illustration of conventional antibodies, scFvs, F_{ab}, camelid hcAbs and DARPins. (IgG) Conventional antibodies (IgGs) contain constant regions from the heavy chains (C_H1-3) and light chains (C_L), as well as variable regions from heavy (V_H) and light chains (V_L). The paratope, the entity conferring antigen-specificity, is represented by the V_H and V_L. Disulfide bonds present in IgGs are depicted in grey lines. **(scFv)** Single-chain variable fragments are only composed of the variable regions (V_H and V_L) of IgGs that are connected to each other via a synthetic linker. **(F_{ab})** Antigen-binding fragments (F_{ab}) are composed of one constant (C_H1 and C_L) and one variable domain (V_H and V_L) of each of the heavy and the light chain. **(hcAbs)** Heavy chain antibodies (hcAbs) lack light chains and C_H1, instead C_H2 is directly fused to the variable domain (VHH) of the heavy chain antibody. A schematic drawing of the VHH domain is depicted. The so-called conserved framework regions (FR1-4) are depicted in grey, the complementarity determining regions (CDR1-3) are shown in other colors. **(DARPins)** Designed Ankyrin Repeat Proteins (DARPins) are composed of three to six ankyrin repeats (AR) that are flanked by a N-terminal and C-terminal cap. The cartoon depicts a DARPin with three ankyrin repeats (AR1-3, in green) and the respective caps (in blue). Figure modified from Bieli et al., 2016.

1.5.2 Conventional Antibodies, scFvs and F_{ab}

Conventional antibodies (IgGs) are the most commonly known protein binders since they have myriads of applications in cell biology. IgGs are typically composed of two identical large heavy (H) chains (~ 50 KDa) and two identical small light (L) chains (~ 25 kDa). Each of these H and L chains comprises constant (C) and variable (V) regions (**Fig. 1.9**). The H and L polypeptide chains are connected to each other via disulfide bonds, and by this assemble to a heterotetrameric protein complex (~ 150 kDa). For synthetic protein engineering or expression approaches, such a complex organization with various inter- and intramolecular disulfide bridges is of disadvantage. Disulfide bonds can only be formed in an oxidizing environment, such as the ER. In addition, assembly and correct folding of four polypeptide chains to a functional antibody is a complex process.

To circumvent some of these drawbacks, derivatives of IgGs, such as scFvs or F_{ab} fragments, have been constructed (**Fig. 1.9**). The so-called single-chain variable fragment (scFv) is actually not a fragment of an antibody as it might insinuate, but represents a fusion protein of the variable regions of the heavy (V_H) and light chains (V_L) of an IgG. Thereby, V_H and V_L are connected with a synthetic short linker peptide, which typically contains glycine residues for flexibility and serine or threonine residues for solubility (Bird et al., 1988; Chen et al., 2013c; Nelson, 2010), and can either bridge the N-terminus of the V_H with the C-terminus of the V_L, or the opposite direction. Since the V_H of the H and L chain are the functional entities binding to target epitopes, scFvs still retain their specificity despite the absence of the constant regions (CH1-3, CL). scFvs represent one of the most used small protein binder scaffolds, however, they did not find many applications in cell and developmental biology because of a variety of technical caveats, including aggregation, insolubility, and misfolding upon expression in the cytoplasm (Bieli et al., 2016; Cattaneo and Biocca, 1999; Visintin et al., 1999).

Unlike scFvs, antigen-binding fragments (F_{ab}) of IgGs, that are produced by partial proteolysis, are composed of one constant and one variable domain of the H and L chain (Rader, 2009). Even though conventional antibodies, scFvs, and F_{ab} act as useful protein binders, they have the disadvantage that they cannot be expressed in the cytoplasm and are difficult to be synthesized with bacterial expression systems.

1.5.3 Nanobodies

Apart from the expression of heterotetrameric antibodies during immune responses, animals from the family of Camelidae (e.g. camels, llama, alpacas, etc.) and cartilaginous fishes (e.g. nurse sharks) produce a distinct set of antibodies. These antibodies lack light chains and are thus also called homodimeric heavy chain antibodies (hcAbs).

As a result of the above-mentioned limitations of IgGs and their derivatives, the discovery of these naturally occurring hcAbs almost 25 years ago has raised great attraction in the recombinant antibody field (Greenberg et al., 1995; Hamers-Casterman et al., 1993). Due to the lack of variable light chain domains, the functional antigen-binding unit of hcAbs is confined to the variable domain of the heavy chain (VHH). The variable domain of these hcAbs is often referred to as single-domain antibody (sdAb) or more commonly as nanobody. In hcAbs, VHH can be regarded as the functional equivalent of the variable regions (F_V) of conventional antibodies. Since the VHH consists only of one polypeptide chain, it is considerably smaller in size (~ 15 kDa) than the F_v fragment. When mentioning hcAbs, we always refer to the homodimeric heavy chain antibodies derived from camelids, because hcAbs from cartilaginous fishes (the so-called IgNARs) have a slightly different organization in their variable and constant regions.

Nanobodies have numerous technological advantages compared to other small antibody fragments like scFv or F_{ab}. First, only one domain has to be cloned and expressed to generate a functional protein binder. There is no need to assemble to higher oligomeric structures to gain antigen specificity. Second, specific nanobodies can be selected with standard screening technologies. Nowadays, companies (e.g. the company Hybribody) produce VHHs on demand and select them using the phage display or yeast two-hybrid technology. And third, nanobodies are highly soluble, stable (heat-stable to ~ 70°C) and characterized by high affinity after selection (Kaiser et al., 2014; Muyldermans, 2001).

All nanobodies share a common conserved framework (FR) structure consisting of 9 β-strands that fold into two 4- and 5-stranded β-sheets, yielding a so-called β-sandwich structure (**Fig. 1.9**). Apart from the FR, nanobodies typically contain three hypervariable regions that are called complementarity-determining regions (CDRs). The CDRs are present within the loops that connect one β-strand to the next to form a continuous surface mediating recognition of the target antigen (Muyldermans, 2013; Muyldermans et al., 1994). While the paratope of conventional antibodies consists of six CDR loops (three each from V_H and V_L), the paratope of nanobodies comprises three loops only. The CDR loops from nanobodies, however, are considerably longer and confer similar variability and specificity as those present in conventional antibodies (Bieli et al., 2016; Muyldermans, 2013). As the CDR loops are longer, they have to be stabilized, and this is mainly conferred by an intramolecular disulfide bond between CDR1 and CDR3. This intramolecular single cystine has been shown to favor a strong paratope-epitope interaction (Muyldermans, 2013). However, bacterially or cytosolically expressed selected nanobodies do not seem to necessarily require this disulfide bond to confer proper epitope recognition, though.

Most of the nanobodies so far characterized bind to three-dimensional folded structures of antigens, which make them suitable to study proteins in living cells. Since nanobodies have a small size, high solubility, specificity, and stability, they are ideal protein binder scaffolds that can be further functionalized depending on the research interests.

1.5.4 DARPins

To operate like nanobodies as suitable protein scaffolds, other scaffold derivatives must replicate the virtues of antibodies and overcome their shortcomings. Repeat proteins turned out to be a very attractive choice for protein binders, since in nature repetitive structural motifs were found in a considerable number of proteins to be involved in specific protein-protein interactions. Repeat proteins are typically composed of repeat modules that tightly stack on each other to give rise to a compact folded structure with variable surface residues to create an extended paratope-epitope interface.

The probably most developed protein repeat scaffold is based on ankyrin repeats, and thus this class of protein binders is called DARPins, derived from Designed Ankyrin Repeat Proteins (Pluckthun, 2015). The structural repeats of DARPins are comprised of two anti-parallel α-helices, one β-turn and one loop (Kohl et al., 2003) with a length of 33 amino acids in total. DARPins contain three to six of these structural motifs, resulting in a molecular weight of about 14-22 kDa. To enhance solubility and stability of DARPins, the stacked repeats are modified with N-terminal and C-terminal hydrophilic synthetic caps. Capping is crucial, otherwise DARPins cannot properly fold when expressed in bacteria (Interlandi et al., 2008). Apart from the need of capping, capping also brings along the advantage to create a larger interaction surface to bind to even more possible epitopes (Schilling et al., 2014).

Due to their compact, stacked and unique structure, DARPins are extremely stable and less prone to aggregation. Compared to nanobodies, DARPins lack any disulfide bonds, which makes it easy to express these protein binders in bacteria or in the cytoplasm of any model system. Since their initial description mainly by Andreas Plückthun, DARPins have found quite a number of applications in basic and medical research (Pluckthun, 2015).

1.5.5 Other Protein Binder Scaffolds

The description and application of nanobodies and DARPins has stimulated the search for additional scaffolds with similar or additional features. Therefore, it is not surprising that over 50 different scaffolds have been reported so far (Helma et al., 2015). Depending on the type of scaffold, a number of different protein binders have been established, among them adhirons, affimers, alphabodies, anticalins, centryins, obodies, pronectins, repebodies, and more (Skrlec et al., 2015). Since most of these belong to the youngest generation of protein binders, they are not that well established as nanobodies or DARPins.

1.6 Aim of the Thesis

At all levels of the secretory pathway, anterograde transport of membranes and cargo is counterbalanced by retrograde traffic to maintain compartment identity and whole cell homeostasis. In particular, retrieval of ligand-free cargo receptors from endosomes is essential in order to replenish receptor pools in the TGN, thus allowing receptors to capture newly synthesized ligands for export. A number of distinct sorting machineries have been shown to confer retrograde transport from endosomes to the TGN, including the AP-1/clathrin machinery. Importantly, the AP-1/clathrin machinery plays an exceptional role, since it has not only been reported to mediate retrograde transport from endosomes to the TGN, but also anterograde TGN-to-endosome traffic.

While anterograde traffic mediated by AP-1 is well established, there is still uncertainty about its involvement in retrograde transport, mainly because there are other well described sorting machineries, or because most of the reported findings were based on indirect readouts (KD and KO). Such readouts may be misleading, because the observed phenotype can be an indirect effect of AP-1 depletion. Additionally, cells might upregulate alternative pathways to compensate for the reduced or missing protein, thereby potentially masking the true phenotype. Although there are also several AP-1 readouts based on acute inactivation of the trafficking complex, it is hard to interpret them since they have been obtained from quantitative proteomics profiling. Directional and more rapid approaches, such as biochemically tracking AP-1-dependent cargo from endosomes to the TGN, have not been established on a routine basis.

With the aim to study the contribution of AP-1 in endosome-to-TGN transport, we sought to set up a more generic approach to follow proteins during their retrograde itinerary from the plasma membrane. To this end, we defined the following two aims:

- Establishment of a versatile nanobody-based approach conferring recombinant protein cargo to be tracked from the cell surface by biochemical techniques, by live cell imaging, and by electron microscopy.
- Investigation of the involvement of AP-1 in endosome-to-TGN transport by using the knocksideways technique in combination with the here established approach based on functionalized nanobodies.

2 Material & Methods

2 Material and Methods

2.1 Material

2.1.1 Primary Antibodies

Antibody	Host	Used for	Dilution	Supplier	Product Number
Anti-GFP	Mouse monoclonal	WB	1:5000	Sigma-Aldrich	11814460001-Roche
Anti-GFP	Rabbit polyclonal	EM	1:100	Abcam	ab6556
Anti-myc	Rabbit polyclonal	WB	1:5000	Sigma-Aldrich	C3956
Anti-myc	Rabbit polyclonal	EM	1:2000	Abcam	ab9106
Anti-HA	Mouse monoclonal	WB	1:10000	Homebrew	12CA5 hybridoma
Anti-HA	Mouse monoclonal	IF	1:1000	GeneTex	GTX115044
Anti-FLAG	Rabbit polyclonal	IF	1:500	Cell Signaling Technology	2368
Anti-FLAG	Mouse monoclonal	WB	1:1000	Cell Signaling Technology	8146
Anti-His_6	Rabbit polyclonal	WB	1:10000	Bethyl Laboratories	A190-114A
Anti-T7	Rabbit polyclonal	WB	1:10000	Bethyl Laboratories	A190-117A
Anti-SNX1	Mouse monoclonal	WB	1:500	BD Biosciences	611482
Anti-VPS26	Rabbit polyclonal	WB	1:1000	Bethyl Laboratories	A304-801A
Anti-VPS35	Rabbit polyclonal	WB	1:1000	Bethyl Laboratories	A304-727A
Anti-SNX2	Rabbit polyclonal	WB	1:2000	Bethyl Laboratories	A304-544A-M
Anti-MTCO2	Mouse monoclonal	IF	1:1000	Abcam	ab3298
Anti-Actin	Mouse monoclonal	WB	1:100000	EMD Millipore	MAB1501
Anti-γ-adaptin (100/3)	Mouse monoclonal	IF/WB	1:500/ 1:5000	Homebrew	100/3 hybridoma
Anti-γ-adaptin	Mouse monoclonal	WB	1:5000	BD Biosciences	610385
Anti-α-adaptin	Mouse monoclonal	WB	1:5000	BD Biosciences	610501
Anti-μ1-adaptin	Mouse polyclonal	WB	1:1000	Abnova	H00008907-A01
Anti-CHC17	Mouse monoclonal	WB	1:200	Homebrew	TD.1 hybridoma
Anti-TfR (H68.4)	Mouse monoclonal	WB	1:1000	Thermo Fisher Scientific	13-6890

Antibody	Host	Used for	Dilution	Supplier	Product Number
Anti-TfR	Mouse monoclonal	IF	1:1000	Homebrew	OKT8 hybridoma
Anti-TGN46	Sheep polyclonal	IF/WB	1:1000	Bio-Rad	AHP500GT
Anti-CDMPR46	Mouse monoclonal	IF	1:200	Jack Rohrer	22D4 hybridoma
Anti-CIMPR (2G11)	Mouse monoclonal	IF	1:1000	Abcam	ab2733
Anti-CIMPR	Rabbit polyclonal	WB	1:1000	GeneTex	GTX130109
Anti-TIP47	Rabbit polyclonal	WB	1:1000	Proteintech	10694-1-AP
Anti-LAMP1	Rabbit monoclonal	WB	1:1000	Cell Signaling Technology	9091
Anti-Calnexin	Mouse monoclonal	WB	1:2000	BD Biosciences	610523
Anti-LAMP1	Rabbit monoclonal	WB	1:1000	Cell Signaling Technology	9091
Anti-Tom20	Mouse monoclonal	WB	1:1000	BD Biosciences	612278
Anti-vti1a	Mouse monoclonal	WB	1:1000	BD Biosciences	611220
Anti-vti1b	Mouse monoclonal	WB	1:1000	BD Biosciences	611404
Anti-Rab4	Rabbit polyclonal	WB	1:5000	Bruno Goud	n.a.
Anti-Rab5	Mouse monoclonal	WB	1:1000	Cell Signaling Technology	3547
Anti-Rab7	Rabbit monoclonal	WB	1:1000	Cell Signaling Technology	9367
Anti-Rab9	Rabbit monoclonal	WB	1:1000	Cell Signaling Technology	5118
Anti-GM130	Rabbit monoclonal	IF	1:1000	Cell Signaling Technology	12480
Anti-α-adaptin	Goat polyclonal	IF	1:1000	Everest Biotech	EB11875
Anti-β-1,4-GalT	Rabbit polyclonal	WB	1:1000	Novus Biologicals	NBP1-88654
Anti-TPST1	Rabbit polyclonal	WB	1:2500	Abcam	Ab100972
Anti-TPST2	Rabbit polyclonal	WB	1:1000	GeneTex	GTX46685
Anti-α-mannosidase II	Rabbit polyclonal	WB	1:1000	LifeSpan BioSciences	LS-C163982
Anti-CD44	Mouse monoclonal	WB	1:2500	Novus Biologicals	NBP1-47386SS
Anti-phospho S6 (Ser235/236)	Rabbit monoclonal	WB	1:2500	Cell Signaling Technology	2211
Anti-S6	Rabbit monoclonal	WB	1:2500	Cell Signaling Technology	2217
Anti-COXIV	Rabbit monoclonal	WB	1:2500	Cell Signaling Technology	4850
Anti-GAPDH	Rabbit monoclonal	WB	1:10000	Cell Signaling Technology	5174

Antibody	Host	Used for	Dilution	Supplier	Product Number
Anti-β-1/2-adaptin	Mouse monoclonal	WB	1:5000	BD Biosciences	610381
Anti-σ1-adaptin	Rabbit polyclonal	WB	1:1000	Bethyl Laboratories	A305-396A-M
Anti-FKBP12	Mouse monoclonal	IF	1:250	BD Biosciences	610808
Anti-FKBP12	goat polyclonal	IF	1:250	Santa Cruz Biotechnology	sc-6174
Anti-FKBP12 (DmrA)	Mouse monoclonal	IF	1:250	Clontech (Takara Bio)	635089
Anti-EEA1	Mouse monoclonal	IF	1:1000	BD Biosciences	610456
Anti-PGK1/2	Mouse monoclonal	WB	1:10000	Santa Cruz Biotechnology	sc-166432

2.1.2 Secondary Antibodies

Antibody	Host	Used for	Dilution	Supplier	Product Number
Anti-mouse Alexa 488	Donkey polyclonal	IF	1:500	Thermo Fisher Scientific	A-21202
Anti-rabbit Alexa 488	Donkey polyclonal	IF	1:500	Thermo Fisher Scientific	A-21206
Anti-goat Alexa 488	Donkey polyclonal	IF	1:500	Thermo Fisher Scientific	A-11055
Anti-mouse Alexa 568	Donkey polyclonal	IF	1:500	Thermo Fisher Scientific	A-10037
Anti-rabbit Alexa 568	Donkey polyclonal	IF	1:500	Thermo Fisher Scientific	A-10042
Anti-rabbit Alexa 647	Donkey polyclonal	IF	1:500	Thermo Fisher Scientific	A-31573
Anti-Sheep Cy3	Donkey polyclonal	IF	1:200	Jackson Laboratories	713-165-147
Streptavidin-HRP	not applicable	WB	1:10000	Thermo Fisher Scientific	434323
Anti-rabbit HRP	Goat polyclonal	WB	1:10000	Sigma-Aldrich	A-0545
Anti-mouse HRP	Goat polyclonal	WB	1:10000	Sigma-Aldrich	A-0168
Anti-sheep HRP	Donkey polyclonal	WB	1:5000	Sigma-Aldrich	A-3415

2.1.3 Fluorochromes

Antibody	Specificity	Used for	Dilution	Supplier	Product Number
DAPI	Nuclei	IF	1:1000	Sigma-Aldrich	D9542
Transferrin Alexa 568	TfR	IF	20 μg/mL	Thermo Fisher Scientific	T-23365
Streptavidin Alexa 647	Biotinylated proteins	IF	Assay-dependent	Thermo Fisher Scientific	S-32357

2.1.4 Functionalized Nanobodies

Name of Nanobody	Specificity	Epitope and Domain Organization
VHH_{GFP}-control	GFP and variants thereof	T7-VHH_{GFP}-HA-BAP-His_6
VHH_{GFP}-TEV-control	GFP and variants thereof	T7-VHH_{GFP}-TEV-HA-BAP-His_6
VHH_{GFP}-myc	GFP and variants thereof	T7-VHH_{GFP}-myc-HA-BAP-His_6
VHH_{GFP}-1xTS	GFP and variants thereof	T7-VHH_{GFP}-1xTS-HA-BAP-His_6
VHH_{GFP}-2xTS	GFP and variants thereof	T7-VHH_{GFP}-2xTS-HA-BAP-His_6
VHH_{GFP}-TEV-2xTS	GFP and variants thereof	T7-VHH_{GFP}-TEV-2xTS-HA-BAP-His_6
TS-VHH_{GFP}-TS	GFP and variants thereof	T7-1xTS-VHH_{GFP}-HA-BAP-1xTS-His_6
VHH_{GFP}-APEX2	GFP and variants thereof	T7-VHH_{GFP}-APEX2-HA-BAP-His_6
VHH_{GFP}-TEV-APEX2	GFP and variants thereof	T7-VHH_{GFP}-TEV-APEX2-HA-BAP-His_6
VHH_{GFP}-mCherry	GFP and variants thereof	T7-VHH_{GFP}-mCherry-HA-BAP-His_6

2.1.5 Chemicals and Reagents

Chemical or Reagent	Supplier	Product Number
DMSO (for cell culture)	Applichem	A3672
D-biotin	Sigma-Aldrich	B4501
5-aminolevuilnic acid hydrochloride	Sigma-Aldrich	A3785
Hexadimethrine bromide (polybrene)	Sigma-Aldrich	H9268
DAB tetrahydrochloride hydrate	Sigma-Aldrich	D5637
Sodium cacodylate trihydrate	Sigma-Aldrich	C0250
DNasel from bovine pancreas	Applichem	A3778
AP21967 (A/C Heterodimerizer)	Clontech (Takara Bio)	635056
Rapamycin	Sigma-Aldrich	R0395
Biotin-Phenol (biotin tyramide)	Adipogen/Chemodex	CDX-B0270
Sodium ascorbate	Sigma-Aldrich	A7631
Sodium azide	Applichem	A1430
Trolox	Sigma-Aldrich	238813
Brefeldin A (BFA)	Sigma-Aldrich	B5936
Lysozyme	Sigma-Aldrich	00000001803705900l-Roche
ProTEV Plus	Promega	V6101
Factor X activated (Xa)	Sigma-Aldrich	F9302
Hygromycin B	Invivogen	ant-hg-5
Puromycin	Invivogen	ant-pr-1
Blasticidin	Invivogen	ant-bl-1
Penicillin/Streptomycin	BioConcept	4-01F00-H
L-glutamine	Applichem	A3704
DMEM - high glucose 4500 mg/L	Sigma-Aldrich	D5796
DMEM - high glucose 4500 mg/L (-pr)	Sigma-Aldrich	D1145
Opti-MEM I	Thermo Fisher Scientific	31985070

Chemical or Reagent	Supplier	Product Number
Sodium pyruvate	Sigma-Aldrich	S8636
Hydrogen peroxide (H_2O_2)	Sigma-Aldrich	216763
Sulfur-35 as sodium sulfate	Hartmann Analytics	ARS0105
FuGENE HD	Promega	E2311
Lipofectamine RNAiMAX	Thermo Fisher Scientific	13778150
IPTG	Applichem	A1008
Carbenicillin	Applichem	A1491
Kanamycin	Applichem	A1493
Coomassie-R (Brilliant Blue)	Sigma-Aldrich	B-0149
Trypsin-EDTA (10x)	Sigma-Aldrich	T4174
Formaldehyde solution	Sigma-Aldrich	F8775
Paraformaldehyde (PFA)	Applichem	A3813
Glutaraldehyde (GA)	Sigma-Aldrich	G7651
Osmium tetroxide solution	Sigma-Aldrich	75632
Bovine serum albumin (BSA)	Sigma-Aldrich	00000001071145400l-Roche
Fetal calf serum (FCS)	Biowest	S181B-500
UA conjugate - streptavidin 5 nm gold	BBI solutions	EM.STP5
Fluoromount-G	Southern Biotech	0100-01
Ni Sepharose High Performance	GE Healthcare	17-5268-01
HC Streptavidin Agarose Resin	Thermo Fisher Scientific	20357
Phusion HF DNA Polymerase	New England BioLabs	M0530L
Q5 HF DNA Polymerase	New England BioLabs	M0491S
DNA ligase T4	Sigma-Aldrich	10481220001-Roche

2.1.6 Kits and Others

Kits	Supplier	Product Number
His GraviTrap columns	GE Healthcare	GE11-0033-99
His buffer kit	GE Healthcare	GE11-0034-00
Disposable PD10 desalting columns	GE Healthcare	GE17-0851-01
NucleoSpin plasmid kit	Macherey-Nagel	740588.50
Jetstar plasmid purification kit	Genomed	210050
iDimerize heterodimerization system	Takara Bio (Clontech)	635067
Pierce BCA protein assay kit	Thermo Fisher Scientific	23225
Mini-Protean TGX gels, 4-20%, 15-well	Bio-Rad	456-1096
Immobilon Western HRP substrate	Merck-Millipore	WBKLS0500
GOLD Conjugation Kit (10 nm, 20 OD)	abcam	ab201808
GOLD Conjugation Kit (20 nm, 20 OD)	abcam	ab188215
His-Spin Protein Miniprep	Zymo Research	P2001
Micro spin desalting columns	Thermo Fisher Scientific	89877
µ-slide dishes (4-well, ibiTreat)	Vitaris	80426-IBI

2.2 Methods

2.2.1 Plasmids and Molecular Cloning

Empty Retro-X vectors, pQCXIH and pQCXIP, as well as the iDimerize Inducible Heterodimer System were purchased from Takara Bio. The vector pQCXIB w297-1 (Addgene plasmid #22800) was a gift from Eric Campeau (Program in Gene Function and Expression, University of Massachusetts Medical School, Worcester, USA). Template AP-1 KS plasmids encoding siRNA-resistant γ-FKBP (pLXIN-Ap1g1-FKBP, Addgene plasmid #46946) and Mitotrap (pEYFP-Mitotrap, Addgene plasmid #46942) were previously described (Robinson et al., 2010) and kindly provided by Margaret Robinson (CIMR, Cambridge, United Kingdom). The plasmid encoding GFP-CI-MPR (pCIpreEGFP-CIMPRtail) was previously published (Waguri et al., 2003) and kindly provided by Bernard Hoflack and Mihaela Anitei (Biotechnology Center, Technische Universität Dresden, Germany). A plasmid containing the anti-GFP nanobody (NSlmb-vhhGFP4) was formerly described (Caussinus et al., 2011; Caussinus et al., 2013) and generously provided by Emmanuel Caussinus (Institute of Molecular Life Sciences, University of Zurich, Switzerland) and Markus Affolter (Biozentrum, University of Basel, Switzerland). The pET-24a template vector containing an anti-GFP nanobody fusion construct, and a template plasmid containing BirA was mercifully provided by Dietmar Schreiner (Institut für Neuroanatomie und Zellbiologie, Medizinische Hochschule Hannover, Germany). The cDNA for APEX2 was obtained from the input vector pcDNA3 APEX2-NES (Addgene plasmid #49386) and was a generous gift from Alice Ting (Department of Chemistry, MIT, Cambridge, USA). The sequences containing TPST1-EGFP (Addgene plasmid #66617) or TPST2-EGFP (Addgene plasmid #66618) were kind gifts from David Stephens. A plasmid containing a cDNA encoding MBP-TEV (pRK1043) was a kind gift from David Waugh (Addgene plasmid #8835). A vector encoding the mCherry nanobody (Addgene plasmid #70696), iRFP670 (Addgene plasmid #45466), TagRFP657 (Addgene plasmid #31959), mCardinal2 (Addgene plasmid #52631), mNeptune2.5 (Addgene plasmid #51310), or mTagBFP2 (Addgene plasmid #55322) were kindly provided by Kazuhisa Nakayama, Vladislav Verkhusha (2x), Michael Lin (2x) or Michael Davidson, respectively. EGFP-ERGIC53 was previously described (Ben-Tekaya et al., 2005) and kindly provided by Houchaima Ben-Tekaya. A sequence encoding clathrin light chain a (CLCa) was a generous gift of Steve Royle (WMS –Cell Development Biology, University of Warwick, Coventry, UK). A sequence template encoding GalT-EGFP was kindly provided by Jennifer Lippincott-Schwartz (Cell Biology and Metabolism Branch, NIH, Bethesda, USA). The sequence encoding human full-length calnexin (SC108288) was purchased from Origene. All other cDNA templates were resources from the Spiess Laboratory.

To generate EGFP reporters and other fusion proteins as presented in this study, they were initially assembled in the pCMV6 entry vector (Origene) or in another CMV promoter-based expression vector from the iDimerize kit (Takara Bio) with standard molecular cloning techniques using polymerase chain reaction (PCR) and restriction enzyme digestion. All PCRs were performed using Phusion or Q5 High-Fidelity DNA polymerase (NEB). Primers with restriction enzyme overhangs were synthesized and purchased from Microsynth. Amplified PCR products and digested vectors were purified from agarose

gels with the NucleoSpin Gel and PCR Clean-up kit (Macherey-Nagel) according to the manufacturer's instructions. Purified constructs were cut with restriction enzymes (NEB and/or Roche) and ligation was performed using T4 DNA ligase (Roche). The resulting constructs were transformed into chemo-competent E. Coli TOP10 cells. All sequences were verified using Barcode Economy Run Service Sanger sequencing (Microsynth).

For generating AP-1 KS cell lines using retroviral transduction, the generated Mitotrap sequence (Tom70-FRB-3xFLAG) was subcloned into the pQCXIH vector using NotI and PacI restriction sites, and the obtained γ-FKBP was inserted into the pQCXIP vector using overhangs for PacI and EcoRI. EGFP reporters were inserted into the pQCXIP vector via NotI and PacI restriction ends. In addition, EGFP-CDMPR and EGFP-CIMPR were also subcloned into the pQCXIB vector to establish reporter-expressing AP-1 KS cells using the same restriction overhangs. The molecular cloning of the used functionalized nanobodies is described below (see 2.2.4).

2.2.2 Cell Culture and Retroviral Transduction

Parental and retrovirally transduced HeLa α cells were maintained in high glucose Dulbecco's modified Eagle's medium (DMEM) supplemented with 10% fetal calf serum (FCS), 100 units/mL streptomycin, 2 mM L-glutamine and proper selection antibiotics at 37°C in 7.5% CO_2. HeLa α cells stably expressing EGFP reporter proteins were grown in complete medium containing 1.5 μg/mL puromycin, AP-1 KS HeLaα cells in complete medium containing 1.5 μg/mL puromycin and 1000 μg/mL hygromycin B, and AP-1 KS cells stably expressing EGFP-CIMPR or EGFP-CDMPR in complete medium containing 1.5 μg/mL puromycin, 1000 μg/mL hygromycin B and 7.5 μg/mL blasticidin. Phoenix Ampho packaging cells (kind gift of Erich Nigg, Biozentrum, University of Basel, Switzerland) were grown only for a few passages in complete medium supplemented with 1 mM sodium pyruvate. Selection antibiotics (hygromycin B and Diphtheria toxin) were excluded due to short culturing periods for this cell line.

To generate stable cell lines, packaging cells were transiently transfected with genes of interest in Retro-X Q vectors conferring resistance against puromycin (pQCXIP), hygromycin B (pQCXIH) or blasticidin (pQCXIB) as outlined above. Phoenix Ampho cells were transiently transfected with 15-20 μg plasmid DNA and 30-40 μL FuGENE HD (Promega) per 100 mm cell culture plate. After 48-72 h of transfection, the viral supernatant was harvested, passed through a 0.45 μm filter, supplemented with 15 μg/mL polybrene and added to target HeLa α cells overnight. In case target HeLa α cells were maintained in any antibiotics beforehand, the medium was accordingly supplemented during the transduction period. Selection was started by refreshing cells with complete medium containing the proper selection antibiotics one or two days after retroviral transduction.

Cell lines stably expressing EGFP reporters were subjected to cell sorting (FACSAria IIIu) for having a genetically heterogeneous, but expression-wise homogenous cell pool. To achieve an AP-1 KS system in our cell line, single clones were analyzed on the basis of expression and the ability to sequester γ-FKBP on mitochondria after rapamycin addition. For AP-1 KS experiments, we typically used concentrations at 500 nM rapamycin.

2.2.3 RNA Interference, DNA Transfections and CRISPR/Cas9 Knockout

For RNA interference experiments, cells were reverse-transfected with target siRNA in Opti-MEM I using Lipofectamine RNAiMAX (both Thermo Fisher Scientific) following the manufacturer's instructions. To silence γ-adaptin in AP-1 KS experiments, the siRNA sequence 5'-GAAGAUAGAAUUCACCUUUrUrU-3' as previously described (Hirst et al., 2012a; Robinson et al., 2010) was used. The siRNA for knocking down endogenous γ-adaptin was applied at a final concentration of 100 nM, and cells were transfected twice (day 1 and 3) and assayed at day 5 after a 96 h-interval of knockdown.

For a conventional knockdown of AP-1, the sequence 5'-AAGGCAUCAAGUAUCGGAAGAdTdT-3' against the μ1A-subunit of the heterotetrameric complex was used as formerly reported (Hirst et al., 2005; Hirst et al., 2003; Hirst et al., 2009). For RNA interference with retromer complex, we applied siRNA duplexes with the sequence 5'-AACUCCUGUAACCCUUGAGdTdT-3' targeting Vps26 as described in previous studies (Popoff et al., 2009; Popoff et al., 2007a). To specifically silence Rab9 or TIP47, we applied the siRNA sequence 5'-GUUUGAUACCCAGCUCUUCdTdT 3' for Rab9 (Ganley et al., 2004; Kucera et al., 2016b; Reddy et al., 2006) or 5'-CCCGGGGCUCAUUUCAAACdTdT-3' for TIP47 (Bulankina et al., 2009). We used the non-targeting siRNA 5'-UAAGGCUAUGAAGAGAUACdTdT-3' as control siRNA (Salazar et al., 2009). All siRNAs were used at a final concentration of 50 nM and were purchased from Microsynth.

Transient plasmid transfections into HeLa α cells were performed using FuGENE HD (Promega) according to the supplier's instructions. Experiments were performed 24 h post transfection.

To generate a γ-adaptin KO HeLa α cell line, we purchased a CRISPR/Cas9 knockout plasmid from Santa Cruz Biotechnology (sc-403986). Briefly, cells were transfected with 2 μg γ-adaptin KO plasmid containing a GFP cassette and 4 μL FuGENE HD (Promega) in a six-well cluster. After 24 h of expression, cells were subjected to fluorescence-activated cell sorting (FACS) and single cell clones or a pool of GFP-positive cells were collected in a 96-well plate or 100 mm cell culture dish, respectively. After isolation of expanded single clones or pooled clones, lack of γ-adaptin expression was assessed by Western blotting. To avoid problems and risks with single cell clones, we used a pool of cells having reduced γ-adaptin expression.

2.2.4 Bacterial Expression and Purification of Functionalized Nanobodies

All described VHH_{GFP} nanobody fusions or myc-BirA were prepared in pET-24a or pET-21d vectors (Novagen, Merck Millipore), respectively, with standard molecular cloning techniques using polymerase chain reaction (PCR) and restriction enzymes.

The established control nanobody termed VHH_{GFP}-control contains SpeI and EcoRI restriction sites between VHH_{GFP} and the C-terminal tag cassette. Using these sites, annealed oligonucleotides encoding a single or tandem tyrosine sulfation (TS) consensus of procholecystokinin, amplified mCherry or APEX2 could be subcloned.

For bacterial protein expression and purification, nanobody fusions together with myc-BirA were transformed into Rosetta DE3 chemocompetent cells and plated on LB plates supplemented with 50

μg/mL kanamycin and 50 μg/mL carbenicillin. A single colony was picked and inoculated overnight in 20 mL LB medium containing the respective antibiotics. The overnight culture was further diluted in 1 L LB medium with antibiotics and grown to an OD_{600} of 0.6-0.7 at 37°C. Expression of myc-BirA and functionalized nanobodies was then induced with 1 mM isopropyl-β-D-thiogalactopyranosid (IPTG). To allow site-specific biotinylation of all fusions by coexpressed myc-BirA, the 1 L LB culture was supplemented with 200 μM D-Biotin. For APEX2-nanobody derivatives, the LB medium was additionally complemented with 1 mM 5-aminolevulinic acid hydrochloride to promote higher heme incorporation as previously described (Delcarte et al., 2003; Kery et al., 1995; Lam et al., 2015). Depending on the VHH_{GFP} nanobody fusion derivatives, IPTG induction and thus expression was performed either at 16°C overnight (VHH_{GFP}-mCherry), at 20°C overnight (VHH_{GFP}-APEX2 and VHH_{GFP}-TEV-APEX2) or at 30°C for 4 h (VHH_{GFP}-control, VHH_{GFP}-TEV-control, VHH_{GFP}-myc, VHH-1xTS, VHH_{GFP}-2xTS, VHH_{GFP}-TEV-2xTS and TS-VHH_{GFP}-TS).

Following protein expression, bacteria were pelleted at 5'000 x g at 4°C for 45 min. If not stored at -80°C, the bacterial pellet was directly prepared for protein isolation and purification using immobilized metal affinity chromatography (IMAC) according to the manufacturer's instructions (His GraviTrap columns and His buffer kit, GE Healthcare Life Sciences). Briefly, the pellet obtained from 1 L was resuspended in a total volume of 30 mL sample binding buffer (PBS with 20 mM imidazole). To perform enzymatic lysis of the bacterial suspension, the binding buffer was modified with 200 μg/mL lysozyme, 20 μg/mL DNase I, 1 mM $MgCl_2$ and 1 mM PMSF, incubated for 10 min at RT, followed by 1 h at 4°C at an end-over-end rotator. Next, mechanical lysis was carried out using a tip sonicator with 3 x 30 sec continuous pulses and cooling periods of 1 min. The enzymatically and mechanically broken cells were then spun for 1 h at 15'000 x g at 4°C to pellet unbroken cells and debris. The cleared lysates were then loaded onto equilibrated His GraviTrap columns, washed with sample binding buffer, and His_6-tagged VHH_{GFP} nanobody fusions were finally eluted with 2 mL PBS supplemented with 500 mM imidazole. To remove the excess of imidazole from the eluate, the purified nanobody was loaded onto a PBS-equilibrated PD-10 desalting column. Desalted and purified nanobody fusions were subsequently eluted with 2 mL PBS and protein concentration was determined using a BCA assay. Aliquots of recombinant fusions were concentrated, flash-frozen in liquid nitrogen and stored at -80°C.

Apart from VHH_{GFP} derivatives and myc-BirA, also maltose binding protein (MBP)-tagged TEV protease was bacterially expressed by subcloning it into pET24-a. Induction was performed for 4 h at 30°C and the recombinant protein was isolated as described above. However, following buffer exchange using a PD-10 desalting column, the MBP moiety was specifically removed by incubation with factor Xa to yield tag-free TEV protease. Typically, 1 mg of MBP-TEV fusion protein was incubated with 10 μg of factor Xa for 2.5 h at 37°C. Depending on the yield, factor Xa was proportionally upscaled. After proteolytic removal of the MBP-tag by factor Xa, the reaction was diluted in PBS to a volume of 30 mL and again passed through a His GraviTrap and PD-10 desalting column. Purified TEV protease was stored in 50 mM HEPES (pH 7.5), 300 mM NaCl, 1 mM DTT, 1 mM EDTA, 50% glycerol, 0.1% Triton X-100 or in PBS. Since no activity difference between MBP-tagged or -free TEV protease was observed, we conducted our experiments mainly with the tagged version.

2.2.5 Uptake of Functionalized Nanobodies

For all uptake assays, cells were usually harvested with lysis buffer (1% Triton X-100, 0.5% deoxycholate in PBS) supplemented with 2 mM PMSF and 1 x protease inhibitor cocktail (PIC) if not differently stated. Following centrifugation at 20'000 x g for 15 min to obtain the postnuclear supernatant, the concentration of the lysates was measured using a BCA assay and accordingly adjusted. The samples were mixed with SDS sample buffer containing reducing agents and boiled at 95°C for 5 min for subsequent SDS-PAGE.

For uptake of functionalized nanobodies by EGFP reporter-expressing cell lines, complete medium containing the respective antibiotics was supplemented with 2-5 μg/mL of purified nanobody as indicated. To measure endocytic uptake kinetics into steady-state, 2 μg/mL (~ 100 nM) of VHH_{GFP}-control was added to cells grown in 30 mm dishes that were then harvested with supplemented lysis buffer after the indicated time points. Uptake was stopped by placing dishes onto ice, immediately followed by five washes with ice-cold PBS to remove any free nanobody. Internalization of VHH_{GFP}-1xTS and -2xTS for subsequent Western blot analysis was also performed at a concentration of 2 μg/mL. If not differently stated, VHH_{GFP}-mCherry and -APEX2 uptakes were performed at a concentration of 5 μg/mL to keep equimolar ratios (~ 100 nM). Purified MBP-TEV protease was used at a concentration of 50-100 μg/mL.

2.2.6 SDS-PAGE, Western Blotting and Coomassie Staining

Protein samples were run on 5-15% polyacrylamide separating gels or on 4-20% Mini-PROTEAN TGX precast gels (Bio-Rad). For immunoblotting, separated proteins were transferred to Immobilon-P^{SQ} PVDF membranes (Millipore), followed by blocking with 5% non-fat dry milk in TBS with 0.1% Tween-20 (TBST) for 1 h. The membranes were probed with primary antibodies in 1% BSA in TBST for 2 h at RT or overnight at 4°C, and subsequently incubated with HRP-coupled secondary antibodies in 1% BSA in TBST for 1 h at RT.

For protein detection, Immobilon Western Chemiluminescent HRP Substrate (Millipore) was used and membranes were imaged using a Fusion Vilber Lourmat Imaging System (Witec). For Coomassie stainings, separated proteins were incubated with 5% of 10g/L Coomassie-R solution in fixation solution (45% methanol, 10% acetic acid) for 30-60 min and destained with destaining solution (15% methanol, 7.5% acetic acid) overnight or up to several days. The gel was imaged using a Fusion Vilber Lourmat Imaging System (Witec) in combination with a conversion screen. Signals from Western blots and Coomassie stainings were analyzed using the Fiji software.

2.2.7 Immunofluorescence and Confocal Microscopy

For immunofluorescence staining, cells were grown on 18 mm coverslips (No. 1.5H) in six-well clusters and fixed with 3% paraformaldehyde (PFA) for 10 min at RT. After three washes with PBS, fixed cells were incubated with 50 mM NH_4Cl in PBS for 5 min to quench the unreacted PFA. Cells were then permeabilized with 0.1% Triton X-100 in PBS for 10 min, washed three times and blocked with 1% BSA in PBS for 15 min. Coverslips with fixed cells were incubated upside down on a droplet of primary antibody in 1% BSA in PBS for 2 h, washed three times and stained with fluorochrome-tagged secondary antibodies

in 1% BSA in PBS for 1 h. After a 5 min staining with DAPI and several washes with PBS, coverslips were mounted in Fluoromount-G (Southern Biotech). Staining patterns were imaged using a Zeiss Point Scanning Confocal LSM700 upright microscope.

2.2.8 Live Cell Imaging, Image Processing and Data Analysis

To determine uptake kinetics of EGFP-labeled reporters to steady-state, stable cells were seeded into ibidi µ-slide dishes one day before the actual experiment started. Uptake was initiated by adding pre-warmed 150 µL of VHH_{GFP}-mCherry (2 x) diluted in complete cell culture medium lacking phenol red to cells in 150 µL of the same medium. Live cell imaging was performed on an automated inverted widefield microscope (FEI MORE) equipped with a sCMOS camera (Hamamatsu ORCA flash 4.0) using an U Plan S Apo 100 x NA 1.4 oil objective at 37°C and 5% CO_2. EGFP (mCherry) fluorescence was excited at 470/24 nm (550/15 nm) and the emitted light was collected at 517/20 nm (590/20 nm) using an LED lightsource (SpectraX) and single band pass filters (AHF), respectively. Per condition > 10 fields of view (FOV) with an average of 3-4 cells per FOV were recorded before (1 frame) and after VHH_{GFP}-mCherry addition for about 100 frames every ~ 36 seconds (EGFP-CDMPR) or 60 frames every ~ 39 seconds (TfR-EGFP) in both channels sequentially.

Subsequent image processing was performed in ImageJ. Time laps images acquired after nanobody addition were corrected for lateral drift using the MultiStackReg plugin on the EGFP channel and the resulting transformation was reused for the mCherry channel. Regions of interest (ROI) were selected manually per image and cell (i.e. whole cell) and their average intensity per frame in both channels was measured across all images before and after nanobody addition.

Data analysis was performed in python on the measured means per ROI and time point. To correct for background and autofluorescence, the mCherry signal before nanobody addition was subtracted from the mCherry signal after. In a second step, the mCherry signal was divided (i.e. normalized) by the EGFP signal to additionally account for intensity fluctuations other than nanobody uptake (e.g. by organelle movement, cell contraction, axial drift, illumination instabilities etc.). Artifacts at the beginning (e.g. from medium addition) or end (e.g bleaching) of the time laps were excluded from the analysis. Resulting curves were modeled to a first order kinetic process that results from assuming two reaction compartments (i.e. outside and inside of a cell) and fit individually to a single exponential decay function

$$I(t) = A \cdot (1 - e^{-k(t+t_0)}),$$

where I(t) is the normalized intensity at time t, and t_0 accounts for the time delay between nanobody addition and the start of the time laps recording (Phair and Misteli, 2001). Each accumulation process is then described by its unique rate constant k and amplitude A. In contrast, t_0 was treated as a global variable across all ROIs and FOVs within an experiment. From the rate constant k, the half-life $\tau_{1/2}$ of the process can be calculated as

$$\tau_{1/2} = -\frac{\ln(0.5)}{k}$$

The end of the uptake process is then defined after $5 \cdot \tau_{1/2}$, where 97% of the reaction is completed. As a simple 'two compartments' model described the recorded data well, we refrained from modeling further compartments in order to avoid overfitting.

In order to convert time laps images to movies, ImageJ was used. Representative raw time laps images were adjusted for optimal display as follows. In the mCherry channel, the minimum display value was set to slightly above the autofluorescence as measured in the reference image, while the maximum display value was set to ~ 66% of the maximum intensity value across the time laps. In the EGFP channel, the display values were set to the minimum and 66% of the maximum intensity value across the respective time laps. MP4 movie files were then saved using the SaveAsMovie plugin at 5 frames per second.

2.2.9 Sulfation Analysis, Kinetics and Autoradiography

To analyze retrograde transport and kinetics of EGFP-labeled reporters to the compartment of sulfation, HeLa α or AP-1 KS cells were incubated with 1 mL sulfate-free medium for 1 h at 37°C and 7.5% CO_2, and then pulse-labeled with sulfate-free medium reconstituted with 0.5 mCi/mL [^{35}S]sulfate (Hartmann Analytics) that was supplemented with 2 μg/mL of purified nanobody (VHH_{GFP}-control, VHH_{GFP}-1xTS, VHH_{GFP}-2xTS or TS-VHH_{GFP}-TS) for the indicated time.

For experiments with AP-1 KS cells or BFA treatment, the labeling medium containing VHH_{GFP}-2xTS was additionally modified with 500 nM rapamycin or 2 μg/mL BFA, respectively. After the pulse, cells were washed twice with ice-cold PBS, lysed in 1 mL lysis buffer supplemented with 2 mM PMSF and 1 x PIC, scraped and transferred into microcentrifuge tubes. After centrifugation at ~ 10'000 x g for 15 min at 4°C, postnuclear supernatants were collected and incubated with 20 μL Nickel sepharose high performance beads to affinity-isolate sulfated VHH_{GFP}-2xTS. A fraction (~ 50-100 μL) of the postnuclear supernatant was saved as reference for the total amount of cell-associated VHH_{GFP}-2xTS or as loading control. After 1 h of incubation, beads were washed at least three times with supplemented lysis buffer containing 20 mM imidazole, boiled in SDS sample buffer and analyzed by 12.5% polyacrylamide SDS midi gel electrophoresis and autoradiography on BAS Storage Phosphor Screens (GE Healthcare Life Sciences). Signals were detected with a Typhoon FLA7000 IP phosphorimager (GE Healthcare Life Sciences) and quantified using Fiji.

2.2.10 Biochemical Inactivation of Compartments

To inactivate intracellular compartments of EGFP reporter proteins by DAB crosslinking, we used a modified protocol established by Stoorvogel and collaborators (Stoorvogel, 1998; Stoorvogel et al., 1989; Stoorvogel et al., 1988). Cells stably expressing EGFP reporter proteins were seeded into 6-well clusters and incubated in complete DMEM containing 5 μg/mL of purified VHH_{GFP}-APEX2 for 1 h at 37°C to reach steady-state. After three washes with ice-cold PBS, cells were incubated with either 1 mg/mL DAB or 0.03% H_2O_2 separately as controls, or with a combination thereof in PBS to yield a productive ablation

reaction. After 90 min of incubation at 4°C in the dark, cells were washed twice with ice-cold PBS-5% BSA to stop the DAB crosslinking reaction, followed by three additional washes before lysis.

2.2.11 Electron Microscopy

To label the retrograde route of EGFP-modified reporters by a DAB-based peroxidase reaction, stable cells were grown in 100 mm culture dishes and incubated with 5 µg/mL VHH_{GFP}-APEX2 for 1 h to reach steady-state. Cells were then subsequently washed twice with buffer (100 mM sodium cacodylate with 2 mM $CaCl_2$, pH 7.4), fixed using RT 2% glutaraldehyde in buffer and further processed with minor modifications according to a protocol as previously published by Ting and collaborators (Hung et al., 2017; Hung et al., 2016; Lam et al., 2015; Martell et al., 2012). Following 45 min of fixation, cells were moved onto ice, rinsed 5 x 2 min each in chilled buffer, treated with 20 mM glycine in chilled buffer for 5 min to quench remaining glutaraldehyde, and subsequently rinsed by another 5 x 2 min incubations in chilled buffer. To peroxidase-label retrograde transport compartments, a freshly prepared and filtered solution of 1 mg/mL DAB tetrahydrochloride hydrate was combined with 0.03% H_2O_2 in chilled buffer, and the solution was added to cells for 30-60 min. To stop the reaction, the DAB/H_2O_2 mixture was removed and cells were immediately rinsed 5 x 2 min with chilled buffer. Postfixation staining was performed with 2% (w/v) osmium tetroxide for 1 h in chilled buffer. Cells were rinsed 5 x 2 min each in chilled distilled water and then placed in chilled 2% (w/v) uranyl acetate (Electron Microscopy Sciences) in ddH_2O overnight. Cells were brought to RT, washed in distilled water, and then carefully scraped off the dish, resuspended, and centrifuged at 700 x g for 1 min to generate a cell pellet. The supernatant was removed, and the pellet was dehydrated in a graded ethanol series (20%, 50%, 75%, 90%, 95%, 100%, 100%, 100%, 100%), for 10 min each time, then infiltrated in EMBED-812 (Electron Microscopy Sciences) using 1:1 (v/v) resin and anhydrous ethanol for 1 h, followed by two changes into 100% resin before letting sit overnight. Finally, the sample was exchanged once more with 100% resin before transfer to fresh resin and polymerization at 60°C for 48 h. Embedded cell pellets were cut with a diamond knife into 70 nm sections and imaged on a Phillips CM100 electron microscope.

For immunoelectron microscopy, EGFP-modified reporter cell lines were grown in 100 mm culture dishes and incubated with 2 µg/mL VHH_{GFP}-myc for 1 h to reach steady-state. Cells were then washed twice with 1 x PBS, and fixed in 3% formaldehyde and 0.2% glutaraldehyde overnight at 4°C. Cells were then scraped, pelleted, resuspended, and washed three times in PBS, incubated with 50 mM NH_4Cl in PBS for 30 min, washed three times in PBS, dehydrated and infiltrated with LR-GOLD resin according to the manufacturer's instructions (London Resin, London, UK), and allowed to polymerize for one day at -10°C. For immunogold labeling, sections of 60-70 nm were collected on carbon-coated Formvar-Ni-grids, and then incubated overnight with an anti-GFP and an anti-myc antibody that were preconjugated to either 10 nm- or 20 nm-sized (abcam) gold nanoparticles according to the manufacturer's instructions. Grids were washed five times for 5 min in PBS, and then five times in H_2O, before staining for 10 min in 4% uranyl acetate and 2 minutes with lead citrate (Reynolds solution). Sections were viewed with a Phillips CM100 electron microscope.

2.2.12 Crude Isolation of Mitochondria from Cell Culture

To isolate crude mitochondria from cell culture, two 100 mm plates of confluent AP-1 KS cells were prepared. Following addition of DMSO or 500 nM rapamycin in complete medium for 10 min at 37°C in 7.5% CO_2, cells were washed with ice-cold PBS and then incubated in 1000 µL homogenization buffer (20 mM HEPES pH 7.4, 10 mM KCl, 2 mM $MgCl_2$, 1 mM EDTA, 1 mM EGTA) freshly supplemented with 1 mM DTT, 2 mM PMSF, 1 x PIC either containing DMSO or rapamycin on a rocking platform at 4°C for 5 min. After gentle scraping, the cell suspension was passed through a 27-gauge needle for 15 times. The homogenized suspension (Hom) was left on ice for 20 min before centrifugation at 700 x g for 5 min to pellet nuclei and unbroken cells. The supernatant was transferred into a new tube and spun at 10'000 x g for 5 min to pellet mitochondria from cytosol and membranes. The mitochondrial pellet was subsequently washed three times with supplemented homogenization buffer. The mitochondrial pellet was lysed in 200 µL TBS containing 0.1% SDS, 2 mM PMSF and 1 x PIC to yield the mitochondrial fraction (Mito).

The supernatant on top of the mitochondrial pellet was ultracentrifuged at 100'000 x g to separate membranes (Mem) from cytosol (Cyto). The membrane pellet was subsequently washed twice with 500 µL homogenization buffer containing 1 mM DTT, 2 mM PMSF and 1 x PIC, and lysed in the same buffer as for mitochondria (in the same volume as the cytosol fraction).

2.2.13 Biotin-Phenol Labeling

To perform biotin-phenol labeling in mammalian cells, we used a modified protocol established by Ting and collaborators (Hung et al., 2017; Hung et al., 2016; Lam et al., 2015; Rhee et al., 2013). Briefly, cells stably expressing EGFP reporters were incubated with 5 µg/mL VHH_{GFP}-APEX2 for 1 h to reach steady-state. Following three washes with growth medium, biotin-phenol labeling was initiated by adding fresh complete medium containing 500 µM biotin-phenol for 30 min at 37°C in 7.5% CO_2. Afterwards, H_2O_2 at a final concentration of 1 mM was added to the cells to start the reaction. After 3 minutes of labeling, the reaction was halted by washing three times with quencher solution (10 mM sodium azide, 10 mM sodium ascorbate, and 5 mM Trolox in PBS). Following lysis and centrifugation at 20'000 x g for 15 min to obtain the postnuclear supernatant, an aliquot of the cleared cell lysate was saved and the rest was used for precipitation using high-capacity streptavidin agarose resin. Cell lysates and pull-downs were mixed with SDS sample buffer containing reducing agents, and boiled at 95°C for 5 min for subsequent SDS-PAGE.

3 Results

3 Results

3.1 Design and Expression of Functionalized Nanobodies

To investigate retrograde transport biochemically, by live cell imaging, and by electron microscopy, we sought to establish a versatile approach where proteins of interest can be labeled at the cell surface with high specificity and affinity. We use protein binders as our basic tool to specifically label proteins of interest. A well-characterized protein binder in this regard is the anti-GFP nanobody (VHH_{GFP}), a camelid single-chain domain antibody specifically recognizing folded GFP in a 1:1 stoichiometry with nanomolar affinity (Kubala et al., 2010; Rothbauer et al., 2008; Rothbauer et al., 2006). Using VHH_{GFP} as basic binder module for cell surface labeling, there is the need of reporter proteins to contain an extracellular/lumenal GFP moiety. Accordingly, GFP fusion proteins that transiently appear at the cell surface will be specifically labeled with derivatized VHH_{GFP}. Along with the need to modify fusion reporters with GFP, fluorescent tagging also has the benefit to simply visualize and monitor their subcellular localization in vivo. Moreover, since myriads of GFP-labeled reporter proteins already exist, our tool exploiting GFP binding might be widely applicable. To track GFP reporters of interest from the plasma membrane, VHH_{GFP} domains need to be further modified in order to assess their itinerary through diverse compartments. We designed, bacterially expressed, and purified a number of functionalized VHH_{GFP} nanobodies conferring all of our methodological needs (**Fig. 3.1 A** and **B**).

All of these functionalized nanobodies share the VHH_{GFP} domain (~ 12 kDa), an N-terminal T7 tag epitope, and a C-terminal cassette comprised of an HA tag, a biotin acceptor peptide (BAP), and a hexahistidine (His_6) epitope for immunodetection and affinity purification. We refer to this basic arrangement as VHH_{GFP}-control, while any further functionalization to this generic sequence is highlighted in the name (**Fig 3.1 A**).

In order to biochemically assess PM-to-TGN transport, we took advantage of the exclusive localization of tyrosylprotein sulfotransferases in the trans-Golgi/TGN and thus modified VHH_{GFP}-control with either one or two tyrosine sulfation (TS) consensus sequences derived from the rat cholecystokinin precursor to yield VHH_{GFP}-1xTS and VHH_{GFP}-2xTS (**Fig 3.1 A**).

To monitor retrograde transport itineraries by live cell imaging, we engineered an anti-GFP nanobody derivative comprising a fluorescent mCherry moiety (~ 27 kDa). Addition of VHH_{GFP}-mCherry to GFP reporter-expressing cell lines enables us to quantitate how long it takes for a given reporter to reach steady-state with its target compartments.

For ultrastructural visualization of retrograde transport compartments by electron microscopy, we followed a cytochemical labeling strategy (Connolly et al., 1994; Futter et al., 1995) that makes use of internalized peroxidases catalyzing the H_2O_2-dependent polymerization of 3,3'-diaminobenzidine (DAB) into a local precipitate that gives EM contrast after treatment with osmium tetroxide (OsO_4). However, instead of horseradish peroxidase (HRP), the most established peroxidase for such applications, we used

the recently described monomeric ascorbate peroxidase, APEX2 (**Fig 3.1 A**) (Hung et al., 2017; Hung et al., 2016; Lam et al., 2015; Martell et al., 2012). APEX2 is the improved version of APEX, a peroxidase derived from dimeric pea or soybean ascorbate peroxidases (Hung et al., 2014; Rhee et al., 2013). Unlike HRP, APEX2 is considerably smaller (28 kDa versus 44 kDa) and does not contain any disulfide bonds, thereby allowing the protein to be expressed in the reducing environment of bacteria.

In addition to its application in electron microscopy, APEX2 can also be used for biochemical ablation of target compartments (Stoorvogel, 1998; Stoorvogel et al., 1989; Stoorvogel et al., 1988) or promiscuous proximity biotinylation (Hung et al., 2017; Hung et al., 2016; Lam et al., 2015). In the former approach, DAB polymerization is exploited to chemically crosslink or encapsulate lumenal and trans-membrane proteins to yield an insoluble fraction that can be precipitated. Hence, to inactivate intracellular compartments of target proteins, we can feed VHH_{GFP}-APEX2 into steady-state of EGFP-labeled fusion reporters. Ablation, moreover, allows us to biochemically determine the localization of reporters within intracellular compartments.

APEX2 can also be used to perform proximity labeling of proteins using biotin-phenol as substrate (Hung et al., 2017; Hung et al., 2016; Hwang and Espenshade, 2016; Lam et al., 2015). APEX2 generates biotin-phenoxyl radicals, highly reactive and short-lived species that conjugate to endogenous proteins (mainly tyrosine side chains) in close proximity. By enriching biotinylated proteins using streptavidin resins, proteins in close proximity to APEX2 can be detected (e.g. by mass spectrometry or Western blotting). Nanobody modified with APEX2 could therefore be used to qualitatively assess PM-to-TGN transport by immunodetection of endogenous TGN-resident proteins after streptavidin pull-down.

The outlined functionalized VHH_{GFP} (**Fig. 3.1 A**, see also **Tab. S2** for protein sequences) were bacterially expressed in the presence of recombinant biotin ligase (BirA) and excess of D-biotin to modify the BAP site (also known as AviTag). Biotinylated nanobodies do not only facilitate their own biochemical detection by streptavidin-HRP, but also allow their high-affinity isolation by avidin-based purification resins. In addition, they can be further functionalized by coupling commercially available streptavidin conjugates (e.g. Alexa Fluor streptavidin conjugates, streptavidin-gold, etc.). We could for instance couple streptavidin-Alexa Fluor 647 or streptavidin gold to VHH_{GFP}-control and others in vitro (**Fig. S1**). Such additionally functionalized nanobodies are very useful since our simplest nanobody fusion (VHH_{GFP}-control) could be taken as main building block to achieve biochemical or fluorescent derivatization.

While VHH_{GFP}-APEX2 requires additional 5-aminolevulinic acid as supplement for efficient heme incorporation, expression of all other VHH_{GFP} derivatives was either induced for several hours at 30°C, or overnight at 16°C or 24°C, respectively, and then subsequently purified using Nickel columns. As seen in **Figure 3.1 B** (lanes 1-5), all nanobody-based retrograde transport trackers could be efficiently isolated from crude bacterial cell lysates to high purity and yield. Differences in their molecular weights are due to the specific functionalization with either peptide tags (TS-tags, **Fig. 3.1 B**, lanes 2 and 3) or entire protein domains (APEX2 and mCherry, **Fig. 3.1 B**, lanes 4 and 5). All bacterially expressed VHH_{GFP} derivatives were free of visible degradation, with the exception of VHH_{GFP}-mCherry that seems to be partially, but negligibly clipped after purification into two parts corresponding probably to a C-terminal mCherry (~ 28 kDa) and an N-terminal VHH_{GFP} (~ 22 kDa) fragment (see also **Fig. 3.2 A**).

Since detection and affinity purification of VHH_{GFP} derivatives from mammalian cell lysates will be crucial for monitoring endocytosed anti-GFP nanobody derivatives by immunoblotting, we addressed the question whether we can detect them with antibodies targeting the various epitopes present in these fusions. To do so, we separated and transferred as little as 10 ng of purified VHH_{GFP} derivatives using SDS-PAGE/immunoblotting and probed membranes with antibodies or streptavidin-HRP recognizing the HA, His_6 and T7 epitope or biotin, respectively (**Fig. 3.2 A**).

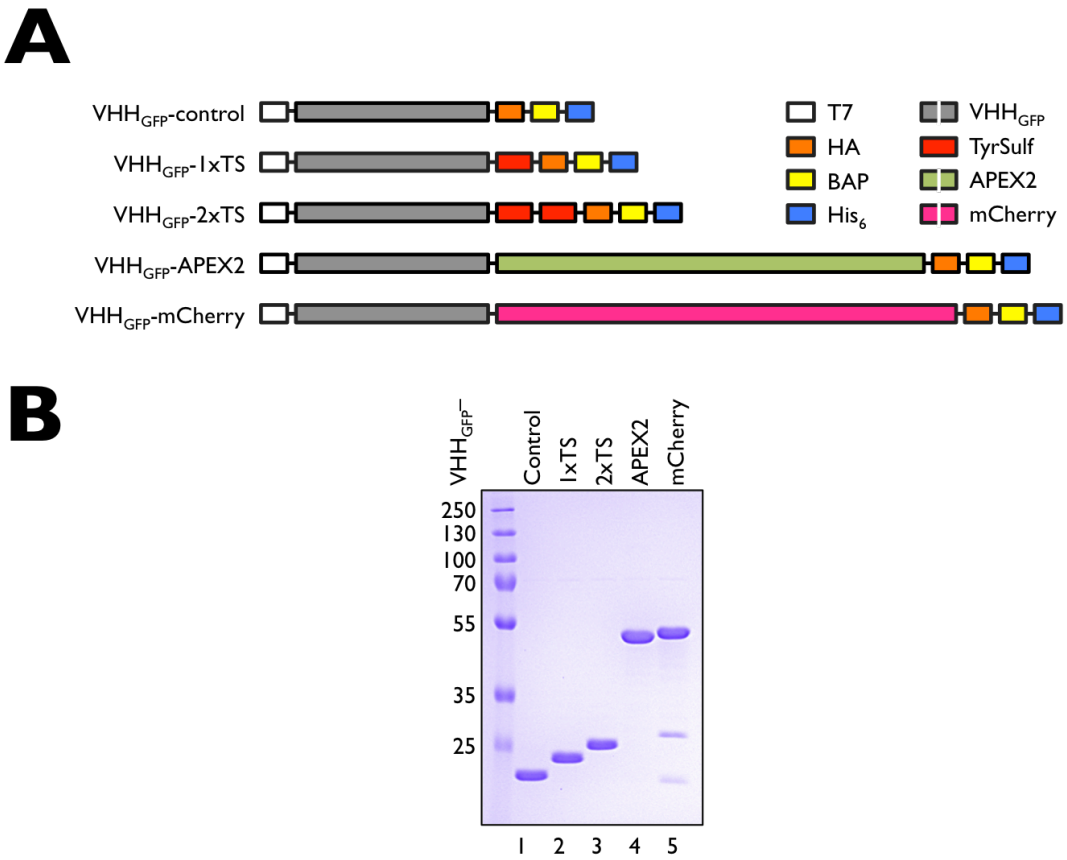

Figure 3.1: Design and bacterial expression of functionalized anti-GFP nanobodies. (A) Schematic cartoon of generated functionalized nanobodies. The basic arrangement of the GFP binder is composed of an N-terminal T7 epitope, followed by the VHH_{GFP} nanobody domain and a cassette comprising an HA, BAP and hexahistidine epitope. To track PM-to-TGN transport, nanobodies with either one or two tyrosine sulfation (TS) consensus sequences were produced (VHH_{GFP}-1/2xTS). To be able to follow EGFP-labeled reporters from the cell surface to any intracellular compartment by live cell imaging, functionalization was performed by recombinantly adding fluorescent mCherry (VHH_{GFP}-mCherry). To ultrastructurally visualize retrograde transport by electron microscopy, the peroxidase reporter APEX2 was subcloned into VHH_{GFP} to yield VHH_{GFP}-APEX2. The peroxidase reporter can also be used to perform compartment ablation or proximity biotin labeling. Cartoon is not drawn to scale. **(B)** Bacterial expression of functionalized nanobodies. 30 µg of purified and desalted protein was loaded onto a SDS-PAGE gel and then subjected to Coomassie staining. Purified proteins were considerably pure and stable. Only a small fraction of VHH_{GFP}-mCherry seems to be unstable since two bands are visible at ~ 22 kDa and ~ 28 kDa. While the upper degradation fragment corresponds to clipped mCherry, the lower one represents clipped VHH_{GFP} (see also Fig 3.2 A). Numbers along the markers correspond to molecular weight in kDa.

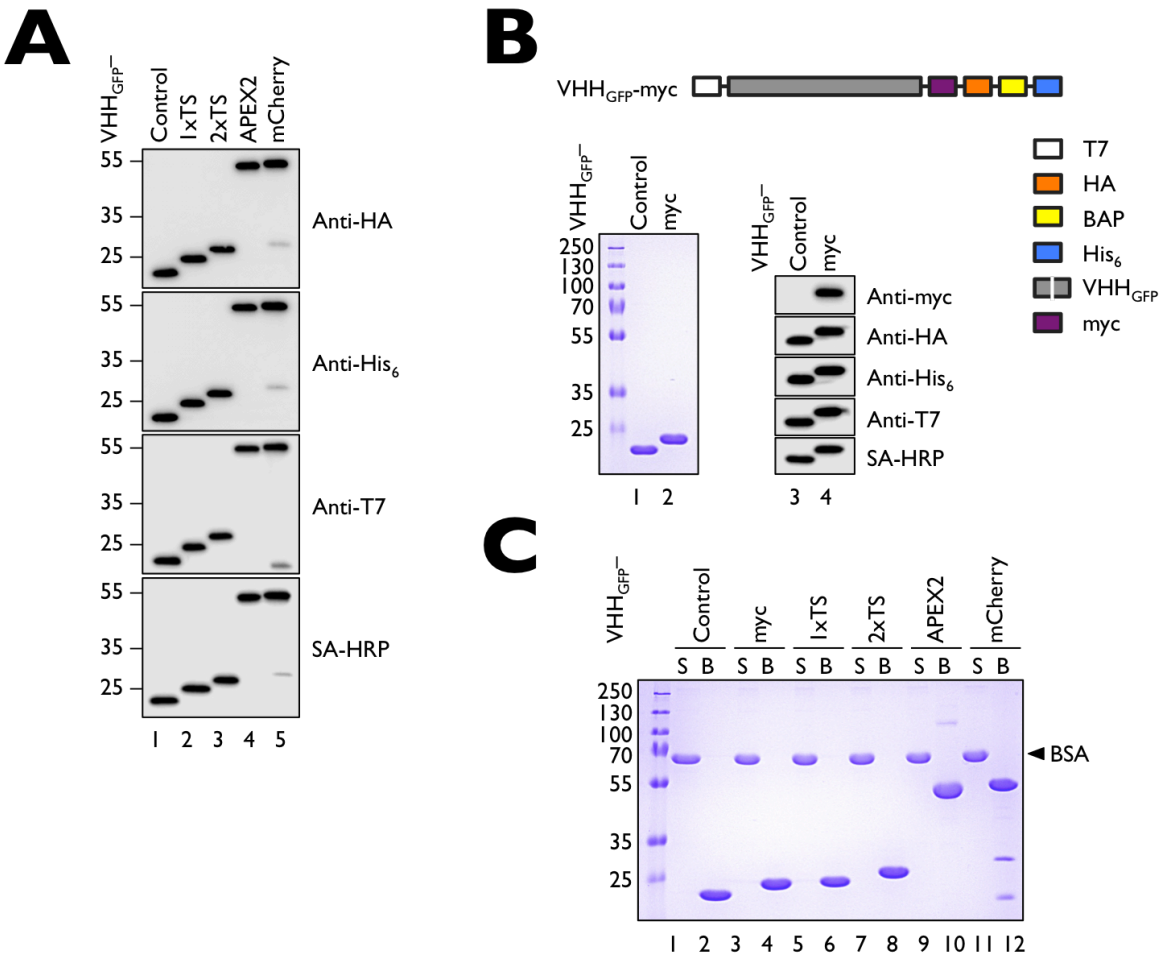

Figure 3.2: Detection and biotinylation efficiency of bacterially expressed anti-GFP nanobodies. (A) 10 ng of purified functionalized nanobody was loaded onto a SDS-PAGE gel, blotted and subjected to immunodetection using antibodies against the HA, hexahistidine and T7 epitope, as well as streptavidin-HRP. Functionalized nanobodies migrate to their expected molecular weights. As mentioned in Fig 3.1 B, VHH$_{GFP}$-mCherry is to a subtle extent prone to degradation since two fragments can be observed. The upper degradation fragment corresponds to a product comprising mCherry, the lower to VHH$_{GFP}$. **(B)** Bacterial expression of functionalized nanobody containing a myc epitope. 30 μg (lanes 1-2) or 10 ng (lanes 3-4) of purified and desalted protein was loaded onto a SDS-PAGE gel and then subjected to Coomassie staining (lanes 1-2) or Western blotting (lanes 3-4), respectively. As the other functionalized nanobodies, VHH$_{GFP}$-myc could be expressed to high yields and to high purity. Cartoon is not drawn to scale. **(C)** Functionalized nanobodies are completely biotinylated by coexpressed BirA. To assess biotinylation efficiency of bacterially expressed nanobodies, ~ 100 μg of nanobody and bovine serum albumin (BSA) each were mixed in a total volume of 100 μL. To the nanobody-BSA mixture, 20 μL of high capacity streptavidin agarose were then added. After incubation for 1 h at 4°C, the supernatant (S) was removed and the beads (B) were extensively washed (7x) with PBS containing extra salts. Beads were finally resuspended in the same volume as the supernatant and boiled in SDS sample buffer. A volume of ~ 25 μL was loaded onto a SDS-PAGE followed by Coomassie staining. While BSA was excluded from the pull-downs (B, beads) and only present in the supernatant (S), the nanobody fusions were exclusively found on the beads indicating that BirA-mediated biotinylation with our conditions was very efficient, namely ~ 100%. Numbers along the markers correspond to molecular weight in kDa.

Epitope tags of all VHH$_{GFP}$ trackers were efficiently detected with the respective antibodies (**Fig. 3.2 A**, lanes 1-5). As reported previously in **Fig. 3.1 B**, only VHH$_{GFP}$-mCherry showed degradation fragments (**Fig 3.2 A**, lane 5). Since the upper degradation fragment is detected with an anti-HA, anti-His$_6$ or streptavidin-HRP, it contains the C-terminal epitope cassette and most of mCherry to yield a

molecular weight above 25 kDa. The lower degradation fragment on the contrary was only positive for the T7 epitope, corresponding to an N-terminal portion containing VHH_{GFP} to make it run at ~ 20 kDa.

Studying retrograde protein transport by electron microscopy cannot only be accomplished by VHH_{GFP}-APEX2 performing polymerization of DAB, but also by immunogold electron microscopy by simply staining for internalized functionalized VHH_{GFP}. Since there is a good anti-myc antibody available that has been previously used in our hands with success (Beuret et al., 2017; Stettler et al., 2009), we generated an additional VHH_{GFP} derivative containing a myc epitope (**Fig 3.2 B**, see also **Tab. S2** for protein sequences). This nanobody fusion, termed VHH_{GFP}-myc, was as well expressed as the other functionalized nanobodies (**Fig 3.2 B**, lanes 1-4).

We also determined the biotinylation efficiency of our VHH_{GFP} derivatives during bacterial induction and expression (**Fig. 3.2 C**). To do so, pure BSA was mixed with bacterially expressed nanobodies and incubated with streptavidin resin. After 1 h of incubation, the supernatant (S) was collected and saved. Beads (B) were extensively washed and prepared for analysis by SDS-PAGE and Coomassie staining. The nanobodies were found to be completely biotinylated by overexpressed BirA during induction (**Fig. 3.2 C**). A high biotinylation efficiency for downstream applications, such as pull-downs or labeling with commercially available streptavidin conjugates, is of benefit. Otherwise, we would miss all non-biotinylated nanobodies in our experiments when we exploit streptavidin-based interactions.

The so far outlined results demonstrate that functionalized anti-epitope (here anti-GFP) nanobodies can be efficiently expressed, detected and biotinylated. They thus fulfill all our needs to act as versatile tool to study retrograde transport itineraries of GFP-labeled proteins from the cell surface.

3.2 Design and Expression of EGFP-Labeled Reporter Proteins

To establish a versatile nanobody-based approach to study retrograde traffic of GFP-labeled proteins from the cell surface to the endo-lysosomal system and to the TGN, there is the indispensable need of GFP reporter proteins traversing through these intracellular compartments. For our study, we decided to use bonafide retrograde transport transmembrane proteins to give basic proof-of-concept evidence.

Among the best-characterized retrograde transport cargo proteins belong the two MPRs, CDMPR and CIMPR (Bonifacino and Rojas, 2006; Duncan and Kornfeld, 1988; Ghosh et al., 2003a; Griffiths et al., 1988). As previously mentioned, their basic function is to deliver newly synthesized lysosomal acid hydrolases from the TGN to endosomes from where they are shuttled back to undergo additional cycles of cargo capturing and release. However, to a certain extent, they occasionally travel out to the plasma membrane from where they are rapidly retrieved by AP-2/clathrin-mediated endocytosis (Ghosh et al., 2003a; Lobel et al., 1989; Prydz et al., 1990; Schweizer et al., 1997).

Other transmembrane cargo proteins that are retrogradely transported from the plasma membrane to the TGN are the trans-Golgi network integral membrane proteins TGN38/46/51, which are all thought to behave identically. The best studied among these is TGN46. Though TGN46 is considered as TGN-resident protein, it is well established that a minor population of it is also present at the cell surface in steady-state (Banting et al., 1998; Banting and Ponnambalam, 1997; Ponnambalam et al., 1996; Rajasekaran et al., 1994; Saint-Pol et al., 2004). Even the molecular transport carriers that mediate TGN exit of TGN46, the CARTS (Pfeffer, 2012; Wakana et al., 2015; Wakana et al., 2012; Wakana et al., 2013), have been identified, highlighting that TGN46 and its isoforms constantly cycle at the TGN-to-PM interface.

Even though we are aware of additional retrograde transport integral membrane proteins such as APP (Choy et al., 2012), WLS (Eaton, 2008; Harterink and Korswagen, 2012; Harterink et al., 2011; Yu et al., 2014), furin (Chia et al., 2011), ANK (Seifert et al., 2016), and more, we decided to follow our studies with the well-established acid hydrolase receptors (CD-/CIMPR) and TGN46.

In order to have a negative control for TGN arrival, we sought to have a reporter that is only transported to the endocytic system (i.e. to endosomes). Prominent candidates for this are the recycling receptors, such as the transferrin receptor (TfR), the asialoglycoprotein receptor (ASGPR) and low-density lipoprotein receptor (LDLR) that all deliver cell surface-bound ligands to early/recycling endosomes from where the ligand-free receptors are returned to the plasma membrane. Since TfR is ubiquitously expressed and a well-established recycling receptor, we have chosen this reporter to be our negative control for our approach. To be noted, however, there are also published reports, suggesting TfR to return to the TGN (Shi et al., 2012b; Snider and Rogers, 1985). With our nanobody-based tool exploiting tyrosine sulfation, we can basically directly assess whether TfR is facing the TGN lumen (compartment of sulfation) after internalization from the plasma membrane.

The basic design of our GFP fusion reporters is outlined in **Figure 3.3 A** (see also **Tab. S1** for protein sequences). Depending on the membrane protein topology (Goder and Spiess, 2001), GFP (more precisely EGFP; from now on, we will use the terminology EGFP) needs to be either N-terminally or C-

terminally located. Since CIMPR, CDMPR and TGN46 are all type I transmembrane proteins, EGFP needs to be present at the N-terminus, directly preceded by a cleavable signal sequence for ER targeting. TfR, conversely, is a type II transmembrane protein and thus needs to have the EGFP domain at the C-terminus so that it might be accessible by functionalized anti-GFP nanobodies at the cell surface.

Apart from CIMPR, we only included full-length sequences in our studies. Due to the large protein size of ~ 300 kDa and thus ~ 7800 bp, we used instead a truncated and simplified version for CIMPR that is composed of its transmembrane and cytosolic domain, only. Such a truncated version has been previously published (Waguri et al., 2003), and since then successfully used in other studies (Amessou et al., 2007; Amessou et al., 2006; Anitei et al., 2014; Billcliff et al., 2016; Girard et al., 2014; Stahlschmidt et al., 2014), because it seems to behave as the full-length counterpart. To generate a truncated secretory EGFP-tagged CIMPR fusion reporter (EGFP-CIMPR), we made use of the well-characterized ER targeting sequence of hemagglutinin (SS-HA), followed by EGFP and the transmembrane and cytosolic domain of murine CIMPR. To establish EGFP-labeled CDMPR and TGN46, we took their respective human full-length sequences, excluding wild-type ER targeting signal, and assembled them in the same signal sequence-EGFP cassette as EGFP-CIMPR to yield EGFP-CDMPR or EGFP-TGN46, respectively. TfR-EGFP was generated using the human TfR sequence followed by EGFP. To also have a second negative control in our assays, we used EGFP without signal sequence, a protein reporter that does not enter the secretory pathway and that stays exclusively cytosolic.

Having these constructs in our inventory bag pack, we moved onwards and established HeLa cells stably expressing either EGFP, EGFP-CIMPR, EGFP-CDMPR, EGFP-TGN46 or TfR-EGFP. Stable reporter expression is important to avoid overexpression artifacts as they may occur during transient transfections. Stable cell lines were generated using retroviral transduction and further improved by fluorescent-activated cell sorting (FACS) to achieve cell pools with homogeneous expression levels.

Figure 3.3 B shows the expression levels of the stable HeLa cells. All EGFP-tagged reporters migrate to their expected molecular weight as monitored by SDS-PAGE and immunoblotting using an anti-GFP antibody (**Fig. 3.3 B**). EGFP-CDMPR runs as a double band, suggesting a high-mannose glycosylated ER form and a complex glycosylated mature form (**Fig. 3.3 B**, lane 4). The lower band that might most likely correspond to the ER form is more dominant, evoking the impression that the EGFP-tagged reporter is inefficiently folded. However, when we expressed an EGFP-free version of CDMPR (SHMY-CDMPR), we also observed a dominant lower band, indicating that the EGFP does not impair reporter folding (**Fig. S2 A**). Since SHMY-CDMPR only contains an N-terminal cassette of short epitope tags (signal sequence, His_6-, myc- and TS-tag), we can assume that it is not much different in protein structure and folding compared to overexpressed tag-free CDMPR. We thus think that the observed double band (**Fig. 3.3 B**, lane 4) represents the natural state of the protein in HeLa cells. Unfortunately, we were not able to confirm that since we did not come across antibodies detecting endogenous levels of CDMPR. As discussed later on, the lower band is in fact composed of two populations, one that is accessible to functionalized nanobody, the other not (**Fig. S2 B**). We only detected single bands for EGFP-tagged CIMPR, TGN46 and TfR at this percentage of the gel. For EGFP-CIMPR, at least, this is not surprising since it lacks any N-glycosylation attachment sites.

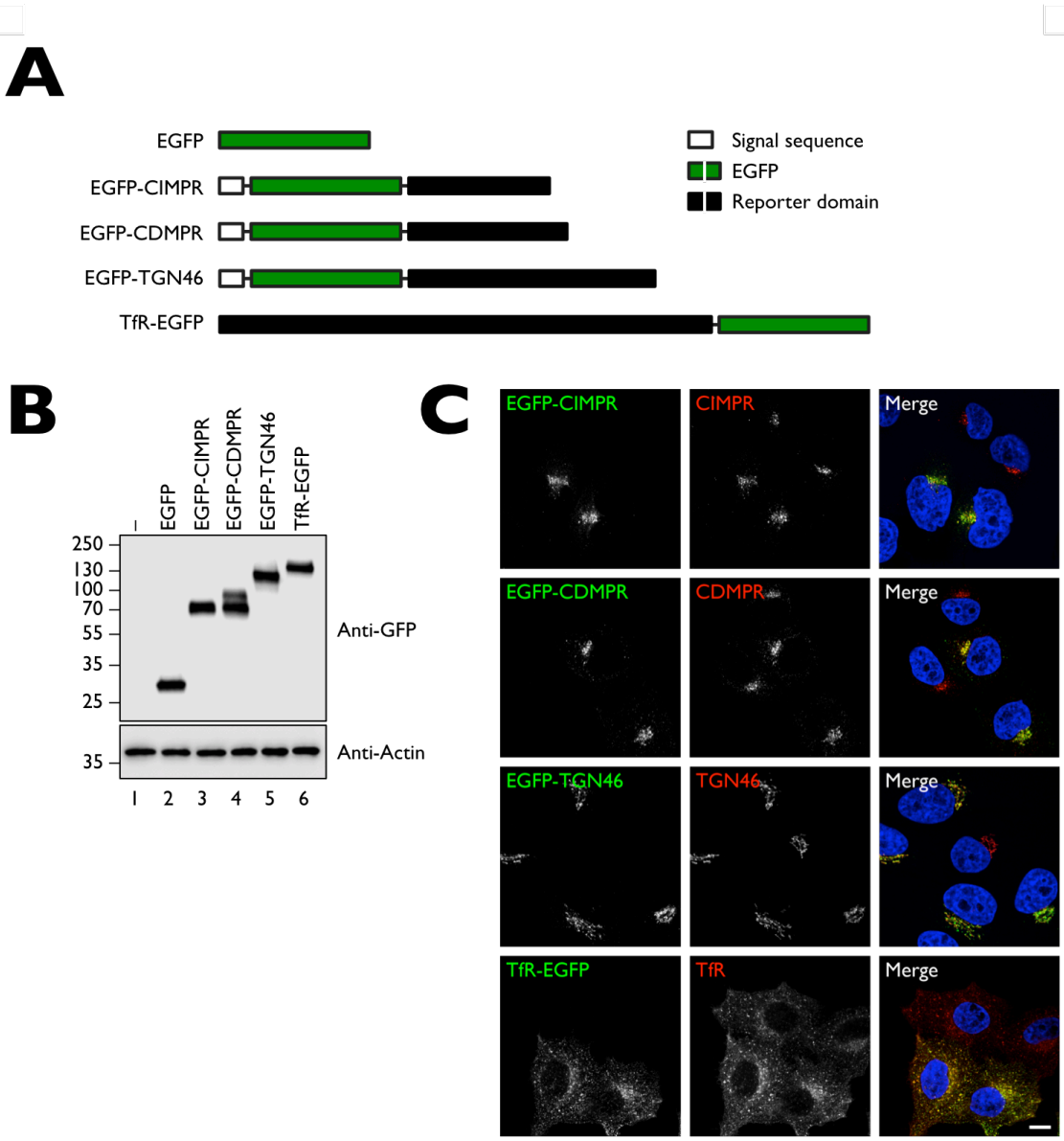

Figure 3.3: Design, expression and localization of EGFP-labeled reporter proteins. (A) Schematic outline of the EGFP reporter proteins. Selected type I transmembrane proteins (CIMPR, CDMPR and TGN46) all contain a well-established cleavable ER signal sequence derived from hemagglutinin (white), followed by EGFP (green) and the reporter sequence (black) without natural ER targeting signal. Apart from CIMPR, only full-length sequences were included in our studies. Since TfR has reverse topology (type II), the EGFP domain is following the reporter sequence. Cytosolic EGFP was used as control for a non-secretory reporter protein. Cartoon is not drawn to scale. **(B)** HeLa cells stably expressing EGFP-tagged reporters. Lysates of the respective reporter cell lines were prepared and analyzed by SDS-PAGE/Western blotting. Fusions run at their expected molecular weights, with EGFP-CDMPR having a double band. **(C)** Intracellular localization of EGFP-tagged reporters. Reporter-expressing and parental HeLa cells were mixed and stained with antibodies targeting the endogenous counterparts. The distribution pattern of the EGFP reporter was similar to the endogenous version. Numbers along the markers correspond to molecular weight in kDa. Scale bar: 10 μm.

To examine whether our EGFP-labeled reporter proteins have the same distribution pattern as their endogenous counterparts and are not too much overexpressed, we analyzed their intracellular localization by fluorescence confocal microscopy (**Fig. 3.3 C**). To do so, we mixed parental HeLa cells with cells stably expressing either EGFP-CIMPR, EGFP-CDMPR, EGFP-TGN46 or TfR-EGFP, seeded them

on the same coverslip and proceeded with immunofluorescence staining by labeling the endogenous counterparts of the EGFP-tagged reporters. Since we used full-length EGFP-tagged reporters (apart from CIMPR) all our antibodies do not only crossreact with the EGFP reporters, but also with the endogenously present counterparts.

As seen in the first panel of **Figure 3.3 C**, EGFP-CIMPR is mainly clustered in small vesicular and tubular elements in the juxtanuclear region in addition to peripheral, endosomal structures overlapping with endogenous CIMPR, demonstrating proper localization of the reporter to its homing compartments in our cells. This is consistent with previous reports (Anitei et al., 2014; Waguri et al., 2003), and additionally shows that stable and modest protein expression does not alter compartment identity since we could not see any morphological changes between reporter-expressing and -lacking HeLa cells. Moreover, as mentioned above, the antibody targeting endogenous CIMPR reacts with the lumenal domain of the receptor, a domain that is completely absent in our EGFP-tagged reporter. This even more supports the notion that our reporter expression levels are in an acceptable range (with regard to unaltered compartment morphology).

We can do a similar statement for the other EGFP-tagged reporters. EGFP-CDMPR, EGFP-TGN46 and TfR-EGFP all colocalize with their endogenous counterparts (**Fig. 3.3 C**). For EGFP-CDMPR- and EGFP-TGN46-expressing cells, the signal obtained by staining with an anti-CDMPR or anti-TGN46 antibody, respectively, did not produce an obvious increase of the signal compared to untransfected HeLa cells. This confirms that these two fusion proteins are not significantly overexpressed. Even though we anticipated having a considerable ER staining for EGFP-CDMPR based on our Western blot analysis (**Fig. 3.3 B**), we predominantly detected a strong perinuclear labeling pattern (similar to EGFP-CIMPR). This confirms our suspicion that the faster migrating band of EGFP-CDMPR cannot exclusively represent high-mannose glycosylated ER form (**Fig. S2 B**).

When considering the mixed population of HeLa cells stably expressing TfR-EGFP with untransfected ones, stronger TfR staining was observed in stable transductants. As discussed and outlined later on (**Fig. 3.10 A**), we reported a three- to four-fold higher expression of TfR in our stable cells. This became also evident when fluorescently labeled transferrin (Tf) was administrated to a mixed population of HeLa and stable transductants. In such an experiment, more Tf endocytosed in the EGFP reporter cell line (**Fig. S2 C**). This experiment furthermore also revealed that our recombinant TfR is still functional to shuttle transferrin through the endocytic-recycling compartments. Since the distribution pattern of the fusion is similar to the wild-type TfR, we are not concerned about the expression levels of our recombinant TfR protein.

The results above confirm that the used EGFP-modified reporters have similar intracellular localization pattern as their endogenous counterparts. By this, we have the methodological basis for studying retrograde transport and sorting itineraries of the selected reporters from the cell surface.

3.3 Analysis of Endocytic Uptake and Recycling Kinetics

We next apply our nanobody-based toolkit to study endocytic uptake and recycling kinetics of EGFP-labeled reporter proteins biochemically and by live cell imaging. To follow up on that, we first needed to address to most relevant and critical question to our approach, that it is whether bacterially expressed and functionalized nanobodies are at all taken up by reporter-expressing cells.

3.3.1 Biochemical Uptake of VHH_{GFP}-control and -mCherry

To examine whether functionalized nanobodies are specifically taken up from the cell culture medium, we incubated cells with 2 μg/mL VHH_{GFP}-control. After 1 h of incubation at 37°C, we prepared cell lysates and probed them for internalized and cell-associated nanobody. Cells stably expressing cytosolic EGFP did not show any uptake of VHH_{GFP}-control (**Fig 3.4 A**, lane 1). This is very plausible, since EGFP was not accessible from the extracellular environment. The nanobody also did not significantly enter the cells by fluid phase uptake. In contrast, cells stably expressing any of the other reporter proteins show cell surface binding and uptake of VHH_{GFP}-control (**Fig 3.4 A**, lane 3, 5, 7 and 9). To be mentioned is the fact that not all reporters take up nanobodies to the same extent. The amount of internalized nanobody is mainly dependent on two reporter characteristics, namely its cell surface fraction and how long it takes until the post-Golgi reporter fraction has faced the plasma membrane (i.e. when steady-state is reached). These characteristics are unique to every reporter, and hence, it is not surprising that we monitor differences in internalized nanobody between EGFP reporters after 1 h of uptake. Most crucially, our uptake experiment has revealed that the intended approach of using nanobodies and nanobody epitope-containing reporters to study retrograde transport works and thus fulfills our major criterion.

Since we also wanted to monitor uptake kinetics by live cell imaging, we also performed the internalization experiment with VHH_{GFP}-mCherry. Similar to VHH_{GFP}-control, VHH_{GFP}-mCherry was only internalized by EGFP reporter cell lines (**Fig 3.4 A**, lane 4, 6, 8 and 10). It seems that relatively more VHH_{GFP}-mCherry is internalized when comparing to the fluorophore-free version (**Fig 3.4 A**, lanes 1-10). The reason for this is unknown. The most plausible explanation is that these two proteins were not equally transferred or retained on the blotting membrane due to differences in molecular weight.

Having VHH_{GFP}-mCherry, not only we can monitor reporter-mediated nanobody uptake by immunoblotting, but also by fluorescence microscopy using fixed cells. VHH_{GFP}-mCherry as such has the advantage that it is fluorescent by itself. To demonstrate uptake by fluorescence microscopy, cells on coverslips were fed with 5 μg/mL VHH_{GFP}-mCherry for 1h at 37°C and subsequently processed for confocal microscopy. As seen in **Figure 3.4 B**, mCherry-labeled VHH_{GFP} shows the identical labeling pattern as the corresponding EGFP reporters, indicating that the nanobody binds the reporter's EGFP moiety at the cell surface and is trafficked piggyback to its homing compartments. There is also no uptake by cells stably expressing cytosolic EGFP (**Fig S2 D**). It appears that for most of the reporters, steady-state has already been reached after 1 h of incubation. For our experiments, it is important to know how long it takes until a given reporter has reached its steady-state, the time after which no additional

nanobody uptake will occur anymore. This can be figured out by measuring endocytic uptake kinetics of the reporters, either biochemically or by live cell imaging.

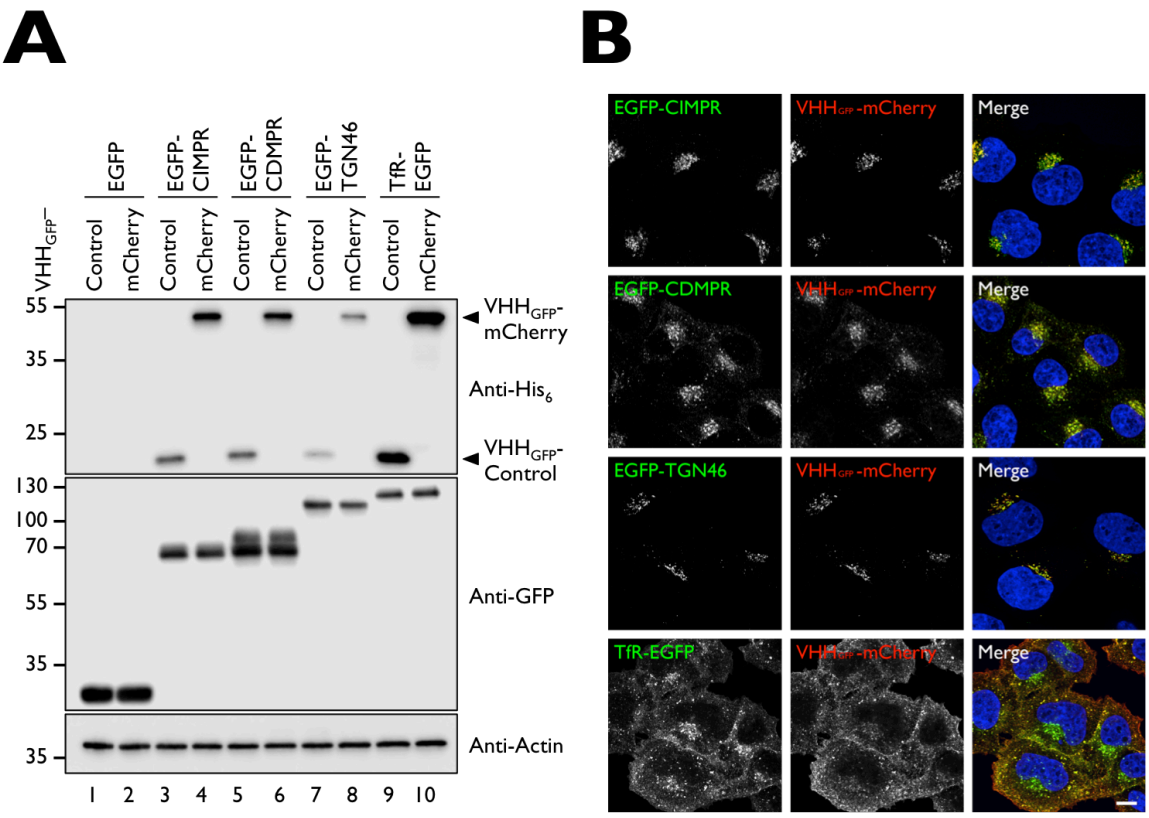

Figure 3.4: Biochemical uptake of VHH$_{GFP}$-control and VHH$_{GFP}$-mCherry by EGFP reporter cell lines. **(A)** Functionalized nanobodies are specifically taken up by reporters presenting an EGFP moiety to the extracellular environment. HeLa cells stably expressing EGFP reporters were incubated in the presence of either 2 µg/mL VHH$_{GFP}$-control or 5 µg/mL VHH$_{GFP}$-mCherry for 1 h at 37°C. Following uptake, cell lysates were prepared and probed with anti-His$_6$, anti-GFP and anti-actin antibodies. **(B)** Similar procedure as in (A). Cells on coverslips were fed with 5 µg/mL VHH$_{GFP}$-mCherry and processed for fluorescence confocal microscopy. Numbers along the markers correspond to molecular weight in kDa. Scale bar: 10 µm.

3.3.2 Biochemical Uptake Kinetics with Functionalized Nanobodies

To biochemically measure endocytic uptake kinetics, we administrated 2 µg/mL VHH$_{GFP}$-control for up to 120 min, extensively washed the cells to get rid of any cell-associated nanobody, and finally lysed the cells for immunoblot analysis (**Fig. 3.5**). As known from previous studies (Ciechanover et al., 1983; Grant and Donaldson, 2009; Hirschmann et al., 2015; Iacopetta and Morgan, 1983; Wauben-Penris et al., 1988), iodinated or fluorescently labeled Tf is rapidly endocytosed with a half time ($\tau_{1/2}$) of ~ 4-5 min, and reaching steady-state distribution at ~ 20 min. In our assay (**Fig. 3.5 D** and **E**), functionalized nanobody phenocopied transferrin as ligand during endocytosis. We determined identical rates and kinetics for nanobody riding along with TfR-EGFP, namely $\tau_{1/2}$ of ~ 5 min and steady-state at ~ 20 min. This means that after ~ 20 min, all TfR-EGFP in post-Golgi compartments are saturated by nanobody and no additional uptake can occur anymore. Our nanobody-based uptake approach is thus very close to the classical one where endogenous TfR is targeted with radiolabeled or fluorescently labeled Tf. Further-

more, it confirms that recombinant and endogenous TfR behaves similarly. So there is rapid binding of nanobody to EGFP, at least as fast as Tf to TfR.

In comparison to the use of labeled Tf as ligand to monitor retrograde transport of TfR to the endosomal system, our nanobody-based approach has even an advantage. While cells need to be serum-starved to deplete intracellular Tf during a classical uptake assay, there is no requirement to do this with our tool. To be noted is that serum starvation affects signaling of kinases that sense the supply of nutrients, such as the mTOR kinase (Gonzalez and Hall, 2017; Shimobayashi and Hall, 2016). Indeed, a previous report has shown compelling evidence that the canonical TfR recycling pathway is under regulation of mTORC1 (Dauner et al., 2017). Serum starvation or rapamycin treatment led to the rapid degradation of TfR and other recycling receptors. To which extent mTORC1 signaling is affecting the kinetic readout during a classical, serum-starved Tf uptake assay is unknown. By using nanobodies that phenocopy Tf or other ligands, mTOR signaling can be cleverly circumvented since our assay is devoid of nutrient starvation.

To the best of our knowledge, uptake kinetics of TGN46 or the MPRs have never been directly assessed and reported so far. This is probably mainly due to either lacking or not routinely established ligands. TGN46 for instance is even most likely not a cargo receptor at all.

As true for TfR, which undergoes endocytosis with the same rate in the presence or absence of bound ligand (Hopkins et al., 1985), MPRs also traffic from the TGN or plasma membrane independently of mannose-6-phosphate (M6P)-tagged cargo load (van Meel and Klumperman, 2014). Using our reporter-binding nanobody to determine endocytic uptake kinetics, we could show that both MPRs have half-lives ($\tau_{1/2}$) at ~ 8-10 min and reach their plateau at ~ 40-45 min (**Fig. 3.5 A**, **B** and **E**). Since both receptors have similar function and intracellular distribution, the observation of similar $\tau_{1/2}$ is not much of a surprise. The longer time to reach $\tau_{1/2}$ or steady-state compared to TfR are conceivable, too. While the main fraction of TfR is cycling between (sorting and recycling) endosomes (~ 85%) and the plasma membrane (~ 15%), MPRs have a more complex steady-state distribution, with pools present in the TGN, plasma membrane, early and late endosomes. Also the receptor's itineraries along these compartments are not as clear as for TfR's. It thus needs much more time for all post-Golgi MPR copies to come out from these individual pools to appear at the cell surface. Following this idea for TGN46, with predominant localization to the TGN, we would then even expect a longer time interval until steady-state is reached. Indeed, this is also what we observe. The half time of steady-state is reached at ~ 25-30 min and the process of nanobody uptake is completed > 60 min.

Our nanobody-based approach to measure endocytic uptake kinetics has not only confirmed previously reported steady-state rates as exemplarily for TfR, but has also revealed rates of membrane proteins with more complex sorting routes (MPRs) or onesided intracellular distribution (TGN46). Our tool to assay uptake kinetics is basically applicable to any protein reporter that cycles via the cell surface and contains an EGFP at the extracellular/lumenal site. Furthermore, by introducing any perturbations to membrane-mediated traffic (e.g. small molecule inhibitors, RNAi, etc.), we can study how $\tau_{1/2}$ and steady-state of reporters of interest will be affected.

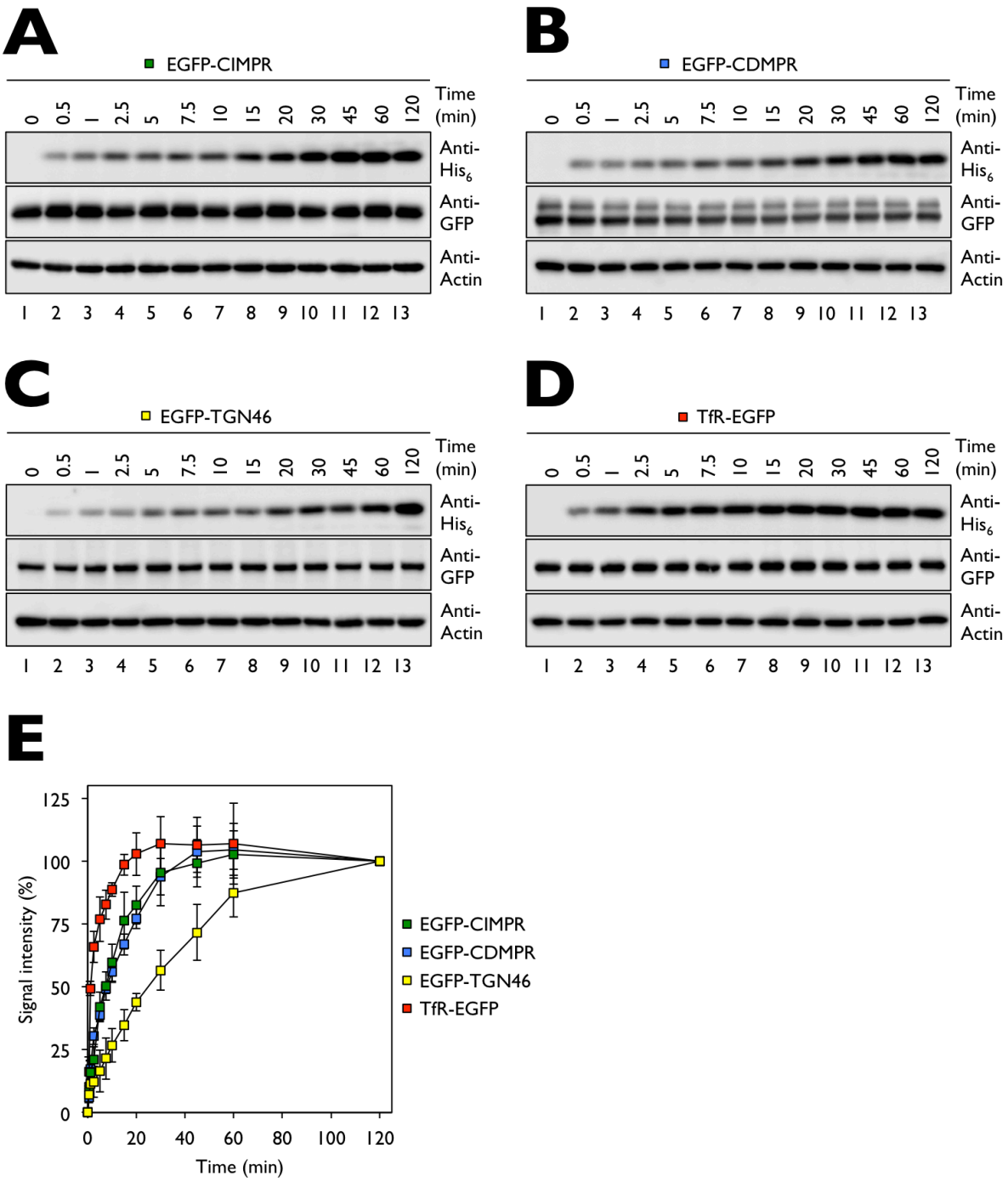

Figure 3.5: Endocytic uptake kinetics of EGFP reporter cell lines. (A)-(D) To biochemically measure uptake kinetics of EGFP-CIMPR, EGFP-CDMPR, EGFP-TGN46 and TfR-EGFP, stable cells were incubated with 2 µg/mL VHH_{GFP}-control for up to 120 min, followed by cell lysis to harvest total cell-associated nanobody (intracellular and plasma membrane). Cell-associated nanobody was detected using an anti-His_6 antibody, internal controls were made with anti-GFP or anti-actin antibodies. **(E)** Quantification of endocytic uptake kinetics. Quantification of three independent experiments is shown (average ± SD). Signal intensities of each time point is expressed as the percentage of the signal intensity after 120 min.

3.3.3 Biochemical Recycling Kinetics with Functionalized Nanobodies

Apart from measuring only uptake kinetics of reporters into steady-state, we also invested attempts in looking at both endocytosis and recycling of target proteins with one functionalized nanobody. To be able

to perform so, we modified our simplest nanobody, VHH_{GFP}-control, with a TEV cleavage site (**Fig. S3 A-B**). TEV cleavage site-modified nanobodies can be cleaved upon appearance at the cell surface with recombinant TEV protease, thereby causing removal of the C-terminal epitope cassette.

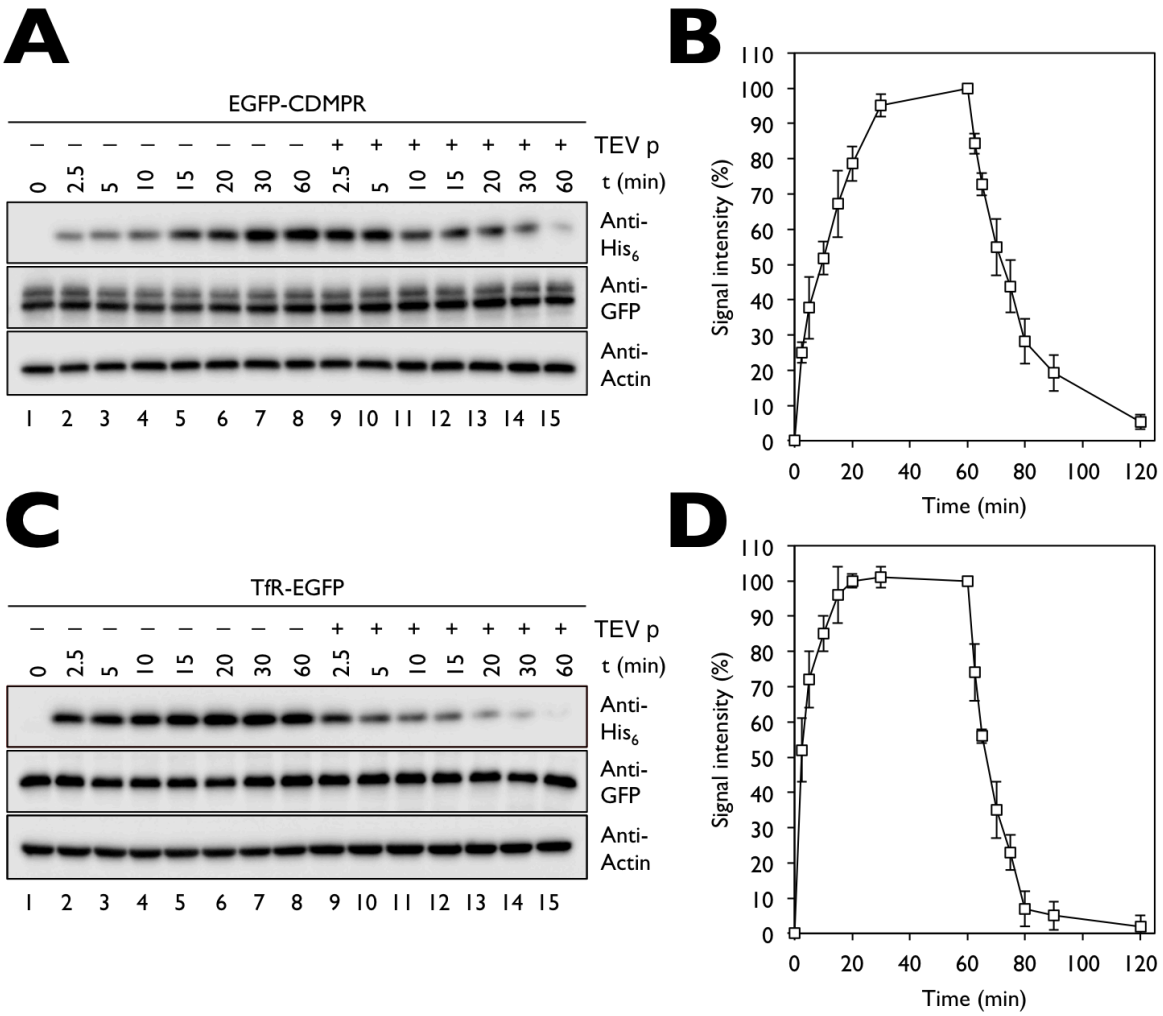

Figure 3.6: Endocytosis and recycling kinetics of EGFP-CDMPR and TfR-EGFP. (A) and **(C)** To biochemically measure endocytic uptake and recycling of EGFP-CDMPR and TfR-EGFP, stable cells were first incubated with 2 µg/mL VHH_{GFP}-TEV-control for up to 60 min, followed by several washes, and then recombinant TEV protease was added for up to 60 min (starting from 2.5) to cleave nanobody arriving at the cell surface. Cells were lysed and the total cell-associated nanobody (intracellular and plasma membrane) was detected using an anti-His_6 antibody, internal controls were made with anti-GFP or anti-actin antibodies. **(B)** and **(D)** Plotting of endocytic uptake and recycling kinetics. Quantification of three independent experiments is shown (average ± SD). Signal intensities of each time point (endocytosis and recycling) is expressed as the percentage of the signal intensity after 60 min.

To illustrate the use of our functionalized nanobody termed VHH_{GFP}-TEV-control, we performed an endocytosis-recycling assay using EGFP-CDMPR and TfR-EGFP as receptor reporters. Similar to the experimental setup in **Figure 3.5**, we administrated 2 µg/mL VHH_{GFP}-control for up to 60 min, washed the cells to get rid of any cell-associated nanobody, and then added purified TEV protease into the cell culture medium at 37°C for up to 60 min before cell lysis was performed.

In **Figure 3.6**, endocytic uptake/recycling kinetics of EGFP reporters are shown. As observed before (**Fig. 3.5 B** and **D**), we could report similar uptake kinetics for the receptors. The presence of TEV protease in the cell culture medium over the chase period caused a robust decrease of the nanobody signal, showing that the extracellular protease faces exocytosed nanobody and cleaves it. Strikingly, rates of recycling and uptake are similar for each individual EGFP reporter. While we observed steady-state to be reached after 20 min in an uptake experiment for TfR-EGFP, we reported < 7% of nanobody to be intracellularly present for the same period of time in the recycling assay (**Fig 3.6 C** and **D**). The minute difference is probably restricted to technical reasons. While the uptake assay relies on nanobody internalization only, the recycling assay is also dependent on the cleavage efficiency of TEV protease. It is likely that the used conditions (cell culture medium, temperature) do not mimic the most optimal working environment for the protease to confer complete TEV site removal, even though it has been added in 'excess' to compensate for this potential limitation. As for TfR-EGFP, we could see a similar trend for EGFP-CDMPR regarding endocytic uptake and recycling rates. After 60 min of recycling for instance, we could only detect minor traces (< 5%) of uncleaved VHH_{GFP}-TEV-control (**Fig. 3.6 A** and **B**). We did not monitor significant levels of TEV protease to be unspecifically taken up during our assayed time.

Even though rates of endocytosis and recycling are not completely identical, primarily because of technical caveats, our results demonstrate the potential use of TEV site-tagged nanobodies to monitor recycling from intracellular compartments to the plasma membrane. We can principally use such a setup to assay recycling of any cycling transmembrane cargo and perturb its traffic with any means.

3.3.4 Live Cell Imaging Uptake Kinetics with Functionalized Nanobodies

As previously mentioned, uptake kinetics so as recycling kinetics cannot only be measured biochemically by nanobody feeding and cell harvesting as performed in **Fig. 3.5**-**3.6**, but also by live cell imaging. Live cell imaging has the advantage that we can 'visualize' the process of endocytosis and quantitate the process of uptake more easily. In light of this notion, we established a semi-automated live cell imaging approach to quantitatively assess uptake using VHH_{GFP}-mCherry.

The live cell imaging approach is based on an inverted widefield microscope and a data analysis program correcting for any live cell perturbances. It also allows us to compute characteristic values describing the uptake process, among them the apparent rate constant k_{app}, half-life $\tau_{1/2}$ of the endocytic process, as well as the time T where uptake is completed (steady-state).

To measure uptake kinetics of our two EGFP receptor reporters, EGFP-CDMPR and TfR-EGFP, we imaged cells in selected fields of view (FOV) before and after nanobody addition. Before adding nanobody, regions of interest (ROI) in the EGFP emission channel of selected FOV were marked in which nanobody (mCherry) increase over time was then quantitated. Since we considered endocytic uptake, whole cells were marked as ROI, but principally, we could mark any defined intracellular compartment. The frame rate was set to 1 frame per 30 seconds, meaning that a picture will be taken every 30 seconds after initial nanobody addition for up to 30 min or 50 min for TfR-EGFP or EGFP-CDMPR, respectively. **Figure 3.7 A** and **C** shows as selected series of silent pictures for the uptake of VHH_{GFP}-mCherry by

cells stably expressing EGFP-CDMPR or TfR-EGFP. Selected insets are enlarged to qualitatively visualize the uptake process.

As seen in both picture series (see also movies **Mov. 3.1** for EGFP-CDMPR, and **Mov. 3.2** for TfR-EGFP), retrograde transport compartments receive robust mCherry fluorescence over time, indicating that the process of endocytic uptake can be visualized with our nanobody tool. Image processing and data analysis of multiple recorded raw movies allowed us to plot endocytic uptake kinetics and to determine k_{app}, $\tau_{1/2}$ and T for EGFP-CDMPR or TfR-EGFP. The respective values as well as the uptake graphs are depicted in Figure **3.7 B** and **D**. We calculated a rate constant of $k_{app} = 1.33 \cdot 10^{-3}\ s^{-1}$, a half-life of $\tau_{1/2} \sim 9$ min, and a steady-state time of T ~ 43 min, with all having a relative error of 20%, for EGFP-CDMPR. For TfR-EGFP, we found a rate constant of $k_{app} = 2.89 \cdot 10^{-3}\ s^{-1}$, a half-life of $\tau_{1/2} \sim 4$ min, and a steady-state time of T ~ 20 min, with all having a relative error of 25%. The computed values for TfR-EGFP impressively demonstrate how well our live cell imaging approach is technically working. We obtained similar values for the endocytic uptake and recycling process, in particular with regard to the half-lives $\tau_{1/2}$.

A similar statement can be made for EGFP-CDMPR. We for instance observed that no additional nanobody will be taken up after 45 min (**Fig. 3.5 B**). This is also reflected by our live cell imaging data that showed the process of uptake to be completed at ~ 43 min (**Fig. 3.7 B** and **D**). Apart from selecting whole cells only, we could principally also mark defined subcellular compartments (ROIs), in particular, the prominent perinuclear region seen in cells stably expressing EGFP-CDMPR or TfR-EGFP. The perinuclear region of EGFP-CDMPR represents a cohort of distinct post-Golgi compartments, including the Golgi, early as well as late endosomes, while for TfR-EGFP, these perinuclear compartments mainly embody early endosomes. Our initial idea to track retrograde transport from the cell surface to the TGN using our EGFP-CDMPR reporter cell line in combination with VHH_{GFP}-mCherry is, because of the ambiguous compartment representation, thus not directly measurable. Then, we do not know which parts of this perinuclear region actually correspond to the Golgi/TGN. We performed nevertheless such an uptake analysis by selecting the perinuclear compartments of EGFP-CDMPR-expressing cells in different FOVs, and found that it took about 60 minutes until nanobody has reached steady-state in these ROIs. The apparently longer time it took for EGFP-CDMPR to come to steady-state in the perinuclear region is obvious, then the receptor needs to pass a much longer route to come to this region. Though 'whole cell' uptake analysis also includes the perinuclear region, there is also the cell surface fraction and the peripheral endosome fraction that causes steady-state of total cell to be reached faster than in the perinuclear region. A strategy to specifically define compartments of interest to monitor retrograde transport is the coexpression of fluorophore-tagged organelle markers. We are currently implementing fluorophore-tagged TGN reporter proteins (TPST1, TPST2 and GalT) as reference markers to assess retrograde transport of EGFP-CDMPR. However, the results of these go beyond the scope of this study. Our established live cell imaging approach provided the basis to analyze endocytic uptake into cells, but also to address further experimental questions.

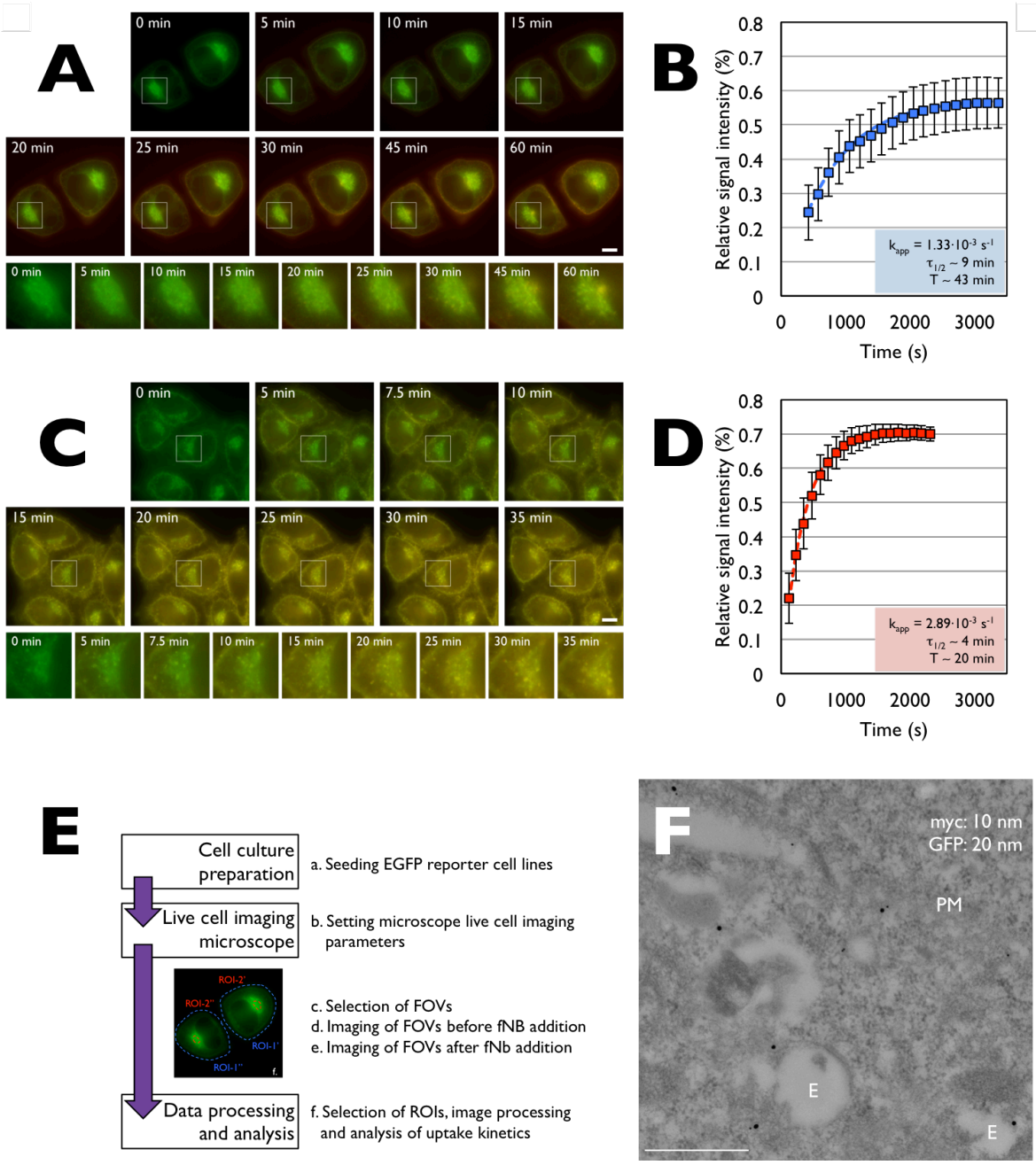

Figure 3.7: Live cell imaging kinetics of EGFP-CDMPR and TfR-EGFP, and immunoelectron microscopy. **(A)** and **(C)** To measure endocytic uptake of EGFP-CDMPR (A) and TfR-EGFP (C), the procedure as outlined in (E) was performed. Image processing was performed using Fiji, data analysis was done in phyton. (A) and (C) illustrate a series of silent pictures of a chosen recorded movie for either EGFP-CDMPR (A) or TfR-EGFP (C). Scale bar: 10 µm. **(B)** and **(D)** Plotting of endocytic uptake kinetics. Quantification of three independent experiments is shown (average ± SD). Characteristic values for each EGFP reporter are also depicted. See material and methods for data analysis. Curve starts delayed > 0 s, because of nanobody addition and curve fitting. **(E)** Typical workflow of live cell imaging acquisition. EGFP reporter cell lines were seeded into ibidi dishes (a). The following day, medium was exchanged to phenol red-free medium and prepared for acquisition. After having set the microscope (37°C, 5% CO_2) and other parameters (b), FOVs were chosen in ibidi dishes (c). FOVs were imaged before (d) and after (e) addition of functionalized nanobody (fNb). Depending on the EGFP reporter, the number of recorded frames was changed. Following image recording, ROIs were selected and processed with ImageJ/Fiji. Analysis of uptake kinetics was performed in phyton (f). **(F)** Immunoelectron microscopy of endocytosed VHH_{GFP}-myc by cells stably expressing TfR-EGFP. GFP was labeled with 20 nm-, myc with 10 nm-collidoal gold particles. Legend: E, endosome; PM, plasma membrane. Scale bar: 500 nm.

Within the interest to visualize endocytic uptake by various methods, we also sought to use immunoelectron microscopy. Then, fluorescence microscopy cannot really resolve the identity of the perinuclear compartment that contains not only TGN, but also endosomes and lysosomes. As previously introduced, we established VHH_{GFP}-myc for this purpose since there is a good anti-myc antibody for this application. For illustration purposes, we decided to use TfR-EGFP to visualize endocytic uptake ultrastructurally, mainly because TfR-EGFP has a relatively high cell surface population (15%), and because it reaches steady-state fast. Following internalization of VHH_{GFP}-myc for 1 h, cells were fixed, processed for electron microscopy and double-labeled with an anti-myc and anti-GFP antibody that were detected with coupled collidoal gold particles.

Figure 3.7 F visualizes uptake by cells expressing TfR-EGFP. We could predominantly observe small and big collidoal gold particles in early endosomes, at the plasma membrane or in transport carriers between these subcellular locations. In many labeled structures, small and big gold particles were seen to cluster together, in agreement with the notion that nanobody is captured at the cell surface and then transported piggyback to intracellular compartments. The observation of single labeled structures is due to the limited double labeling efficiency with colloidal gold particles. Then virtually 1 h of uptake is more than sufficient to label the entire TfR-EGFP population in post-Golgi compartments. We can also exclude unspecific labeling since the antibodies were initially titrated. We also tried to immunolabel EGFP-CDMPR for electron microscopy, however, but rarely detected substantial amounts of endocytosed VHH_{GFP}-myc in these cells. It seems that the immunoelectron microscopy approach is not sensitive enough to detect endocytosed nanobodies by receptor reporters which only have a small cell surface fraction in steady-state. Thus, a more sensitive approach is required to ultrastructurally visualize endocytic and retrograde transport compartments.

3.4 Analysis of Retrograde Transport by Peroxidase Labeling

Ultrastructural investigation of retrograde transport itineraries by electron microcopy can be performed either by immunogold staining of cell surface-labeled and endocytosed reporters (as performed in **Fig. 3.7**) or by peroxidase-mediated labeling. Stoorvogel and colleagues were one of the first who made use of the peroxidase HRP to label and study the endocytic pathway by electron microscopy and by biochemical approaches (Geuze et al., 1988; Stoorvogel, 1998; Stoorvogel, 2008; Stoorvogel et al., 1987; Stoorvogel et al., 1991). By coupling HRP to receptor ligands or to recombinant fusions, ultrastructural and biochemical insights of target compartments were possible.

Since the heart of our approach relies on bacterial expression of nanobody fusion proteins, we could not use HRP due to its secretory properties (e.g. disulfide bonds). We instead used APEX2. By fusing the enzymatic domain of APEX2 to VHH_{GFP}, we can basically label and track any EGFP fusions from the cell surface to finally study their ultrastructural localization, as well as to biochemically characterize the compartments in which they 'nest' by compartment ablation and proximity-dependent biotin labeling.

3.4.1 Biochemical Uptake of VHH_{GFP}-APEX2

To see whether VHH_{GFP}-APEX2 is internalized as the other functionalized nanobodies (**Fig 3.4**), medium of EGFP reporter cell lines was supplemented with 5 μg/mL VHH_{GFP}-APEX2. After 1 h of uptake at 37°C, cell lysates were prepared and probed against cell-associated nanobody. VHH_{GFP}-APEX2 is efficiently taken up by all via the cell surface cycling reporters (**Fig 3.8 A**), but not by cytosolic EGFP-expressing cells. To be noted is that despite the size of the enzyme (same for mCherry), it is taken up to the same extent as VHH_{GFP}-control, if not even more. This means that functionalization even with bigger protein domains can be accomplished and internalized, provided that VHH_{GFP} still acts as 'vector' for endocytic uptake by EGFP reporters. As expected because of previous observations, internalized VHH_{GFP}-APEX2 also follows its reporters into steady-state as revealed by immunofluorescence microscopy (**Fig 3.8 B**). We thus can feed VHH_{GFP}-APEX2 to EGFP reporter cell lines and perform DAB cytochemistry.

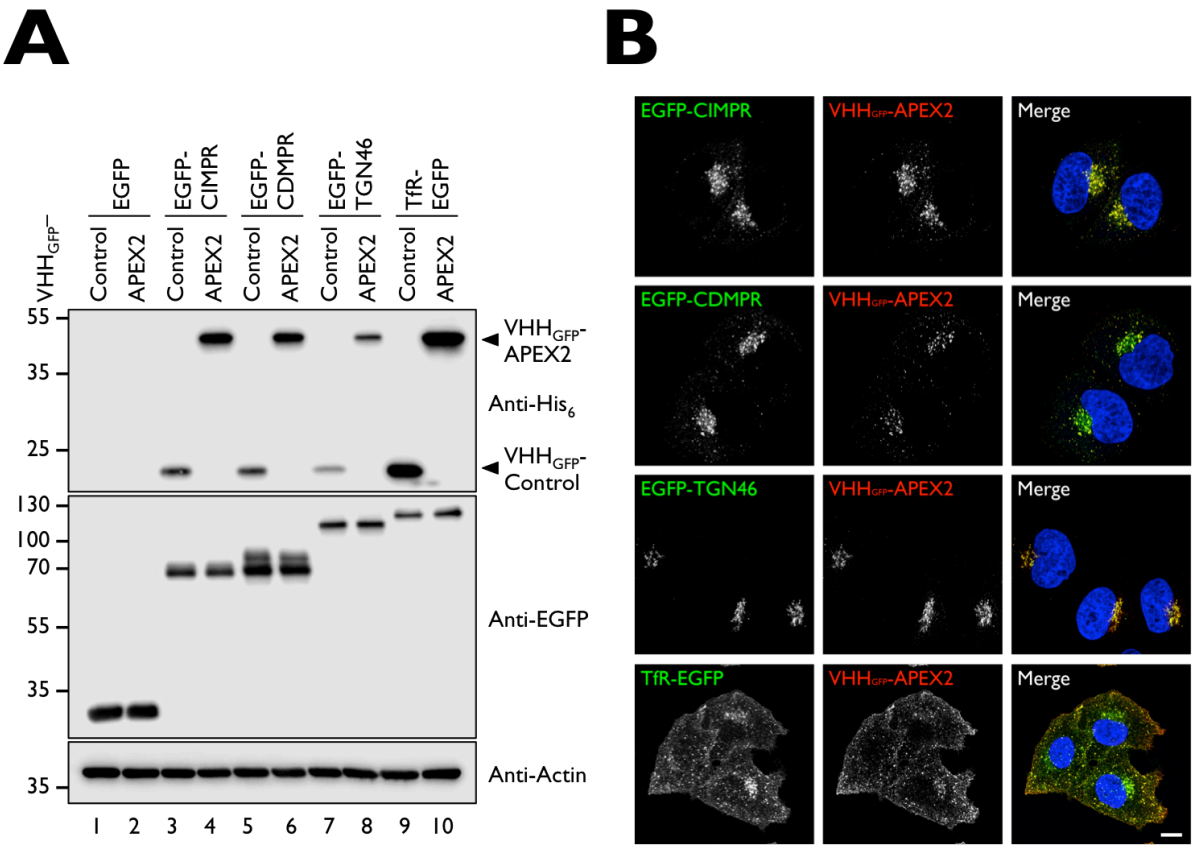

Figure 3.8: Endocytic uptake of VHH$_{GFP}$-control and VHH$_{GFP}$-APEX2 by EGFP reporter cell lines. (A) Functionalized nanobodies are specifically taken up by reporters presenting an EGFP moiety to the extracellular environment. HeLa cells stably expressing EGFP reporters were incubated in the presence of either 2 μg/mL VHH$_{GFP}$-control or 5 μg/mL VHH$_{GFP}$-APEX2 for 1 h at 37°C. Following uptake, cell lysates were prepared and probed with anti-His$_6$, anti-GFP and anti-actin antibodies. **(B)** Similar procedure as in (A). Cells on coverslips were fed with 5 μg/mL VHH$_{GFP}$-APEX2 and processed for fluorescence confocal microscopy. APEX2 was detected using an anti-HA antibody. Numbers along the markers correspond to molecular weight in kDa. Scale bar: 10 μm.

3.4.2 Electron Microscopy of Target Compartments with VHH$_{GFP}$-APEX2

A general and important note to be shared in advance is that Golgi appearance is strongly dependent on the applied EM method. It is thus crucial to be aware that a 'typical' Golgi is not always an array of nicely stacked cisternae. Depending on the sectioning and post-fixation procedures, Golgi architecture might look different from what we are familiar with from textbooks.

To specifically peroxidase-label endocytic compartments, cell lines stably expressing EGFP reporters were incubated with 5 μg/mL VHH$_{GFP}$-APEX2 for 1-2 h to reach steady-state. After fixation and DAB/H_2O_2 cytochemistry, cells were stained with osmium tetroxide for electron microscopy. Cells that do not possess any EGFP reporter, but have undergone cytochemistry, do not show any visible DAB precipitates due to missing APEX2 internalization (**Fig 3.9 A**). The only structures that are stained after osmium tetroxide in control cells are peroxidase-containing compartments, such as peroxisomes. The Golgi area was typically identified by the presence of a discernible cluster of elongated tubular/vacuolar-shaped membranes in close proximity to the nucleus. To prove and compare that compartment labeling with our approach productively worked for EGFP-modified reporter proteins, we first used TfR-EGFP. As

established for TfR/Tf-HRP (Laulagnier et al., 2011; Stoorvogel et al., 1988; Theos et al., 2005), DAB precipitates are preferentially formed in compartments of the endosomal network. For TfR-EGFP (**Fig. 3.9 B**), we observed DAB depositions outlining or filling endocytic compartments reminiscent of early and recycling endosomes. In addition, also stained vesicular structures (presumably endocytic CCV) and invaginated membranes (e.g. CCP) from the plasma membranes could be observed. Thus, APEX2 can very well substitute for HRP as peroxidase to label target compartments. Furthermore, the specific and local deposition of DAB also showed that APEX2, unlike HRP, can operate in both an oxidative and reductive cellular environment. So far, APEX2 has been only applied for cytosolic expression. We are not aware of studies using APEX2 in the secretory or endocytic pathway.

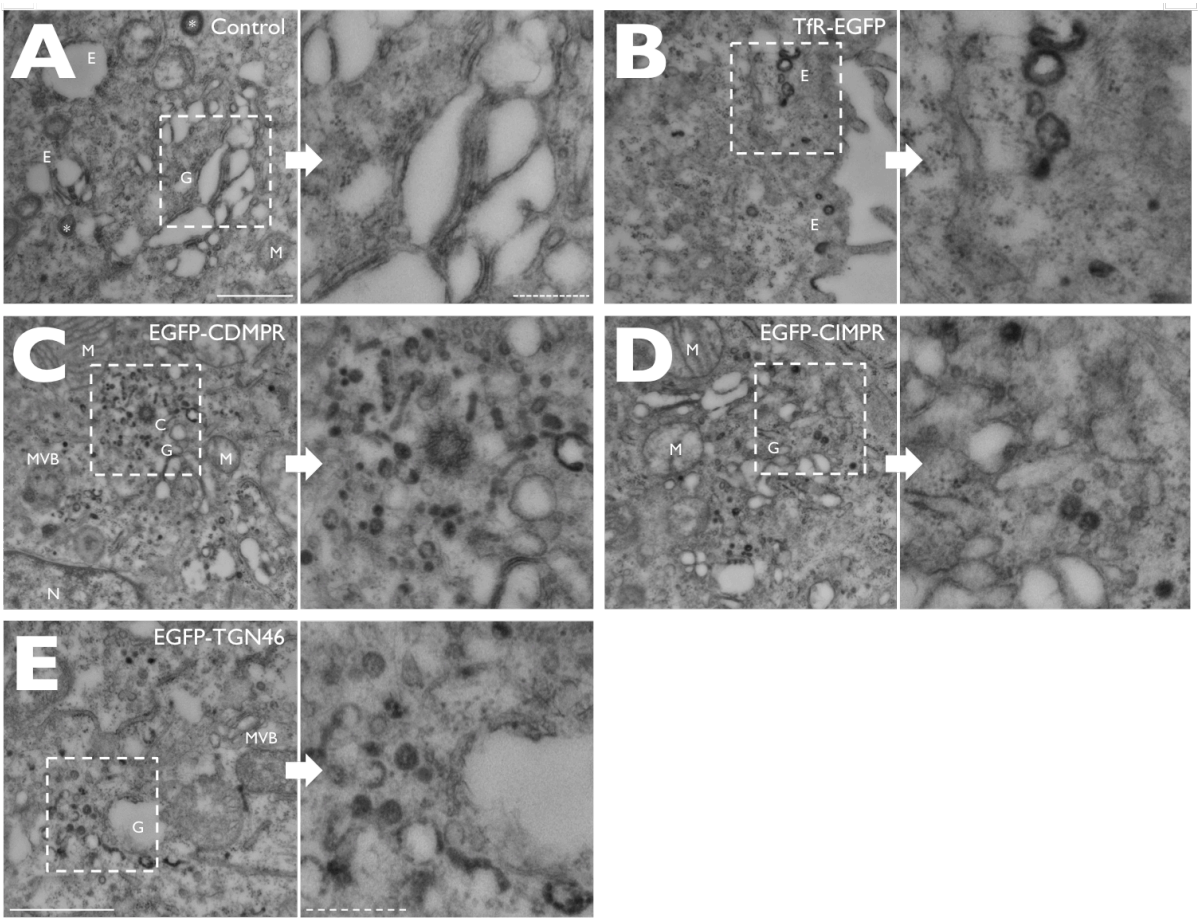

Figure 3.9: DAB/H_2O_2 cytochemistry and electron microscopy of EGFP reporter cell lines. (A)-(E) Control and EGFP reporter cell lines were incubated with 5 µg/mL VHH_{GFP}-APEX2 for 1-2 h at 37°C to reach steady-state. After fixation with 2% glutaraldehyde, cells were treated with DAB/H_2O_2 to yield a local and productive DAB polymerization reaction. The picture on the right of an alphabetic series refers to the enlargement of the respective selected area (dotted square). Straight lines correspond to 1000 nm (A-D or E), dotted lines to 380 nm (A-D or E). Legend: C, centrosome; E, endosome; G, Golgi; M, mitochondrium; MVB, multivesicular body; N, nucleus; Asterix (*), peroxidase-containing compartments (e.g. peroxisomes).

In a next step, we wanted to see what kind of ultrastructural architecture compartments beyond endosomes, i.e. the TGN, have. Following this idea, we first considered to look at DAB-positive structures in cells expressing EGFP-CDMPR (**Fig. 3.9 C**). Apart from DAB-positive peripheral and perinuclear endosomes, we often found a concentrated pattern of small vesicular and tubular elements

adjacent to the Golgi cisternae. The labeled tubular elements varied in length and often had branched extensions (see also **Fig. S4 A**). In agreement with former reports that made use of wheat germ agglutinin (WGA)-HRP to label endocytic and Golgi compartments (Iida and Shibata, 1989; Klumperman, 2011; Pavelka et al., 2008), our observed vesicular-tubular arrangement of membranes represents indeed TGN at ultrastructural resolution. Some of these tubular elements seem to be even interconnected with the trans-Golgi cisternae, thereby turning into integrated parts of the Golgi complex. The TGN varied in size, morphology, and also in the number of vesicular-tubular elements. It is therefore not a surprise that the TGN pattern of EGFP-CIMPR and EGFP-TGN46 (**Fig. 3.9 D-E**) does not look identical, but similar. Compared to WGA-HRP as retrograde tracer, our nanobody-based technique to label the retrograde route to the TGN is by far more specific. WGA is an N-acetyl-glucosamine- and sialic acid-binding lectin (Goldstein and Hayes, 1978) and thus labels and conveys a broad spectrum of glycosylated cargo proteins. As demonstrated by Iida and Shibata (Iida and Shibata, 1989) almost three decades ago, WGA-HRP can chart beyond the TGN and even label Golgi cisternae. The nanobody approach, in contrast, allows specific labeling of the steady-state ultrastructural distribution of a given EGFP reporter.

3.4.3 Inactivation of Target Compartments with VHH_{GFP}-APEX2

Another application of peroxidases to study retrograde traffic is biochemical ablation (Stoorvogel, 1998; Stoorvogel et al., 1988). As mentioned previously, ablation describes the selective compartment inactivation by crosslinking and/or encapsulation of lumenal and integral membrane proteins using peroxidase-mediated DAB/H_2O_2 cytochemistry. Since polymerized DAB is water-insoluble and dense, the crosslinked proteins can be easily precipitated by centrifugation. Ablation is thus very much suitable to figure out to which intracellular compartments a reporter localizes and above all through which it traffics. By peroxidase labeling of endocytic compartments with HRP conjugated to Tf in combination with ablation, sorting itineraries of a number of proteins could be assessed through TfR-positive membranes (Hashiramoto and James, 2000; Livingstone et al., 1996; Mihov et al., 2015; Stoorvogel et al., 1989; Stoorvogel et al., 1988). The APEX2-labeled anti-GFP nanobody offers us a direct way to specifically ablate compartments, and to identify the subcellular localization of EGFP reporters.

To assess the efficiency and specificity of the ablation reaction on living cells, we took advantage of the well-studied endocytic reporter TfR. Cells stably expressing TfR-EGFP were loaded with APEX2-labeled VHH_{GFP} for 1 h at 37°C, washed with ice-cold PBS to halt membrane transport and then incubated with a mixture of DAB/H_2O_2 to initiate crosslinking at 4°C for 90 min in the dark. Cells were harvested and the postnuclear supernatant was separated from the DAB crosslinking precipitate. Immunoblot analysis of cell lysates showed more than 90% elimination of recombinant TfR, demonstrating that not only intracellular levels (~ 85%), but presumably also cell surface fractions were affected (**Fig. 3.10 A**). The almost complete ablation of TfR-EGFP is in agreement with the observed auto-ablation of APEX2. APEX2 itself namely is completely ablated from the soluble fraction, highlighting that DAB precipitates can be potentially formed locally at distinct plasma membrane niches. Indeed, close to TfR-EGFP, we even often observed DAB precipitates along the extracellular rim of the plasma membrane by electron microscopy (**Fig. S4 B-C**), further confirming the existence of plasma membrane-associated

precipitations. As for the recombinant TfR with three to four fold higher protein expression, we reported productive elimination of the endogenous counterpart to the same extent (**Fig. 3.10 A**, blot lane with TfR). This result might suggest that some of the TfR are heterodimers, composed of an endogenous and recombinant subunit, otherwise we would not observe ablation of more than > 85% for endogenous TfR. The plasma membrane overall in general was not significantly affected by DAB crosslinking since we could monitor rather stable levels of the cell surface marker CD44. However, it has to be mentioned that CD44, a CIE cargo, probably populate plasma membrane domains where TfR, a CME cargo, might be absent. Missing ablation of overall cell surface proteins (including CD44) was probably mainly due to the high reaction volume provided by the extracellular space, thereby making DAB crosslinking considerably inefficient. While the concentration of APEX2 for a productive reaction in endocytic compartments is high, it is vanishingly small in the extracellular space despite constant amounts of DAB/H_2O_2.

Other endogenous proteins that were affected by DAB polymerization were CIMPR and the endosomal SNARE proteins vti1a and vti1b (**Fig. 3.10 A**). All of these proteins are known to pass early endosomes to perform their individual functions as cargo receptor or membrane targeting, respectively. Even though reported to mainly localize to the TGN and to late endosomes in steady-state, we found a reproducible elimination of ~ 50% for CIMPR, revealing a rather dominant localization of the hydrolase receptor to TfR-positive endosomes and peripheral structures. Our results are supported by a previous study of Kornfeld and colleagues (Ghosh et al., 2003b) who showed the presence of ~ 60% CIMPR in endosomes and 'scattered elements' by quantitative immunogold labeling in HeLa cells. In agreement with endosomal localization of vti1a and vti1b (Hirst et al., 2004; Hirst et al., 2003), we consistently observed ablation of these proteins in TfR-positive compartments, even though these proteins have only an extremely short lumenal tail. Ablation from the soluble fraction is thus probably not only caused by covalent chemical protein crosslinking, but also contributed by encapsulation of soluble proteins into the DAB polymer meshwork (Stoorvogel et al., 1989; Stoorvogel et al., 1988; Stoorvogel et al., 1987). In a study of James and colleagues where recycling of the GLUT4 transporter from endosomal compartments in 3T3-L1 adipocytes was investigated using Tf-HRP, ablation of other post-Golgi SNAREs with short lumenal tails (syntaxin 6 and VAMP2) could be observed (Hashiramoto and James, 2000).

In contrast to endosomal markers, proteins which predominantly localize to the TGN (TGN46, GalT, TPSTs), to the medial Golgi cisternae (ManII), or peripherally associate with endosomal membranes (Rab4, Rab5, Rab7 and Rab9) were not noticeably ablated. This is in line with the observation that TfR mainly cycles through endosomal compartments with only insignificant shortcuts to the TGN and beyond. LAMP1 was also not affected by APEX2-mediated compartment ablation, most likely because there is only a poor fraction in TfR-positive endosomes in steady-state. Other compartments of the secretory pathway (e.g. ER) or other organelles (e.g. mitochondria) were also not affected by endocytic DAB/H_2O_2 cytochemistry, as demonstrated by immunoblotting against calnexin or Tom20 (**Fig. 3.10 A**).

With proof in hand that APEX2-mediated ablation principally works in TfR-EGFP-expressing cells, we next investigated which retrograde transport compartments and intermediates are inactivated in cells expressing EGFP-CDMPR. Western blots probed against GFP showed mature recombinant CDMPR to be depleted from postnuclear supernatants (**Fig. 3.10 B**). As discussed previously, the lower band of EGFP-

CDMPR does not exclusively represent high-mannose glycosylated ER form, but is rather composed of two bands that can be hardly separated by gel electrophoresis. Parts of the lower band of EGFP-CDMPR indeed were accessible by the nanobody that was provided in the cell culture medium, indicating an additional mature form of the receptor (**Fig. S2 B**). We therefore also observed a decline in protein levels of the lower band of EGFP-CDMPR.

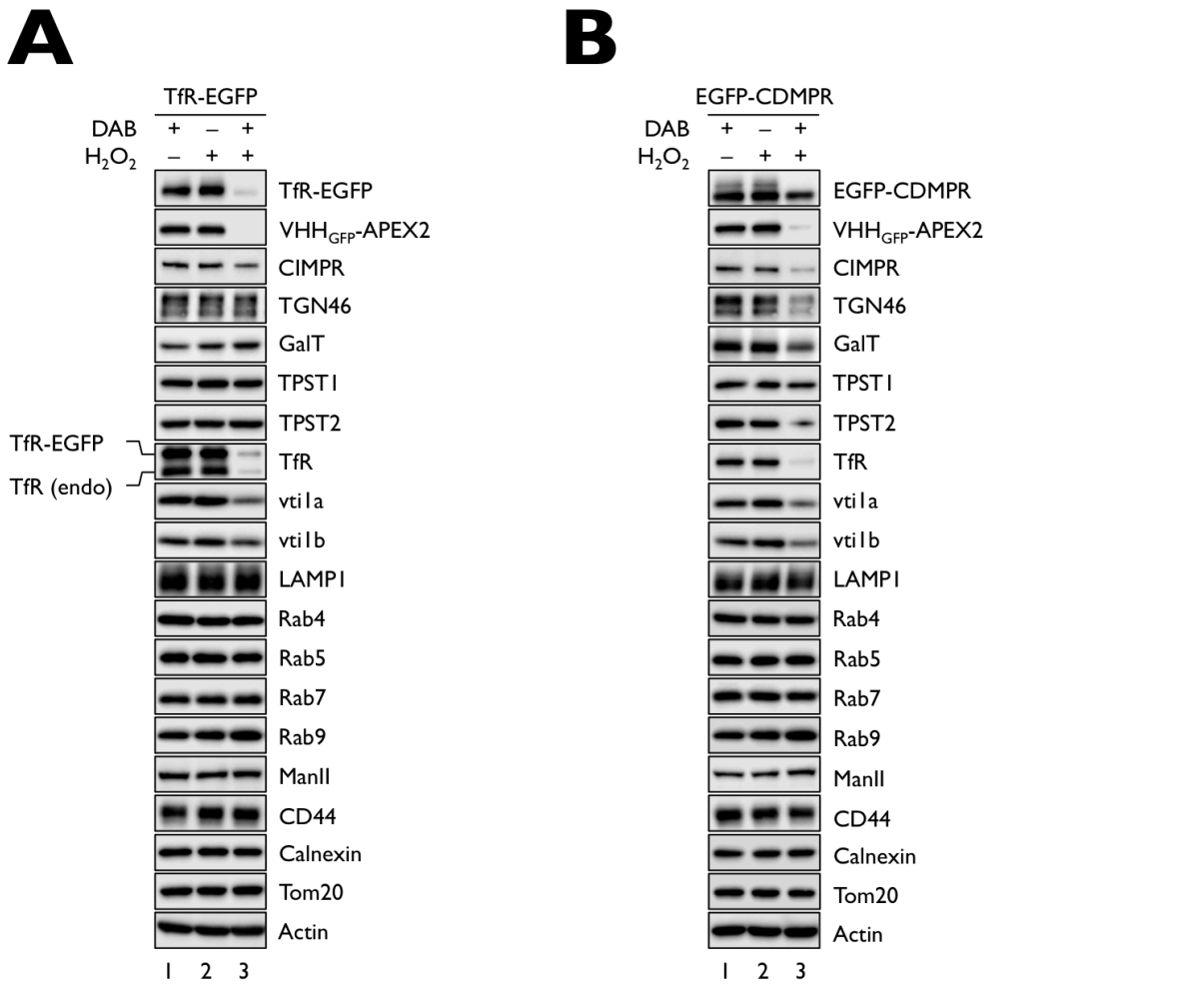

Figure 3.10: Biochemical compartment ablation analysis of TfR-EGFP and EGFP-CDMPR. (A)-(B) To inactivate endocytic or retrograde compartments of TfR-EGFP or EGFP-CDMPR, cells were prepared in 6-well clusters and incubated in complete DMEM containing 5 µg/mL of purified VHH_{GFP}-APEX2 for 1 h at 37°C to reach steady-state. After three washes with ice-cold PBS, cells were incubated with either 1 mg/mL DAB or 0.03% H_2O_2 separately as control, or a combination thereof in PBS to yield a productive ablation reaction. After 90 min of incubation at 4°C in the dark, cells were washed twice with ice-cold PBS-5% BSA to stop the DAB crosslinking reaction, followed by three additional washes before lysis. Legend: GalT, β-1,4-galactosyl-transferase; TPST, tyrosylprotein sulfotransferase; ManII, α-mannosidase II. Experiments have been repeated at least three times.

As observed for TfR-EGFP as positive control, APEX2 was also ablated in cells expressing EGFP-CDMPR to almost undetectable levels. Since both MPRs are implicated to have similar function and transport itineraries, we expected CIMPR to be ablated, too. Indeed, we noticed a concomitant 70-80% depletion of endogenous CIMPR after DAB/H_2O_2 cytochemistry. Similar to recombinant TfR, we also observed ablation of endogenous TfR and the endosomal SNARE proteins vti1a and vti1b in the EGFP-

CDMPR reporter cell line. Because MPRs need to capture newly synthesized lysosomal hydrolases from the TGN, there is a requirement of continuous receptor retrieval from endosomes. It is thus obvious that the reporter must go back to the TGN where it will occasionally encounter and face more resident marker proteins.

To examine whether our EGFP-CDMPR indeed undergoes the return route from the cell surface to the TGN via endosomes, we probed our lysates against TGN46, GalT and the two tyrosylprotein sulfotransferase isoforms (TPST1 and TPST2). We observed depletion of TGN46, GalT and TPST2 in the condition with productive DAB polymerization, consistent with the notion that EGFP-CDMPR undergoes retrograde transport to the TGN. TPST1 instead was maximally depleted by ~ 20%, thereby potentially suggesting that this isoform is not localized to the TGN to the same extent as TPST2. The literature is unclear regarding the precise localization of TPSTs, either in the trans-Golgi or TGN (Baeuerle and Huttner, 1987; Huttner, 1988; Stone et al., 2009). It thus might be that either TPST1 is preferentially localized to the trans-Golgi cisterna in steady-state and thus is less ablated, or it just resides in a 'TGN subdomain' where MPRs are not passing through.

Although MPRs are reported to traverse late endosomes to reach the TGN (Barbero et al., 2002; Bonifacino and Rojas, 2006; Diaz and Pfeffer, 1998; Lombardi et al., 1993; Reddy et al., 2006), we did not find any ablation of the marker LAMP1 that is also present in late endosomes to a certain degree (Humphries et al., 2011; Saftig and Klumperman, 2009). However, we can also not exclude that APEX2 is rendered inactive in more acidic late endosomes. In agreement with the view that MPRs do not retrogradely traffic beyond the TGN, we did not observe any ablation of medial-Golgi compartments (ManII) or the ER (calnexin). Also Rab GTPases that are peripherally recruited to inactivatable compartments were not ablated.

Our assay provides means to assess whether EGFP reporters undergo transport to the TGN just by assaying for ablation of TGN-resident markers. This approach can be expanded to other EGFP-modified reporters.

3.4.4 Proximity-Dependent Biotin Labeling of Target Compartments

Instead of biochemically ablating the TGN, retrograde EGFP reporters can also be exploited to escort protein modifiers. Such a protein modifier will then have the task to substrate-label interactors or neighbors in close proximity. Valuable protein modifiers for proximity-dependent labeling in this regard are the promiscuous BirA mutant (BirA*) and peroxidases (Kim and Roux, 2016). The former has been developed and improved by Roux and colleagues (Kim et al., 2016a; Roux et al., 2012) and since then used in a wide number of applications ranging from immunoblot analysis to mass spectrometry (De Munter et al., 2017; Kim et al., 2016b; Le Sage et al., 2016; Li et al., 2017; Mehus et al., 2016; Roux, 2013; Roux et al., 2013). BirA* uses D-biotin as substrate and has a mutation within the biotin- and biotin-AMP-binding domain that causes it to be released and reactive with primary amines within a diameter of approximately 10 nm.

While the enzymatic activity of BirA*-mediated biotinylation is slow, peroxidase-driven labeling is more rapid. Peroxidases can generate short-lived free radicals from substrates such as phenolic aryl azide

derivatives or tyramide derivatives in combination with H_2O_2 (Gross and Sizer, 1959; Honke and Kotani, 2011), and conjugate them to electron-dense side chains (e.g tyrosine and tryptophan) (Kim and Roux, 2016).

Based on the idea of Ting and colleagues who initially demonstrated proximity-dependent biotinylation using APEX2 (Hung et al., 2017; Hung et al., 2016; Hung et al., 2014; Lam et al., 2015; Rhee et al., 2013), we sought to send our nanobody fusion along with our EGFP reporters. A pulse with the peroxidase substrate biotin-phenol (biotin tyramide) would then lead to biotin transfer to APEX2-proximal proteins. Biotinylation strictly depends on the steady-state distribution of the reporter, and thus reporter undergoing retrograde transport to the TGN might most likely biotinylate resident proteins in this compartment. Subsequently, biotinylated proteins from lysates can be enriched using streptavidin-based purification and probed with antibodies recognizing TGN-specific markers. This approach is thus a simple way to assess retrograde traffic to the TGN or basically to any other target compartment.

To detect APEX2-mediated biotinylation of TGN-resident proteins, we decided to use again TfR-EGFP and EGFP-CDMPR as model proteins. Cells expressing these EGFP reporters were loaded with 5 µg/mL VHH_{GFP}-APEX2 for 1 h to reach steady-state. Following three washes, biotin-phenol labeling was initiated by adding fresh complete medium containing 500 µM biotin-phenol for 30 min at 37°C. Afterwards, H_2O_2 at a final concentration of 1 mM was added to the cells to start the reaction. After 3 minutes of labeling, the reaction was halted and quenched. Cleared cell lysates were then incubated with streptavidin beads followed by immunoblot analysis.

We first studied whether APEX2 can perform promiscuous biotinylation when present in the endocytic or retrograde pathway and, hence, checked our lysates with streptavidin-HRP. As seen in **Figure 3.11**, we observed a robust biotinylation in the condition where both biotin-phenol and H_2O_2 were present. We even observed some discrete bands corresponding to biotinylated proteins in control cells lacking any EGFP reporter when biotin-phenol and H_2O_2 were both present. This most likely reflects the ability of endogenous peroxidases to transfer biotin onto neighboring proteins. We also observed bands at ~ 70 kDa and ~ 130 kDa (see black arrows in **Fig. 3.11**) in the condition where only one peroxidase substrate was present and thus no productive biotinylation reaction could occur. These bands correspond to endogenous biotinylated proteins, that are pyruvate carboxylase (~ 130 kDa) and propinyl-CoA carboxylase (~ 70 kDa). In both lysates and pull-downs, we observed a visible biotinylation reaction by APEX2 that was transported piggyback by EGFP-CDMPR or TfR-EGFP to intracellular compartments, demonstrating that the peroxidase can be exploited to label proteins in close proximity.

To see whether we could use proximity-dependent biotinylation as qualitative readout to assess TGN arrival of proteins of interest, we probed our streptavidin pull-downs from cells expressing EGFP-CDMPR with antibodies targeting TPST2, TGN46 and GalT. If these resident markers are in close proximity to the EGFP reporter, that cycles through the TGN, then they should be modified with biotin. For unknown reasons, we could not detect any biotinylated TPST2 or TGN46, suggesting that these proteins are either not in close proximity, sterically not well positioned for biotin modification or the amount of these proteins is just too scarce for detection. GalT, in contrast, was found in our streptavidin pull-downs, implicating that EGFP-CDMPR must have passed a GalT-positive compartment. In steady-

state, GalT is mainly localized to the trans-Golgi/TGN. However, it has to be noted that the signal derived from GalT in the streptavidin pull-downs was quite weak. We did not report any GalT to be present in streptavidin pull-downs derived from TfR-EGFP, in agreement with the notion that TfR and GalT only have poor colocalization in steady-state. As reported previously (**Fig. 3.10**), other endomembranes beyond the TGN (ER, calnexin) are not affected by biotinylation. Surprisingly, we could not recover the same relative amounts of EGFP-CDMPR/APEX2 in our pull-downs when compared to TfR-EGFP/APEX2. The reason for this is unknown.

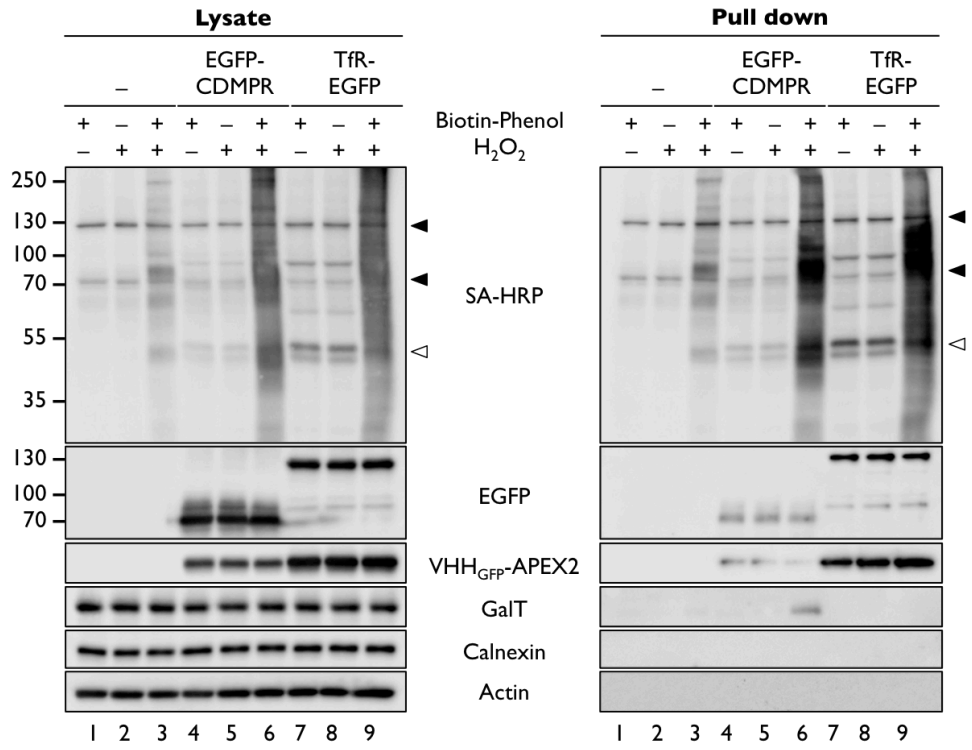

Figure 3.11: Proximity-dependent biotinylation analysis of EGFP-CDMPR and TfR-EGFP. Cells stably expressing either EGFP-CDMPR or TfR-EGFP were loaded with 5 μg/mL VHH_{GFP}-APEX2 for 1 h to reach steady-state. Following three washes, biotin-phenol labeling was initiated by adding fresh complete medium containing 500 μM biotin-phenol for 30 min at 37°C. Afterwards, H_2O_2 at a final concentration of 1 mM was added to the cells to start the reaction. After 3 minutes of labeling, the reaction was halted and quenched. Cleared cell lysates were then incubated with streptavidin beads followed by immunoblot analysis. Left panel with blots correspond to total cell lysate, right panel with blots correspond to streptavidin pull-downs. Black arrows indicate endogenous biotinylated proteins, the white arrow corresponds to APEX2 whose BAP epitope has been modified (even though no biotin was added during bacterial expression here). The faint smear (in SA-HRP) running in lane 3 (control cells) at nanobody migration speed does not correspond to VHH_{GFP}-APEX2. Legend: SA-HRP, streptavidin conjugated to HRP; GalT, β-1,4-galactosyltransferase. Numbers along the blots correspond to molecular weight in kDa. Experiments have been repeated at least three times.

An other perplexing finding we have made was that when we incubated with H_2O_2 too long (> 10 min), our antibody signal strongly declined in our cell lysates and pull-downs (even those from VHH_{GFP}-APEX2 and the EGFP reporters). It thus seems that extended biotinylation destroys epitopes for antibody recognition. While promiscuous BirA* can only modify lysine residues, peroxidases can modify much

more amino acids (tyrosines, tryptophans, and even histidines and cysteines). The risk of destroying epitopes for antibody recognition is thus considerably higher.

We have exemplified that APEX2-driven reactions can also be exploited to test whether a given protein of interest faces TGN-resident markers. We thus could use an improved system to test other reporters for appearance in the TGN using this proximity-dependent labeling approach. An alternative strategy to look more globally at biotinylated proteins by EGFP reporter/APEX2 complexes is by mass spectrometry. Indeed, Ting and colleagues have established and used this biotinylation-based setup to detect interaction partners of their proteins of interest by the means of proteomics (Branon et al., 2017; Hung et al., 2017; Hung et al., 2016; Hung et al., 2014; Lam et al., 2015; Rhee et al., 2013). Whenever there is a need to test weak or transient interactions, we can call in mind that APEX2 is suitable for this experimental endeavor.

3.5 Analysis of Retrograde Transport to the TGN

Although the previously described functionalized nanobodies could be used for studying cell surface-to-TGN transport, they have the disadvantage that retrograde transport kinetics cannot be directly measured. For VHH_{GFP}-mCherry, there is the indispensable requirement of stable overexpression of a fluorescent TGN-resident marker to perform live cell imaging, while for VHH_{GFP}-APEX2, only qualitative and no quantitative conclusions can be drawn concerning TGN arrival and localization. To overcome the drawbacks of each of these with regard to TGN arrival, we established nanobodies that can be modified by sulfation. Sulfation of tyrosines is a posttranslational modification that is exclusively restricted to the trans-Golgi/TGN (Baeuerle and Huttner, 1987; Huttner, 1988) where TPSTs reside and PAPS supply is high. Hence, by using tyrosine-sulfatable nanobodies that ride piggyback with EGFP reporters, we cannot only monitor arrival, but also determine retrograde transport kinetics to the TGN.

3.5.1 Biochemical Uptake of VHH_{GFP}-1xTS and -2xTS

To increase the efficiency of tyrosine sulfation, we preventively constructed nanobodies not only with one, but also with two tyrosine sulfation (TS) consensus sequences derived from of the rat cholecystokinin precursor (**Fig. 3.1 A** and **B**). To verify that VHH_{GFP}-1xTS and VHH_{GFP}-2xTS are efficiently internalized by EGFP reporter cell lines as previously monitored for VHH_{GFP}-control, VHH_{GFP}-mCherry and VHH_{GFP}-APEX2 (**Fig. 3.4** and **3.8**), nanobodies were applied for immunoblot and immunofluorescence analysis (Fig. **3.12 A-C**).

As reported for the other functionalized nanobodies (**Fig. 3.4** and **3.8**), TS-tagged derivatives are also internalized and distribute themselves along the same compartments as the reporters. Knowing that EGFP-CDMPR rides to the TGN as revealed by our APEX2 studies, we can biochemically test our nanobodies for TGN return using sulfate-radiolabeled nanobody as readout.

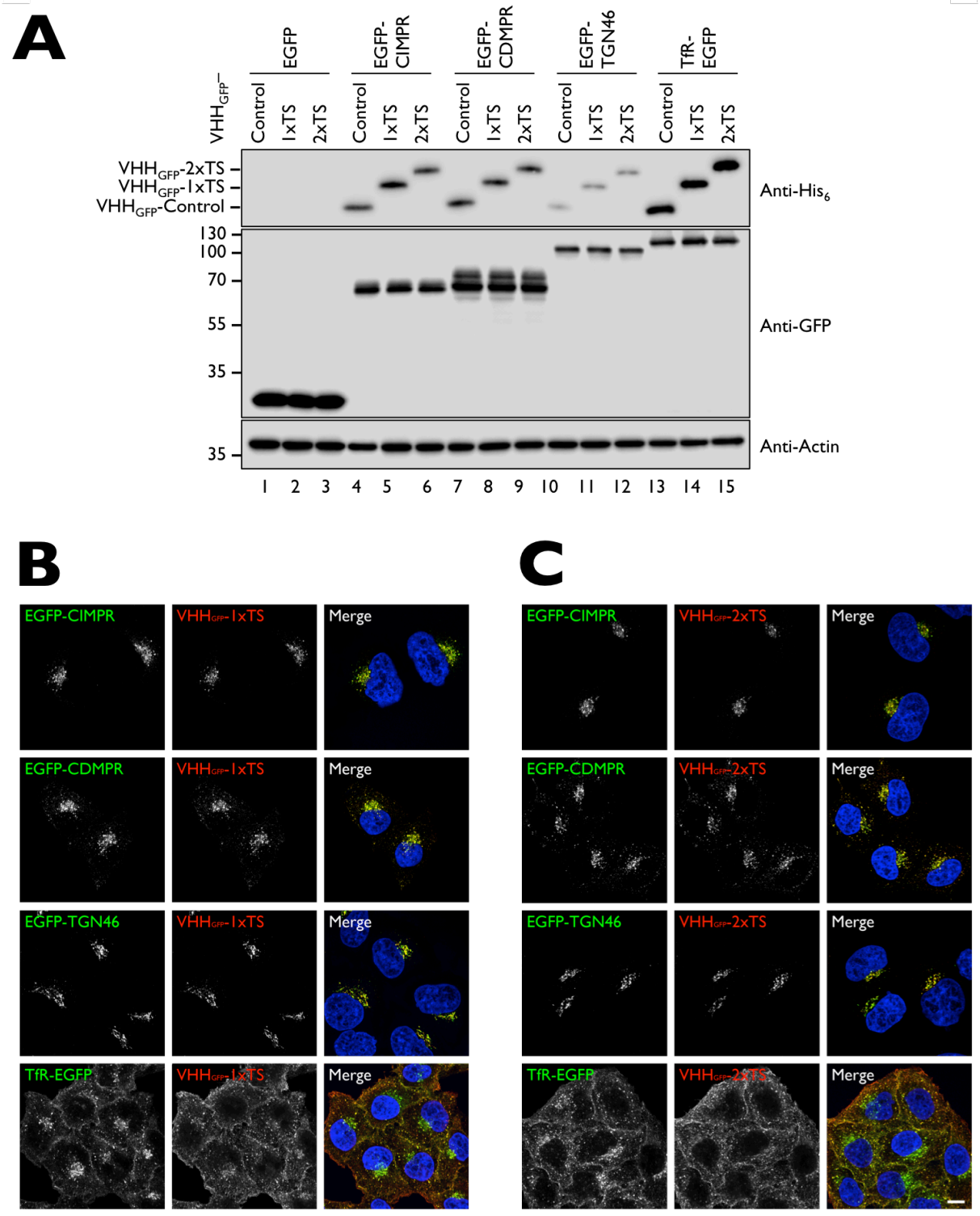

Figure 3.12: Endocytic uptake of VHH_{GFP}-1xTS and VHH_{GFP}-2xTS by EGFP reporter cell lines. (A) Functionalized nanobodies are specifically taken up by reporters presenting an EGFP moiety to the extracellular environment. HeLa cells stably expressing EGFP reporters were incubated in the presence of either 2 μg/mL VHH_{GFP}-control, VHH_{GFP}-1xTS or VHH_{GFP}-2xTS for 1 h at 37°C. Following uptake, cell lysates were prepared and probed with anti-His_6, anti-GFP and anti-actin antibodies. **(B)-(C)** Similar procedure as in (A). Cells on coverslips were fed with 2 μg/mL VHH_{GFP}-1xTS (B) or VHH_{GFP}-2xTS (C) and processed for fluorescence confocal microscopy. TS-tagged nanobodies were detected using an anti-HA antibody. Numbers along the markers correspond to molecular weight in kDa. Scale bar: 10 μm.

3.5.2 TGN Arrival Sulfation Analysis with VHH_{GFP}-1xTS and -2xTS

To analyze sulfation, cells expressing cytosolic EGFP or secretory reporters were incubated with functionalized nanobodies in the presence of radiolabeled [^{35}S]sulfate at 37°C for 1 h. The postnuclear supernatant was harvested and incubated with Nickel sepharose beads to affinity-isolate potentially sulfated VHH_{GFP} derivatives. In parallel, a fraction of the postnuclear supernatant was saved as reference for the total amount of cell-associated VHH_{GFP}-1xTS/2xTS or as loading reference. Radioactive signals were assessed by SDS gel electrophoresis and autoradiography, while uptake and the loading reference was evaluated by immunoblot analysis (**Fig. 3.13**).

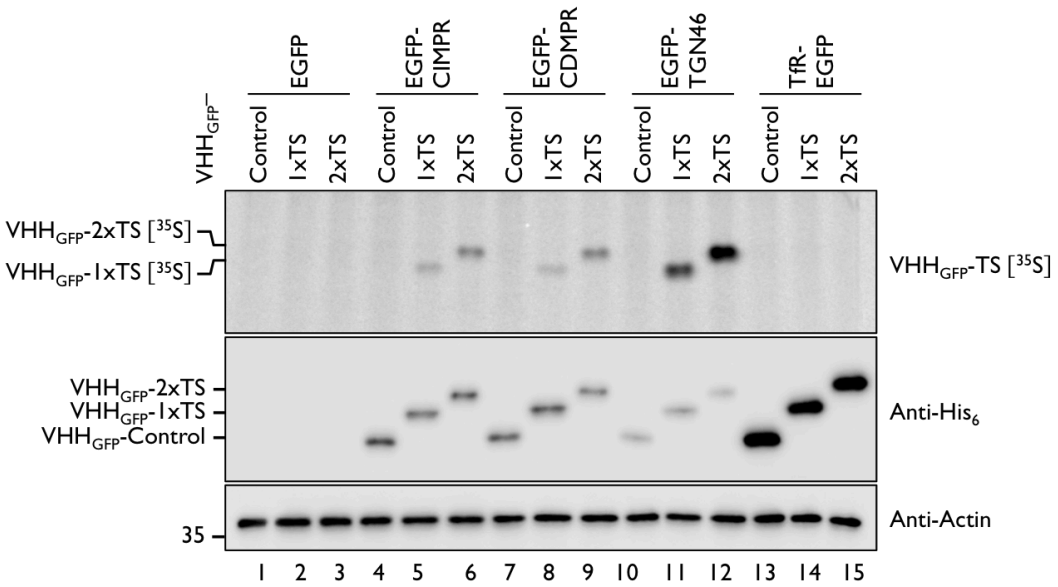

Figure 3.13: TGN arrival sulfation analysis in EGFP reporter cell lines. Cells stably expressing cytosolic EGFP or secretory reporter proteins were starved in sulfate-free medium for 1 h at 37°C and 7.5% CO_2, and then pulse-labeled with sulfate-free medium reconstituted with 0.5 mCi/mL [^{35}S]sulfate supplemented with 2 µg/mL of either VHH_{GFP}-control, VHH_{GFP}-1xTS or VHH_{GFP}-2xTS for up to 75 min. Postnuclear supernatants were collected and incubated with Nickel beads to affinity-isolate nanobodies. A fraction of the postnuclear supernatant was saved as reference for the total amount of cell-associated nanobody or as loading control. Proteins were separated using gel electrophoresis and prepared for autoradiography. Cell-associated nanobody was detected using an anti-His_6 antibody. Numbers along the markers correspond to molecular weight in kDa.

As expected from previous results, there is no visible nanobody uptake by cells expressing cytosolic EGFP (**Fig. 3.13**, lanes 1-3). Conversely, cells expressing recombinant MPRs show a specific sulfation signal at the molecular weight of the respective TS-modified nanobody (**Fig. 3.13**, lanes 5-6 and 8-9), while there is no signal from the nanobody lacking a TS motif in these reporters (**Fig. 3.13**, lanes 4 and 7). In addition, the degree of sulfation between the MPR reporters is similar, but in general with more incorporation of radiolabeled sulfate into VHH_{GFP}-2xTS. Even though we monitored sparse uptake of nanobodies into cells expressing EGFP-TGN46 relative to the other reporters throughout this study, we observed a higher degree of sulfation for TGN46 (**Fig. 3.13**, lanes 11 and 12), and this even under conditions where TGN46 is not yet in steady-state (see also **Fig. 3.5 C** and **E**). The higher degree of sulfation is most likely explained by the longer residence time of the reporter in the compartment of

labeling. MPRs, on the contrary, dynamically move in and out from the TGN, thus having a much shorter time to face the sulfation machinery.

To complete our uptake experiments and demonstrate the overall specificity of nanobody uptake by confocal immunofluorescence microscopy, we fed VHH_{GFP}-2xTS (any other derivatives are possible, too) to cells expressing either cytosolic EGFP or fusions residing in the early secretory pathway (**Fig. S5**). Popular markers for the early secretory pathway are the quality control chaperone calnexin (ER) and the lectin ERGIC53 (ERGIC). We did not see any nanobody uptake by cells expressing either cytosolic EGFP, EGFP-calnexin or EGFP-ERGIC53, indicating that a reporter presenting an EGFP moiety to the extracellular environment is a prerequisite for VHH_{GFP} internalization (see also **Fig. S3 D**).

Since there was stronger sulfate incorporation into VHH_{GFP}-2xTS (**Fig. 3.13**), we continued to use this version for our future studies. Apart from VHH_{GFP}-1xTS and VHH_{GFP}-2xTS, we also generated and bacterially expressed a TS-tagged version (TS-VHH_{GFP}-TS), where the sulfation consensus was present both at the N- and C-terminus. However, this nanobody was much worse than VHH_{GFP}-2xTS, but comparable if not even worse to VHH_{GFP}-1xTS (**Fig. S6**).

Our nanobody-based approach offers us a direct way to biochemically study cell surface-to-TGN transport of EGFP fusion proteins using sulfation. Our attempts are not only restricted to do qualitative statements based on simple pulse experiments, but also can be expanded to quantitative analysis of kinetic transport to the TGN.

3.5.3 TGN Arrival Kinetics of MPRs with VHH_{GFP}-2xTS

As proof-of-concept to study retrograde transport kinetics to the TGN, we chose MPRs as reporters. After AP-2/clathrin-mediated endocytosis, endosome-to-TGN transport of MPRs has been reported to be mediated by different sorting machineries, including retromer (Arighi et al., 2004; Seaman, 2004), epsinR- (Saint-Pol et al., 2004) and AP-1/clathrin-coated carriers (Meyer et al., 2000; Robinson et al., 2010) from early endosomes, as well as Rab9/TIP47-dependent transport (Diaz and Pfeffer, 1998; Lombardi et al., 1993) from late endosomes (discussed in the introduction). It is suggested that the overlapping or orchestrated action of these pathways might mediate retrieval of the hydrolase cargo receptor to the TGN. It remains elusive and to be determined what the individual contribution of each of these pathways is to ensure proper TGN relocalization of MPRs.

To generally interfere with retrograde transport, we decided to use the fungal metabolite Brefeldin A (BFA) that inhibits guanine exchange factors (GEFs) of the ARF protein family. ARF proteins, mainly ARF1, have been shown to recruit adaptors, such as AP-1 and epsinR, to endosomal membranes, but not retromer complex and Rab9/TIP47 which membrane-associate in an ARF-independent manner. To follow transport kinetics to the compartment of labeling using VHH_{GFP}-2xTS, we pulsed cells stably expressing EGFP-CIMPR and EGFP-CDMPR for up to 75 min with [^{35}S]sulfate in the presence or absence of BFA (**Fig. 3.14 A-D**). Cells were harvested after each time point, incubated with nickel beads and analyzed by autoradiography. As before, nanobody uptake by the MPRs reached steady-state after 45 min. In contrast, sulfation started only after a lag time of > 15 min and did not yet reach maximum after 75 min.

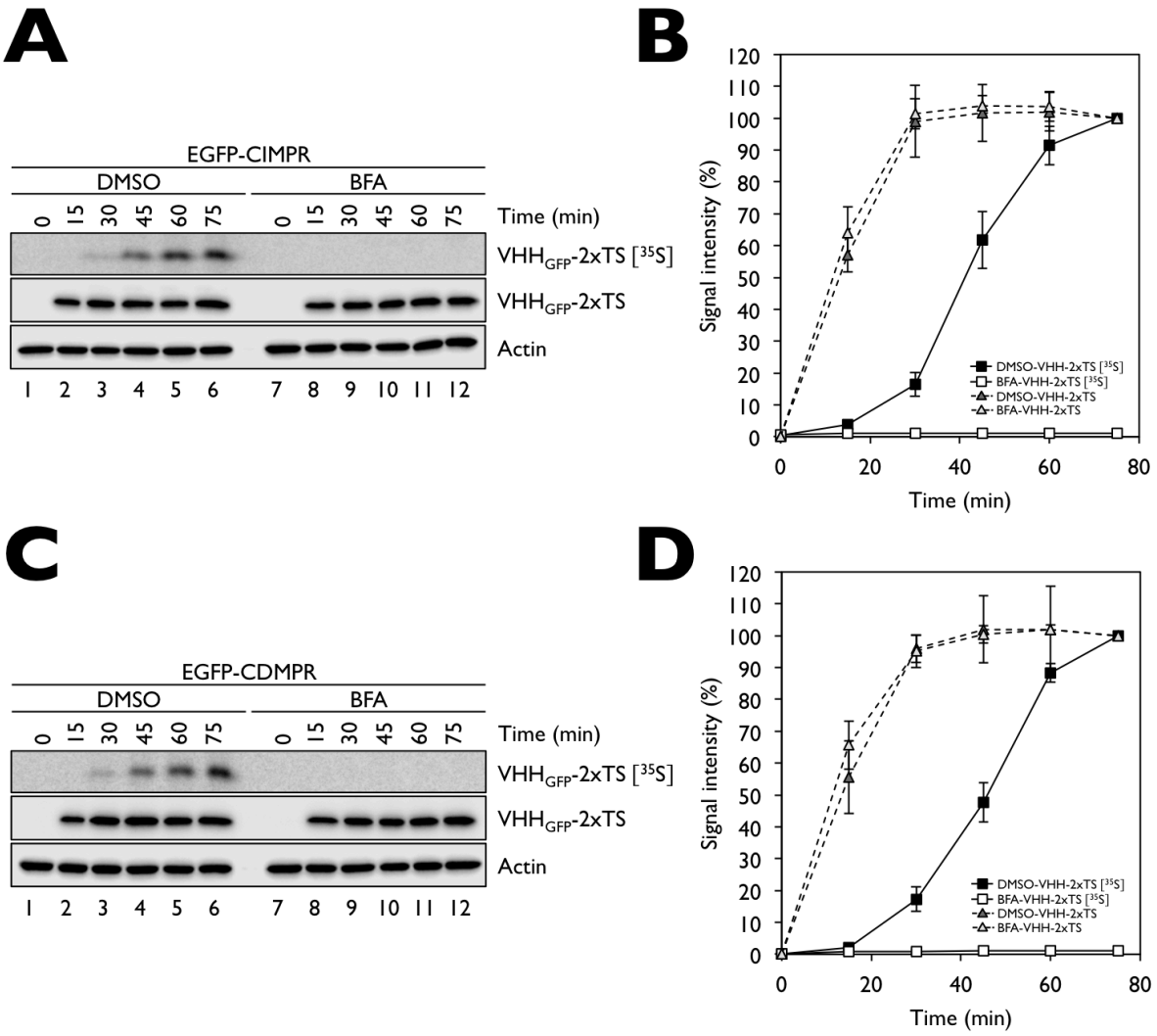

Figure 3.14: Cell surface-to-TGN transport kinetics of MPRs. (A) and **(C)** Cells stably expressing either EGFP-CIMPR or EGFP-CDMPR were starved in sulfate-free medium for 1 h at 37°C and 7.5% CO_2, and then pulse-labeled with sulfate-free medium reconstituted with 0.5 mCi/mL [^{35}S]sulfate supplemented with 2 µg/mL of VHH$_{GFP}$-2xTS for up to 75 min. BFA was used at 2 µg/mL during the pulse. Postnuclear supernatants were collected and incubated with Nickel beads to affinity-isolate sulfated nanobody. A fraction of the postnuclear supernatant was saved as reference for the total amount of cell-associated VHH$_{GFP}$-2xTS or as loading control. Proteins were separated using gel electrophoresis and prepared for autoradiography. Cell-associated VHH$_{GFP}$-2xTS nanobody was detected using an anti-His$_6$ antibody. **(B)** and **(D)** Quantification of retrograde transport kinetics. Quantification of three independent experiments is shown (average ± SD). Signal intensities of each time point is expressed as the percentage of the signal intensity after 75 min. Black and white squares belong to kinetics of sulfation, grey triangles correspond to kinetics of cellular uptake. Data points of sulfation kinetics between DMSO and BFA were at least $p < 0.05$ statistical significant.

The observed difference between maximal uptake and sulfation of nanobody can have diverse reasons. First, and most relevantly, MPRs have a complex retrograde transport itinerary, with trajectories through early endosomes, late endosomes, and possibly even with multiple round trips in these compartments before reaching the TGN. Additionally, MPR-captured nanobody could also reencounter the cell surface for other rounds before migrating to the TGN for being sulfated. Second, sulfation of the nanobody likely depends on the residence time and one transit through the TGN will only cause partial

sulfation of the four tyrosines present that might be completed only after multiple cycling rounds. Another point in light of dwelling time in the TGN is the inherent feature of the receptor to dynamically cycle at the endosome-to-TGN interface. Consequently, the delayed increase in sulfation might be a consequence of all these parameters.

Consistent with the notion of BFA to inhibit retrograde transport (Amessou et al., 2007; Mallard et al., 1998), we observed a robust, if not complete block in retrograde transport to the compartment of labeling (**Fig. 3.14 A-D**). We even reported inhibition of retrograde transport at concentrations lower than 2 μg/mL of BFA, indicating that the observed effect is due to inhibition of ARF-dependent processes, rather than of reported secondary effects of the fungal metabolite (Fjeldstad et al., 2002). Interestingly and surprisingly, while retrograde transport was blocked by BFA, uptake of nanobody into cells and above all steady-state levels were not significantly affected. This suggests that the pool of MPRs residing in the TGN is not trapped and still able to traffic out to the cell surface. Otherwise similar levels of internalized nanobody in the presence or absence of BFA would not have been detected. It has been previously shown that BFA in general does not impair cellular uptake into cultured cells (Damke et al., 1991; Hunziker et al., 1992; Lippincott-Schwartz et al., 1991; Prydz et al., 1992).

3.6 Knocksideways of AP-1-Dependent Retrograde Transport

As discussed in the introduction, the precise contribution of AP-1 in retrograde transport is still unclear. Most of the conclusions regarding directionality were based on mislocalization of AP-1-dependent cargo deduced from altered steady-state distribution. Furthermore, most of these studies were conducted with indirect approaches or such with possible secondary effects. Our tyrosine-sulfatable nanobody (VHH_{GFP}-2xTS) offers us the opportunity of studying kinetics. To selectively and rapidly interfere with the AP-1 transport machinery, we used the recently described knocksideways technique (Robinson and Hirst, 2013; Robinson et al., 2010).

3.6.1 Rapid Inactivation of AP-1 by Knocksideways

The knocksideways (KS) approach, pioneered by Margaret Robinson (Robinson et al., 2010), describes the rapid sequestration and thus inactivation of FKBP-modified target proteins onto mitochondria by rapamycin-induced heterodimerization with a FRB-tagged mitochondrial bait protein called Mitotrap (see also introduction 1.4). Compared to a conventional knockdown or knockout, the knocksideways technique has the advantage of eliminating the problem of gradual or long-term protein loss during which the cell might switch on compensatory pathways, or accumulate indirect effects of protein depletion over time. Since protein traffic in the retrograde pathway and, hence, at the endosome-to-TGN interface, is a concerted action of a vast number of cytosolic factors (i.e. ARF and Rab GTPases, coat adaptors, tethering factors, lipid kinases and phosphatases, etc.) in a complex network, rapid inactivation rather than siRNA-mediated gradual depletion of proteins is strongly favored in order to look at immediate consequences of impaired traffic.

We established the AP-1 knocksideways system (with minor modifications) in our HeLa cells. To mitochondrially trap FKBP-tagged AP-1, we generated a Mitotrap composed of the targeting sequence of the yeast mitochondrial outer membrane protein Tom70p, followed by a mutant FRB domain, and a 3xFLAG epitope. The mutant FRB domain has a threonine to leucine point mutation that enables it to bind not only rapamycin, but also the rapalog AP21967. The latter, however, can no longer bind to the full-length wild-type FRB-containing domain of mTOR. As AP-1 prey, we used the same protein sequence as previously described (Robinson et al., 2010). Using these constructs, we first retrovirally transduced our parental HeLa to generate a Mitotrap cell line, and then with the AP-1 prey to obtain the AP-1 knocksideways cells line. Single clones were picked and analyzed.

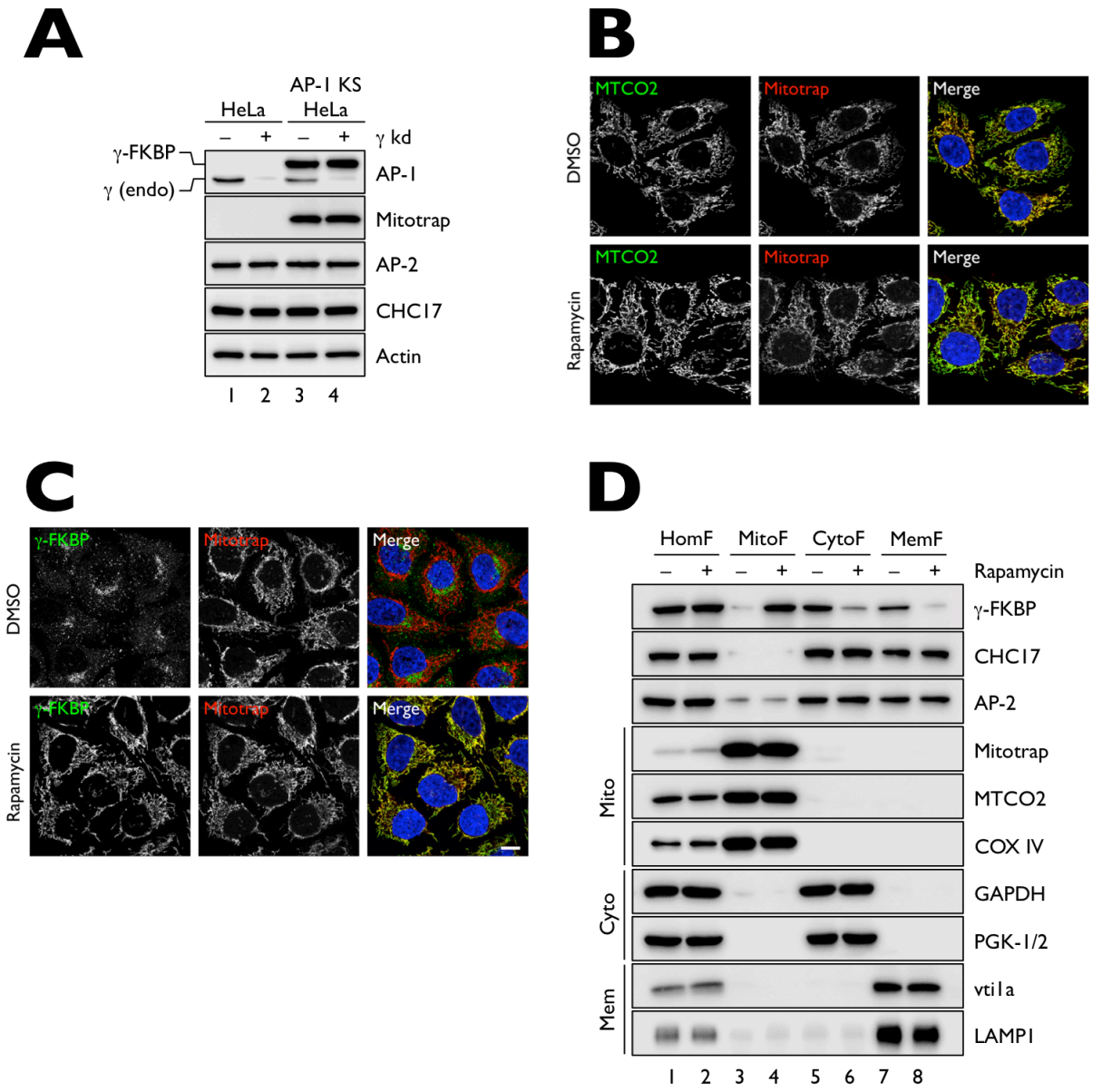

Figure 3.15: Characterization of the AP-1 knocksideways cell line. (A) Lysates from AP-1 KS cells were prepared and probed against AP-1 (γ-adaptin), Mitotrap (anti-FLAG), AP-2 (α-adaptin) and clathrin (CHC17). Equal amounts of proteins were loaded. **(B)** siRNA-treated AP-1 KS cells were seeded on coverslips, treated with 500 nM rapamycin and processed for fluorescence confocal microscopy. Mitochondria were detected with an antibody targeting MTCO2, Mitotrap was labeled with an anti-FLAG antibody. **(C)** siRNA-treated AP-1 KS cells were seeded on coverslips, treated with 500 nM rapamycin for 10 min and processed for fluorescence confocal microscopy. Recombinant γ-FKBP was specifically detected using an antibody targeting a recombinant epitope present in the neuronal splice variant of α-adaptin, Mitotrap was labeled with an anti-FLAG antibody. **(D)** Crude isolation of mitochondria from AP-1 KS cells. Confluent 100 mm dishes containing AP-1 KS cells were treated with DMSO or 500 nM rapamycin for 10 min, homogenized, and fractions of mitochondria, cytosol and membranes were collected. Fractions were probed with antibodies targeting membranes (vti1a, LAMP1), cytosol (GAPDH and PGK-1/2), mitochondria (Mitotrap, MTCO2, COX IV) and CCV machinery components (γ-FKBP of AP-1, α-adaptin of AP-2, CHC17). Scale bar: 10 μm.

Figure 3.15 A shows a typical lysate harvested from clone 9 of our generated AP-1 KS HeLa cell line. As shown by immunoblotting using an anti-FLAG antibody, only AP-1 knocksideways cells showed expression of recombinant Mitotrap (**Figure 3.15 A**, lanes 3-4). Since only the recombinant, functional

and siRNA-resistant AP-1 subunit (γ-adaptin) should take over, knocksideways requires the preceding depletion of the endogenous counterpart of the prey. In parental HeLa cells, we typically observed KD efficiencies of > 85% for endogenous γ (**Figure 3.15 A**, lanes 1-2). AP-1 KS cells, which show a higher recombinant γ-FKBP expression, are, as expected, not affected by RNAi with regard to the recombinant construct. Surprisingly, AP-1 KS cells showed a considerably lower expression of endogenous γ-adaptin than their parental cell line. This observation is most likely explained by the competition between endogenous and the recombinant subunit. Unbound free γ-adaptin is rapidly degraded, and hence, since there is excess of the recombinant subunit, it is preferentially assembled into the functional heterotetrameric adaptor complex compared to the endogenous one (**Figure 3.15 A**, lanes 1 and 3). In both the parental and stable cell line, there is no change in the expression of other trafficking components, such as of clathrin (CHC17) or α-adaptin (AP-2), due to silencing of AP-1.

Since we decided to use rapamycin rather than the rapalog AP21967 to heterodimerize FKBP- and FRB-fusion proteins, we first checked whether addition of rapamycin influences overall mitochondrial morphology. The reason for applying rapamycin rather than the synthetic heterodimerizer was that the latter needs to be applied at much higher concentrations to get comparable heterodimerization phenotypes, as previously already reported for getting a robust knocksideways of prey proteins (Robinson and Hirst, 2013). In general, we did not see striking differences between DMSO and rapamycin-treated cells, as judged by stainings of the mitochondrial marker MTCO2 and Mitotrap (**Figure 3.15 B**). In contrast, recombinant FKBP-tagged AP-1 was almost completely rerouted to mitochondria after 10 min of rapamycin addition (**Fig. 3.15 C**), consistent with previous reports illustrating the principle of AP-1 KS (Hirst et al., 2012a; Robinson et al., 2010).

Since rapamycin interferes with mTOR signaling, we were wondering to which magnitude the mTOR pathway is affected in our KS system. It would be a drawback of the KS technique if an observed phenotype would be a result of both mitochondrial prey sequestration and impaired mTOR downstream pathways. To check the extent of mTOR inhibition in our AP-1 KS cell line, we treated parental HeLa and AP-1 KS cells with rapamycin for up to 75 min, harvested the cells and immunoblotted against the mTORC1 downstream target ribosomal protein S6 (**Fig. S7 A**). As expected from previous studies, parental HeLa cells quickly responded to rapamycin treatment after 30 min of incubation and had almost undetectable levels of Phospho-S6 (Ser235/236) at 75 min. Surprisingly, our AP-1 KS cells did not show that a significant reduction in Phospho-S6 (Ser235/236) levels after 75 min. This thus suggests that the AP-1 KS cell line is partially resistant to rapamycin administration, as judged by reduced mTOR inhibition. The reason for the decreased susceptibility might be explained by the fact that apart from γ-FKBP also endogenous FKBP12 is trapped on mitochondria, thereby not only knocking sideways AP-1, but also 'the mTORC1 pathway' to a certain extent. The same statement might be the case for a Mitotrap-only-expressing cell line. Unfortunately, due to the lack of working antibodies (**Fig. S7 B-D**), we could not prove our hypothesis of mitochondrial FKBP12 sequestration. There was no specific signal present for any antibodies. Additionally, we also do not know whether the FKBP subunit present in γ-FKBP can heterodimerize with the FRB domain of mTOR1 to inhibit downstream effectors. However, our data

suggest that the mTOR pathway is only partially affected upon rapamycin administration within the assessed time of 75 min.

To biochemically demonstrate rapamycin-triggered mitochondrial relocalization of FKBP-modified AP-1, subcellular fractionation was performed to enrich mitochondria, cytosol and membranes. While recombinant AP-1 was substantially rerouted to the mitochondrial fraction with concomitant loss from the cytosolic and membrane fraction in rapamycin-treated cells (**Fig. 3.15 D**), other coats or coat components (AP-2, CHC17) did not follow AP-1 onto mitochondria. The residual and minor levels of γ-FKBP in the cytosol or on membranes indicate that either mitochondrial trapping was not as complete as the immunofluorescence suggested, preparation by homogenization might have caused AP-1 to be disconnected from membranes, or that a subpopulation of AP-1 has a longer residence time (longer k_{off}) on membranes, respectively. However, the biochemical readout obtained by mitochondria isolation reflects what we have observed by immunofluorescence, i.e. sequestration of AP-1 onto mitochondria upon rapamycin addition.

3.6.2 Retrograde Transport of MPRs Is Impaired by AP-1 Knocksideways

Having established the basis for rapid AP-1 inactivation, we now combined it with our nanobody assay to study its involvement in retrograde transport. To this end, we set out to establish a triple stable cell line expressing the knocksideways components (γ-FKBP and Mitotrap) and either EGFP-CIMPR or EGFP-CDMPR, respectively. Cell lines were generated by retroviral transduction of the described AP-1 KS cell line (**Fig. 3.15**) with the corresponding MPR reporters, followed by blasticidin selection and FACS. Since reporter-transduced AP-1 KS cell lines were derived from our characterized clone 9, we did not see any changes in fusion protein expression (γ-FKBP, Mitotrap) or endogenous markers (CHC17, AP-2), apart from that we have additional expression of either EGFP-CIMPR or EGFP-CDMPR (**Fig. 3.16 A** and **C**).

To confirm the functionality of our AP-1 KS cell lines, we looked at the steady-state distribution of the recombinant MPR reporters after AP-1 inactivation. To do so, we silenced endogenous γ-adaptin, treated cells for 1 h with rapamycin, and proceeded with immunofluorescence. We detected a higher ratio of peripheral to juxtanuclear steady-state localization of both EGFP-modified reporters (**Fig. 3.16 B** and **D**). This observation is in agreement with previous reports after knockouts (Medigeshi and Schu, 2003; Meyer et al., 2000), after knockdowns (Robinson et al., 2010), after drug-mediated inhibition (Stahlschmidt et al., 2014), or after knocksideways (Robinson et al., 2010). Since we considered here total protein (**Fig. 3.16 B** and **D**), the mislocalization phenotype is less pronounced than in the anti-CIMPR antibody uptake experiment (Robinson et al., 2010), though.

Rather than doing antibody uptake experiments to look at peripherally clustered and accumulated CIMPR in AP-1-inactivated cells by immunofluorescence, we sought to use VHH_{GFP}-2xTS in combination with a sulfation assay to look at the contribution of AP-1 in retrograde transport. For this purpose, AP-1 KS cells stably expressing EGFP reporters were pulsed with radiolabeled sulfate in the presence of VHH_{GFP}-2xTS and rapamycin for up to 75 min, harvested and analyzed by autoradiography (**Fig 3.17 A-D**).

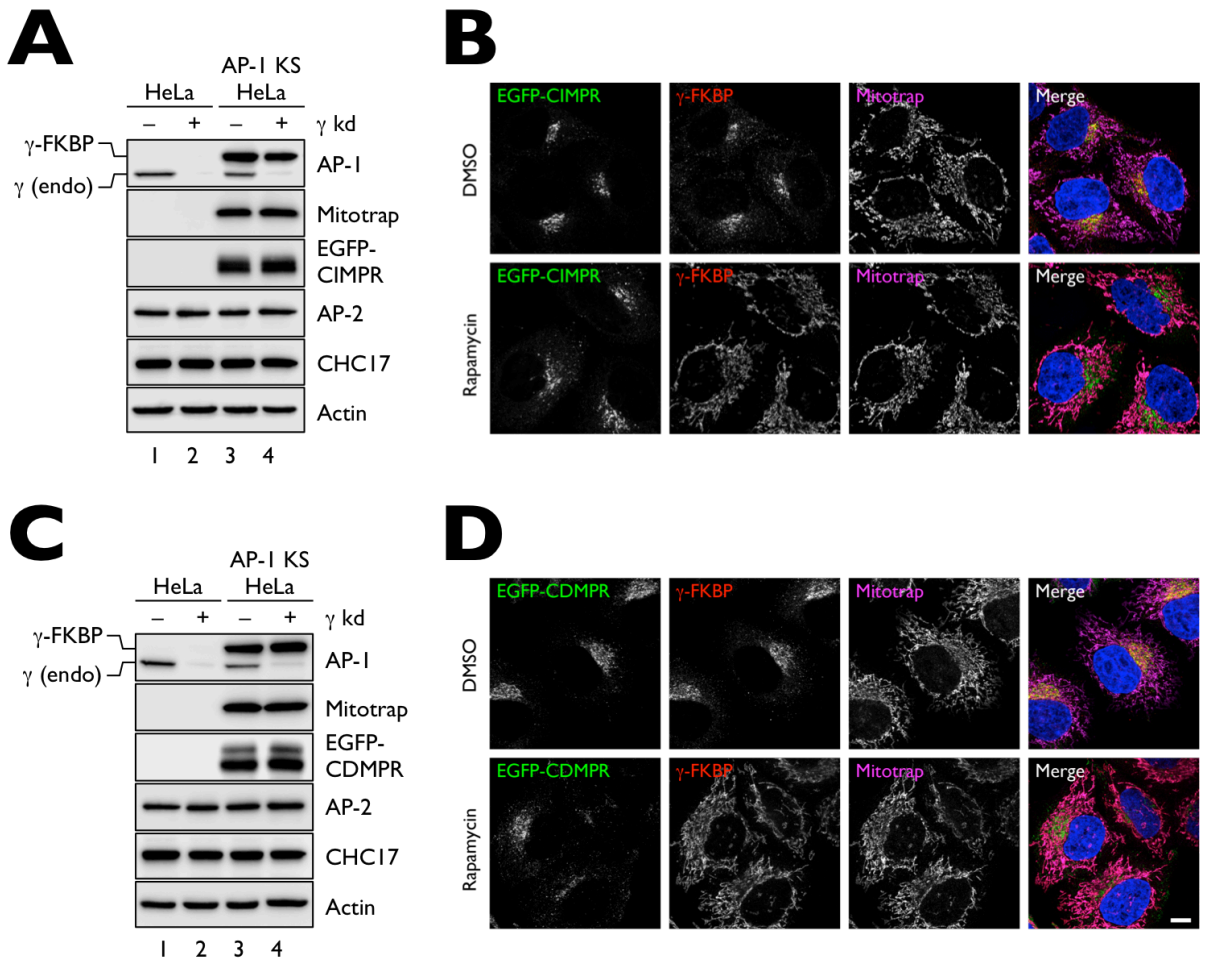

Figure 3.16: AP-1 knocksideways cells stably expressing EGFP-tagged MPR reporters. (A) and **(C)** Lysates from AP-1 KS cells stably expressing EGFP-CIMPR or EGFP-CDMPR were prepared and probed against AP-1 (γ-adaptin), Mitotrap (anti-FLAG), EGFP-CIMPR or EGFP-CDMPR (anti-GFP), AP-2 (α-adaptin) and clathrin (CHC17). Equal amounts of proteins were loaded. **(B)** and **(D)** siRNA-treated AP-1 KS cells stably expressing EGFP-CIMPR or EGFP-CDMPR were seeded on coverslips, treated with 500 nM rapamycin for 1 h and processed for fluorescence confocal microscopy. Recombinant γ-FKBP was specifically detected using an antibody targeting a recombinant epitope present in the neuronal splice variant of α-adaptin, Mitotrap was labeled with an anti-FLAG antibody. Scale bar: 10 μm.

For both MPRs, we observed a delay in sulfation in rapamycin-treated (AP-1-inactivated) cells. At 75 min, for instance, the level of sulfation is reduced by a third when compared to control cells. While the degree of sulfation between rapamycin-treated and -untreated cells differed, we did not see apparent alterations in nanobody uptake over the measured time (**Fig 3.17 A-D**). These results suggest AP-1 to be partially involved in retrograde transport from endosomes to the TGN.

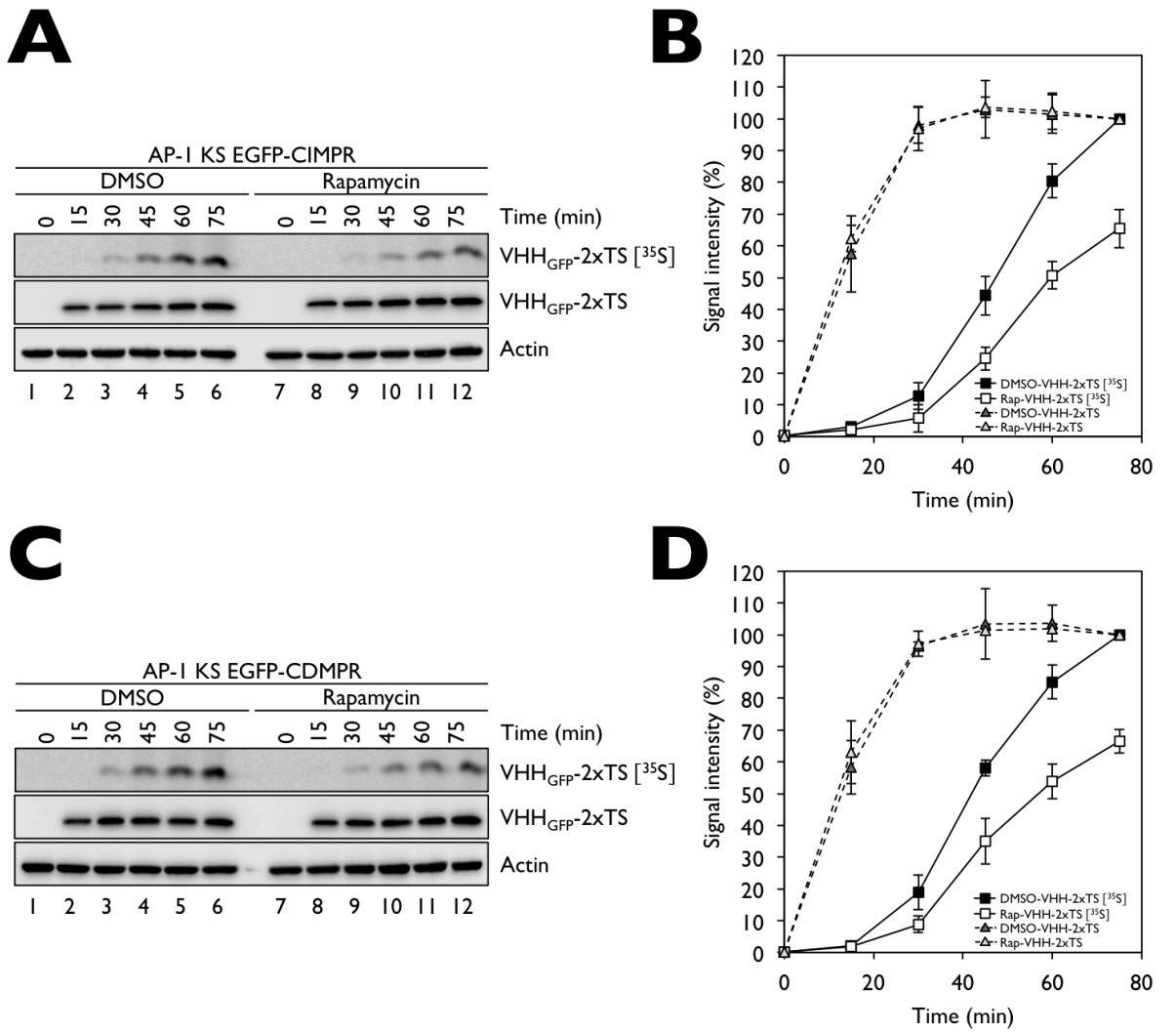

Figure 3.17: Cell surface-to-TGN transport kinetics of MPRs in AP-1 knocksideways cells. (A) and **(C)** AP-1 KS cells stably expressing either EGFP-CIMPR (A) or EGFP-CDMPR (C) were starved in sulfate-free medium for 1 h at 37°C and 7.5% CO_2, and then pulse-labeled with sulfate-free medium reconstituted with 0.5 mCi/mL [^{35}S]sulfate supplemented with 2 µg/mL of VHH_{GFP}-2xTS for up to 75 min. Rapamycin was used at a concentration of 500 nM during the pulse. Postnuclear supernatants were collected and incubated with Nickel beads to affinity-isolate sulfated nanobody. A fraction of the postnuclear supernatant was saved as reference for the total amount of cell-associated VHH_{GFP}-2xTS or as loading control. Proteins were separated using gel electrophoresis and prepared for autoradiography. Cell-associated VHH_{GFP}-2xTS nanobody was detected using an anti-His_6 antibody. **(B)** and **(D)** Quantification of retrograde transport kinetics. Quantification of three independent experiments is shown (average ± SD). Signal intensities of each time point is expressed as the percentage of the signal intensity after 75 min. Black and white squares belong to kinetics of sulfation, grey triangles correspond to kinetics of cellular uptake. Data points of sulfation kinetics between DMSO and rapamycin were at least $p < 0.05$ statistical significant.

3.7 Alternative Retrograde Transport Pathways to the TGN

The only partial reduction of sulfated VHH_{GFP}-2xTS nanobody in knocksideways cells suggests that AP-1-independent retrograde transport routes for MPRs from endosomes coexist. Indeed, evidence for alternative sorting machineries operating from early, recycling or late endosomes to deliver cargo back to the TGN have been reported (see also introduction), among them retromer (Arighi et al., 2004; Bonifacino and Hurley, 2008; Carlton et al., 2004; Carlton et al., 2005; Hierro et al., 2007; Seaman, 2004), epsinR/clathrin (Saint-Pol et al., 2004) and Rab9/TIP47 (Carroll et al., 2001; Diaz and Pfeffer, 1998; Diaz et al., 1997; Riederer et al., 1994). It is thus likely that the concerted action of these trafficking machineries, and not of AP-1 alone only, facilitates retrograde transport to the TGN. This hypothesis is supported by the notion of MPRs to have a multitude of diverse cytosolic sorting determinants that might permit TGN retrieval from any level of the endocytic pathway by diverse machineries.

To examine to which extent transport of MPRs is dependent on such alternative pathways, we sought to individually interfere with them. Ideally, knocksideways of these machinery components would be the best choice for specific and rapid interference. Since establishing a knocksideways system for every machinery component is a cumbersome procedure and would go beyond the scope of our topic, we decided to target individual machinery coat components by RNAi-mediated knockdown.

To this end, we set out to assay retrograde transport of MPRs in Vps26 (retromer)-, TIP47-, and Rab9-depleted HeLa cells using VHH_{GFP}-2xTS. We did not consider to include epsinR in our studies since Ludger Johannes and colleagues (Saint-Pol et al., 2004) have previously demonstrated that this monomeric adaptor is not only involved in retrograde transport of Shiga toxin and TGN46, but also of CIMPR.

3.7.1 Interference with Alternative Retrograde Transport Pathways

RNAi-Mediated Depletion of Alternative Retrograde Transport Components

To assess the knockdown efficiencies of Vps26-, Rab9- and TIP47-depleted cells, we transiently reverse-transfected HeLa cells with specific and well-described siRNA duplexes (Bulankina et al., 2009; Ganley et al., 2004; Hirst et al., 2005; Hirst et al., 2003; Popoff et al., 2009; Popoff et al., 2007a; Reddy et al., 2006). After a period of 96 h, cells were harvested and immunoprobed against various markers. Since we were also curious about readouts of an AP-1 knockdown, we also included AP-1-depleted cells in our studies. Apart from TIP47, we reached robust depletion of Vps26, Rab9 and AP-1 with knockdown efficiencies greater than 90% (**Fig. 3.18 A** and **B**).

As expected for a multimeric protein coat such as AP-1 and retromer complex, we observed concomitant depletion of other coat complex subunits. While siRNA-mediated depletion of μ1A-adaptin resulted in the concomitant and partial loss of γ-adaptin, Vps26-depleted cells showed a slight reduction in Vps35 levels. The sorting nexins 1 and 2 (SNX1 and SNX2), conversely, were not significantly affected. This is in agreement with previous reports suggesting the pentameric retromer complex to be composed of an independent dimeric (with SNX1 or SNX2) and trimeric (Vps26-Vps29-Vps35) subcomplex (Fuse et

al., 2015; Rojas et al., 2007a; Rojas et al., 2008). As expected, depletion of neither Rab9 nor TIP47 affected the stability of the other markers (**Fig. 3.18 A** and **B**).

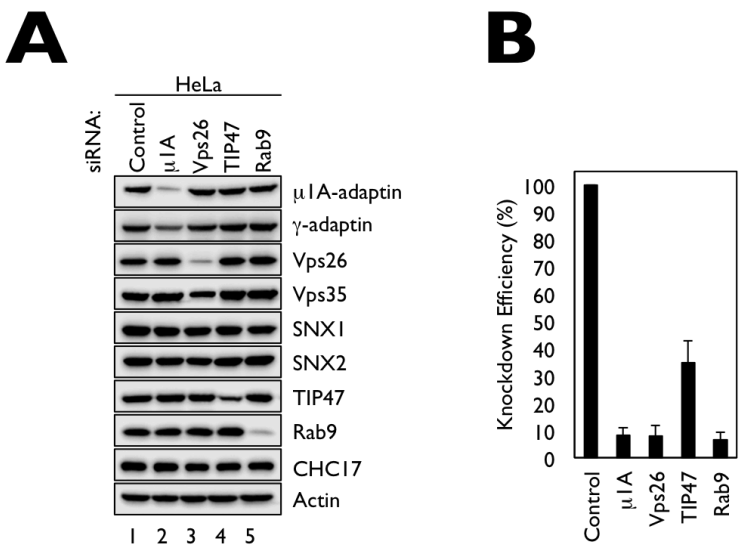

Figure 3.18: Knockdown of alternative transport pathways. (A) HeLa cells were reverse-transfected with the indicated siRNAs and harvested after 96 h. Immunoblots were probed with markers against μ1A-adaptin, γ-adaptin (both AP-1), Vps26, Vps35, SNX1, SNX2 (all retromer complex), TIP47, Rab9 and clathrin. Actin was used as reference. **(B)** Quantification of knockdown efficiencies. Quantification of three independent experiments is shown (average ± SD). Signal intensities of each knockdown is expressed as the percentage of the control.

RNAi-Mediated Inhibition of the Retromer Complex Pathway

We next wanted to see how retrograde transport of MPRs is affected in cells depleted of Vps26, TIP47, Rab9 and μ1A. We decided to use EGFP-CDMPR as our reporter in this part of the study since it represents, unlike EGFP-CIMPR, the full-length receptor version. In order to study retrograde cell surface-to-TGN transport of EGFP-CDMPR, we reverse-transfected stable cells with siRNAs for 96 h and performed a sulfation assay as described beforehand.

We observed a significant reduction of sulfation of VHH_{GFP}-2xTS riding piggyback with the recombinant receptor to the TGN in Vps26-depleted cells (**Fig. 3.19 A** and **B**). After 75 min of labeling, we could observe a ~ 50% reduction in sulfation, while nanobody uptake into cells was not altered significantly. It has been previously reported that retromer is acting as one of the prime machineries in delivering the empty hydrolase receptor from an endosomal compartment to the TGN. However, all what we know about its function in CIMPR retrieval is based on protein-protein interaction studies and immunofluorescence data. Our nanobody-based approach allowed us to investigate retrograde traffic from endosomes in a different manner. Instead of looking at steady-state reporter redistribution in fixed cells, we could measure transport kinetics to the compartment of labeling. However, as a drawback, the endosomal transit stations en route to the TGN cannot be deciphered directly with any previous knowledge.

Concerning the retromer complex, literature is inconsistent on which endosomal compartment (early or late) it assembles. Electron microscopy studies have demonstrated the retromer complex to

assemble on tubular elements of tubular-vacuolar structures reminiscent of early endosomes. In addition to that, retromer complex colocalizes with EEA1 and Tf, markers characteristic to early endosomes. Moreover, there are also a vast number of reports showing the complex to functionally cooperate with clathrin in sequential staging during carrier formation (Johannes and Wunder, 2011; Popoff et al., 2009; Popoff et al., 2007a). Clathrin, so far, has been shown to localize only to early, but not late endosomes. Conversely, retromer complex is membrane-recruited by Rab7, a GTPase typically found on late endosomes (Rojas et al., 2008; Seaman, 2004; Seaman et al., 2009). Although still elusive, it might be that this controversy is due to the generally accepted notion that retrograde sorting is a progressive process that is part of endosomal maturation.

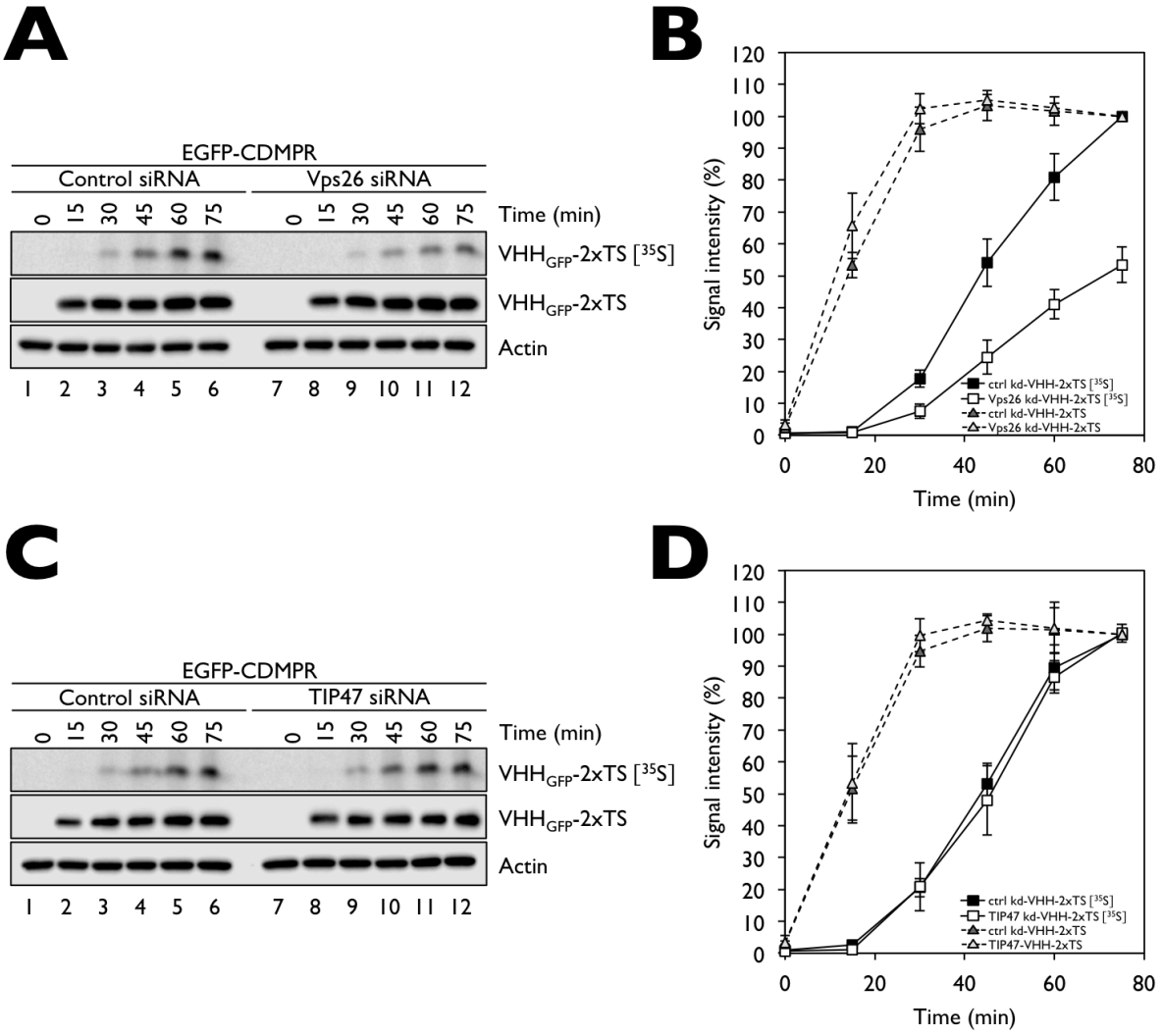

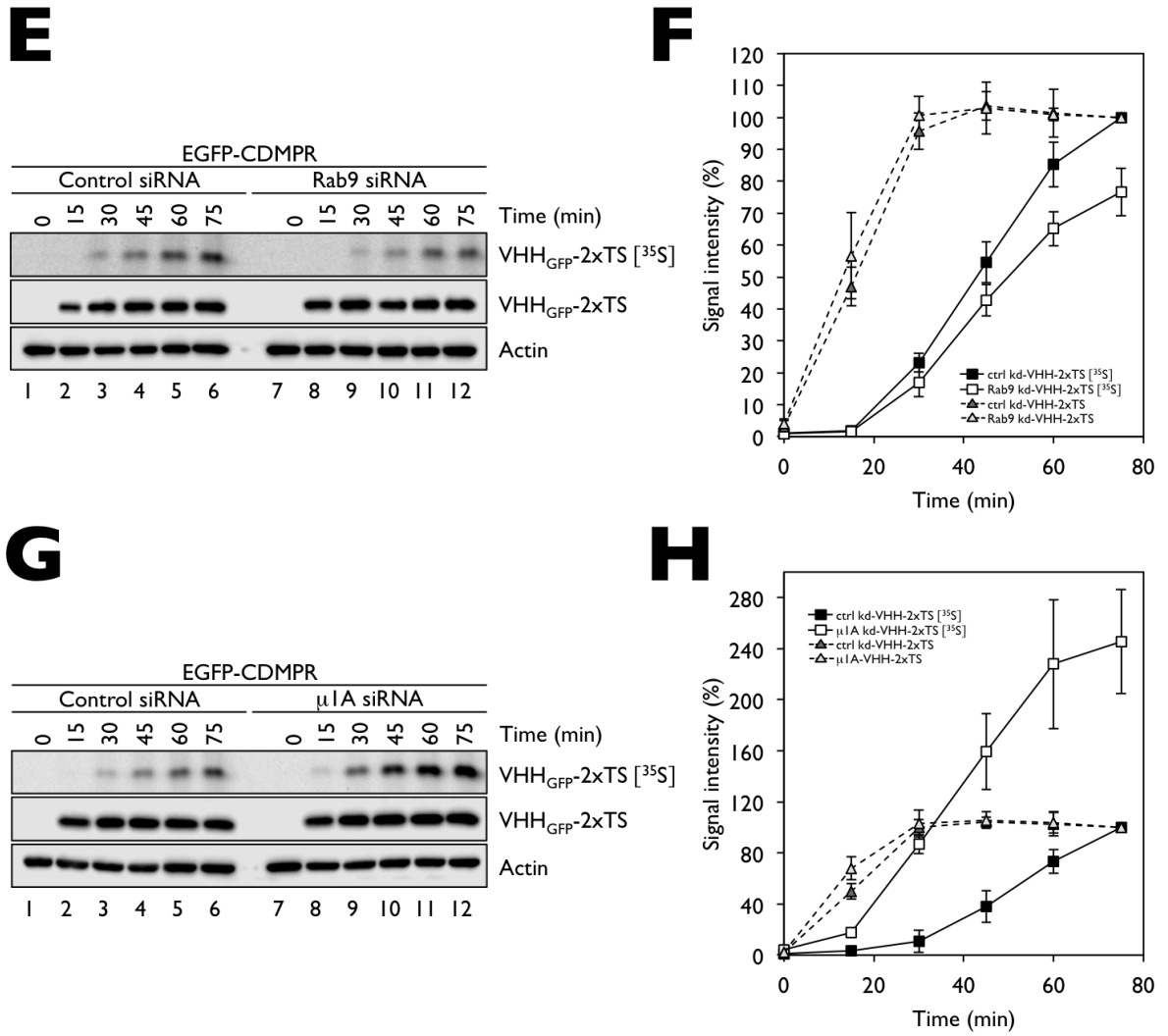

Figure 3.19: Cell surface-to-TGN transport kinetics of EGFP-CDMPR in retromer complex-, TIP47-, Rab9- and AP-1-depleted HeLa cells. (A, C, E, G) HeLa cells stably expressing EGFP-CDMPR were RNAi-mediated silenced with specific duplexes against Vps26 (A), TIP47 (C), Rab9 (E) or μ1A-adaptin (G). After 96 h of knockdown, cells were starved in sulfate-free medium for 1 h at 37°C and 7.5% CO_2, and then pulse-labeled with sulfate-free medium reconstituted with 0.5 mCi/mL [^{35}S]sulfate supplemented with 2 μg/mL of VHH_{GFP}-2xTS for up to 75 min. Postnuclear supernatants were collected and incubated with Nickel beads to affinity-isolate sulfated nanobody. A fraction of the postnuclear supernatant was saved as reference for the total amount of cell-associated VHH_{GFP}-2xTS or as loading control. Proteins were separated using gel electrophoresis and prepared for autoradiography. Cell-associated VHH_{GFP}-2xTS nanobody was detected using an anti-His_6 antibody. **(B, D, F, H)** Quantification of retrograde transport kinetics. Quantification of three independent experiments is shown (average ± SD). Signal intensities of each time point is expressed as the percentage of the signal intensity after 75 min. Black and white squares belong to kinetics of sulfation, grey triangles correspond to kinetics of cellular uptake. Data points of sulfation kinetics between control and target KD were at least $p < 0.05$ statistical significant.

RNAi-Mediated Inhibition of the Rab9/TIP47 Pathway

While the localization of retromer complex based on previous reports is not fully conclusive, TIP47, on the contrary, has been described to operate from late endosomes, exclusively (Diaz and Pfeffer, 1998; Diaz et al., 1997; Lombardi et al., 1993). To examine the role of TIP47 in MPR sorting from late endosomes, we performed a sulfation assay in TIP47-depleted cells. To our surprise, we did not see any

difference in the rate of sulfation or nanobody uptake over 75 min between control- and TIP47-depleted cells (**Fig. 3.19 C** and **D**). The reason for the absence of an effect on transport could be either due to the incomplete knockdown (**Fig. 3.18 A** and **B**) where a small pool of the cargo adaptor (~ 35%) is still able to perform its job, or because TIP47 is not involved in MPR retrieval from late endosomes. Given the fact that the applied siRNA has been described previously with similar depletion efficiencies, but observed an effect on TIP47-mediated processes, we can conclude that the residual levels of TIP47 at least are not sufficient to perform their normal task.

In addition, we initially also performed experiments with siRNAs as suggested by Pfeffer and colleagues (Ganley et al., 2004). However, knockdown efficiency was not strikingly better using their described duplexes. Albeit unsuccessful, we even tried to improve our results with anti-TIP47 antibodies raised and kindly provided by Susan Pfeffer, but with no success. Another explanation for the missing effect on MPR sorting might be EGFP-CDMPR. Though functionally identical to CIMPR, CDMPR has been previously shown to have subtle differences during segregation into endosomal sorting elements for TGN delivery (Klumperman et al., 1993), with CDMPR to segregate earlier and more rapidly. This would propose that CDMPR would escape more preferentially from early rather than from late endosomes during maturation. However, this is rather unlikely since TIP47 has been shown to interact with both hydrolase receptors with high-fidelity in vitro and in vivo (Diaz and Pfeffer, 1998). As mentioned in the introduction, TIP47 has been recently described more prominently as a lipid droplet protein that is required for lipid droplet biosynthesis (Bulankina et al., 2009; Wolins et al., 2001). Further investigations from our side are required to figure out whether TIP47 acts as MPR-specific cargo adaptor.

Depletion of Rab9, that is acting upstream of TIP47, showed a partial reduction of ~ 30% in retrograde transport of EGFP-CDMPR to the compartment of labeling (**Fig. 3.19 E** and **F**). This observation is in agreement with former studies indicating CIMPR to redistribute to peripheral compartments like for AP-1 and retromer complex depletion (Barbero et al., 2002; Ganley et al., 2004; Kucera et al., 2016b; Progida et al., 2010; Progida et al., 2012). However, it has to be mentioned that Rab9 acts as platform for many downstream effectors (Kucera et al., 2016a; Stenmark and Olkkonen, 2001; Zhen and Stenmark, 2015). It is thus very plausible that MPR traffic is likely affected not as a direct consequence of Rab9 depletion, but rather due to a misbalance of endosome homeostasis and dysregualtion of endosome maturation.

RNAi-Mediated Inhibition of the AP-1 Pathway

For the sake of completeness, we also performed the sulfation assay experiment in cells silenced for AP-1. Surprisingly and unexpectedly, the levels of sulfated VHH_{GFP}-2xTS did not decline over 75 min in AP-1-depleted cells, but were strongly elevated on the contrary (**Fig. 3.19 G** and **H**). This readout suggested AP-1 not to be not involved in retrograde transport to the TGN and is in disagreement with reported immunofluorescence stainings showing MPRs to accumulate in peripheral compartments in antibody uptake experiments (Meyer et al., 2000; Robinson et al., 2010). The experiment (**Fig. 3.19 G** and **H**) not only shows that sulfation starts earlier in AP-1-depleted cells, but also that it seems to head towards

steady-state soon after 75 min. The observation and phenotype of 'hypersulfation' under certain experimental conditions is not a new discovery and will be addressed in detail in the discussion.

Concerning our AP-1 KD phenotype, explanations for the observed hypersulfation of VHH_{GFP}-2xTS in AP-1 KD cells may be due to either more MPR being faster transported to the TGN, more efficient sulfation in the TGN, accumulation in the TGN or mislocalization of the sulfation machinery to post-Golgi compartments.

Faster kinetic transport to the TGN is rather unlikely since AP-1 is thought to mediate retrograde transport and not prevent receptor recycling to the cell surface. Moreover, imaging data suggest trapping of MPRs in peripheral EEA1-positive endosomes (Meyer et al., 2000; Robinson et al., 2010), not accelerated transport to the TGN. We also did not report striking differences in nanobody uptake between control and AP-1-depleted cells. In general, we do not think that activity of TPST1 and TPST2 is increased by knocking down AP-1. Actually, it would be rather plausible when AP-1 depletion would cause reduced TPST activity since a knockdown would rather induce a misbalance than a balance in conferring efficient tyrosine sulfation.

Another possibility responsible for hypersulfation is the missorting of TPSTs and PAPS transporters to peripheral compartments, thereby making sulfation possible earlier and multicompartmentalized than only TGN-specific. We indeed reported that sulfation occurred already after 15 min in AP-1-depleted cells, while their control counterparts showed initial sulfation at similar levels after 30 min. The leakage of the sulfation machinery to post-Golgi membranes rather than only localization to the TGN would be in line with more efficient sulfation of cycling MPRs due to higher dwelling times in compartments. It would also explain why steady-state kinetics of sulfation are reached faster. To test this hypothesis, we generated HeLa cell lines stably expressing TPST1-EGFP or TPST2-EGFP and checked for their post-Golgi localization after knocking down AP-1 by RNAi (**Fig. S8 A-B**). We did not see any difference between control and AP-1-silenced cells when we costained with the endosomal marker EEA1, suggesting no effect on TPST localization upon AP-1 knockdown. We did not invest any attempts in quantifying colocalization between EEA1 and TPSTs since no difference could be detected by eye.

We also transiently overexpressed TPST1-EGFP or TPST2-EGFP in an AP-1 KO HeLa cell line, however, we did not observe any effect here either (**Fig. S8 C-D**). Which extent of sulfation machinery mislocalization would be required to cause the observed hypersulfation is not known. It could be just a little fraction that cannot be detected by optical means.

Furthermore, what is the exact nature and identity of the perinuclear compartment? Our opinion is that it primarily reflects Golgi/TGN, however, at the same time it is also of our awareness that a number of overexpressed Rab proteins (Rab5, Rab6, Rab7, Rab9, etc.) localize to the same perinuclear region. It thus might be that some of the perinuclear structures represent post-Golgi compartments with endosomal identity. Ultrastructural resolution could give us more precise localizations of TPSTs in control- and AP-1-depleted cells in this regard. These are experimental attempts we might be addressing in the near future to nail down TPST localization in AP-1-depleted cells more precisely.

Testing whether increased sulfation is a consequence of MPR-nanobody accumulation in the TGN would make sense. Apart from AP-1 to operate in the retrograde route, there is also a considerable body

of evidence for its involvement in anterograde TGN-to-endosome transport in polarized and non-polarized cells (Deborde et al., 2008; Doray et al., 2002; Folsch et al., 1999; Gonzalez and Rodriguez-Boulan, 2009; Gravotta et al., 2012b; Mardones et al., 2007; Robinson, 2004). We did not find a suitable way how to convincingly show that MPR-nanobody complexes are stuck in the TGN.

But, why is the knocksideways readout different to the knockdown phenotype? Schu and colleagues (Meyer et al., 2000) have previously shown biochemical proof for AP-1-mediated retrograde transport apart from anti-CIMPR antibody uptake experiments. They have demonstrated that cell surface-desialylated MPR got resialylated in control-, but to a lesser extent in μ1A-deficient fibroblast cells, indicating that retrograde transport to the TGN is severely impaired in these cells. Using an in vitro approach, Medigeshi and Schu (Medigeshi and Schu, 2003) also demonstrated that the competence of membranes from AP-1-deficient cells for endosome-to-TGN transport was strongly compromised.

3.7.2 AP-1 Knockout Does Not Phenocopy AP-1 Knocksideways

The controversial readout of nanobody hypersulfation in AP-1 knockdown cells made us curious to see whether our phenotype is a result of gradual rather than rapid protein loss. During the gradual elimination of a protein, it might be possible that cells adapt or accumulate the indirect consequences of 4 days (96 h) of protein loss. The observed readout and interpretation of the former would be compensation, of the latter secondary effects.

To see whether also long-term depletion of AP-1 resulted in increased sulfation of VHH_{GFP}-2xTS imported by MPR reporters, we set out to establish a HeLa cell line with a genetic deletion of AP-1 using the CRISPR/Cas9 technology. We decided to induce double-strand breaks in loci encoding the γ-adaptin subunit of AP-1. Genetic deletion of the γ-adaptin subunit also allows us to exclude potential siRNA off-target effects originating from the μ1A duplexes. Then, we targeted μ1A for knockdowns, while γ-adaptin was inactivated in KS and KO experiments. To achieve genetic elimination of γ-adaptin, we transiently transfected our parental HeLa cell line with a commercial pool of three plasmids containing specific sgRNAs and NLS-tagged Cas9-2A-GFP. A pool of or single GFP-positive cells were collected using FACS and cultured to confluency. We continued with a pool of cells to avoid clonal variations.

To verify the genetic deletion of γ-adaptin, we harvested HeLa and HeLa AP-1 KO cells and subjected cell lysates for immunoblot analysis (**Fig. 3.20 B**). We could report absence of γ-adaptin protein expression in HeLa AP-1 KO cells, confirming its genetic deletion. To prove that loss of γ-adaptin expression resulted in overall AP-1 complex instability, we probed our cell lysates also against β1-, μ1A- and σ1A-adaptin. We observed a strong reduction of μ1A and σ1A protein levels, β-adaptin was only partially affected. The reason for this is that the antibody targeting β-adaptin crossreacts with both β1 (from AP-1) and β2 (from AP-2). Since there are estimated higher intracellular protein levels of β2 than for β1 (Hirst et al., 2012b), most of the β-adaptin is represented by the version from AP-2. Cellular levels of AP-2 and clathrin were not affected in the KO cell line.

To examine whether loss of γ-adaptin did not only affect adaptor complex stability, but also AP-1-mediated traffic, we transiently transfected γ-FKBP into AP-1 KO HeLa cells, followed by an anti-CIMPR

antibody uptake assay for 45 min (**Fig. 3.20 C**). As reported previously (Meyer et al., 2000), we found that the antibody failed to reach the perinuclear region over 45 min and that it clustered in peripheral endosomal spots. This observation is in agreement with the common consensus about the involvement of AP-1 in retrograde transport of CIMPR. Expression of recombinant γ-adaptin in the AP-1 KO cells could partially rescue the phenotype of CIMPR mislocalization (**Fig. 3.20 C**, see also **Fig. S9 A-C**). We could also show that two AP-1-dependent SNARE proteins vti1a and vti1b (Hirst et al., 2004; Hirst et al., 2003) were also affected in their steady-state localization in AP-1-deficient HeLa cells (**Fig. S9 D-E**). TGN46, on the contrary, was not affected in its steady-state localization in AP-1 KO cells (**Fig. S9 F**), in agreement with previously reported AP-1 KD readouts (Ishizaki et al., 2008).

Having the proof for genetic and functional absence of AP-1 in HeLa cells, we can now test whether MPR-nanobody complexes are sulfated preferentially more in these AP-1 KO cells. To do so, EGFP-CDMPR was transiently transfected into HeLa and HeLa AP-1 KO cells, followed by a sulfation assay using VHH_{GFP}-2xTS. After 60 min of labeling, we observed increased sulfation of VHH_{GFP}-2xTS in cells lacking AP-1 (**Fig. 3.20 D**, lane 2). This phenotype is in agreement with our observations from AP-1 KD cells (**Fig. 3.19 G** and **H**), showing that the lack of AP-1 expression causes increased levels of sulfated VHH_{GFP}-2xTS.

Since immunofluorescence readouts of CIMPR mislocalization were not phenocopied by our sulfation analysis experiments, we started to consider both of them critically. Could it be that the peripheral compartments in which internalized anti-CIMPR antibody accumulates does not solely represent early endosomes? The report by Schu and colleagues (Meyer et al., 2000) at least suggested a redistribution of MPRs to EEA1-positive compartments. However, not all of the MPR-positive peripheral and juxtanuclear punctates were also EEA1-positive. A considerable number of the observed peripheral structures were EEA1-negative (Meyer et al., 2000). They could represent TGN-derived or -scattered membranes as result of AP-1 deficiency. We can also express our uncertainty concerning AP-1 readouts by asking the other way around. Why do we observe increased sulfation at all when we can see internalized CIMPR to have severe problems to shuttle to the perinuclear region from EEA1-positive compartments? Why do we not monitor increased accumulation of internalized CIMPR in the perinuclear region by immunofluorescence when believing the kinetic sulfation readouts? We can only speculate why the readouts are inconclusive and look like this. An interesting observation we have made, however, was that we could detect sulfation of MPR-nanobody complexes to start earlier in AP-1 KD cells (**Fig. 3.19 G** and **H**). Earlier onset could mean that sulfation might occur to some extent also in post-Golgi compartments like early endosomes. Following this notion, this would implicate that also proteins that usually do not cycle back to the TGN could be sulfated to a certain extent.

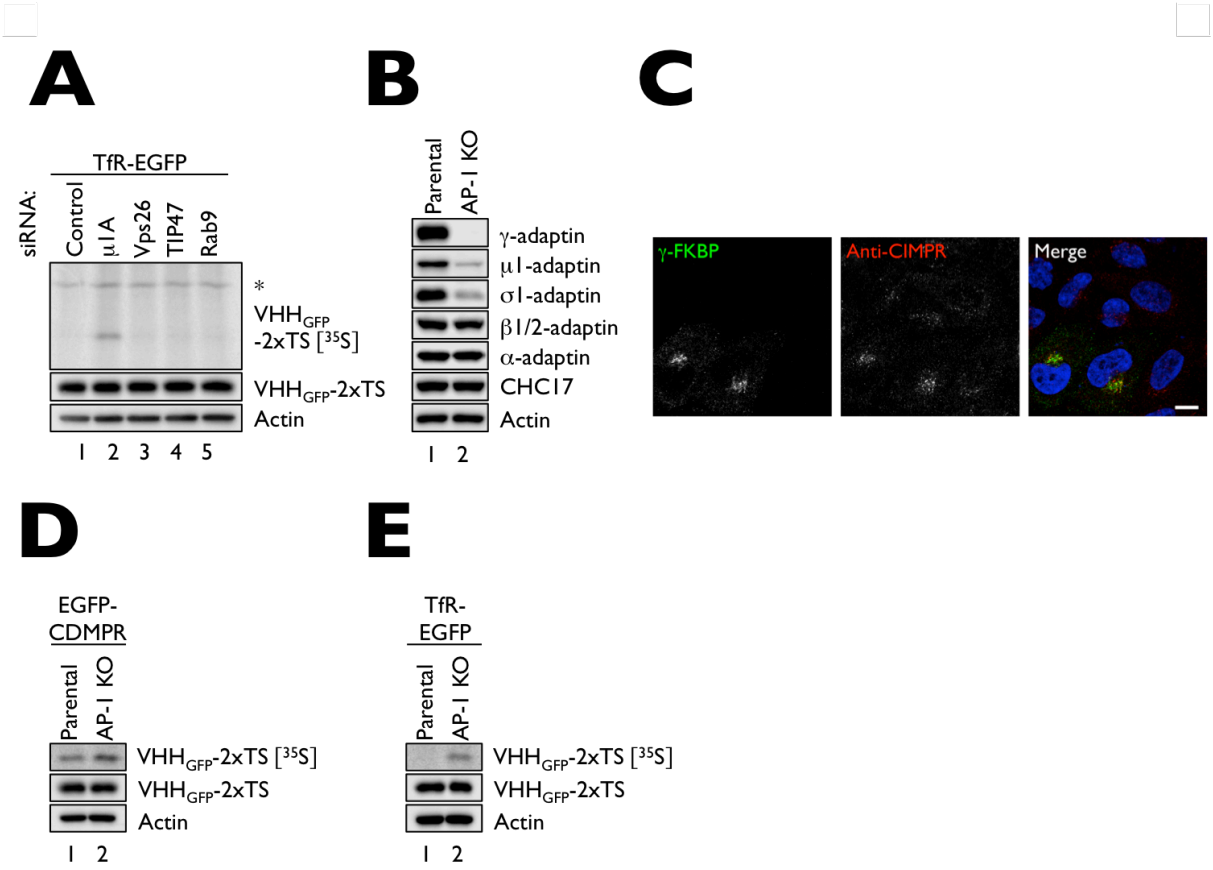

Figure 3.20: AP-1 knockdowns and knockouts can cause indirect effects. (A) HeLa cells stably expressing TfR-EGFP were RNAi-mediated silenced with specific duplexes against μ1A-adaptin, Vps26, TIP47 and Rab9. After 96 h of knockdown, cells were starved in sulfate-free medium for 1 h at 37°C and 7.5% CO_2, and then pulse-labeled with sulfate-free medium reconstituted with 0.5 mCi/mL [^{35}S]sulfate supplemented with 2 μg/mL of VHH_{GFP}-2xTS for 1 h. Postnuclear supernatants were collected and incubated with Nickel beads to affinity-isolate sulfated nanobody. A fraction of the postnuclear supernatant was saved as reference for the total amount of cell-associated VHH_{GFP}-2xTS or as loading control. Proteins were separated using gel electrophoresis and prepared for autoradiography. Cell-associated VHH_{GFP}-2xTS nanobody was detected using an anti-His_6 antibody. **(B)** Parental and AP-1 KO HeLa cells were lysed and probed against γ-, μ1A-, σ1A-, β1/2-adaptin, α-adaptin (AP-2) and CHC17. **(C)** AP-1 rescue with anti-CIMPR antibody uptake assay. AP-1 KO HeLa cells were transiently transfected with recombinant γ-FKBP for 24 h and incubated with a 1:5000 dilution of anti-CIMPR antibody for 45 min. Cells were then processed for fluorescence confocal microscopy. Recombinant γ-FKBP was specifically detected using an antibody targeting a recombinant epitope present in the neuronal splice variant of α-adaptin, internalized mouse anti-CIMPR was directly detected with a fluorochrome-tagged secondary antibody. **(D-E)** AP-1 KO HeLa cells were transiently transfected with either EGFP-CDMPR (D) or TfR-EGFP (E). After 24 h of overexpression, cells were starved in sulfate-free medium for 1 h at 37°C and 7.5% CO_2, and then pulse-labeled with sulfate-free medium reconstituted with 0.5 mCi/mL [^{35}S]sulfate supplemented with 2 μg/mL of VHH_{GFP}-2xTS for 1 h. Postnuclear supernatants were collected and incubated with Nickel beads to affinity-isolate sulfated nanobody. A fraction of the postnuclear supernatant was saved as reference for the total amount of cell-associated VHH_{GFP}-2xTS or as loading control. Proteins were separated using gel electrophoresis and prepared for autoradiography. Cell-associated VHH_{GFP}-2xTS nanobody was detected using an anti-His_6 antibody. Scale bar: 10 μm.

Since TfR does not undergo retrograde transport to the TGN at substantial levels, we took advantage of cells stably expressing TfR-EGFP in combination with RNAi-mediated AP-1 knockdown. Indeed, recombinant TfR-nanobody complexes were moderately sulfated in AP-1-silenced cells (**Fig. 3.20 A**), while under the same conditions they were not with the other knockdowns. We performed the

same experiment with transiently transfected AP-1 KO HeLa cells (**Fig 3.20 E**). Also here, we could observe sulfation of recombinant TfR-nanobody complexes. Although these results point towards sulfation to occur also in post-Golgi compartments, we do not know which fraction of nanobody-bound TfR reporter is sulfated. It might be a very tiny and negligible amount, only. As a matter of fact, we had to expose cassettes containing these samples much longer. We do not think that AP-1 depletion favors TfR to recycle to the TGN. But, previous reports have shown that depletion of AP-1 from endosomes can affect Tf recycling indirectly (Chamberland et al., 2016; D'Souza et al., 2014; Perrin et al., 2013). However, the main finding out of this experiment was that we observed a potentially dysregulated system upon AP-1 depletion. Otherwise nanobody riding with TfR-EGFP would not have been sulfated. It thus might be that AP-1 sorting not only contributes to the correct targeting of a number of membrane proteins to their acceptor compartments, but perhaps also contributes to TGN/endosome homeostasis to certain degree. We will follow up on this topic in more detail in the discussion.

4 Discussion

4 Discussion

4.1 A Versatile Nanobody-Based Toolkit

In the present study, we have established the basis for a methodological approach to investigate retrograde transport of reporter proteins from the cell surface. The approach to track proteins from the cell surface to any intracellular compartment relies on binding of functionalized VHH_{GFP} to recombinant EGFP-modified reporter proteins. Depending on the functionalization, we can use specific cell surface labeling to biochemically determine retrograde transport kinetics, to monitor endocytic uptake by fluorescence live cell imaging, or to ultrastructurally visualize retrograde transport compartments by electron microscopy. In particular, a nanobody featuring a consensus motif for tyrosine sulfation (e.g. VHH_{GFP}-2xTS) allows us to assay whether a reporter reaches the TGN or not. We cannot only qualitatively examine whether a reporter is shuttled to the TGN by simply detecting sulfated nanobody, but we can also determine transport kinetics.

Below, we would like to compare previously described strategies for TGN arrival, thereby highlighting the advantages and disadvantages of our approach to others. In addition to that, we will also discuss the other 'cargo trackers' (TEV-based VHH_{GFP}, VHH_{GFP}-mCherry, VHH_{GFP}-APEX2), thereby also emphasizing how they can be powerfully used in a wide number of other applications.

4.1.1 Sulfatable Nanobodies Are Superior to Other Approaches

Radiolabel and Radiolabel-Free Sulfation-Based Approaches to Study TGN Arrival

We are not the first to develop an experimental toolkit to biochemically study retrograde transport to the TGN. Over the last decades, approaches have been established that rely on in vitro or in vivo sulfation, reglycosylation or artificially introduced modifications at the cell surface to assess TGN arrival. Previously, Ludger Johannes, Sjur Olsnes, Kirsten Sandvig, Bo van Deurs and colleagues have independently developed sulfation site sequences that can be expressed in the context of recombinant cargo proteins or can be chemically coupled to them (Amessou et al., 2006; Johannes et al., 1997; Mallard et al., 1998; Rapak et al., 1997; Sandvig and van Deurs, 1994). In brief, they constructed recombinant fragments of ricin and Shiga toxin subunits that were modified with a sulfation site (Johannes et al., 1997; Mallard and Johannes, 2003; Rapak et al., 1997; Shiba et al., 2010; Utskarpen et al., 2006). Using these recombinant toxin subunits, they could show that the fragments were sulfated, revealing that they must have passed the TGN en route to the ER from where they reached the host cytoplasm. These studies paved the way for exploiting sulfation as PTM, not only to study TGN exit as part of the secretory pathway, but also to assess TGN arrival from the retrograde route.

Ludger Johannes and colleagues pioneered sulfation peptide chemistry approaches to cell surface-label proteins or antibodies (Amessou et al., 2007; Amessou et al., 2006; Christiano et al., 2010; Saint-Pol et al., 2004). Concerning the latter, they coupled sulfation site-containing peptides to anti-GFP or anti-TGN46 antibodies in order to study retrograde transport of recombinant GFP-CI-MPR or endogenous TGN46. In the study of Ludger Johannes and collaborators (Saint-Pol et al., 2004), such an approach showed epsinR to be partly involved in endosome-to-TGN transport of the above proteins. The anti-GFP antibody chemically modified with a sulfation site resembles our functionalized TS-tagged nanobodies. Using such an antibody-based approach to monitor retrograde traffic brings along many technical and experimental caveats.

First, while our VHH_{GFP} domain is only capable of binding GFP in a 1:1-stoichiometry, an anti-GFP antibody has the potential of binding more than one GFP epitope with its two paratopes. Such a setup is likely prone to cause crosslinking of GFP-CI-MPR reporters at the cell surface. Crosslinking of reporters might result in local aggregates, reduced mobility and altered endocytosis rates. The possibility and risk of cell surface crosslinking by antibodies is higher when the antibody is of polyclonal nature. Although Johannes and colleagues (Amessou et al., 2007; Amessou et al., 2006; Saint-Pol et al., 2004) used a commercial 'monoclonal' anti-GFP antibody to couple sulfation site-containing peptides, the antibody is actually a pool of two monoclonal antibodies (clone 7.1 and 13.1), thereby making it biclonal at the end.

Second, modification of antibodies with sulfation peptides occurs in a random fashion. Crosslinking can occur in the variable regions that can cause the antibody to fail binding the GFP epitopes. Additionally, the random and uncontrolled modifications of the antibody might cause disruption of important intramolecular interactions, resulting in structural changes and increased instability. Also, the modified anti-GFP antibodies are quite heterogeneous, some might have none, one, two or more chemically crosslinked sulfation peptide tags (batch-to-batch variation). Whether all of these sulfation tags are functional and efficiently modified by endogenous TPSTs due to sterical hindrance remain in question.

Third, detection of sulfated antibody proves difficult in autoradiography-based readouts since peptide modifications occur in both heavy and light chains. Separation via a reducing SDS-PAGE does not then result in a single sharp band, but rather in two dissimilarly strong sulfation signals corresponding to light or heavy chain, respectively (Amessou et al., 2007). Our functionalized nanobody in contrast is monovalent, has a specific tyrosine sulfation consensus sequence close to the C-terminus and can be separated as a single band. Since we bacterially express our nanobody fusions, we can achieve high amounts and yields in one single step.

The other approach, conversely, requires commercially available antibody that has to be first chemically crosslinked with sulfation peptide sequences prior to use. Overall, both antibody- and nanobody-based approaches are powerful tools to study transport to the TGN, with a plus to the nanobody-based technique, however.

A drawback, admittedly, which both approaches presumably have, is the low efficiency of tyrosine sulfation. We were surprised to realize that the steady-state of nanobody uptake and sulfation were not similar after 75 min of labeling (see for instance **Fig. 3.14** or **3.17**). Steady-state of sulfation was in most cases not yet reached after this time interval. The best explanation for this observation is that not every

nanobody passing through the TGN is completely sulfated during the first transit. Incorporating more than two sequences cannot avoid this phenomenon. Even though more tandem TS sequences would permit a stronger sulfation signal, it would also increase the risk that more retrieval rounds at the endosome-to-TGN interface are required to complete sulfation. Sulfation signal strength and reaching of steady-state of sulfation are thus standing in conflict with each other. We can circumvent or partially abolish this problem when we can identify a sulfation consensus sequence that is modified with a higher efficiency during the first transit than ours. One of our future attempts to improve the sulfation assay will thus include to screen and test additional tyrosine sulfation consensus sequences, this either by testing already described sequences or by simulating and finding the most suitable ones with the help of bioinformatics (Bundgaard et al., 1997; Kehoe and Bertozzi, 2000; Nedumpully-Govindan et al., 2014; Rosenquist and Nicholas, 1993). Incomplete sulfation, however, might be an inherent feature of endogenous secretory proteins (Bundgaard et al., 1997; Nedumpully-Govindan et al., 2014). This raises the issue that completed sulfation after one transit through the TGN lumen might be unlikely at all.

A less elegant, but acceptable approach, also based on sulfation, to study retrograde transport of receptor proteins from the cell surface to the TGN has been described in the study of Pfeffer and colleagues (Sincock et al., 2003), and Kutsche and collaborators (van Rahden et al., 2012). Instead of using a cell surface label, the protein of interest can be directly tagged with a site conferring tyrosine sulfation. To study endosome-to-TGN transport in this manner, cells expressing TS-tagged reporters are first incubated in sulfate-free medium containing excess of chlorate to prevent sulfation of newly synthesized proteins. Chlorate is a reversible inhibitor of sulfation (Humphries and Silbert, 1988; Safaiyan et al., 1999) and competitively interferes with the formation of PAPS. The reporter is then chased to its steady-state localization, while new synthesis is blocked with the addition of cycloheximide. Reporter transport from endosomes to the TGN is then measured by incubating cells in the presence of radiolabeled sulfate and cycloheximide, after removal of chlorate. An approach in this setup has been used to monitor retrograde transport of a modified version of CDMPR (HMY-MPR46) containing an N-terminal cassette with a His_6-, myc-, and TS-tag. Using this reporter, the authors proposed that the endosomal OCRL phosphatase (van Rahden et al., 2012) and TIP47 (Sincock et al., 2003) are involved in retrograde transport of MPRs. The disadvantage of their strategy is that one has to chemically block sulfation over several days by adding excess of chlorate. Blocking sulfation over a long time range causes natural proteoglycans and other proteins not to be sulfated anymore and might render them unfunctional as a consequence. Since the assay also makes use of cycloheximide to block de novo reporter synthesis, we probably also have to cope with indirect effects (cell stress, ribosome pausing, etc.) that might be finally reflected in the results.

Another drawback of this assay is that we can hardly measure cell surface-to-TGN kinetics. After having substituted chlorate for radiolabeled sulfate, reporters momentarily residing in the Golgi lumen will be sulfated. Also reporter on the way to the TGN or prior to exit from endosomes will have earlier access to the sulfation machinery. In particular, when the assay is performed in combination with a knockdown with additional possible indirect and/or compensatory effects, the assay is stretched to its limits and solid interpretations of the obtained results are hard to be made. The advantage of this assay is

that TGN exit and arrival of a reporter-expressing cell line can be monitored without the need of any cell surface modifications (e.g. nanobodies). However, our nanobody approach is much more suitable to determine retrograde transport kinetics. It is not only free of any inhibitors like chlorate and cyclo-heximide, but also circumvents adverse experimental setups.

An alternative, radiolabel-free approach to study TGN arrival is by using anti-sulfotyrosine antibodies. The only existing antibody detecting sulfotyrosine as epitope independently of sequence context has been described in the publication of Moore and colleagues (Hoffhines et al., 2006). Protein arrival in the TGN could then by easily measured by detecting 'cold'-sulfated nanobody from a pull-down. Even though we tried to apply the anti-sulfotyrosine antibody (sulfo-1C-A2) on precipitates containing sulfated VHH_{GFP}-2xTS nanobody, no antigen cross-reactivity could be monitored. Antibody detection of nanobodies would simplify all of our radioactive assays. We also plan to test natural and artificial peptide sequences that have previously been shown to crossreact with sulfo-1C-A2 antibody (Cha et al., 2009; Cimbro et al., 2014; Friedman et al., 2012; Hoffhines et al., 2006; Seko et al., 2015; Yang, 2009). The reason why the sulfotyrosines within our SAEDYEYPS-based peptide from the cholecystokinin precursor are not recognized is unknown.

In addition to conventional biochemical approaches relying on radiolabeling, assays have been developed to monitor kinetics of sulfation using a fluorescence-based probe readout (Chen et al., 2013a; Zhou et al., 2014). Such probes are converted to fluorescence once they have become substrates for TPSTs. Fluorescence detection could then be taken as readout for TGN arrival. However, both of the cited publications have the huge drawback that probes are not yet directly applicable for the use in a cell culture system. Convertible probes attached to VHH_{GFP} that turn fluorescent after reaction with TPSTs would manifest as ideal tool for radiolabel-free detection other than biochemical ones.

A Desialylation-Resialylation-Based Approach to Study TGN Arrival

An other approach to assess PM-to-TGN transport has been initially described by Duncan and Kornfeld (Duncan and Kornfeld, 1988). Instead of making use of the endogenous sulfation machinery, their assay relies on oligosaccharide processing of retrogradely transported cargo proteins. To do so, mature oligosaccharides units of cell surface receptors are desialylated so that they become substrates for sialyltransferase, a marker of the trans-Golgi/TGN. If the deglycosylated receptor then returns to this compartment, the oligosaccharides regain sialic acid. This approach and variants thereof have been widely used in the past (Draper et al., 1990; Goda and Pfeffer, 1988; Goda and Pfeffer, 1989; Jin et al., 1989; Prydz et al., 1990; Riederer et al., 1994), above all to study retrograde transport of MPRs. Indeed, this kind of assay has been used to test whether AP-1 is involved in MPR receptor return to the TGN by Schu and colleagues (Meyer et al., 2000). Our AP-1 KD phenotype based on a sulfation assay did not support the observations made by Schu and coworkers using a resialylation assay.

As reported previously, since our AP-1 KD and KO readouts of increased sulfation might be indirect consequences specifically of sulfation machinery mislocalization, a sulfation-independent approach

would have been very useful, too. In order to quantitatively measure return to the TGN by still using our tools, one could try to apply a modified protocol derived from the study of Duncan and Kornfeld (Duncan and Kornfeld, 1988). Cells expressing EGFP reporters could be specifically cell surface-labeled with VHH_{GFP} derivatives at 4°C or 37°C, and digested with neuraminidase to remove terminal sialic acid residues from mature glycans. Internalized desialylated EGFP reporters carrying VHH_{GFP} derivatives in a piggyback mode can then be terminally resialylated when facing the lumen of trans-Golgi/TGN. To easily analyze compartment arrival from the retrograde route, the assay could make use of radiolabeled sialic acid. The total fraction of cell surface-to-TGN transported cargo can then be collected by affinity precipitation of the bound VHH_{GFP} derivatives and analyzed by autoradiography.

Even though Golgi PTM machineries are considered to 'remain' static and unaffected upon interferences (RNAi, knockout, inhibitors), what they probably will not do, it is of a big advantage to have more than just one detection strategy. If, for instance, readouts of two or even more approaches (sulfation and resialylation) are consistent with each other, then final conclusions of an experiment can be drawn more convincingly. If, however, they do not balance each other, then one or more PTM machineries are affected by the applied interferences, directly or indirectly. We are currently part of such an experimental readout discrepancy. On the one hand, we know from literature that in AP-1-deficient mouse fibroblasts retrograde transport of MPR is severely impaired, as judged by a resialylation approach (Meyer et al., 2000). On the other hand, conversely, we reported increased sulfation of recombinant CDMPR in AP-1-depleted (KD and KO) HeLa cells using sulfation as PTM. The biochemical readout based on sulfation would then rather favor AP-1 not be involved in retrograde transport. However, when we rapidly inactivate AP-1 using the knocksideways approach, we could not see any increase, but a partial decrease in sulfation, thus favoring AP-1 to be involved in endosome-to-TGN retrieval.

The suggested resialylation approach in combination with nanobody as described above might be an alternative strategy to reconcile the observed AP-1 phenomenon.

A Proteomics-Based Approach to Study TGN Arrival

Proteomics has gained fundamental importance over the last decade, and therefore it is not surprising that attempts have been undertaken to analyze retrograde transport using the power of mass spectrometry. Ludger Johannes and collaborators (Shi et al., 2012a) have previously presented a SNAP-tag-based proteomics approach to study cell surface-to-TGN transport of endogenous proteins. They created a TGN-localized trap composed of truncated GalT fused to GFP and a SNAP-tag. Cargo that has been chemically cell surface-labeled with benzylguanine (BG) can react and be covalently bonded to the recombinant resident trap (GalT-GFP-SNAP) if retrograde transport to the TGN has occurred.

Applying this approach, the authors (Shi et al., 2012a) could present a list of 20 proteins, including GPCRs, transporters, kinases and more, that undergo retrograde traffic to the TGN. Among the hits, TfR, the first proposed endogenous retrograde cargo protein (Snider and Rogers, 1985), was detected, too. This observation is in contrast to the general notion that recycling receptors, such as TfR or ASGPR, only pass early endosomes before being recycled to the cell surface.

By using our versatile nanobody approach, we could not detect significant amounts of sulfated nanobody riding along with recombinant TfR-EGFP, or at least vanishingly minute traces relative to other retrograde transport cargoes. In contrast to the publication of Johannes and collaborators (Shi et al., 2012a) whose results are based on the overexpression of a recombinant TGN trap, we made use of the endogenous sulfation machinery to detect retrograde cargo. Overexpression systems might have the risk that they are not as tight as their endogenous counterparts. Although GalT is generally considered a bonafide TGN-resident protein because of its function, GalT is naturally also moving out to the cell surface (Hathaway et al., 2003). Johannes and collaborators (Shi et al., 2012a) used a well-established truncated version of GalT, composed of its cytosolic tail, transmembrane domain and stem region, an arrangement that is mimicking full-length GalT regarding traffic. The recombinant GalT-GFP-SNAP thus likely contains the trafficking determinants to distribute to the post-Golgi environment. Thus, there is a high risk that the covalent reaction between the BG-modified cell surface cargo and SNAP-tag-based trap may also occur somewhere at the TGN-to-PM interface, and not exclusively in the TGN. Using HeLa cells stably expressing GalT-EGFP, we could detect significant uptake of VHH_{GFP} derivatives, indicating that this protein transiently appears at the cell surface (**Fig. S10**). Even more, we could reveal that nanobody bound to GalT-EGFP is sulfated, suggesting that GalT might be actively cycling for- and backwards at the TGN-to-PM interface. Since mass spectrometry is one of the most sensitive approaches, it is likely that SNAP-tagged crosslinked TfR is mainly reflected by peripheral non-Golgi GalT distribution.

Surprisingly and interestingly, the SNAP-tag-based proteomics approach (Shi et al., 2012a) failed to detect MPRs and TGN46, thereby indicating that the mass spectrometry methodology can also pass over relevant candidates that are amenable with classical biochemical approaches. Moreover, there was no follow-up publication so far for the other detected retrograde cargo proteins (Shi et al., 2012a).

Nonetheless, the idea of specific cell surface labeling (or modification) and trapping represents a strategy to identify novel cargo proteins traversing respective compartments of interest. A similar SNAP-tag-based approach to investigate retrograde transport to the ER has been presented by the group of Ari Helenius (Geiger et al., 2012).

Towards a Novel Approach to Study TGN Arrival

Inspired by ideas derived from publications originating from the lab of Ludger Johannes and Ari Helenius (Geiger et al., 2012; Shi et al., 2012a), we thought that we could establish an approach ourselves for measuring PM-to-TGN transport based on an artificial TGN-restricted modification that is free of any radiolabel. To this end, we designed a fusion construct composed of shortened GalT (shGalT) fused to mCherry and wild-type BirA, referred to as shGalT-mCherry-BirA-3xFLAG. As reported previously in the lab of Barry Shur (Hathaway et al., 2003), two alternate forms of GalT exist that only differ in the length of their cytoplasmic domains. They demonstrated that the long cytoplasmic and transmembrane domains of GalT is capable of targeting a reporter protein to the cell surface, whereas the short cytoplasmic and transmembrane domains (shGalT) do not have this property, but remain stuck in the Golgi instead. This is the reason why we introduced shGalT in our TGN-localized modifier, and not GalT that contains sorting determinants for exocytic traffic. While mCherry was incorporated for fluorescence

visualization and cell sorting, BirA confers the specific transfer of activated D-biotin onto a BAP (AviTag) epitope. Reporters that bring along a BAP motif will then be specifically modified by TGN-hooked BirA. To channel BAP-containing proteins into the retrograde pathway, we followed the versatility in domain organization of our nanobody fusions. Instead of bacterially modifying them with D-biotin during induction, we grew bacteria under biotin-reduced conditions to avoid functionalization of the BAP epitope. Purified nanobody under these conditions is then mainly biotin-free and can be used for piggyback transport conveyed by EGFP reporters. Kinetics of de novo biotinylation of internalized nanobody into BirA-containing compartments can be taken as readout for TGN arrival. Since radiolabeling with sulfate takes advantage of the endogenous sulfation apparatus rather than of a recombinant artificial machinery, we gave the sulfation approach priority. However, the basis for such a biotinylation approach exists, including the above-mentioned BirA-modifier HeLa cell line and several nanobodies devoid of biotinylation.

Using non-biotinylated VHH_{GFP}-2xTS and EGFP reporters in combination with a BirA-modifier HeLa cell line, we will be able to directly and simultaneously compare the increase in sulfation and biotinylation over time. Biotinylation might also overcome the problem of inefficient sulfation that we have observed, so that in best case, steady-state of nanobody uptake and biotinylation are not so strongly shifted from each other as it is the case for sulfation.

Taken together, the described approach would offer us an alternative, radiolabel-free method to study retrograde transport from the cell surface to the TGN. Other TGN-hooked BirA fusions need to be established in case of leakiness of shGalT-based fusions.

4.1.2 TEV Site-Modified Nanobodies to Study Endocytosis and Recycling

We have not only established an approach to monitor uptake kinetics into steady-state, but also to simultaneously investigate recycling of receptor proteins to the plasma membrane. To do so, we have generated nanobodies with a TEV cleavage site after the VHH_{GFP} domain. Once internalized TEV site-modified functionalized nanobodies have appeared at the cell surface, they can be specifically shaved using TEV protease. By using such a TEV site-modified nanobody (e.g. VHH_{GFP}-TEV-control), we could confirm the rates of endocytosis and recycling of the well-studied TfR. In addition to that, we could study endocytosis and recycling of CDMPR.

To be mentioned is that TEV cleavage site-containing nanobodies allow us to investigate uptake and recycling kinetics of 'difficult-to-study' receptor proteins, assuming that nanobody binding does not affect receptor properties. They include proteins that either have no ligands, less well-established ligands or antibodies failing to detect their extracellular domain for uptake assays. Among these are for instance recycling receptors such as LDLR or H1 with no suitable ligands (for recycling), stimuli-triggered internalized cargo proteins such as GPCRs or GLUT4, or other proteins with no detailed information about their final fate after endocytosis from the cell surface. In all such cases, a nanobody with a TEV site can help us to narrow down the endocytic and recycling fate of EGFP-modified receptor proteins. A physiological relevant process in whole-body glucose homeostasis is the translocation of the GLUT4 to cell surface upon insulin signaling in cells. Insulin initiates GLUT4-mediated uptake of glucose into the cell, however, once glucose and hence insulin levels decrease, the transporter is endocytosed and kept in

storage endosomes (Bryant et al., 2002; Rea and James, 1997; Stockli et al., 2011). Using our TEV site-containing nanobody, we can basically follow the transporter's endocytic route after decreasing levels of insulin, and follow again how GLUT4 is retranslocated to the cell surface when insulin levels increase again.

For other approaches of interest, we can even apply expressed VHH_{GFP}-TEV-2xTS for studying exocytosis rates of sulfated proteins, or VHH_{GFP}-TEV-mCherry for monitoring how long it takes until a certain compartment is depleted of nanobody after having reached steady-state by live cell imaging. Ongoing attempts in investigating retrograde traffic of a number of EGFP-tagged proteins will include the use of these TEV site-containing nanobodies.

4.1.3 APEX2-Modified Nanobody for Electron Microscopy and Ablation

We demonstrated that VHH_{GFP}-APEX2 could label retrograde transport compartments as analyzed by electron microscopy using DAB cytochemistry. To label TfR-positive compartments, Tf coupled to HRP has previously served as tool to dissect which other receptors travel through these endocytic organelles. Using our nanobody approach, we could not only follow receptor proteins where a known ligand (e.g. Tf), that channels the peroxidase moiety for DAB cytochemistry into the cell, but could look more generally at reporters of interest. Based on the knowledge that MPRs and TGN46 cycle back to the TGN, and also that internalized nanobody strongly overlapped with TGN-resident markers by immunofluorescence, we could ultrastructurally visualize membranes of TGN identity in the perinuclear region by DAB/H_2O_2-cytochemistry. Unlike to the clearly identifiable trans-Golgi compartment, a distal cisterna in the perinuclear region, the TGN is structurally less well defined. It often appears as a scattered network of tubular, but mostly vesicular membrane elements. Our observed vesicular and tubular elements look like the membrane structures previously labeled by bacterial toxins or WGA coupled to HRP that traffic to the TGN (Iida and Shibata, 1989; Llorente et al., 1998; Sandvig et al., 1989; van Deurs et al., 1986). These observations from almost more than 30 years ago already gave evidence that the detected vesicular-tubular structures of different sizes are indeed representing TGN. We are curious to know and elucidate what kind of retrograde DAB labeling patterns, we are obtaining from other EGFP-labeled cargo proteins we are investigating in the future.

Even though APEX2-mediated DAB cytochemistry has worked to our satisfaction, we would have appreciated having more pronounced DAB precipitation for detection by electron microscopy. Comparing our results using APEX2 with results published on HRP conjugates, it is clear that HRP generates more pronounced DAB precipitates than APEX2 does. This is also reflected by the finding of Ting and colleagues who have recently outlined that APEX2 turns over ~ 3000-4000 times before becoming permanently inactivated in the presence of 1 mM H_2O_2 and peroxidase substrate, while HRP survives > 130'000 turnovers under these conditions (Lam et al., 2015). Due to the higher turnover rates and thus labeling effectivity of HRP, we started to generate HRP-coupled nanobody probes. We are currently testing whether VHH_{GFP}-APEX2 or VHH_{GFP} coupled to HRP is as better retrograde transport tracker for electron microscopy.

Peroxidase-mediated compartment ablation is also strongly depended on the enzyme being used. HRP conjugates might be much more effective in generating DAB polymers than APEX2. This is above all

then of crucial importance when only a very small amount of EGFP fusions is present at the cell surface that might only generate a decent signal with APEX2-driven polymerization. Thus, HRP conjugates might not only be beneficial for electron microscopy, but also for our biochemical approaches including ablation and peroxidase-mediated biotinylation. It has to be mentioned that the strength of our APEX2-mediated DAB labeling reaction was in the range as previously reported by Parton and colleagues (Ariotti et al., 2015a; Follett et al., 2016). The great advantage of APEX2 is that we can simply express it in the reducing environment of bacteria, while HRP derivatives are obtained the easiest way by coupling peroxidase to our nanobody.

4.1.4 mCherry-Modified Nanobody for Live Cell Imaging

Apart from considering retrograde transport by immunofluorescence on fixed cells, we also had VHH_{GFP}-mCherry in our toolbox to study uptake by live cell imaging microscopy. Using a semi-automated widefield microscope in combination with quantitative image analysis, we could determine uptake kinetics of EGFP reporter cell lines. While the biochemical approach only allows to measure uptake into steady-state of total cell, the live cell imaging approach would have additionally enabled us to selectively mark regions of interest, such as perinuclear compartments, peripherally associated endosomes, or other fluorescently marked compartments. We used EGFP-CDMPR and TfR-EGFP as cargo proteins to illustrate our live cell imaging approach, mainly to study uptake kinetics into steady-state. Although not studied in depth because of experimental and technical constraints, we could test that kinetics of nanobody uptake into steady-state in the perinuclear region and into total cell differed. This is in line with the biochemical observation that it takes longer to reach compartments beyond early endosomes. Longer nanobody internalization rates for EGFP-CDMPR into steady-state in the perinuclear region is obvious since the nanobody is passing late endosomes and the TGN. Surprisingly, although TfR is being transported through the endosomal network only, we also observed for this receptor a difference between reaching steady-state in the perinuclear compartment and total cell in preliminary experiments. It thus seems that the observed perinuclear compartment in cells expressing TfR-EGFP does not solely represent sorting endosomes. Since TfR recycles to the cell surface in different modes, Rab4-dependent 'fast recycling' from sorting endosomes and Rab11-dependent 'slow recycling' from recycling endosomes (Maxfield and McGraw, 2004), differences in the observed kinetics could be explained by different recycling pathways. However, we need to investigate this more carefully, above all by coexpression with fluorophore-tagged Rabs to specifically mark compartments.

The approach based on a nanobody suitable for live cell imaging has the advantage that we can also determine kinetics of uptake in transiently transfected cells with good expression levels. This is particularly important when stable cells lines are difficult to be obtained, or when many EGFP-labeled cargo proteins are to be studied and compared. Since apparent rates (k_{app}) of uptake are specific for every receptor protein, it might be interesting to determine many of these rates from receptors of interest and compare them with those from proteins with well-established sorting itineraries.

Future experimental attempts using VHH_{GFP}-mCherry will not only include to determine half-lives of other receptors, but also to combine the assay with additionally expressed fluorophore-tagged markers to reveal the identity of the receptor-passing retrograde transport compartments.

4.1.5 Functionalized Nanobodies as Ideal Biochemical Tool

In the present study, we have introduced a number of functionalized nanobodies that can be used to study retrograde traffic by various methods. Because of their advantageous features (size, high stability, affinity, binding to folded epitopes, etc.), nanobodies have been used in a wide number of applications in multicellular organisms or in cell culture systems. In particular, VHH_{GFP} has been used in a number of recent studies.

Using a strategy based on VHH_{GFP}, a novel method to induce protein degradation called deGradFP (degrade Green Fluorescent Protein) was recently introduced (Caussinus et al., 2011). The idea behind this turnover tool is to exploit the ubiquitin pathway by supplying a new substrate recognition domain interacting with GFP. This is accomplished by functionally tagging a component of the E3 ubiquitin ligase complex with VHH_{GFP} to send GFP-labeled proteins for rapid proteasomal destruction. This method is not only applicable to induce turnover of cytosolic, but also of transmembrane proteins (Caussinus et al., 2011).

Another powerful strategy based on VHH_{GFP} is morphotrap (Rothbauer et al., 2006). Morphotrap was developed in Drosophila as a tool to modify the extracellular distribution of secreted GFP-modified proteins, either by retaining them on the cell surface of producing cells or by sequestering them on target cells in the surrounding environment. The rationale for morphotrap is similar as for deGradFP. For morphotrap, VHH_{GFP} is incorporated into the extracellular portion of mouse CD8 transmembrane protein where receptor expression mediates trapping of secreted GFP-tagged proteins. Morphotrap has been used among others to address the importance of morphogen spreading in Drosophila wing disc development (Harmansa et al., 2015). Very recently, the idea of synthetic traps has been expanded to capture GFP-tagged proteins along the apical-basal axis of polarized cells (Harmansa et al., 2017).

While the studies above were mainly performed in multicellular organisms, functionalized nanobodies as tool have also been used in unicellular eukaryotes and prokaryotes. An interesting application is the fluorescent-three-hybrid (F3H) system, a method to visualize protein-protein interactions in vivo (Herce et al., 2013). In this system, a GFP binder module is anchored to a specific subcellular compartment. To probe putative interaction between two proteins, one is labeled with GFP, the other with RFP. As a result, the GFP-tagged protein will be recruited by the nanobody to the subcellular compartment. If the RFP-labeled protein interacts with the GFP-labeled protein, a colocalization of the green and red fluorescent signal will be observed.

Another application of nanobodies is their use as inhibitors or activity modulators. Previously, it was shown that enzymes, such as lysozyme, could be inhibited by nanobodies that bind to the enzyme's active site (De Genst et al., 2006). In another study, diverse nanobodies against human FIC domain-containing proteins, proteins that can AMPylate target substrates, were demonstrated to not only inhibit,

but instead overactivate target AMPylation (Truttmann et al., 2015). Modulating a protein with nanobodies does not only apply for altering enzymatic activity, but also for inducing conformational changes of proteins to have different fluorescent properties (Kirchhofer et al., 2010). Nanobodies were also used to drug influenza nucleoprotein to disrupt the replication of virus particles (Ashour et al., 2015).

As outlined with only a few examples, nanobodies represent a versatile device to study protein-protein interactions, properties and functions. Their broad range applicability in basic science makes them a powerful tool. Being aware of the nanobodies' versatility, we established a tool to track proteins from the cell surface to intracellular compartments. To our knowledge, we are the first who made use of bacterially expressed functionalized nanobodies to follow the retrograde sorting itineraries of EGFP-modified cargo. The increasing number of nanobodies against different proteins and domains will make it possible to monitor retrograde transport of endogenous, untagged cargo. Our nanobody approach can then be used by replacing VHH_{GFP} by a receptor-specific nanobody to yield functionalized transport trackers.

4.2 Role and Function of AP-1 in Endosome-to-TGN Transport

As mentioned throughout this study, AP-1/clathrin carriers are involved in protein sorting at the TGN-to-endosome interface. Over the last decades, evidence has accumulated that AP-1 does not just simply mediate anterograde transport of proteins from the TGN, but also retrograde transport to the TGN. Therefore, the consensus has arisen that the AP-1 cargo adaptor is involved in bidirectional traffic between the TGN and early endosomes.

We have investigated the question of the involvement of AP-1 in retrograde transport from endosomes using a direct assay with our functionalized, tyrosine sulfatable nanobody (VHH_{GFP}-2xTS). For this, we combined our retrograde nanobody-based 'transport tracker' with protein interference to look at transport to the TGN. We used four different interference approaches, BFA treatment, RNAi, CRISPR/Cas9 and knocksideways, to inactivate AP-1 function. Apart from providing evidence for AP-1 to be involved in retrograde transport to the TGN, some of our results, partially contradict previous findings. In the following, we will briefly discuss the results from the different protein interference approaches and relate them to each other to corroborate the role of AP-1 in retrograde endosome-to-TGN traffic.

4.2.1 BFA-Mediated Interference Blocks Retrograde Transport of MPRs

We used the fungal metabolite BFA to generally interfere with retrograde transport. As mentioned before, BFA inhibits sensitive ARFGEFs, resulting in missing recruitment of ARF GTPases to early endosomes and the Golgi. As a consequence of this, ARF GTPase-recruited adaptor proteins will not assemble anymore on these membranes and will rather remain cytosolic, thereby precluding productive ARF1-dependent carrier formation from endosomes. We observed a complete block in retrograde transport of recombinant CIMPR and CDMPR to the TGN in the presence of BFA, as assessed by sulfation analysis of bound nanobody. These results are in agreement with previous studies on retrograde transport using BFA (Amessou et al., 2007; Mallard et al., 1998). BFA does not only result in the immediate dissociation of several adaptors from the membranes, but also in Golgi complex disassembly and redistribution of Golgi enzymes into the ER (Klausner et al., 1992; Lippincott-Schwartz et al., 1991).

Recently, there was also a report that high BFA concentrations can indirectly affect sulfation in the TGN (Fjeldstad et al., 2002). Proteins from the biosynthetic pathway were sulfated at reduced levels due to impaired uptake of PAPS into the lumen of the Golgi apparatus after BFA administration. However, we used concentrations at 2 μg/mL of BFA where sulfation was not significantly affected. We thus can conclude that the lack of signal in BFA-treated cells is not due to inhibition of sulfation by TPSTs, but rather a consequence of impaired transport to the TGN or Golgi dysfunction. We also do not think that the lack of sulfation is a result of complete relocalization of the sulfation machinery to ER upon BFA treatment. In such a case, the sulfation assay would measure transport to the dispersed Golgi/ER rather than the TGN.

To our surprise, steady-state nanobody uptake levels of BFA-treated cells reached the same plateau as control cells after 75 min. Even though AP-1 is dissociating from TGN membranes by acute

BFA treatment, the fungal metabolite also induces highly dynamic tubular extensions from the TGN that fuse with endosomes to yield a tubular network with endosomal characteristics (Waguri et al., 2003). This finding may explain why also the TGN-resident recombinant MPR pool reaches the cell surface in BFA-treated cells.

Furthermore, as previously shown in our lab, there was no effect on in vitro TGN carrier formation of MPR-containing transport intermediates in the presence of BFA (Kobialka, unpublished). Although BFA causes a block in retrograde transport of MPRs, we cannot specifically reduce this phenotype to AP-1 inactivation only.

4.2.2 AP-1 Knocksideways Partially Blocks Retrograde Transport of MPRs

Unlike BFA that has a broader spectrum of action than only affecting AP-1, the knocksideways approach was established to specifically and acutely inactivate the AP-1 pathway. Fast approaches to rapidly block and thus to look at immediate consequences of AP-1 depletion became necessary since knockout and knockdown studies have produced misleading results regarding directionality of transport and function. In some studies, cargo proteins were found to accumulate in peripheral endosomal (Meyer et al., 2000) or postendosomal (Foote and Nothwehr, 2006) compartments, whereas, in others, they accumulated in the perinuclear Golgi region (Canuel et al., 2008) or even at the cell surface (Lubben et al., 2007). From these phenotypes, it was concluded that AP-1 is involved in anterograde and retrograde carrier transport, thereby not considering the possibility of indirect effects or cell adaptation. In case of indirect effects, a possible scenario might be that during gradual depletion, the sorting of cargo proteins is likely to become less and less efficient as the levels of AP-1 decrease. Some of the transported cargo proteins may be themselves components of the trafficking machinery, including SNAREs or tethers. Thus, by the time the cells are ready for an experiment, other proteins may have been missorted, not as a consequence of AP-1 depletion, but as secondary effect, due to the mislocalization of machinery components (Robinson et al., 2010). On the other hand, it might also be possible, that the cell compensates for the loss of AP-1 by upregulating other sorting pathways. Indeed, a cellular adaptation in such regard has been previously described. It was reported that when the formation of clathrin-coated vesicles was inhibited by knockdown of either CHC17 or auxilin, AP-4 vesicle formation was stimulated without affecting protein levels (Hirst et al., 2012b). Also, as shown for instance in a different study, specific depletion of any GGA adaptor resulted in a partial decrease of the others (Ghosh et al., 2003b), pointing out that a 'specific' knockdown might affect more components than just the protein of interest. Another study also showed that levels of active ARF-GTP are drastically increased in cells depleted of either CHC17 or AP-1 by RNAi (Matsudaira et al., 2015). Thus, gradual depletion can indeed lead to biochemical changes.

In the present study, we thus applied the currently most reliable way of inactivating a protein, knocksideways. By using the AP-1 knocksideways system, we were revisiting the role of AP-1 in retrograde transport and thereby found that endosome-to-TGN transport of recombinant MPRs was partially, by far not completely blocked. This observation is in line with other studies supporting AP-1 to operate in retrograde transport (Meyer et al., 2000; Robinson et al., 2010) on top of its undisputed role in anterograde traffic. Given the fact that retrograde transport of CIMPR to the TGN was strongly impaired

as judged by immunofluorescence (Robinson et al., 2010), we were a little bit disappointed to only see a mild reduction of about a third. We thus speculate that the other two thirds are transported by alternative, AP-1-independent sorting machineries, including retromer complex, epsinR and Rab9/TIP47. Although knocksideways is more specific than BFA and less indirect than a knockdown, it has to be mentioned that rapamycin-induced AP-1 rerouting also relocalizes AP-1 binding partners, including epsinR, aftiphilin and γ-synergin, to mitochondria (Hirst et al., 2012a; Robinson et al., 2010). One can thus not formally rule out the possibility that the observed reduction in sulfation of piggyback-transported nanobody is caused or contributed by relocalization of these factors, in particular that of epsinR. EpsinR has been suggested to traffic MPRs from early endosomes to the TGN (Saint-Pol et al., 2004), and the respective study reported a reduction of ~ 30% in MPR transport to the TGN in epsinR-depleted cells. The extent of epsinR relocalization by mitochondrially sequestered AP-1 is unknown (Hirst et al., 2012a; Robinson et al., 2010), however, it has to be mentioned that ~ 50% reduction of epsinR levels was sufficient to cause an inhibition of ~ 30% in retrograde MPR transport (Saint-Pol et al., 2004). When knocking down AP-1 by RNAi, epsinR still normally localizes to its target membranes. Thus, in the case of a knockdown, epsinR distribution does not depend on AP-1 (Hirst et al., 2004; Hirst et al., 2003). However, since knockdown readouts might bring along the risk of indirect or compensatory effects, we should also skeptically regard gradual epsinR depletion phenotypes. It thus remains to be figured out what the precise contribution of epsinR in our rapid inactivation approaches is. Robinson and colleagues established an epsinR KS cell line and could show that this adaptor seems to have a more global role than just acting as SNARE-specific cargo adaptor. It would thus be very interesting to test to which extent retrograde traffic of recombinant MPR is affected in cells with rapidly sequestered epsinR.

In general, we think that the contribution of epsinR to retrograde transport during AP-1 knocksideways is neglectable. Even though there is an interdependent action of epsinR and AP-1 in intracellular CCV formation as suggested by Robinson and colleagues (Hirst et al., 2012a; Hirst et al., 2015), epsinR alone nucleates a separate population of transport carriers. Given the fact that cytosolic levels of epsinR are unchanged during an AP-1 knocksideways (Robinson et al., 2010), we believe that there is still enough of the adaptor available to confer epsinR-mediated membrane traffic from early endosomes. We thus think that the partial block in retrograde transport observed for MPRs is mainly due to the inactivation of AP-1.

4.2.3 AP-1 Knockdown/out and Alternative Pathways

To figure out the involvement of other, alternative sorting machineries in retrograde transport of MPRs, we followed an RNAi-based approach by simply monitoring sulfation upon compartment arrival. As reported previously (Arighi et al., 2004; Popoff et al., 2009; Popoff et al., 2007b; Seaman, 2004), depletion of retromer subunits caused an accumulation of MPRs in peripheral compartments. We were thus not much surprised when retromer depletion by targeting Vps26 resulted in decreased nanobody sulfation. The TIP47 adaptor, conversely, did not alter retrograde transport kinetics of CDMPR. TIP47 was initially described as MPR-specific adaptor operating in late endosome-to-TGN transport (Diaz and Pfeffer, 1998; Diaz et al., 1997). Over the years, however, findings have accumulated contradicting TIP47 to be involved

in retrograde MPR transport (Bulankina et al., 2009; Medigeshi and Schu, 2003), but rather in lipid droplet biogenesis. Our results suggest that TIP47 is likely not taking part in retrograde transport of MPRs. Depletion of Rab9, the upstream regulator of TIP47, in contrast caused a slight reduction in nanobody sulfation, indicating the GTPase to be operating in retrograde transport. This was somehow expected since Rab9 acts as a hub for many downstream trafficking events on endosomes (Kucera et al., 2016a; Kucera et al., 2016b). Impaired MPR transport is thus likely not a direct consequence of Rab9 depletion, but rather an indirect effect, including dysregulation of endosome maturation and endosome misbalance.

For completeness sake, we then also performed an AP-1 knockdown, with the idea to confirm our knocksideways readouts. Surprisingly, retrograde transport of CDMPR was affected differently, sulfation of transported nanobody was strongly increased. Also, AP-1 KO HeLa cells showed stronger sulfation of MPR-transported nanobody compared to their parental cells. Both these results suggested AP-1 to not function in retrograde transport, but rather to prevent MPR traffic to the compartment of labeling. In this regard, our results are in disagreement with our and previous reported immunostainings showing MPRs to accumulate in peripheral compartments in antibody uptake experiments (Meyer et al., 2000; Robinson et al., 2010) or in resialylation experiments of cell surface-desialylated MPRs (Meyer et al., 2000). Sulfation analysis of EGFP-CDMPR not only showed sulfation to start earlier in AP-1 KD cells, but also to head towards steady-state of sulfation close after 75 min. As a consequence, nanobody sulfation was higher at every measured time point within 75 min.

How can the AP-1 KD sulfation phenotype be explained? There are many not mutually exclusive explanations for this observation. One idea might be that retrograde transport of MPRs is not dependent on AP-1/clathrin carriers at all, but only on anterograde transport. Following this view, this would explain the enhanced sulfation phenotype where MPR cargo might enter the TGN, but accumulate there since exit is impaired. Impaired exit is in line with prolonged residence time in the TGN, and thus potentially higher sulfation efficiency. Indeed, a previous publication favored an unidirectional rather than a bidirectional role of AP-1 traffic (Canuel et al., 2008). This report suggested AP-1 and retromer to play opposite roles in hydrolase receptor traffic.

Another reason to explain the increased sulfation phenotype is that sulfation machinery localization might be affected by AP-1 perturbances. 'Generally', it is assumed that when perturbances are introduced into a system, the machinery giving rise to the experimental readout, in our case the endogenous sulfation apparatus, remains static. However, this should be rarely the case. We thus thought that parts of the sulfation machinery, among them TPSTs or PAPS transporters, might have shifted their steady-state localizations to post-TGN compartments. In such a model, nanobody sulfation would not only occur earlier after endocytosis, but would also be increased due to higher residence time of MPRs in sulfation-competent compartments. We checked the steady-state distribution of fluorescently tagged TPSTs, but did not see any striking difference by optical means between control and AP-1 KD or KO cells, respectively. Ultrastructural resolution of the perinuclear region by electron microscopy might have allowed determining membrane subcompartments, thus more convincingly providing evidence whether there is a shift in steady-state after interference. But, the current data suggest that there is no significant TPST relocalization to post-TGN membranes in AP-1 KD and KO cells.

We also tried to check other sulfation machinery components such as one member of the PAPS transporters (PAPST2, systematic name: SLC35B3). In our hands, the commercial antibody recognizing this transporter did not work, leaving the question open whether other sulfation machinery components rather than TPSTs are missegregated to endosomal membranes. Recently, however, we have had a closer look at affected cargo proteins from AP-1/CCVs (Hirst et al., 2012a). Robinson and lab listed cargo proteins that were depleted more than two fold from intracellular CCVs after rapid inactivation of AP-1. Interestingly, SLC35B2 (PAPST1), the other out of two PAPS transporters was found among robustly depleted cargo proteins from AP-1/CCVs. This finding is very stimulating since it suggests that AP-1 is either involved in retention or retrieval of this transporter. SLC35B2 had a fold depletion of 2.26, cathepsin Z, a bonafide MPR cargo, had a fold depletion of 2.35 in comparison, showing that SLC35B2 is strongly affected from AP-1/CCVs. In the study of Robinson (Hirst et al., 2012a), SLC35B2 was not further validated, however. While SLC35B2 was depleted from AP-1/CCVs, it was neither from epsinR/CCVs nor GGA2/CCVs, suggesting that the protein is specifically affected by AP-1 inactivation, only. Proteomics profiling of AP-1 KS gives a snapshot which proteins are immediately affected after adaptor sequestration without indirect effects to emerge. As a KD lasts for several days, it might be that SLC35B2 is gradually missorted to peripheral compartments upon RNAi-mediated depletion of AP-1. Other transmembrane proteins found in the list (Hirst et al., 2012a) with more than two fold depletion from AP-1/CCVs include for instance CDMPR (2.68), STX10 (3.04), furin (3.05), STX16 (3.06) or CIMPR (3.12). All these proteins have been previously reported to shift their steady-state distribution to early endosomes upon AP-1 KD. It thus might be that SLC35B2 is also misdistributed using RNAi, making our AP-1 KD readout in general hard to interpret for sulfation experiments. Since AP-1 KS experiments lasted for 75 min at maximum, such changes in steady-state distribution of transmembrane proteins might be unlikely to occur rapidly.

Even though EGFP-tagged TPSTs show an exclusive perinuclear labeling pattern, we could also report TPST1-EGFP and TPST2-EGFP to migrate to the cell surface, since they were both accessible to externally added nanobody to a certain degree (not shown). It thus might be that TPSTs cycle also, but that sulfation nevertheless can only occur in the TGN where PAPS transporters and additional factors coincide to enable sulfation locally. If PAPS transporters really had an altered steady-state distribution towards early endosomes in AP-1 KD and KO cells, then it might be that sulfation could even occur in these compartments due to cycling TPSTs.

Another explanation for the enhanced sulfation phenotype is the possible discrepancy between acute and gradual or long-term protein depletion readouts. This is also the reason why we were favoring knocksideways-based inactivation strategies, since they hardly allow cellular adaption or indirect effects to dominate given the short time of inactivation. In particular for AP-1, a number of striking differences between RNAi- and knocksideways-based experimental readout have been already reported by the group of Robinson (Hirst et al., 2012a; Robinson et al., 2010). While we exploit sulfation to look at immediate consequences of perturbed traffic, Robinson and colleagues performed biochemical and proteomic characterization of isolated CCVs. Western blot analysis of isolated CCVs from AP-1 KS cells and AP-1 KD cells has for instance shown that there was a strong depletion of CIMPR from the former cell line

only (Robinson et al., 2010). This result suggested that during the period of gradual depletion, CIMPR was given a 'lift' by other transport intermediates to find its way to its target organelle. The same CCV isolation experiment also showed that there was more α-adaptin associated with vesicles prepared from AP-1 KD cells, whereas levels from AP-1 KS cells were unaltered. This observation probably reflected compensation for the loss of AP-1 (Robinson et al., 2010). In a follow-up study (Hirst et al., 2012a), Robinson and colleagues even showed a more dramatic difference in loss of AP-1's binding partners on isolated CCVs. Apart from epsinR and other previously known proteins, GGA2 was strongly depleted from AP-1 CCVs, even though not co-rerouted with AP-1 to mitochondria, while the amount of GGA2 in the vesicle fraction of a conventional knockdown was not affected (Hirst et al., 2012a). This result clearly demonstrated that the time from depleting a protein up to phenotype assessment can matter with regard to the readout. Additionally, in the latest study of Robinson (Navarro Negredo et al., 2017), the difference between long-term depletion (KD and/or KO) and knocksideways became apparent once again. While ARF1 was barely affected in CCVs isolated from AP-1 KO cells, it was strongly depleted from CCVs derived from AP-1 KS cells. Based on such previous findings derived from AP-1 KD or KO cells, we were already a little bit 'sensibilized' with possible cellular adaption or indirect effects which might misdirect us. Is thus the increased sulfation of nanobody with recombinant CDMPR a compensatory or indirect effect of gradual AP-1 depletion? We cannot give a definite answer. However, in our studies, we have made an observation that tends towards post-Golgi compartment dysregulation. We observed that in AP-1-depleted cells, nanobody-recombinant TfR complexes became sulfated, while this was not the case in control cells. The amount of nanobody that is sulfated in AP-1-depleted cells is unknown. We think that the sulfated fraction only represents a minor part of total bound nanobody to TfR-EGFP.

We were also wondering whether the phenotype of hypersulfation has been previously already reported for retrograde transport cargo proteins. Indeed, Ludger Johannes and collaborators have demonstrated that HeLa cells depleted of Hsc70, RME-8, or Vps35 have considerably elevated levels (300-400%) of sulfated Shiga toxin B-subunit (STxB), even though the bacterial cargo accumulated in 'peri-Golgi structures' (Popoff et al., 2009). This result was very much surprising since peripheral non-Golgi compartment accumulation of STxB was paralleled by increased sulfation. It has been previously observed that clathrin is involved in retrograde transport of STxB (Saint-Pol et al., 2004) as assessed by sulfation analysis using CHC17 KD. The clathrin uncoating ATPase Hsc70, conversely, which is part of the clathrin interactome and should essentially impair clathrin-dependent transport, played an opposite role. It is very hard to rationalize this finding, since removal of Hsc70 facilitated sulfation rather than preventing it. RNAi-based depletion did not only retain STxB in peri-Golgi tubular structures, but also fluorescently tagged CIMPR, highlighting a similar failure in retrograde delivery to the Golgi. RME-8, which is a 'bridging adaptor' between Hsc70 and the retromer complex via the Hrs protein, produced a similar hypersulfation phenotype. Also here, RME-8 depletion resulted in accumulation of STxB and recombinant MPR in peripheral compartments. Interestingly, Vps35 depletion, but not depletion of Vps26, caused hyper-sulfation of STxB. Even though they are both components of the same retromer subcomplex, and targeting either of them is commonly used to eliminate retromer complex function, interference with one of the subunits produced distinct biochemical phenotypes. While depletion of Vps26 caused an

accumulation in TfR-containing early endosomal tubules and concomitant reduction in sulfation of STxB, decrease in Vps35 expression prevented exit from endosomes, but resulted in increased sulfation. This result is misleading with regard to retromer complex function. Since Vps35 KD caused a stronger concomitant depletion of Vps26 than vice versa, the authors speculated that in Vps35-depleted cells, fusion with TGN/Golgi membranes is uncoupled from retrograde tubules detachment from early endosomes. The authors reasoned that STxB and other cargo might be in contact with sulfotransferases for extended periods of time in tubules in a dynamic manner. However, Ludger Johannes and colleagues could not detect TPSTs in the tubules by fluorescence microscopy. The puzzling observation of hypersulfation might be a result based on indirect effects of RNAi-mediated Hsc70-, RME8-, and Vps35-depletion.

A number of studies from the lab of Kirsten Sandvig have also recently reported unexpected hypersulfation, the cause of which remains unresolved in her studies, too (Dyve Lingelem et al., 2015; Klokk et al., 2011; Tcatchoff et al., 2012). It was shown that either addition of ONO, an inhibitor of cytoplasmic phospholipase A_2, or geldanamycin, an inhibitor of Hsp90, caused increased sulfation of STxB and ricin. In both studies, it was speculated why inhibition culminated in increased cargo sulfation. Also here, it remained to be determined whether increased sulfation had an indirect or direct cause.

In the present study, we have established a toolset of functionalized nanobodies to study retrograde traffic of EGFP-labeled proteins. By combining our nanobody-based tool with protein interference approaches, we readdressed the involvement of AP-1 in endosome-to-TGN transport of MPRs. So far, most of conclusions drawn on traffic at the TGN-to-endosome interface were based on gradual or long-term AP-1 depletion experiments. However, these studies had the caveat that they had neglected possible secondary or cellular adaptation effects. In particular, in the case of a trafficking adaptor like AP-1 that permanently traffics proteins between two intracellular compartments, the question about directionality is more complicated to be addressed in potentially dysregulated cells. On the one hand, RNAi-based or genetic depletion of AP-1 causes accumulation of MPRs in endosomes and depletion from the TGN (i.e. shift of steady-state towards endosomes). This idea supports AP-1 to be involved in retrograde transport. On the other hand, such AP-1-depleted cells have deficits in lysosomal targeting of cathepsin D, a readout that is often used to illustrate AP-1 dysfunction at the TGN. However, it can also be that the lack of efficient lysosomal targeting might be just the result of peripherally redistributed MPRs over the period of a knockdown or knockout, and not a consequence of AP-1 function at the TGN.

To thus investigate the immediate consequences of AP-1 inactivation, the knocksideways approach is preferable, since we have wild-type and unaltered steady-state distribution of trafficking components. We could report a partial reduction in retrograde transport of MPRs to the TGN upon AP-1 KS. Given the fact that nanobody might be trapped in the TGN due to a block in anterograde transport, our AP-1 KS readout might represent even an underestimate because of hypersulfation. In summary, our nanobody toolset in combination with knocksideways allowed us to reinvestigate the contribution of AP-1/clathrin carriers in retrograde transport from early endosomes to the TGN.

5 Perspectives

5 Perspectives

In this thesis, we have presented proof-of-concept of our nanobody-based tool to study retrograde transport from the cell surface to intracellular compartments. In the remainder of this work, we would like to give some perspectives to point out our future research interests and to stress additional experimental endeavors. Already during our pilot studies, we have rationalized the versatility of our nanobody-based toolkit to study intracellular protein traffic. One the way, we were inspired for other derivatized nanobodies with new functions and features to monitor or manipulate intracellular transport. Simultaneous to the expansion of nanobody fusions, we also started to widen the number of EGFP-tagged receptor proteins. In the following, we would like to outline the use of other established EGFP-modified reporter cell lines, functionalized nanobodies and other applications.

With the attempt to establish retrograde transport protein fusions as well as suitable controls, we came up with a list comprising a variety of different cargo proteins. So far, we have made use of MPRs and TGN46 as bonafide PM-to-TGN retrograde cargo proteins for proof-of-concept studies. In addition, we were also aware of APP, WLS, furin, and ANK that have been reported to return to the TGN. Because of the considerable number of reports manifesting their retrograde transport routes and underlying sorting machineries, we decided that time to go for MPRs and TGN46, only. Apart from these two proteins, the most well-described retrograde transport cargo is APP. Schekman and colleagues (Choy et al., 2012) provided some data for APP to undergo retrograde transport from early endosomes to the TGN for efficient amyloid β peptide production, a process that is involved in the development of Alzheimer's disease. The site of APP processing after internalization, however, is actually still debated. While the TGN is considered one of the main APP processing compartments in the study of Schekman (Choy et al., 2012), some others propose the endo-lysosomal system (Tam and Pasternak, 2015; Tam et al., 2014). We also established a stable HeLa cell line expressing EGFP-tagged APP695 (splice variant 695). We found the protein to reach the cell surface, as shown by nanobody internalization in these cells. Using VHH_{GFP}-2xTS in a sulfation assay, we could not detect any sulfated nanobody bound to EGFP-APP695, indicating that there was no substantial delivery of nanobody from the PM/EE pool of APP to the TGN (**Fig. S10**). These preliminary results indicate that APP is probably not a real bonafide retrograde transport cargo. Using our VHH_{GFP}-APEX2 and VHH_{GFP}-mCherry nanobodies, we plan to analyze APP's retrograde journey into the endocytic system in more detail in the future.

While APP was initially considered a bonafide retrograde transport protein, we started with similar premises for the 'Golgi-resident' proteins β-1,4-galactosyltransferase, α-2,6-sialyltransferase and α-mannosidase II, namely that they represent Golgi-resident proteins. However, we noticed that HeLa cells stably expressing GalT-EGFP or SiaT-EGFP could capture nanobody and bring it to the TGN for sulfation (**Fig. S10**). So far, it has never been reported that these glycosyltransferases cycle to the cell surface and come back again. For GalT, it has been shown that a fraction is detectable at the cell surface, potentially

with a function in cell adhesion (Hathaway et al., 2003). For Man II, in contrast, there is so far no evidence for a similar cell surface pool. When we looked at internalized nanobody in fixed HeLa cells stably expressing GalT-EGFP or SiaT-EGFP, we indeed could monitor transport back to the TGN, however, in addition, we also noticed that a considerable fraction of EGFP fusions did not overlap with TGN.

To concretize, it will be our interest to show that putative bonafide retrograde transport cargo proteins (i.e. APP) are not that bonafide as literally documented, and that Golgi marker proteins (i.e. GalT and SiaT), which are considered compartment-resident, are cycling at the TGN-to-cell surface interface. Using our functionalized nanobodies, we can start to look at these cargo proteins in more detail.

In our collection of cell lines, we also established HeLa stably expressing EGFP-LAMP1 and H1-EGFP. While the former can be used to study transport to lysosomes, the latter can be used as an additional recycling receptor reporter. As for recombinant TfR, we could not see any sulfation of nanobody riding along with H1-EGFP. H1 is a little bit more attractive than TfR for use. Then H1 has 50% of its mature protein at the cell surface while TfR only 15%. The versatility of our nanobody-based toolkit makes it possible to simply generate any EGFP fusion of interest and to study its retrograde transport.

Apart from looking at other EGFP cargo proteins with our functionalized nanobodies, we also generated some that could not be discussed within the scope this thesis. With the future attempts to investigate also PM-to-ER traffic, we generated and expressed a nanobody conferring N-glycosylation (VHH_{GFP}-Nglyco). It has been previously shown that N-glycosylation on proteins cannot only occur cotranslationally, but also posttranslationally (Plaut and Carbonetti, 2008). We also expressed a derivative comprising a tyrosine sulfation and N-glycosylation site to be able to measure TGN-to-ER transport (VHH_{GFP}-Nglyco-1xTS). In particular, in order to look at retrograde intra-Golgi transport of proteins, such a nanobody derivative is especially useful. Such a N-glycosylatable and sulfatable nanobody can also be used to determine TGN-to-ER-to-Golgi round trip kinetics by monitoring first sulfation (TGN arrival), detection of a shift because of the addition of an oligosaccharide chain (ER arrival) and by following its maturation to a mature glycan (second Golgi passage). Since a shift from an immature to mature glycan is not always very easy to separate and detect on a SDS-PAGE, we have developed another round trip tracker that is VHH_{GFP}-GAG-TS. It contains a site for glycosaminoglycanation that starts in the ER by the additon of xylose, followed by the attachment of long unbranched polysaccharides and subsequent sulfation during passage through the Golgi.

Even though we have these functionalized nanobodies already for use, we are still lacking an appropriate retrograde cargo protein to the ER. The probably best-established cargo proteins migrating from the cell surface to the ER are bacterial and plant toxins. The only known endogenous membrane protein which travels from the cell surface to the ER is the Wnt ligand receptor, WLS (Yu et al., 2014). WLS encodes a multipass transmembrane protein and has its N- and C-termini both in the cytosol. We have inserted an EGFP moiety into lumenal loops, but so far we did not obtain a functional protein. It is our aim to generate a WLS fusion, which is functional and can be used in our PM-to-ER retrograde and round trip approaches.

Another functionalized nanobody that awaits its further use is VHH_{GFP}-KDEL. KDEL mediates ER retrieval from KDEL receptor (KDELR)-positive compartments. Using such a functionalized nanobody, we might be able to test which EGFP-labeled cargo proteins are passing KDELR-positive compartments, and as second application, to potentially reroute reporters to the ER. Is KDELR also localized to the TGN? We can test this by administrating VHH_{GFP}-KDEL to cells expressing EGFP-tagged MPRs, for instance. In case the KDEL signal overrides the sorting determinants present in the EGFP fusions, then it might be shuttled to ER. The initial goal that we were following with the VHH_{GFP}-KDEL was to perform 'transmembrane protein knocksideways'. This nanobody might relocalize EGFP reporters of interest to the ER and traps them there.

Other functionalized nanobodies that are currently in planning are such which 'force' EGFP-modified cargo to continuously cycle at the endosome-to-PM interface rather than undergoing retrograde transport to the TGN, and such which target proteins for lysosome-mediated degradation. We think to achieve that by fusing either Tf (for 'forced' recycling) or EGF (for lysosomal targeting) to VHH_{GFP}. Unfortunately, there are no established lumenal signals for lysosomal degradation that might facilitate targeting. They typically all reside in the cytosolic tail of proteins.

As already briefly mentioned in the discussion, we are improving our sulfatable nanobodies by introducing other tyrosine sulfation consensus sequences than reported here. Then assessing transport to the TGN remains part of our core interest. New sequences should confer higher sulfation efficiency on the one hand, and guarantee detection by an anti-sulfotyrosine antibody (Sulfo-1C-A2) on the other hand. Using 'cold' rather than 'hot' sulfation would simplify all our future experimental endeavors concerning determination of cell surface-to-TGN transport kinetics.

We do not only want to examine new cargo proteins for retrograde transport to the TGN, but also to test a number of tail mutants of a given protein to elucidate the precise sorting determinants for endosome-to-TGN transport. Some of the motifs required for endosome-to-TGN in the cytosolic tail of CDMPR have been already described (Nair et al., 2003). It would be thus of interest to screen tail mutants of selected EGFP-tagged reporter proteins by feeding a TS-tagged nanobody that is detectable by an anti-sulfotyrosine antibody. By this, we can analyze and screen much faster for signals required for retrograde transport to the TGN. The assay would also enable us to screen whether the same patches of sorting signals are required for endocytosis and endosome-to-TGN transport, or whether they are present on different stretches of the cytoplasmic tail.

The number of available nanobodies is increasing and combining two or more of these in a system brings along many advantages. We have recently produced functionalized anti-mCherry nanobodies (VHH_{mCh}) and reporter cell lines stably expressing both an EGFP- and a mCherry-modified cargo protein. This allows us to study two recombinant fusion proteins at the same time in the same cell line. Accordingly, we have replaced VHH_{GFP} by VHH_{mCh} in some of our existing nanobodies and even prepared new ones (see also **Fig. S11 A-B**). By applying for instance VHH_{GFP}-2xTS and VHH_{mCh}-3xTS (to distinguish MW) to HeLa cells stably expressing EGFP-TGN46 and mCherry-CDMPR, we can follow

sulfation kinetics to the TGN of both these receptors. Simultaneously, we generated also an additional number of fluorophore-tagged VHH_{GFP} and VHH_{mCh} so that we can perform live cell imaging using a four color approach with no overlapping emission spectra (see also **Fig. S11 A**).

As mentioned previously, we are also preparing double stable cell lines expressing both an EGFP- and an mCherry-modified protein for other reasons. To be able to measure cell surface-to-TGN transport by live cell imaging in the future, we need a fluorophore-tagged TGN marker. We already established a repertoire of cell lines expressing for instance GalT-, TPST1-, or TPST2-EGFP with mCherry-CDMPR or TfR-mCherry. In this case, we can use VHH_{mCh}-mTagBFP2 or VHH_{mCh}-iRFP670 to follow mCherry-tagged receptors to endocytic compartments or to the TGN. Another attempt for live cell imaging with our generated nanobodies is to measure vectorial transport from a donor to an acceptor compartment. We can for instance express mTagBFP2-Rab5 (early endosomes) and mCherry-Rab9 (late endosomes) to study transport of EGFP-labeled cargo proteins between these two labeled endocytic compartments using VHH_{mCh}-iRPF670. Other fluorescent compartment markers can be used to label other organelles of interest (i.e. recycling endosomes, TGN, etc.). In light of other nanobody functionalization to monitor traffic of proteins of interest through the endo-lysosomal system, it would be also interesting to chemically couple commercially available pH sensors, like pHrodo, to our nanobodies.

We do not only follow the idea of using nanobodies as transport trackers, but also want to apply them as a tool to inactivate proteins similar to the knocksideways approach. We would like to attempt making use of the type III secretion-based protein delivery tool of Yersinia enterocolitica (Ittig et al., 2015). As presented in the study of Ittig, this bacterial injectosome device can be exploited to deliver proteins into target cells with a high infection rate. They also showed that a myc-tagged VHH_{GFP} could be delivered into cells and bind EGFP fusions (Ittig et al., 2015). We would like to apply NLS- or degron-tagged nanobodies to sequester and inactivate proteins in the nucleus or by the proteasome, respectively. Using such an approach, we could in principal inactivate one or two proteins simultaneously and figure out their interdependence and possibly concerted action. We have already tried such an approach by relocalizing clathrin (EGFP-CLCa or HA-FKBP-CLCa) to the nucleus by delivering a plasmid encoding NLS-VHH_{GFP}-FLAG-NLS or NLS-FRB-NLS by transient transfections. Preliminary results showed that this seemed to work and we are wondering whether we can follow a similar strategy to inactivate two proteins at the same time using the type III delivery tool (**Fig. S12**).

Within the scope of our discussion regarding the interdependence of AP-1 and epsinR adaptors in retrograde endosome-to-TGN traffic, it would be interesting to know what happens when we nuclearily trap one of the adaptor alone or both together (e.g. EGFP-γ-adaptin and mCherry-epsinR). As an alternative, we could also just stably bring a siRNA-resistant copy of mCherry-epsinR into our AP-1 KS EGFP reporter cell line to yield a quadruple stable cell line. Here, there is a requirement of administrating both rapamycin and NLS-tagged VHH_{mCh}.

Another planned and novel strategy to inactivate and reactivate proteins would be by delivering a VHH_{GFP}-VHH_{mCh} fusion into cells expressing both an EGFP-tagged prey and a mCherry-tagged bait protein using the type III delivery tool. In this case, the nanobody fusion acts as a heterodimerizer by connecting

both fluorophores with each other that are themselves linked to proteins of interest. Prey and bait can be analogues to the knocksideways system where we have a cytosolic prey and mitochondrial bait protein. We even think of making cleavable nanobody heterodimerizers by including a TEV cleavage site between the two nanobodies. Subsequent delivery of TEV protease by the type III delivery tool would allow reactivation of the sequestered prey protein.

To round up, we have explored a broad range of applications of our nanobody-based tool or of nanobodies in general in basic science, and recognized its potential for other approaches. We are heading forward to tackle some of these ideas in the near future.

6 Supplementary Material

6 Supplementary Material

Table S1: Protein sequences of the main EGFP-labeled reporter proteins. Signal sequence of hemagglutinin is highlighted in red, EGFP in green, and the cargo sequence in blue. Asterisk (*) marks the end of the protein.

EGFP reporter	Protein sequence
EGFP	MVSKGEELFTGVVPILVELDGDVNGHKFSVSGEGEGDATYGKLTLKFICTTGKLPV PWPTLVTTLTYGVQCFSRYPDHMKQHDFFKSAMPEGYVQERTIFFKDDGNYKTR AEVKFEGDTLVNRIELKGIDFKEDGNILGHKLEYNYNSHNVYIMADKQKNGIKVN FKIRHNIEDGSVQLADHYQQNTPIGDGPVLLPDNHYLSTQSALSKDPNEKRDHM VLLEFVTAAGITLGMDELYK*
EGFP-CIMPR	MKTIIALSYIFCLVFARESMVSKGEELFTGVVPILVELDGDVNGHKFSVSGEGEGDAT YGKLTLKFICTTGKLPVPWPTLVTTLTYGVQCFSRYPDHMKQHDFFKSAMPEGYV QERTIFFKDDGNYKTRAEVKFEGDTLVNRIELKGIDFKEDGNILGHKLEYNYNSH NVYIMADKQKNGIKVNFKIRHNIEDGSVQLADHYQQNTPIGDGPVLLPDNHYLS TQSALSKDPNEKRDHMVLLEFVTAAGITLGMDELYKSGLRSRAVGAVLSLLLVALT GCLLALLLHKKERRETVINKLTSCCRRSSGVSYKYSKVSKEEETDENETEWLMEEIQ VPAPRLGKDGQENGHITTKAVKAEALSSLHGDDQDSEDEVLTVPEVKVHSGRGA EVESSQPLRNPQRKVLKEREGERLGLVRGEKARKGKFRPGQRKPTAPAKLVSFHD DSDEDLLHI*
EGFP-CDMPR	MKTIIALSYIFCLVFARESMVSKGEELFTGVVPILVELDGDVNGHKFSVSGEGEGDAT YGKLTLKFICTTGKLPVPWPTLVTTLTYGVQCFSRYPDHMKQHDFFKSAMPEGYV QERTIFFKDDGNYKTRAEVKFEGDTLVNRIELKGIDFKEDGNILGHKLEYNYNSH NVYIMADKQKNGIKVNFKIRHNIEDGSVQLADHYQQNTPIGDGPVLLPDNHYLS TQSALSKDPNEKRDHMVLLEFVTAAGITLGMDELYKGTTEEKSCDLVGEKDKESK NEVALLERLRPLFNKSFESTVGQGSDTYSYIFRVCREASNHSSGAGLVQINKSNDKE TVVGRINETHIFNGSNWIMLIYKGGDEYDNHCGKEQRRAVVMISCNRHTLAANF NPVSEERGKVQDCFYLFEMDSSLACSPEVSHLSVGSILLVIFASLVAVYIIGGFLYQRLV VGAKGMEQFPHLAFWQDLGNLVADGCDFVCRSKPRNVPAAYRGVGDDQLGEE SEERDDHLLPM*

Table S1 (continued): Protein sequences of the main EGFP-labeled reporter proteins. Signal sequence of hemagglutinin is highlighted in red, EGFP in green, and the cargo sequence in blue. Asterisk (*) marks the end of the protein.

EGFP reporter	Protein sequence
EGFP-TGN46	MKTIIALSYIFCLVFARESMVSKGEELFTGVVPILVELDGDVNGHKFSVSGEGEGDAT YGKLTLKFICTTGKLPVPWPTLVTTLTYGVQCFSRYPDHMKQHDFFKSAMPEGYV QERTIFFKDDGNYKTRAEVKFEGDTLVNRIELKGIDFKEDGNILGHKLEYNYNSH NVYIMADKQKNGIKVNFKIRHNIEDGSVQLADHYQQNTPIGDGPVLLPDNHYLS TQSALSKDPNEKRDHMVLLEFVTAAGITLGMDELYKGTATESVKQEDAGVRPSAG NVSTHPSLSQRPGGSTKSHPEPQTPKDSPSKSSAEAQTPEDTPNKSGAEAKTQKDS SNKSGAEAKTQKGSTSKSGSEAQTTKDSTSKSHPELQTPKDSTGKSGAEAQTPED SPNRSGAEAKTQKDSPSKSGSEAQTTKDVPNKSGADGQTPKDGSSKSGAEDQTP KDVPNKSGAEKQTPKDGSNKSGAEEQGPIDGPSKSGAEEQTSKDSPNKVVPEQPS RKDHSKPISNPSDNKELPKADTNQLADKGKLSPHAFKTESGEETDLISPPQEEVKSS EPTEDVEPKEAEDDDTGPEEGSPPKEEKEKMSGSASSENREGTLSDSTGSEKDDLYP NGSGNGSAESSHFFAYLVTAAILVAVLYIAHHNKRKIIAFVLEGKRSKVTRRPKASD YQRLDQKS*
TfR-EGFP	MMDQARSAFSNLFGGEPLSYTRFSLARQVDGDNSHVEMKLAVDEEENADNNTK ANVTKPKRCSGSICYGTIAVIVFFLIGFMIGYLGYCKGVEPKTECERLAGTESPVREEP GEDFPAARRLYWDDLKRKLSEKLDSTDFTSTIKLLNENSYVPREAGSQKDENLALY VENQFREFKLSKVWRDQHFVKIQVKDSAQNSVIIVDKNGRLVYLVENPGGYVAYS KAATVTGKLVHANFGTKKDFEDLYTPVNGSIVIVRAGKITFAEKVANAESLNAIGV LIYMDQTKFPIVNAELSFFGHAHLGTGDPYTPGFPSFNHTQFPPSRSSGLPNIPVQTI SRAAAEKLFGNMEGDCPSDWKTDSTCRMVTSESKNVKLTVSNVLKEIKILNIFGVI KGFVEPDHYVVVGAQRDAWGPGAAKSGVGTALLLKLAQMFSDMVLKDGFQPS RSIIFASWSAGDFGSVGATEWLEGYLSSLHLKAFTYINLDKAVLGTSNFKVSASPLLY TLIEKTMQNVKHPVTGQFLYQDSNWASKVEKLTLDNAAFPFLAYSGIPAVSFCFC EDTDYPYLGTTMDTYKELIERIPELNKVARAAAEVAGQFVIKLTHDVELNLDYERY NSQLLSFVRDLNQYRADIKEMGLSLQWLYSARGDFFRATSRLTTDFGNAEKTDRF VMKKLNDRVMRVEYHFLSPYVSPKESPFRHVFWGSGSHTLPALLENLKLRKQNNG AFNETLFRNQLALATWTIQGAANALSGDVWDIDNEFRTRIDMVSKGEELFTGVV PILVELDGDVNGHKFSVSGEGEGDATYGKLTLKFICTTGKLPVPWPTLVTTLTYGV QCFSRYPDHMKQHDFFKSAMPEGYVQERTIFFKDDGNYKTRAEVKFEGDTLVNR IELKGIDFKEDGNILGHKLEYNYNSHNVYIMADKQKNGIKVNFKIRHNIEDGSVQL ADHYQQNTPIGDGPVLLPDNHYLSTQSALSKDPNEKRDHMVLLEFVTAAGITLG MDELYK*

Table S2: Protein sequences of the functionalized nanobodies applied in this study. T7 epitope is highlighted in turquoise, HA epitope in orange, BAP epitope in yellow, hexahistidine in blue, TEV cleavage site in brown, myc epitope in violet, the tyrosine consensus sequence in red, APEX2 in olive, and mCherry in pink. Asterisk (*) marks the end of the protein.

Nanobody	Protein sequence
VHH_{GFP}-control	MASMTGGQQMGRGSDQVQLVESGGALVQPGGSLRLSCAASGFPVNRYSMRWY RQAPGKEREWVAGMSSAGDRSSYEDSVKGRFTISRDDARNTVYLQMNSLKPEDT AVYYCNVNVGFEYWGQGTQVTVSSTSEFDYPYDVPDYAGAQPARSGGGLNDIF EAQKIEWHEGALEHHHHHH*
VHH_{GFP}-TEV-control	MASMTGGQQMGRGSDQVQLVESGGALVQPGGSLRLSCAASGFPVNRYSMRWY RQAPGKEREWVAGMSSAGDRSSYEDSVKGRFTISRDDARNTVYLQMNSLKPEDT AVYYCNVNVGFEYWGQGTQVTVSSTSENLYFQSEFDYPYDVPDYAGAQPARSG GGLNDIFEAQKIEWHEGALEHHHHHH*
VHH_{GFP}-myc	MASMTGGQQMGRGSDQVQLVESGGALVQPGGSLRLSCAASGFPVNRYSMRWY RQAPGKEREWVAGMSSAGDRSSYEDSVKGRFTISRDDARNTVYLQMNSLKPEDT AVYYCNVNVGFEYWGQGTQVTVSSTSEQKLISEEDLEFDYPYDVPDYAGAQPAR SGGGLNDIFEAQKIEWHEGALEHHHHHH*
VHH_{GFP}-1xTS	MASMTGGQQMGRGSDQVQLVESGGALVQPGGSLRLSCAASGFPVNRYSMRWY RQAPGKEREWVAGMSSAGDRSSYEDSVKGRFTISRDDARNTVYLQMNSLKPEDT AVYYCNVNVGFEYWGQGTQVTVSSTSSAEDYEYPSEFDYPYDVPDYAGAQPARS GGGLNDIFEAQKIEWHEGALEHHHHHH*
VHH_{GFP}-2xTS	MASMTGGQQMGRGSDQVQLVESGGALVQPGGSLRLSCAASGFPVNRYSMRWY RQAPGKEREWVAGMSSAGDRSSYEDSVKGRFTISRDDARNTVYLQMNSLKPEDT AVYYCNVNVGFEYWGQGTQVTVSSTSSAEDYEYPSAEDYEYPSEFDYPYDVPDYA GAQPARSGGGLNDIFEAQKIEWHEGALEHHHHHH*
VHH_{GFP}-TEV-2xTS	MASMTGGQQMGRGSDQVQLVESGGALVQPGGSLRLSCAASGFPVNRYSMRWY RQAPGKEREWVAGMSSAGDRSSYEDSVKGRFTISRDDARNTVYLQMNSLKPEDT AVYYCNVNVGFEYWGQGTQVTVSSTSENLYFQSSAEDYEYPSAEDYEYPSEFDYP YDVPDYAGAQPARSGGGLNDIFEAQKIEWHEGALEHHHHHH*
VHH_{GFP}-APEX2	MASMTGGQQMGRGSDQVQLVESGGALVQPGGSLRLSCAASGFPVNRYSMRWY RQAPGKEREWVAGMSSAGDRSSYEDSVKGRFTISRDDARNTVYLQMNSLKPEDT AVYYCNVNVGFEYWGQGTQVTVSSTSGKSYPTVSADYQDAVEKAKKKLRGFIAE KRCAPLMLRLAFHSAGTFDKGTKTGGPFGTIKHPAELAHSANNGLDIAVRLLEPLK AEFPILSYADFYQLAGVVAVEVTGGPKVPFHPGREDKPEPPPEGRLPDPTKGSDHLR DVFGKAMGLTDQDIVALSGGHTIGAAHKERSGFEGPWTSNPLIFDNSYFTELLSGE KEGLLQLPSDKALLSDPVFRPLVDKYAADEDAFFADYAEAHQKLSELGFADAEFDY PYDVPDYAGAQPARSGGGLNDIFEAQKIEWHEGALEHHHHHH*

Table S2 (continued): Protein sequences of the functionalized nanobodies applied in this study. T7 epitope is highlighted in turqouise, HA epitope in orange, BAP epitope in yellow, hexahistidine in blue, TEV cleavage site in brown, myc epitope in violet, the tyrosine consensus sequence in red, APEX2 in olive, and mCherry in pink. Asterisk (*) marks the end of the protein.

Nanobody	Protein sequence
VHH_{GFP}-TEV-APEX2	MASMTGGQQMGRGSDQVQLVESGGALVQPGGSLRLSCAASGFPVNRYSMRWY RQAPGKEREWVAGMSSAGDRSSYEDSVKGRFTISRDDARNTVYLQMNSLKPEDT AVYYCNVNVGFEYWGQGTQVTVSSTSENLYFQSGKSYPTVSADYQDAVEKAKK KLRGFIAEKRCAPLMLRLAFHSAGTFDKGTKTGGPFGTIKHPAELAHSANNGLDIA VRLLEPLKAEFPILSYADFYQLAGVVAVEVTGGPKVPFHPGREDKPEPPPEGRLPDPT KGSDHLRDVFGKAMGLTDQDIVALSGGHTIGAAHKERSGFEGPWTSNPLIFDNS YFTELLSGEKEGLLQLPSDKALLSDPVFRPLVDKYAADEDAFFADYAEAHQKLSELG FADAEFDYPYDVPDYAGAQPARSGGGLNDIFEAQKIEWHEGALEHHHHHH*
VHH_{GFP}-mCherry	MASMTGGQQMGRGSDQVQLVESGGALVQPGGSLRLSCAASGFPVNRYSMRWY RQAPGKEREWVAGMSSAGDRSSYEDSVKGRFTISRDDARNTVYLQMNSLKPEDT AVYYCNVNVGFEYWGQGTQVTVSSTSMVSKGEEDNMAIIKEFMRFKVHMEGSV NGHEFEIEGEGEGRPYEGTQTAKLKVTKGGPLPFAWDILSPQFMYGSKAYVKHPA DIPDYLKLSFPEGFKWERVMNFEDGGVVTVTQDSSLQDGEFIYKVKLRGTNFPSD GPVMQKKTMGWEASSERMYPEDGALKGEIKQRLKLKDGGHYDAEVKTTYKAK KPVQLPGAYNVNIKLDITSHNEDYTIVEQYERAEGRHSTGGMDELYKEFDYPYDV PDYAGAQPARSGGGLNDIFEAQKIEWHEGALEHHHHHH*

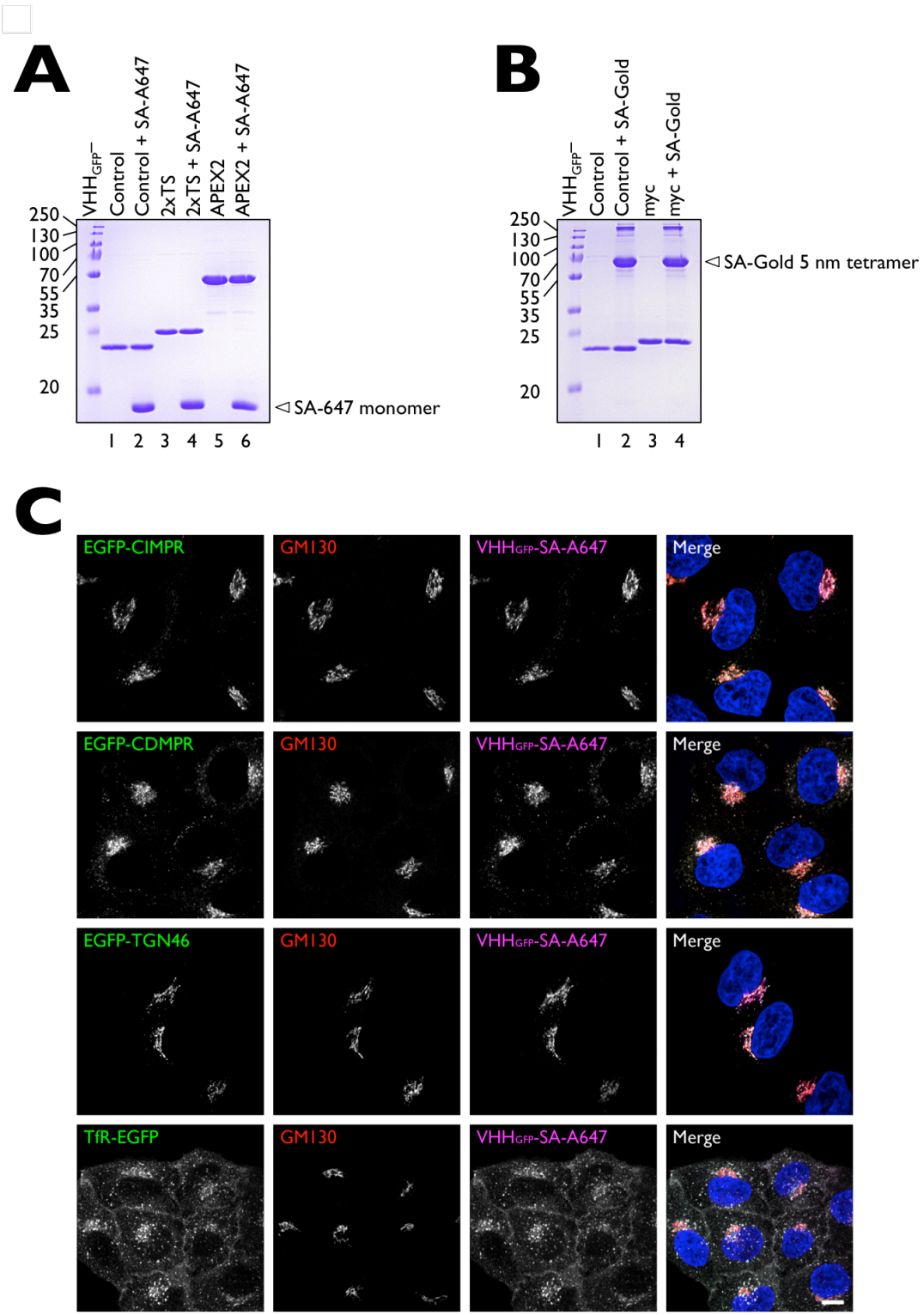

Figure S1: Functionalization of nanobodies with streptavidin conjugates. (A) Biotinylated nanobodies were coupled in vitro to streptavidin Alexa 647. Since one molecule of streptavidin can bind four molecules of biotin, a reaction mixture with 3:1 molarity ratio of nanobody:streptavidin conjugate was prepared. A 3:1 ratio was chosen to have an excess of streptavidin conjugate in the reaction to saturate biotin on nanobodies. Following 1 h of incubation at RT in PBS, the reaction mixture was run on a mini nickel column to remove unbound conjugate. Nanobody-streptavidin conjugates were eluted, desalted and stored in PBS. Typically, 30 ug of nanobody:streptavidin conjugate was loaded on a SDS-PAGE, followed by Coomassie staining (monomers of SA are seen). The step using a mini nickel and desalting column was not necessary. Then we did not see any uptake of streptavidin conjugates. **(B)** The same as in (A), but with streptavidin gold 5 nm. **(C)** 2 μg/mL VHH$_{GFP}$-control coupled to Alexa 647 was added to reporter cell lines and processed for IF. Numbers along the markers correspond to molecular weight in kDa. Scale bar: 10 μm.

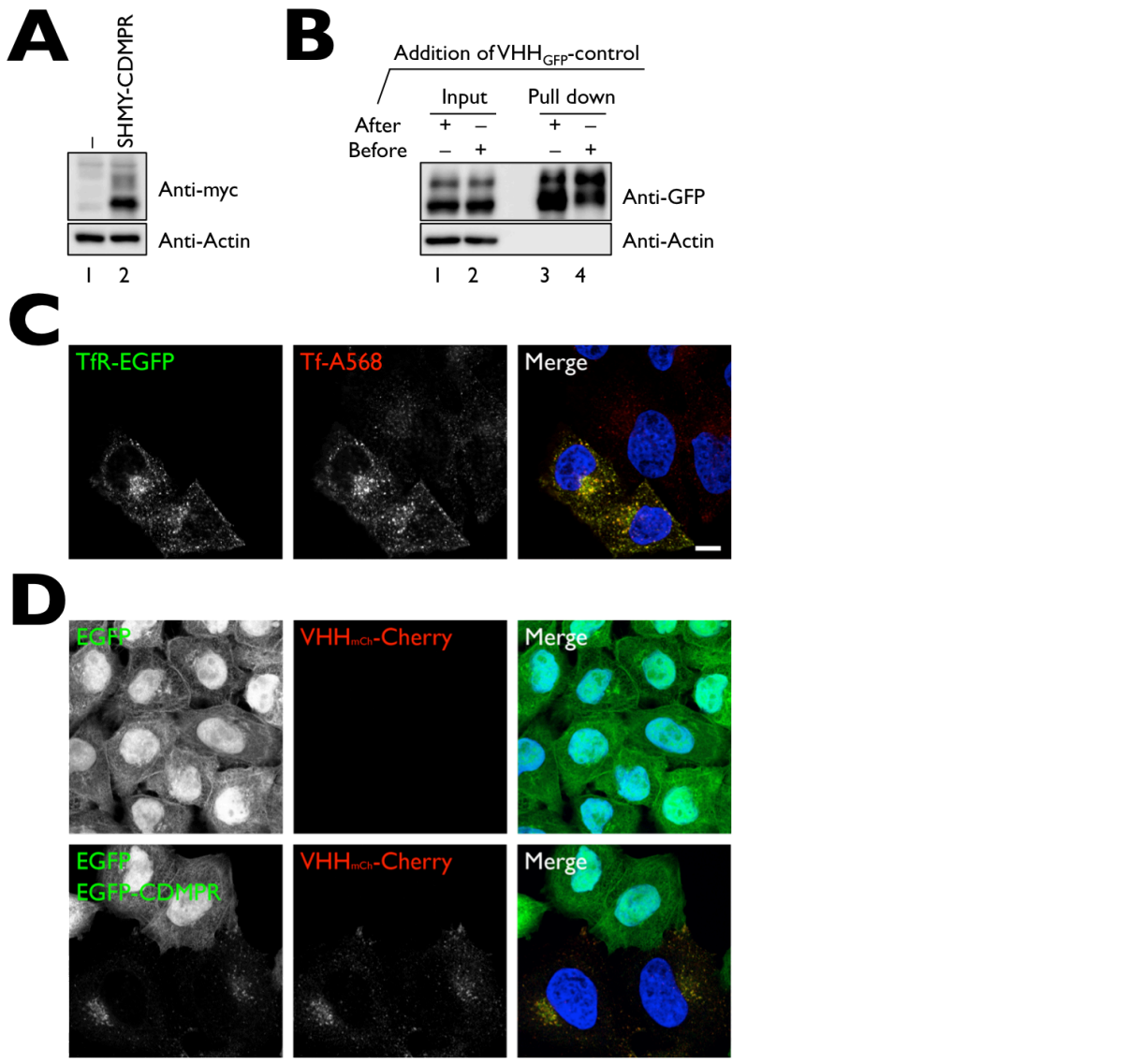

Figure S2: CDMPR protein expression, Tf uptake in TfR-EGFP, and EGFP cell line. **(A)** HeLa cells were transiently transfected with SHMY-CDMPR, harvested after 24 h, and analyzed by SDS-PAGE/Western blotting. SHMY-CDMPR (lane 2) runs as a double band (a strong band at lower MW, and a smear at higher MW). **(B)** In order to find out immature and mature CDMPR forms, we administrated VHH$_{GFP}$-control to cells stably expressing EGFP-CDMPR, where only mature EGFP-CDMPR will internalize nanobody. To figure out, we prepared two dishes with HeLa cells stably expressing EGFP-CDMPR. While one dish remained untreated (here named 'After'), the other was incubated with 2 μg/mL VHH$_{GFP}$-control ('Before') for 1 h at 37°C. Cells were lysed and postnuclear supernatants (from 'After' and 'Before') were prepared. An aliquot of postnuclear supernatant was saved as loading control. 2 μg/mL of VHH$_{GFP}$-control was then added to the untreated postnuclear supernatant ('After'). The individual postnuclear supernatants (~ 1 mL) were subsequently incubated with 15-20 μL streptavidin beads for 1 h at 4°C. Beads were washed and boiled in SDS sample buffer. As seen in lane 3 and 4, the lower band of EGFP-CDMPR (seen in lysates) is composed of two distinct CDMPR forms, one that reaches the cell surface (mature), and one that does not (immature). **(C)** HeLa cells stably expressing TfR-EGFP were mixed with parental HeLa cells and seeded on coverslips. Cells were incubated with 20 μg/mL Tf coupled to Alexa 568 and processed for fluorescence microscopy. Cells expressing additional TfR internalize more Tf, indicating that the recombinant EGFP fusion is still functional as cargo receptor. **(D)** Uptake of 2 μg/mL VHH$_{GFP}$-mCherry with cells stably expressing EGFP, or a mixture of cells expressing EGFP and EGFP-CDMPR. There is no uptake by cells stably expressing EGFP. Scale bar: 10 μm.

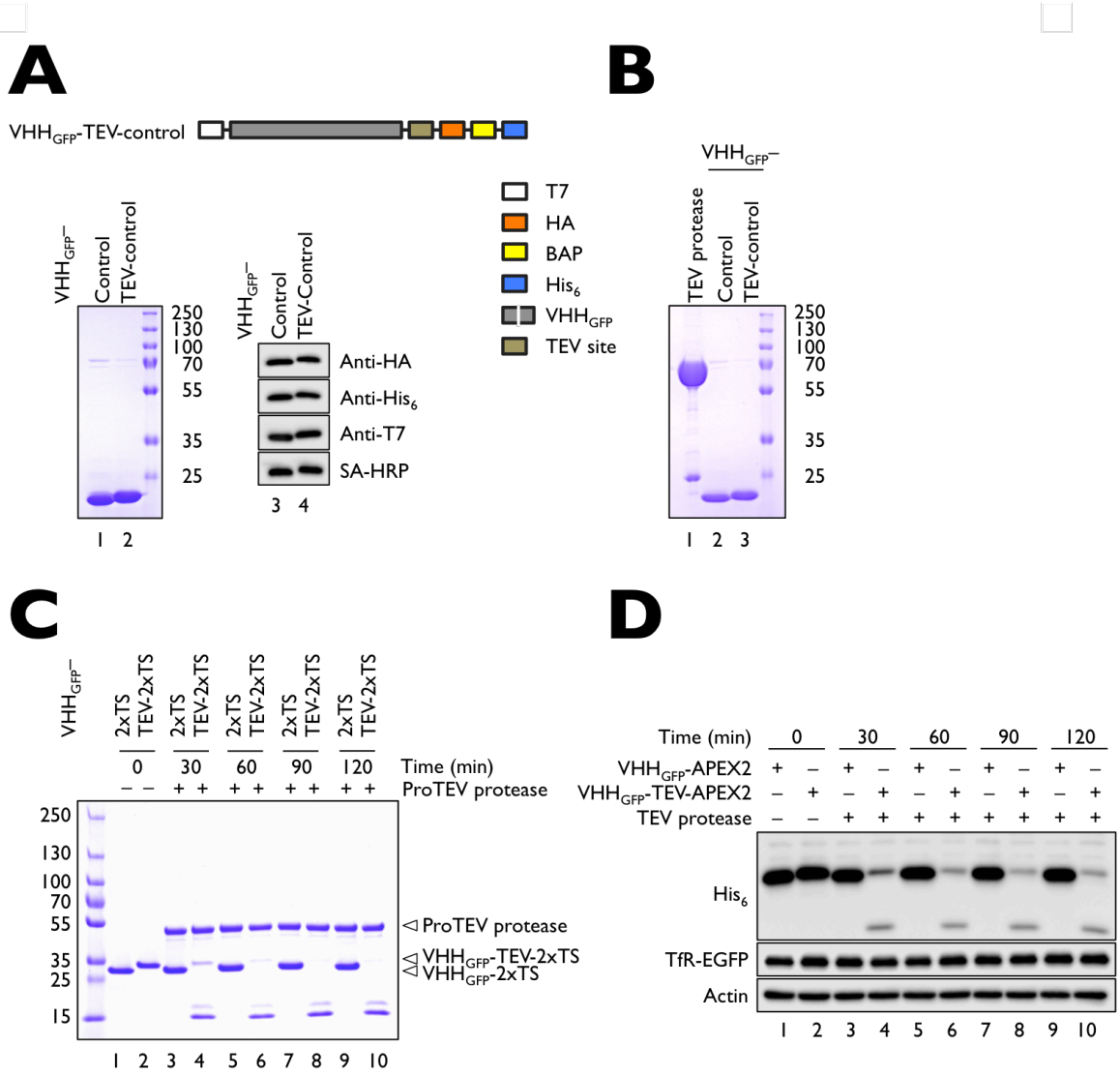

Figure S3: Expression, purification and application of TEV site-modified nanobodies and TEV protease. **(A)** Schematic representation of VHH$_{GFP}$-TEV-control. 30 μg of purified and desalted protein was loaded onto a SDS-PAGE gel and then subjected to Coomassie staining. VHH$_{GFP}$-TEV-control can also be detected by antibodies or SA-HRP targeting specific epitopes. Cartoon is not drawn to scale. **(B)** Expression of maltose-binding protein (MBP)-tagged TEV protease. 60 μg or 20 μg of purified and desalted MBP-TEV, VHH$_{GFP}$-control or VHH$_{GFP}$-TEV-control was loaded onto a SDS-PAGE gel and then subjected to Coomassie staining. **(C)** In vitro cleavage of TEV site-containing nanobody (e.g. VHH$_{GFP}$-TEV-2xTS) by TEV protease. 20 μg of the respective nanobodies were digested with commercial recombinant ProTEV Plus for up to 2 h according to the manufacturer's protocol. While VHH$_{GFP}$-2xTS was not cleaved, VHH$_{GFP}$-TEV-2xTS was almost completely digested after 2 h. **(D)** HeLa cells stably expressing TfR-EGFP were incubated with VHH$_{GFP}$-APEX2 or VHH$_{GFP}$-TEV-APEX2 for 30 min at 4°C. To test digestion efficiency at 4°C, cells were incubated for up to 2 h with ProTEV Plus protease in a total volume of 400 uL according to the manufacturer's instructions. Cells were lysed and analyzed by SDS-PAGE/Western blotting. Membranes were probed with anti-His$_6$, anti-GFP and anti-actin antibodies. Digestion was almost completed after 2 h. Numbers along the markers correspond to molecular weight in kDa.

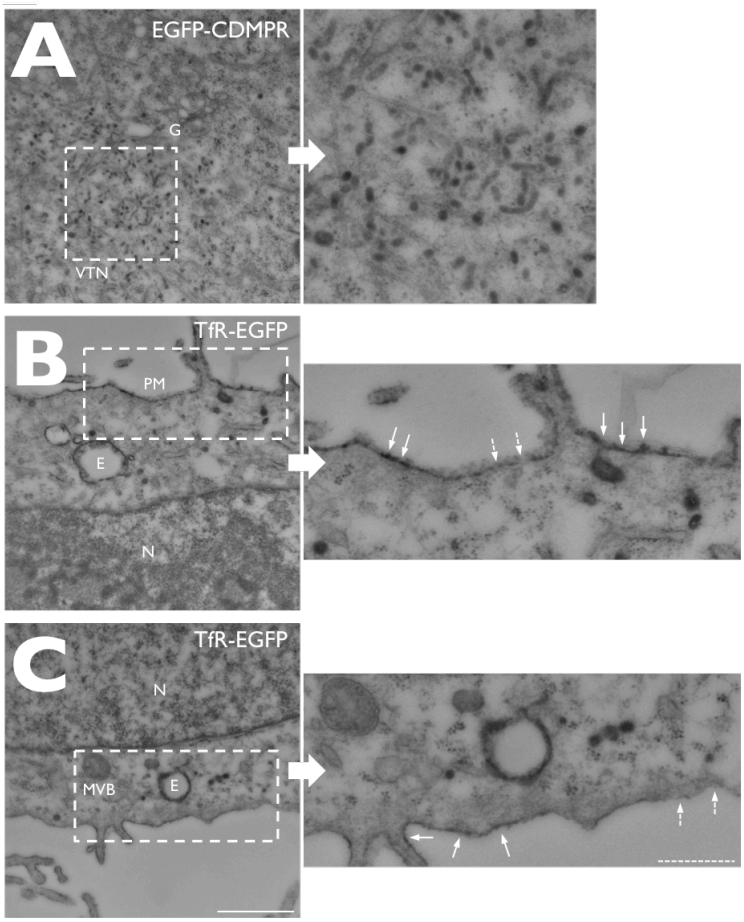

Figure S4: DAB/H_2O_2 cytochemistry and electron microscopy of EGFP-CDMPR and TfR-EGFP. (A)-(C) Same procedure as in Figure 3.9. Cells stably expressing EGFP-CDMPR (A) or TfR-EGFP (B)-(C) were incubated with 5 μg/mL VHH_{GFP}-APEX2 for 1 h at 37°C to reach steady-state. After fixation with 2% glutaraldehyde, cells were treated with DAB/H_2O_2 to yield a local and productive polymerization reaction. Subfigure (A) shows the Golgi region of cells expressing EGFP-CDMPR. The reporter was often found in concentrated patterns of small vesicular and tubular elements adjacent to the Golgi cisternae. The labeled tubular elements varied in length and often had branched extensions. (B) and (C) shows local cell surface DAB polymer precipitations of cells expressing TfR-EGFP (two examples). Some surface regions showed DAB polymer precipitations (lined arrows), some not (dotted arrows), suggesting local or missing deposition and ablation reactions. An inset of every picture is highlighted. Straight bar lines correspond to 1000 nm, dotted lines to 380 nm. Legend: E, endosome; G, Golgi; MVB, multivesicular body; N, nucleus; VTN, vesicular-tubular network.

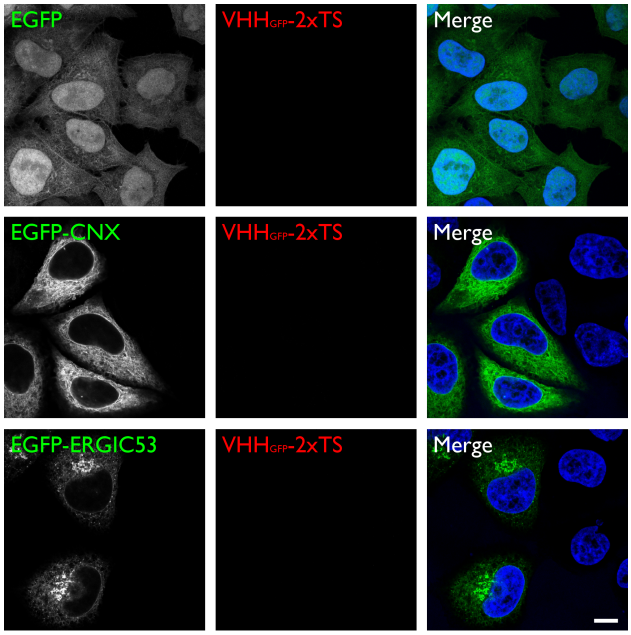

Figure S5: Nanobody is only taken up by EGFP reporters presenting an EGFP moiety at the cell surface. HeLa cells stably expressing EGFP, or transiently expressing EGFP-calnexin (CNX) or EGFP-ERGIC53 were incubated with 2 μg/mL VHH_{GFP}-2xTS for 1 h at 37°C, and processed for immunofluorescence microscopy. VHH_{GFP}-2xTS was detected using an anti-HA antibody. The figure shows that proteins expressed either in the cytosol (EGFP) or in the early secretory pathway (CNX or ERGIC53) do not take up any nanobody. Scale bar: 10 μm.

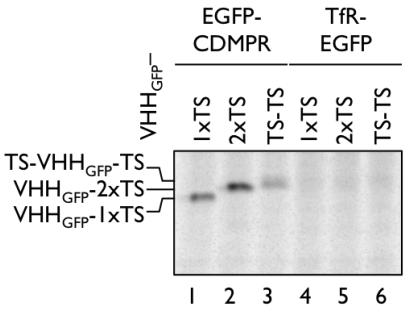

Figure S6: Comparison of sulfatable nanobodies. Cells stably expressing EGFP-CDMPR (lanes 1-3) or TfR-EGFP (lanes 4-6) were starved in sulfate-free medium for 1 h at 37°C and 7.5% CO_2, and then pulse-labeled with sulfate-free medium reconstituted with 0.5 mCi/mL [^{35}S]sulfate supplemented with 2 µg/mL of either VHH_{GFP}-1xTS, VHH_{GFP}-2xTS or TS-VHH_{GFP}-TS for 60 min. Equal amounts of postnuclear supernatants were taken and incubated with Nickel beads to affinity-isolate nanobodies. Proteins were separated using gel electrophoresis and prepared for autoradiography. There was higher sulfate incorporation into VHH_{GFP}-2xTS than into TS-VHH_{GFP}-TS using cells expressing EGFP-CDMPR. As reported before, no sulfated nanobody was detected from cells expressing TfR-EGFP.

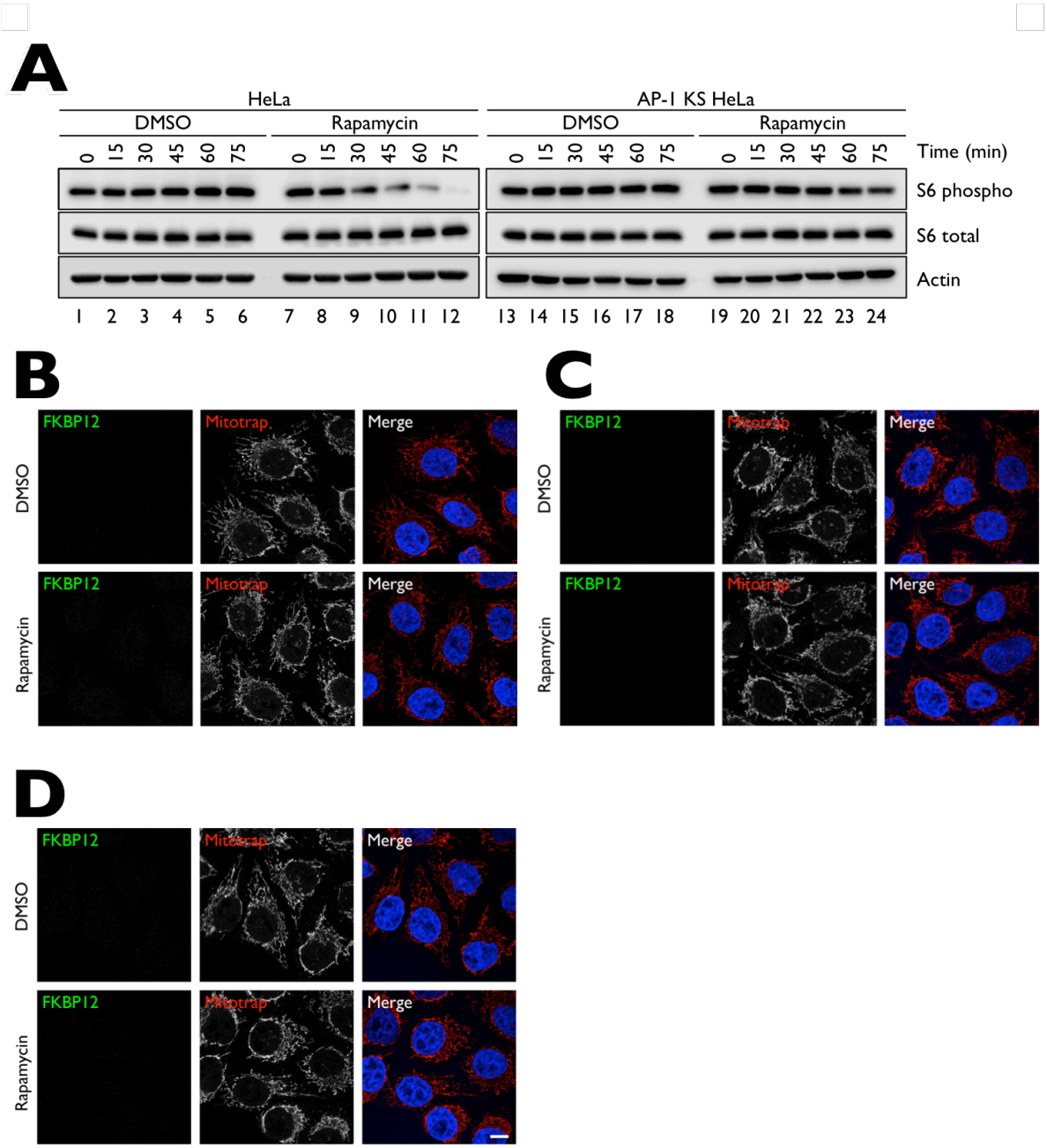

Figure S7: Rapamycin treatment moderately affects mTOR signaling in AP-1 KS cells. (A) Parental HeLa (1-12) and AP-1 KS HeLa (13-24) were treated with DMSO (1-6, 13-18) or 500 nM rapamycin (7-12, 19-24) for up to 75 min. Following postnuclear supernatant preparation, samples were analyzed by SDS-PAGE/Western blotting. Membranes were probed with anti-phospho S6, anti-S6 (total S6) and anti-actin antibodies. While parental HeLa cells showed a significant decrease in S6 phosphorylation, AP-1 KS cells were only moderately affected after 75 min of rapamycin treatment. **(B)-(D)** In order to see whether the moderate decrease in S6 phosphorylation (less mTORC1 activity) is caused by mitochondrial rerouting of endogenous FKBP12, Mitotrap-expressing cells were incubated with 500 nM rapamycin for 30 min. None of the antibodies (BD Biosciences (B), Clontech (C), Santa Cruz (D)) could detect endogenous FKBP12. Mitotrap was labeled with an anti-FLAG antibody. Scale bar: 10 μm.

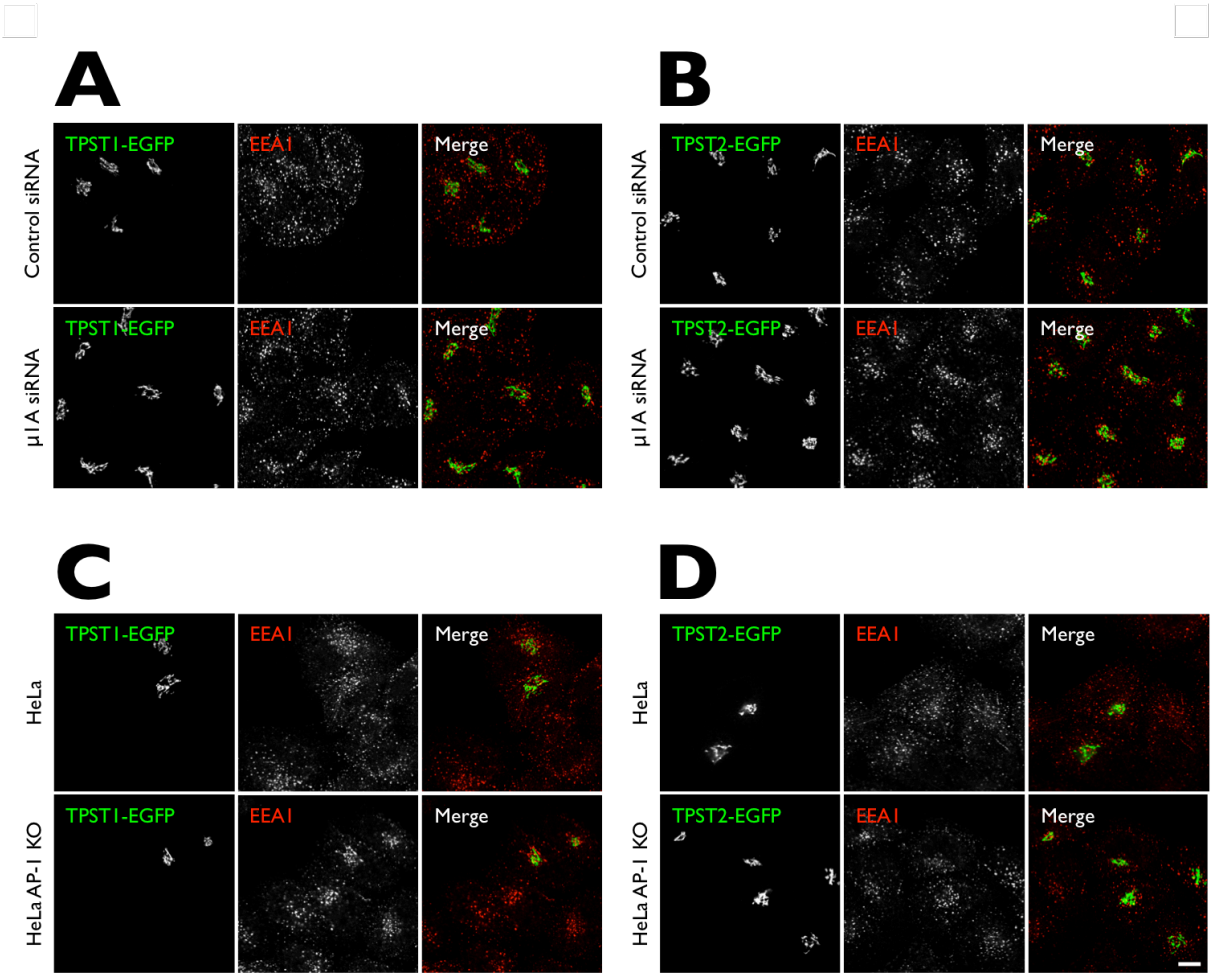

Figure S8: AP-1 knockdown or knockout does not affect localization of TPST1-EGFP and TPST2-EGFP. **(A)-(B)** HeLa cells stably expressing TPST1-EGFP (A) or TPST2-EGFP (B) were treated for 96 h with siRNA targeting AP-1, seeded on coverslips, fixed and processed for immunofluorescence microscopy. **(C)-(D)** Parental or AP-1 KO HeLa cells were transiently transfected with TPST1-EGFP (C) or TPST2-EGFP (D) for 24 h, seeded on coverslips, fixed and processed for immunofluorescence microscopy. Cells were costained with EEA1. An AP-1 knockdown or knockout did not significantly alter the steady-state localization of TPST1-EGFP or TPST2-EGFP towards early endosomes. However, as previously reported by Schu and colleagues (Meyer et al., 2000), the distribution pattern of EEA1 was slightly changed in AP-1-depleted cells. Scale bar: 10 µm.

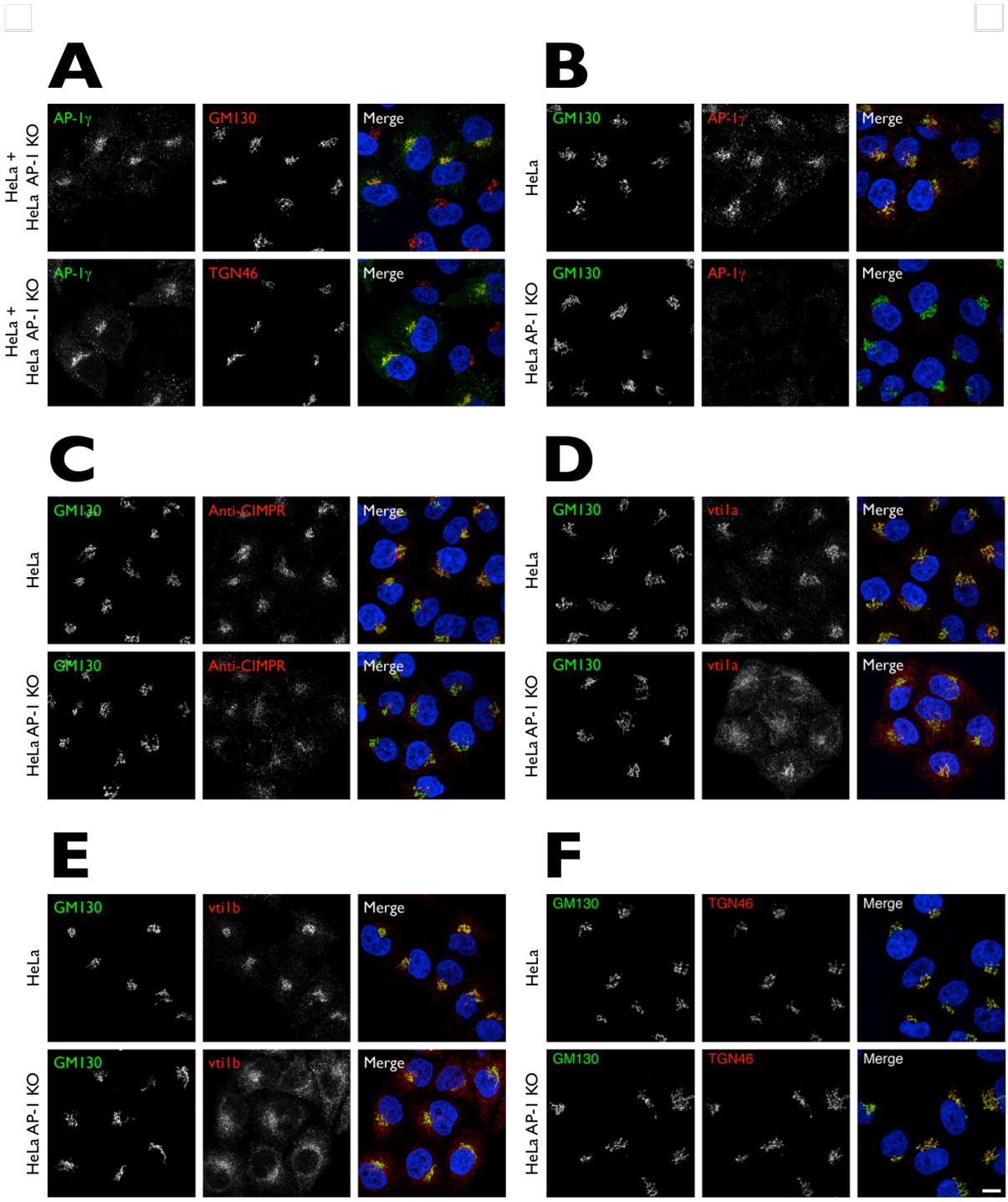

Figure S9: Localization of cargo proteins in AP-1 KO HeLa cells. (A) Parental and AP-1 KO HeLa cells were mixed, seeded on the same coverslip, and prepared for immunofluorescence microscopy. AP-1 KO cells were identified by the lack of γ-adaptin expression. Cells were stained for AP-1 and GM130 or TGN46. GM130 (a peripheral early Golgi protein) and TGN46 (TGN) were not affected in their steady-state distribution in AP-1 KO cells. GM130 was used as reference marker. **(B)** Same as in (A), but parental and AP-1 KO HeLa cells were seeded on different coverslips. **(C)** Parental and AP-1 KO HeLa cells were prepared for an anti-CIMPR antibody uptake assay and processed for immunofluorescence microscopy. While anti-CIMPR antibody localizes to the perinuclear compartment in control cells, this looks less impressive in AP-1 KO cells, suggesting that retrograde endosome-to-TGN transport of CIMPR is affected. **(D)-(E)** Parental and AP-1 KO HeLa cells were prepared for immunofluorescence microscopy. Cells were stained for GM130 and vti1a (D) or vti1b (E). In agreement with previous literature (Hirst et al., 2004), there is a shift in the steady-state localization for both proteins in AP-1-depleted cells. **(F)** Same as in (A), but parental and AP-1 KO HeLa cells were seeded on different coverslips. Scale bar: 10 μm.

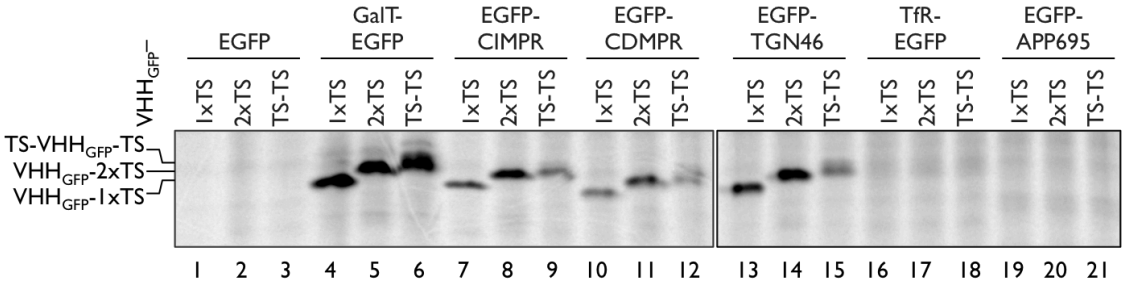

Figure S10: Sulfation analysis of GalT-EGFP and EGFP-APP695. HeLa cells stably expressing EGFP-tagged reporters were starved in sulfate-free medium for 1 h at 37°C and 7.5% CO_2, and then pulse-labeled with sulfate-free medium reconstituted with 0.5 mCi/mL [^{35}S]sulfate supplemented with 2 µg/mL of either VHH$_{GFP}$-1xTS, VHH$_{GFP}$-2xTS or TS-VHH$_{GFP}$-TS for 60 min. Equal amounts of postnuclear supernatants were taken and incubated with Nickel beads to affinity-isolate nanobodies. Proteins were separated using gel electrophoresis and prepared for autoradiography. As reported in Figure S6, there was higher sulfate incorporation into VHH$_{GFP}$-2xTS than into TS-VHH$_{GFP}$-TS (apart from GalT). Apart from the already tested EGFP reporters, GalT-EGFP (lanes 4-6) and EGFP-APP695 (lanes 19-21) were also analyzed. There was a strong sulfation for the former, while no sulfation could be reported for the latter. These results suggest that GalT returns to the compartment of sulfation, while APP695 does apparently not.

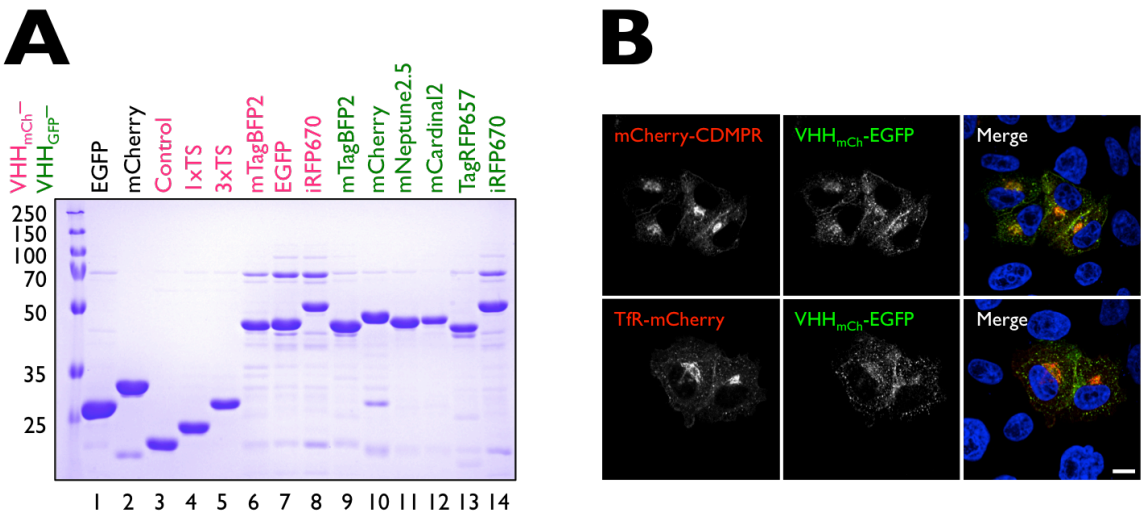

Figure S11: Expression of additional functionalized anti-GFP (VHH$_{GFP}$) and anti-mCherry (VHH$_{mCh}$) nanobodies. **(A)** Bacterial expression of functionalized nanobodies. 30 µg of purified and desalted protein was loaded onto a SDS-PAGE gel and then subjected to Coomassie staining. Most of the shown nanobodies are fused to fluorophores. The color code indicates which nanobody is meant, green when fused to VHH$_{GFP}$, pink when fused to VHH$_{mCh}$. **(B)** HeLa cells transiently expressing mCherry-CDMPR or TfR-mCherry were incubated with VHH$_{mCh}$-EGFP and processed for fluorescence microscopy. As already observed for functionalized VHH$_{GFP}$ nanobodies, functionalized VHH$_{mCh}$ derivatives are also internalized. Scale bar: 10 µm.

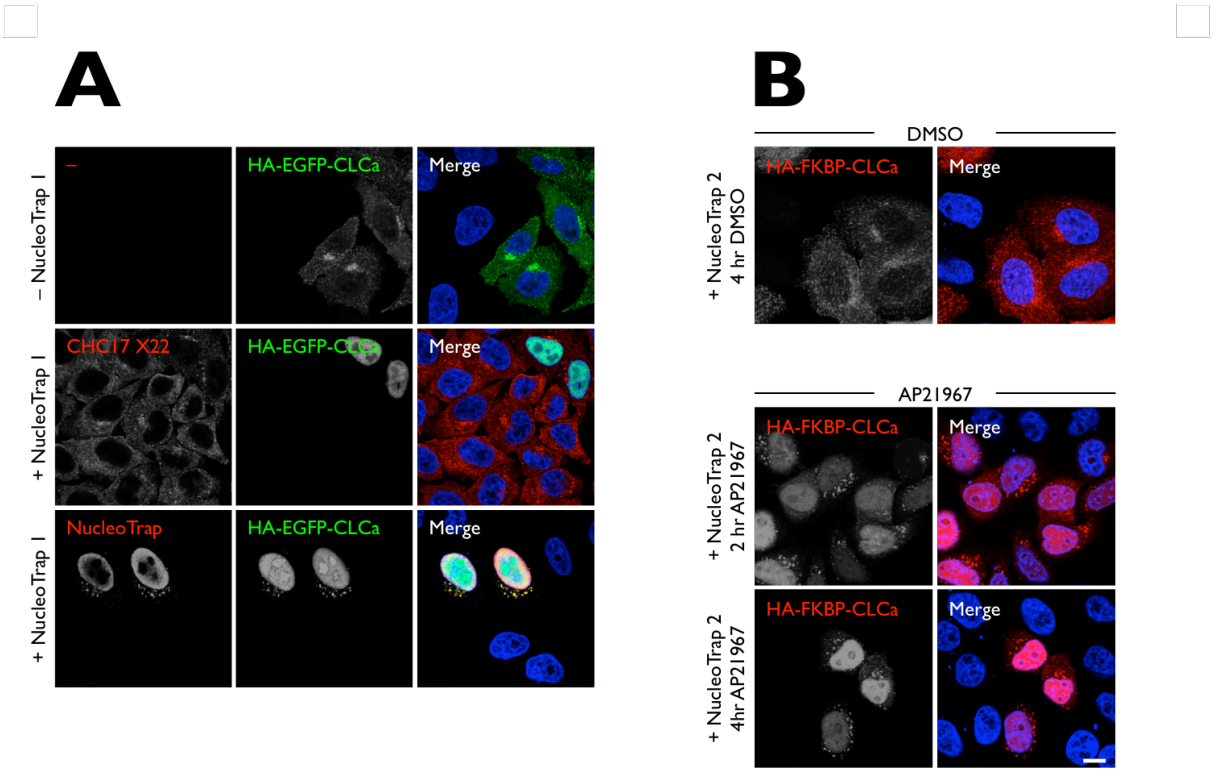

Figure S12: Rerouting of proteins to the nucleus. (A) HeLa cells were transiently transfected with HA-EGFP-CLCa alone, or cotransfected with both HA-EGFP-CLCa and NLS-VHH$_{GFP}$-FLAG-NLS (NucleoTrap 1). In cells with no nuclear trap, HA-EGFP-CLCa localizes to a perinuclear compartment and the plasma membrane. Cells with coexpressed NucleoTrap I show HA-EGFP-CLCa as well as parts of endogenous CHC17 to be removed from the cytosol. Overexpressed HA-EGFP-CLCa mainly localizes to the nucleus in cells with coexpressed NucleoTrap I, CHC17, however, cannot be dominantly found in the nucleus. The reason for this is unknown. It might be that CHC17 is rapidly degraded in the nucleus, since CHC17 is also involved in mitosis. Nuclear localization of CHC17 in interphase might cause dysregulation of the cell cycle. **(B)** HeLa cells were transiently cotransfected with HA-FKBP-CLCa and NLS-FRB-NLS (NucleoTrap 2). Addition of the rapalog AP21967 caused most of HA-FKBP-CLCa to be trapped in the nucleus after 4 h. Scale bar: 10 μm.

7 References

7 References

A

Agostinho, P., A. Pliassova, C.R. Oliveira, and R.A. Cunha. 2015. Localization and Trafficking of Amyloid-beta Protein Precursor and Secretases: Impact on Alzheimer's Disease. *J Alzheimers Dis*. 45:329-347.

Amessou, M., A. Fradagrada, T. Falguieres, J.M. Lord, D.C. Smith, L.M. Roberts, C. Lamaze, and L. Johannes. 2007. Syntaxin 16 and syntaxin 5 are required for efficient retrograde transport of several exogenous and endogenous cargo proteins. *J Cell Sci*. 120:1457-1468.

Amessou, M., V. Popoff, B. Yelamos, A. Saint-Pol, and L. Johannes. 2006. Measuring retrograde transport to the trans-Golgi network. *Curr Protoc Cell Biol*. Chapter 15:Unit 15 10.

Anitei, M., R. Chenna, C. Czupalla, M. Esner, S. Christ, S. Lenhard, K. Korn, F. Meyenhofer, M. Bickle, M. Zerial, and B. Hoflack. 2014. A high-throughput siRNA screen identifies genes that regulate mannose 6-phosphate receptor trafficking. *J Cell Sci*. 127:5079-5092.

Antonny, B., C. Burd, P. De Camilli, E. Chen, O. Daumke, K. Faelber, M. Ford, V.A. Frolov, A. Frost, J.E. Hinshaw, T. Kirchhausen, M.M. Kozlov, M. Lenz, H.H. Low, H. McMahon, C. Merrifield, T.D. Pollard, P.J. Robinson, A. Roux, and S. Schmid. 2016. Membrane fission by dynamin: what we know and what we need to know. *EMBO J*. 35:2270-2284.

Arighi, C.N., L.M. Hartnell, R.C. Aguilar, C.R. Haft, and J.S. Bonifacino. 2004. Role of the mammalian retromer in sorting of the cation-independent mannose 6-phosphate receptor. *J Cell Biol*. 165:123-133.

Ariotti, N., T.E. Hall, J. Rae, C. Ferguson, K.A. McMahon, N. Martel, R.E. Webb, R.I. Webb, R.D. Teasdale, and R.G. Parton. 2015a. Modular Detection of GFP-Labeled Proteins for Rapid Screening by Electron Microscopy in Cells and Organisms. *Dev Cell*. 35:513-525.

Ariotti, N., J. Rae, N. Leneva, C. Ferguson, D. Loo, S. Okano, M.M. Hill, P. Walser, B.M. Collins, and R.G. Parton. 2015b. Molecular Characterization of Caveolin-induced Membrane Curvature. *J Biol Chem*. 290:24875-24890.

Ashour, J., F.I. Schmidt, L. Hanke, J. Cragnolini, M. Cavallari, A. Altenburg, R. Brewer, J. Ingram, C. Shoemaker, and H.L. Ploegh. 2015. Intracellular expression of camelid single-domain antibodies specific for influenza virus nucleoprotein uncovers distinct features of its nuclear localization. *J Virol*. 89:2792-2800.

B

Baeuerle, P.A., and W.B. Huttner. 1987. Tyrosine sulfation is a trans-Golgi-specific protein modification. *The Journal of cell biology*. 105:2655-2664.

Bai, Z., and B.D. Grant. 2015. A TOCA/CDC-42/PAR/WAVE functional module required for retrograde endocytic recycling. *Proc Natl Acad Sci U S A*. 112:E1443-1452.

Banting, G., R. Maile, and E.P. Roquemore. 1998. The steady state distribution of humTGN46 is not significantly altered in cells defective in clathrin-mediated endocytosis. *Journal of cell science*. 111 (Pt 23):3451-3458.

Banting, G., and S. Ponnambalam. 1997. TGN38 and its orthologues: roles in post-TGN vesicle formation and maintenance of TGN morphology. *Biochimica et biophysica acta*. 1355:209-217.

Barbero, P., L. Bittova, and S.R. Pfeffer. 2002. Visualization of Rab9-mediated vesicle transport from endosomes to the trans-Golgi in living cells. *J Cell Biol*. 156:511-518.

Bashkirov, P.V., S.A. Akimov, A.I. Evseev, S.L. Schmid, J. Zimmerberg, and V.A. Frolov. 2008. GTPase cycle of dynamin is coupled to membrane squeeze and release, leading to spontaneous fission. *Cell*. 135:1276-1286.

Behnia, R., and S. Munro. 2005. Organelle identity and the signposts for membrane traffic. *Nature*. 438:597-604.

Belenkaya, T.Y., Y. Wu, X. Tang, B. Zhou, L. Cheng, Y.V. Sharma, D. Yan, E.M. Selva, and X. Lin. 2008. The retromer complex influences Wnt secretion by recycling wntless from endosomes to the trans-Golgi network. *Dev Cell*. 14:120-131.

Ben-Tekaya, H., K. Miura, R. Pepperkok, and H.P. Hauri. 2005. Live imaging of bidirectional traffic from the ERGIC. *J Cell Sci*. 118:357-367.

Bendris, N., and S.L. Schmid. 2017. Endocytosis, Metastasis and Beyond: Multiple Facets of SNX9. *Trends Cell Biol*. 27:189-200.

Beuret, N., F. Hasler, C. Prescianotto-Baschong, J. Birk, J. Rutishauser, and M. Spiess. 2017. Amyloid-like aggregation of provasopressin in diabetes insipidus and secretory granule sorting. *BMC Biol*. 15:5.

Bieli, D., I. Alborelli, S. Harmansa, S. Matsuda, E. Caussinus, and M. Affolter. 2016. Development and Application of Functionalized Protein Binders in Multicellular Organisms. *Int Rev Cell Mol Biol*. 325:181-213.

Billcliff, P.G., C.J. Noakes, Z.B. Mehta, G. Yan, L. Mak, R. Woscholski, and M. Lowe. 2016. OCRL1 engages with the F-BAR protein pacsin 2 to promote biogenesis of membrane-trafficking intermediates. *Mol Biol Cell*. 27:90-107.

Bird, R.E., K.D. Hardman, J.W. Jacobson, S. Johnson, B.M. Kaufman, S.M. Lee, T. Lee, S.H. Pope, G.S. Riordan, and M. Whitlow. 1988. Single-chain antigen-binding proteins. *Science*. 242:423-426.

Birnbaum, J., S. Flemming, N. Reichard, A.B. Soares, P. Mesen-Ramirez, E. Jonscher, B. Bergmann, and T. Spielmann. 2017. A genetic system to study Plasmodium falciparum protein function. *Nat Methods*. 14:450-456.

Bitsikas, V., I.R. Correa, Jr., and B.J. Nichols. 2014. Clathrin-independent pathways do not contribute significantly to endocytic flux. *Elife*. 3:e03970.

Bogan, J.S., and K.V. Kandror. 2010. Biogenesis and regulation of insulin-responsive vesicles containing GLUT4. *Curr Opin Cell Biol*. 22:506-512.

Bonifacino, J.S. 2004. The GGA proteins: adaptors on the move. *Nature reviews. Molecular cell biology*. 5:23-32.

Bonifacino, J.S. 2014. Adaptor proteins involved in polarized sorting. *J Cell Biol*. 204:7-17.

Bonifacino, J.S., and J.H. Hurley. 2008. Retromer. *Curr Opin Cell Biol*. 20:427-436.

Bonifacino, J.S., and R. Rojas. 2006. Retrograde transport from endosomes to the trans-Golgi network. *Nature reviews. Molecular cell biology*. 7:568-579.

Bonifacino, J.S., and L.M. Traub. 2003. Signals for sorting of transmembrane proteins to endosomes and lysosomes. *Annual review of biochemistry*. 72:395-447.

Borner, G.H., R. Antrobus, J. Hirst, G.S. Bhumbra, P. Kozik, L.P. Jackson, D.A. Sahlender, and M.S. Robinson. 2012. Multivariate proteomic profiling identifies novel accessory proteins of coated vesicles. *J Cell Biol*. 197:141-160.

Borner, G.H., M. Harbour, S. Hester, K.S. Lilley, and M.S. Robinson. 2006. Comparative proteomics of clathrin-coated vesicles. *The Journal of cell biology*. 175:571-578.

Boucrot, E., A.P. Ferreira, L. Almeida-Souza, S. Debard, Y. Vallis, G. Howard, L. Bertot, N. Sauvonnet, and H.T. McMahon. 2015. Endophilin marks and controls a clathrin-independent endocytic pathway. *Nature*. 517:460-465.

Boucrot, E., M.T. Howes, T. Kirchhausen, and R.G. Parton. 2011. Redistribution of caveolae during mitosis. *J Cell Sci*. 124:1965-1972.

Branon, T., S. Han, and A. Ting. 2017. Beyond Immunoprecipitation: Exploring New Interaction Spaces with Proximity Biotinylation. *Biochemistry*. 56:3297-3298.

Bright, N.A., L.J. Davis, and J.P. Luzio. 2016. Endolysosomes Are the Principal Intracellular Sites of Acid Hydrolase Activity. *Curr Biol*. 26:2233-2245.

Bright, N.A., M.J. Gratian, and J.P. Luzio. 2005. Endocytic delivery to lysosomes mediated by concurrent fusion and kissing events in living cells. *Curr Biol*. 15:360-365.

Bryant, N.J., R. Govers, and D.E. James. 2002. Regulated transport of the glucose transporter GLUT4. *Nat Rev Mol Cell Biol*. 3:267-277.

Bulankina, A.V., A. Deggerich, D. Wenzel, K. Mutenda, J.G. Wittmann, M.G. Rudolph, K.N. Burger, and S. Honing. 2009. TIP47 functions in the biogenesis of lipid droplets. *J Cell Biol*. 185:641-655.

Bundgaard, J.R., J. Vuust, and J.F. Rehfeld. 1997. New consensus features for tyrosine O-sulfation determined by mutational analysis. *J Biol Chem*. 272:21700-21705.

Burd, C., and P.J. Cullen. 2014. Retromer: a master conductor of endosome sorting. *Cold Spring Harb Perspect Biol*. 6.

Burd, C.G. 2011. Physiology and pathology of endosome-to-Golgi retrograde sorting. *Traffic*. 12:948-955.

C

Canagarajah, B.J., X. Ren, J.S. Bonifacino, and J.H. Hurley. 2013. The clathrin adaptor complexes as a paradigm for membrane-associated allostery. *Protein Sci*. 22:517-529.

Canuel, M., S. Lefrancois, J. Zeng, and C.R. Morales. 2008. AP-1 and retromer play opposite roles in the trafficking of sortilin between the Golgi apparatus and the lysosomes. *Biochem Biophys Res Commun*. 366:724-730.

Carlton, J., M. Bujny, B.J. Peter, V.M. Oorschot, A. Rutherford, H. Mellor, J. Klumperman, H.T. McMahon, and P.J. Cullen. 2004. Sorting nexin-1 mediates tubular endosome-to-TGN transport through coincidence sensing of high- curvature membranes and 3-phosphoinositides. *Curr Biol*. 14:1791-1800.

Carlton, J.G., M.V. Bujny, B.J. Peter, V.M. Oorschot, A. Rutherford, R.S. Arkell, J. Klumperman, H.T. McMahon, and P.J. Cullen. 2005. Sorting nexin-2 is associated with tubular elements of the early endosome, but is not essential for retromer-mediated endosome-to-TGN transport. *J Cell Sci*. 118:4527-4539.

Carroll, K.S., J. Hanna, I. Simon, J. Krise, P. Barbero, and S.R. Pfeffer. 2001. Role of Rab9 GTPase in facilitating receptor recruitment by TIP47. *Science*. 292:1373-1376.

Cattaneo, A., and S. Biocca. 1999. The selection of intracellular antibodies. *Trends Biotechnol*. 17:115-121.

Caussinus, E., O. Kanca, and M. Affolter. 2011. Fluorescent fusion protein knockout mediated by anti-GFP nanobody. *Nat Struct Mol Biol*. 19:117-121.

Caussinus, E., O. Kanca, and M. Affolter. 2013. Protein knockouts in living eukaryotes using deGradFP and green fluorescent protein fusion targets. *Current protocols in protein science / editorial board, John E. Coligan ... [et al.]*. 73:Unit 30 32.

Cha, S.W., E. Tadjuidje, J. White, J. Wells, C. Mayhew, C. Wylie, and J. Heasman. 2009. Wnt11/5a complex formation caused by tyrosine sulfation increases canonical signaling activity. *Curr Biol*. 19:1573-1580.

Chamberland, J.P., L.T. Antonow, M. Dias Santos, and B. Ritter. 2016. NECAP2 controls clathrin coat recruitment to early endosomes for fast endocytic recycling. *J Cell Sci*. 129:2625-2637.

Chater, T.E., and Y. Goda. 2014. The role of AMPA receptors in postsynaptic mechanisms of synaptic plasticity. *Front Cell Neurosci*. 8:401.

Chaumet, A., G.D. Wright, S.H. Seet, K.M. Tham, N.V. Gounko, and F. Bard. 2015. Nuclear envelope-associated endosomes deliver surface proteins to the nucleus. *Nat Commun*. 6:8218.

Cheeseman, L.P., E.F. Harry, A.D. McAinsh, I.A. Prior, and S.J. Royle. 2013. Specific removal of TACC3-ch-TOG-clathrin at metaphase deregulates kinetochore fiber tension. *Journal of cell science*. 126:2102-2113.

Chen, B.H., C.C. Wang, L.Y. Lu, K.S. Hung, and Y.S. Yang. 2013a. Fluorescence assay for protein post-translational tyrosine sulfation. *Anal Bioanal Chem*. 405:1425-1429.

Chen, C., D. Garcia-Santos, Y. Ishikawa, A. Seguin, L. Li, K.H. Fegan, G.J. Hildick-Smith, D.I. Shah, J.D. Cooney, W. Chen, M.J. King, Y.Y. Yien, I.J. Schultz, H. Anderson, A.J. Dalton, M.L. Freedman, P.D. Kingsley, J. Palis, S.M. Hattangadi, H.F. Lodish, D.M. Ward, J. Kaplan, T. Maeda, P. Ponka, and B.H. Paw. 2013b. Snx3 regulates recycling of the transferrin receptor and iron assimilation. *Cell Metab*. 17:343-352.

Chen, X., J.L. Zaro, and W.C. Shen. 2013c. Fusion protein linkers: property, design and functionality. *Adv Drug Deliv Rev*. 65:1357-1369.

Cheng, J.P., and B.J. Nichols. 2016. Caveolae: One Function or Many? *Trends Cell Biol*. 26:177-189.

Chia, P.Z., I. Gasnereau, Z.Z. Lieu, and P.A. Gleeson. 2011. Rab9-dependent retrograde transport and endosomal sorting of the endopeptidase furin. *J Cell Sci*. 124:2401-2413.

Chidambaram, S., N. Mullers, K. Wiederhold, V. Haucke, and G.F. von Mollard. 2004. Specific interaction between SNAREs and epsin N-terminal homology (ENTH) domains of epsin-related proteins in trans-Golgi network to endosome transport. *J Biol Chem*. 279:4175-4179.

Choy, R.W., Z. Cheng, and R. Schekman. 2012. Amyloid precursor protein (APP) traffics from the cell surface via endosomes for amyloid beta (Abeta) production in the trans-Golgi network. *Proc Natl Acad Sci U S A*. 109:E2077-2082.

Christiano, R., M. Amessou, G. Shi, M. Azoulay, A. Blanpain, H. Drobecq, O. Melnyk, J.C. Florent, and L. Johannes. 2010. Chemistry-based protein modification strategy for endocytic pathway analysis. *Biol Cell*. 102:351-359.

Chua, C.E., and B.L. Tang. 2006. alpha-synuclein and Parkinson's disease: the first roadblock. *J Cell Mol Med*. 10:837-846.

Ciechanover, A., A.L. Schwartz, A. Dautry-Varsat, and H.F. Lodish. 1983. Kinetics of internalization and recycling of transferrin and the transferrin receptor in a human hepatoma cell line. Effect of lysosomotropic agents. *J Biol Chem*. 258:9681-9689.

Cimbro, R., T.R. Gallant, M.A. Dolan, C. Guzzo, P. Zhang, Y. Lin, H. Miao, D. Van Ryk, J. Arthos, I. Gorshkova, P.H. Brown, D.E. Hurt, and P. Lusso. 2014. Tyrosine sulfation in the second variable loop (V2) of HIV-1 gp120 stabilizes V2-V3 interaction and modulates neutralization sensitivity. *Proc Natl Acad Sci U S A*. 111:3152-3157.

Cocucci, E., F. Aguet, S. Boulant, and T. Kirchhausen. 2012. The first five seconds in the life of a clathrin-coated pit. *Cell*. 150:495-507.

Connolly, C.N., C.E. Futter, A. Gibson, C.R. Hopkins, and D.F. Cutler. 1994. Transport into and out of the Golgi complex studied by transfecting cells with cDNAs encoding horseradish peroxidase. *J Cell Biol.* 127:641-652.

Cremona, O. 2001. Live stripping of clathrin-coated vesicles. *Developmental cell.* 1:592-594.

Cremona, O., G. Di Paolo, M.R. Wenk, A. Luthi, W.T. Kim, K. Takei, L. Daniell, Y. Nemoto, S.B. Shears, R.A. Flavell, D.A. McCormick, and P. De Camilli. 1999. Essential role of phosphoinositide metabolism in synaptic vesicle recycling. *Cell.* 99:179-188.

Cullen, P.J., and H.C. Korswagen. 2011. Sorting nexins provide diversity for retromer-dependent trafficking events. *Nat Cell Biol.* 14:29-37.

D

D'Souza, R.S., R. Semus, E.A. Billings, C.B. Meyer, K. Conger, and J.E. Casanova. 2014. Rab4 orchestrates a small GTPase cascade for recruitment of adaptor proteins to early endosomes. *Curr Biol.* 24:1187-1198.

Dacks, J.B., and M.S. Robinson. 2017. Outerwear through the ages: evolutionary cell biology of vesicle coats. *Curr Opin Cell Biol.* 47:108-116.

Damke, H., J. Klumperman, K. von Figura, and T. Braulke. 1991. Effects of brefeldin A on the endocytic route. Redistribution of mannose 6-phosphate/insulin-like growth factor II receptors to the cell surface. *J Biol Chem.* 266:24829-24833.

Daumke, O., A. Roux, and V. Haucke. 2014. BAR domain scaffolds in dynamin-mediated membrane fission. *Cell.* 156:882-892.

Dauner, K., W. Eid, R. Raghupathy, J.F. Presley, and X. Zha. 2017. mTOR complex 1 activity is required to maintain the canonical endocytic recycling pathway against lysosomal delivery. *J Biol Chem.* 292:5737-5747.

De Genst, E., K. Silence, K. Decanniere, K. Conrath, R. Loris, J. Kinne, S. Muyldermans, and L. Wyns. 2006. Molecular basis for the preferential cleft recognition by dromedary heavy-chain antibodies. *Proc Natl Acad Sci U S A.* 103:4586-4591.

De Meyer, T., S. Muyldermans, and A. Depicker. 2014. Nanobody-based products as research and diagnostic tools. *Trends Biotechnol.* 32:263-270.

De Munter, S., J. Gornemann, R. Derua, B. Lesage, J. Qian, E. Heroes, E. Waelkens, A. Van Eynde, M. Beullens, and M. Bollen. 2017. Split-BioID: a proximity biotinylation assay for dimerization-dependent protein interactions. *FEBS Lett.* 591:415-424.

Deborde, S., E. Perret, D. Gravotta, A. Deora, S. Salvarezza, R. Schreiner, and E. Rodriguez-Boulan. 2008. Clathrin is a key regulator of basolateral polarity. *Nature.* 452:719-723.

Delcarte, J., M. Fauconnier, P. Jacques, K. Matsui, P. Thonart, and M. Marlier. 2003. Optimisation of expression and immobilized metal ion affinity chromatographic purification of recombinant (His)6-tagged cytochrome P450 hydroperoxide lyase in Escherichia coli. *J Chromatogr B Analyt Technol Biomed Life Sci.* 786:229-236.

Derby, M.C., Z.Z. Lieu, D. Brown, J.L. Stow, B. Goud, and P.A. Gleeson. 2007. The trans-Golgi network golgin, GCC185, is required for endosome-to-Golgi transport and maintenance of Golgi structure. *Traffic.* 8:758-773.

Derkach, V.A., M.C. Oh, E.S. Guire, and T.R. Soderling. 2007. Regulatory mechanisms of AMPA receptors in synaptic plasticity. *Nat Rev Neurosci.* 8:101-113.

Diaz, E., and S.R. Pfeffer. 1998. TIP47: a cargo selection device for mannose 6-phosphate receptor trafficking. *Cell*. 93:433-443.

Diaz, E., F. Schimmoller, and S.R. Pfeffer. 1997. A novel Rab9 effector required for endosome-to-TGN transport. *J Cell Biol*. 138:283-290.

Doherty, G.J., and H.T. McMahon. 2009. Mechanisms of endocytosis. *Annu Rev Biochem*. 78:857-902.

Doray, B., P. Ghosh, J. Griffith, H.J. Geuze, and S. Kornfeld. 2002. Cooperation of GGAs and AP-1 in packaging MPRs at the trans-Golgi network. *Science*. 297:1700-1703.

Doray, B., I. Lee, J. Knisely, G. Bu, and S. Kornfeld. 2007. The gamma/sigma1 and alpha/sigma2 hemicomplexes of clathrin adaptors AP-1 and AP-2 harbor the dileucine recognition site. *Molecular biology of the cell*. 18:1887-1896.

Draper, R.K., Y. Goda, F.M. Brodsky, and S.R. Pfeffer. 1990. Antibodies to clathrin inhibit endocytosis but not recycling to the trans Golgi network in vitro. *Science*. 248:1539-1541.

Duncan, J.R., and S. Kornfeld. 1988. Intracellular movement of two mannose 6-phosphate receptors: return to the Golgi apparatus. *J Cell Biol*. 106:617-628.

Dyve Lingelem, A.B., I.A. Hjelseth, R. Simm, M.L. Torgersen, and K. Sandvig. 2015. Geldanamycin Enhances Retrograde Transport of Shiga Toxin in HEp-2 Cells. *PLoS One*. 10:e0129214.

E

Eaton, S. 2008. Retromer retrieves wntless. *Dev Cell*. 14:4-6.

Erhart, D., M. Zimmermann, O. Jacques, M.B. Wittwer, B. Ernst, E. Constable, M. Zvelebil, F. Beaufils, and M.P. Wymann. 2013. Chemical development of intracellular protein heterodimerizers. *Chemistry & biology*. 20:549-557.

Eyster, C.A., J.D. Higginson, R. Huebner, N. Porat-Shliom, R. Weigert, W.W. Wu, R.F. Shen, and J.G. Donaldson. 2009. Discovery of new cargo proteins that enter cells through clathrin-independent endocytosis. *Traffic*. 10:590-599.

F

Ferguson, S.M., A. Raimondi, S. Paradise, H. Shen, K. Mesaki, A. Ferguson, O. Destaing, G. Ko, J. Takasaki, O. Cremona, O.T. E, and P. De Camilli. 2009. Coordinated actions of actin and BAR proteins upstream of dynamin at endocytic clathrin-coated pits. *Developmental cell*. 17:811-822.

Ferguson, S.S., W.E. Downey, 3rd, A.M. Colapietro, L.S. Barak, L. Menard, and M.G. Caron. 1996. Role of beta-arrestin in mediating agonist-promoted G protein-coupled receptor internalization. *Science*. 271:363-366.

Fjeldstad, K., M.E. Pedersen, T.T. Vuong, S.O. Kolset, L.M. Nordstrand, and K. Prydz. 2002. Sulfation in the Golgi lumen of Madin-Darby canine kidney cells is inhibited by brefeldin A and depends on a factor present in the cytoplasm and on Golgi membranes. *J Biol Chem*. 277:36272-36279.

Fjorback, A.W., M. Seaman, C. Gustafsen, A. Mehmedbasic, S. Gokool, C. Wu, D. Militz, V. Schmidt, P. Madsen, J.R. Nyengaard, T.E. Willnow, E.I. Christensen, W.B. Mobley, A. Nykjaer, and O.M. Andersen. 2012. Retromer binds the FANSHY sorting motif in SorLA to regulate amyloid precursor protein sorting and processing. *J Neurosci*. 32:1467-1480.

Follett, J., A. Bugarcic, Z. Yang, N. Ariotti, S.J. Norwood, B.M. Collins, R.G. Parton, and R.D. Teasdale. 2016. Parkinson Disease-linked Vps35 R524W Mutation Impairs the Endosomal Association of Retromer and Induces alpha-Synuclein Aggregation. *J Biol Chem*. 291:18283-18298.

Folsch, H., H. Ohno, J.S. Bonifacino, and I. Mellman. 1999. A novel clathrin adaptor complex mediates basolateral targeting in polarized epithelial cells. *Cell*. 99:189-198.

Foote, C., and S.F. Nothwehr. 2006. The clathrin adaptor complex 1 directly binds to a sorting signal in Ste13p to reduce the rate of its trafficking to the late endosome of yeast. *The Journal of cell biology*. 173:615-626.

Fotin, A., Y. Cheng, N. Grigorieff, T. Walz, S.C. Harrison, and T. Kirchhausen. 2004. Structure of an auxilin-bound clathrin coat and its implications for the mechanism of uncoating. *Nature*. 432:649-653.

Friedman, J., S.M. Alam, X. Shen, S.M. Xia, S. Stewart, K. Anasti, J. Pollara, G.G. Fouda, G. Yang, G. Kelsoe, G. Ferrari, G.D. Tomaras, B.F. Haynes, H.X. Liao, M.A. Moody, and S.R. Permar. 2012. Isolation of HIV-1-neutralizing mucosal monoclonal antibodies from human colostrum. *PLoS One*. 7:e37648.

Frost, A., R. Perera, A. Roux, K. Spasov, O. Destaing, E.H. Egelman, P. De Camilli, and V.M. Unger. 2008. Structural basis of membrane invagination by F-BAR domains. *Cell*. 132:807-817.

Frost, A., V.M. Unger, and P. De Camilli. 2009. The BAR domain superfamily: membrane-molding macromolecules. *Cell*. 137:191-196.

Fuse, A., N. Furuya, S. Kakuta, A. Inose, M. Sato, M. Koike, S. Saiki, and N. Hattori. 2015. VPS29-VPS35 intermediate of retromer is stable and may be involved in the retromer complex assembly process. *FEBS Lett*. 589:1430-1436.

Futter, C.E., C.N. Connolly, D.F. Cutler, and C.R. Hopkins. 1995. Newly synthesized transferrin receptors can be detected in the endosome before they appear on the cell surface. *The Journal of biological chemistry*. 270:10999-11003.

G

Gallon, M., and P.J. Cullen. 2015. Retromer and sorting nexins in endosomal sorting. *Biochem Soc Trans*. 43:33-47.

Ganley, I.G., K. Carroll, L. Bittova, and S. Pfeffer. 2004. Rab9 GTPase regulates late endosome size and requires effector interaction for its stability. *Mol Biol Cell*. 15:5420-5430.

Garay, C., G. Judge, S. Lucarelli, S. Bautista, R. Pandey, T. Singh, and C.N. Antonescu. 2015. Epidermal growth factor-stimulated Akt phosphorylation requires clathrin or ErbB2 but not receptor endocytosis. *Mol Biol Cell*. 26:3504-3519.

Garcia, C.K., K. Wilund, M. Arca, G. Zuliani, R. Fellin, M. Maioli, S. Calandra, S. Bertolini, F. Cossu, N. Grishin, R. Barnes, J.C. Cohen, and H.H. Hobbs. 2001. Autosomal recessive hypercholesterolemia caused by mutations in a putative LDL receptor adaptor protein. *Science*. 292:1394-1398.

Garmroudi, F., G. Devi, D.H. Slentz, B.S. Schaffer, and R.G. MacDonald. 1996. Truncated forms of the insulin-like growth factor II (IGF-II)/mannose 6-phosphate receptor encompassing the IGF-II binding site: characterization of a point mutation that abolishes IGF-II binding. *Mol Endocrinol*. 10:642-651.

Garrick, M.D., K.G. Dolan, C. Horbinski, A.J. Ghio, D. Higgins, M. Porubcin, E.G. Moore, L.N. Hainsworth, J.N. Umbreit, M.E. Conrad, L. Feng, A. Lis, J.A. Roth, S. Singleton, and L.M. Garrick. 2003. DMT1: a mammalian transporter for multiple metals. *Biometals*. 16:41-54.

Geiger, R., S. Luisoni, K. Johnsson, U.F. Greber, and A. Helenius. 2012. Investigating endocytic pathways to the endoplasmic reticulum and to the cytosol using SNAP-trap. *Traffic*.

Gesbert, F., N. Sauvonnet, and A. Dautry-Varsat. 2004. Clathrin-Independent endocytosis and signalling of interleukin 2 receptors IL-2R endocytosis and signalling. *Curr Top Microbiol Immunol*. 286:119-148.

Geuze, H.J., W. Stoorvogel, G.J. Strous, J.W. Slot, J.E. Bleekemolen, and I. Mellman. 1988. Sorting of mannose 6-phosphate receptors and lysosomal membrane proteins in endocytic vesicles. *The Journal of cell biology*. 107:2491-2501.

Ghosh, P., N.M. Dahms, and S. Kornfeld. 2003a. Mannose 6-phosphate receptors: new twists in the tale. *Nature reviews. Molecular cell biology*. 4:202-212.

Ghosh, P., J. Griffith, H.J. Geuze, and S. Kornfeld. 2003b. Mammalian GGAs act together to sort mannose 6-phosphate receptors. *J Cell Biol*. 163:755-766.

Ghosh, P., and S. Kornfeld. 2004. The GGA proteins: key players in protein sorting at the trans-Golgi network. *European journal of cell biology*. 83:257-262.

Giorgino, T., and G. De Fabritiis. 2011. A High-Throughput Steered Molecular Dynamics Study on the Free Energy Profile of Ion Permeation through Gramicidin A. *J Chem Theory Comput*. 7:1943-1950.

Girard, E., D. Chmiest, N. Fournier, L. Johannes, J.L. Paul, B. Vedie, and C. Lamaze. 2014. Rab7 is functionally required for selective cargo sorting at the early endosome. *Traffic*. 15:309-326.

Glebov, O.O., N.A. Bright, and B.J. Nichols. 2006. Flotillin-1 defines a clathrin-independent endocytic pathway in mammalian cells. *Nature cell biology*. 8:46-54.

Goda, Y., and S.R. Pfeffer. 1988. Selective recycling of the mannose 6-phosphate/IGF-II receptor to the trans Golgi network in vitro. *Cell*. 55:309-320.

Goda, Y., and S.R. Pfeffer. 1989. Cell-free systems to study vesicular transport along the secretory and endocytic pathways. *FASEB J*. 3:2488-2495.

Goder, V., and M. Spiess. 2001. Topogenesis of membrane proteins: determinants and dynamics. *FEBS letters*. 504:87-93.

Goldstein, I.J., and C.E. Hayes. 1978. The lectins: carbohydrate-binding proteins of plants and animals. *Adv Carbohydr Chem Biochem*. 35:127-340.

Gonatas, N.K., A. Steiber, S.U. Kim, D.I. Graham, and S. Avrameas. 1975. Internalization of neuronal plasma membrane ricin receptors into the Golgi apparatus. *Exp Cell Res*. 94:426-431.

Gonzalez, A., and M.N. Hall. 2017. Nutrient sensing and TOR signaling in yeast and mammals. *EMBO J*. 36:397-408.

Gonzalez, A., and E. Rodriguez-Boulan. 2009. Clathrin and AP1B: key roles in basolateral trafficking through trans-endosomal routes. *FEBS letters*. 583:3784-3795.

Grant, B.D., and J.G. Donaldson. 2009. Pathways and mechanisms of endocytic recycling. *Nature reviews. Molecular cell biology*. 10:597-608.

Gravotta, D., J.M. Carvajal-Gonzalez, R. Mattera, S. Deborde, J.R. Banfelder, J.S. Bonifacino, and E. Rodriguez-Boulan. 2012a. The clathrin adaptor AP-1A mediates basolateral polarity. *Developmental cell*. 22:811-823.

Gravotta, D., J.M. Carvajal-Gonzalez, R. Mattera, S. Deborde, J.R. Banfelder, J.S. Bonifacino, and E. Rodriguez-Boulan. 2012b. The clathrin adaptor AP-1A mediates basolateral polarity. *Dev Cell*. 22:811-823.

Greenberg, A.S., D. Avila, M. Hughes, A. Hughes, E.C. McKinney, and M.F. Flajnik. 1995. A new antigen receptor gene family that undergoes rearrangement and extensive somatic diversification in sharks. *Nature*. 374:168-173.

Griffiths, G., B. Hoflack, K. Simons, I. Mellman, and S. Kornfeld. 1988. The mannose 6-phosphate receptor and the biogenesis of lysosomes. *Cell*. 52:329-341.

Grimm, M.O., J. Mett, H.S. Grimm, and T. Hartmann. 2017. APP Function and Lipids: A Bidirectional Link. *Front Mol Neurosci*. 10:63.

Gross, A.J., and I.W. Sizer. 1959. The oxidation of tyramine, tyrosine, and related compounds by peroxidase. *J Biol Chem*. 234:1611-1614.

Gruenberg, J. 2001. The endocytic pathway: a mosaic of domains. *Nat Rev Mol Cell Biol*. 2:721-730.

Gupta, G.D., M.G. Swetha, S. Kumari, R. Lakshminarayan, G. Dey, and S. Mayor. 2009. Analysis of endocytic pathways in Drosophila cells reveals a conserved role for GBF1 in internalization via GEECs. *PLoS One*. 4:e6768.

H

Hamers-Casterman, C., T. Atarhouch, S. Muyldermans, G. Robinson, C. Hamers, E.B. Songa, N. Bendahman, and R. Hamers. 1993. Naturally occurring antibodies devoid of light chains. *Nature*. 363:446-448.

Hancock, M.K., D.J. Haskins, G. Sun, and N.M. Dahms. 2002. Identification of residues essential for carbohydrate recognition by the insulin-like growth factor II/mannose 6-phosphate receptor. *J Biol Chem*. 277:11255-11264.

Hansen, C.G., and B.J. Nichols. 2010. Exploring the caves: cavins, caveolins and caveolae. *Trends Cell Biol*. 20:177-186.

Hao, M., and F.R. Maxfield. 2000. Characterization of rapid membrane internalization and recycling. *J Biol Chem*. 275:15279-15286.

Harmansa, S., I. Alborelli, D. Bieli, E. Caussinus, and M. Affolter. 2017. A nanobody-based toolset to investigate the role of protein localization and dispersal in Drosophila. *Elife*. 6.

Harmansa, S., F. Hamaratoglu, M. Affolter, and E. Caussinus. 2015. Dpp spreading is required for medial but not for lateral wing disc growth. *Nature*. 527:317-322.

Harterink, M., and H.C. Korswagen. 2012. Dissecting the Wnt secretion pathway: key questions on the modification and intracellular trafficking of Wnt proteins. *Acta Physiol (Oxf)*. 204:8-16.

Harterink, M., F. Port, M.J. Lorenowicz, I.J. McGough, M. Silhankova, M.C. Betist, J.R. van Weering, R.G. van Heesbeen, T.C. Middelkoop, K. Basler, P.J. Cullen, and H.C. Korswagen. 2011. A SNX3-dependent retromer pathway mediates retrograde transport of the Wnt sorting receptor Wntless and is required for Wnt secretion. *Nat Cell Biol*. 13:914-923.

Hashiramoto, M., and D.E. James. 2000. Characterization of insulin-responsive GLUT4 storage vesicles isolated from 3T3-L1 adipocytes. *Mol Cell Biol*. 20:416-427.

Hathaway, H.J., S.C. Evans, D.H. Dubois, C.I. Foote, B.H. Elder, and B.D. Shur. 2003. Mutational analysis of the cytoplasmic domain of beta1,4-galactosyltransferase I: influence of phosphorylation on cell surface expression. *J Cell Sci*. 116:4319-4330.

Hayer, A., M. Stoeber, C. Bissig, and A. Helenius. 2010. Biogenesis of caveolae: stepwise assembly of large caveolin and cavin complexes. *Traffic*. 11:361-382.

Helma, J., M.C. Cardoso, S. Muyldermans, and H. Leonhardt. 2015. Nanobodies and recombinant binders in cell biology. *J Cell Biol*. 209:633-644.

Henley, J.M., and K.A. Wilkinson. 2013. AMPA receptor trafficking and the mechanisms underlying synaptic plasticity and cognitive aging. *Dialogues Clin Neurosci.* 15:11-27.

Henley, J.M., and K.A. Wilkinson. 2016. Synaptic AMPA receptor composition in development, plasticity and disease. *Nat Rev Neurosci.* 17:337-350.

Henne, W.M., E. Boucrot, M. Meinecke, E. Evergren, Y. Vallis, R. Mittal, and H.T. McMahon. 2010. FCHo proteins are nucleators of clathrin-mediated endocytosis. *Science.* 328:1281-1284.

Henne, W.M., H. Stenmark, and S.D. Emr. 2013. Molecular mechanisms of the membrane sculpting ESCRT pathway. *Cold Spring Harb Perspect Biol.* 5.

Herce, H.D., W. Deng, J. Helma, H. Leonhardt, and M.C. Cardoso. 2013. Visualization and targeted disruption of protein interactions in living cells. *Nat Commun.* 4:2660.

Hermey, G. 2009. The Vps10p-domain receptor family. *Cell Mol Life Sci.* 66:2677-2689.

Herr, P., G. Hausmann, and K. Basler. 2012. WNT secretion and signalling in human disease. *Trends Mol Med.* 18:483-493.

Hierro, A., A.L. Rojas, R. Rojas, N. Murthy, G. Effantin, A.V. Kajava, A.C. Steven, J.S. Bonifacino, and J.H. Hurley. 2007. Functional architecture of the retromer cargo-recognition complex. *Nature.* 449:1063-1067.

Hill, M.M., M. Bastiani, R. Luetterforst, M. Kirkham, A. Kirkham, S.J. Nixon, P. Walser, D. Abankwa, V.M. Oorschot, S. Martin, J.F. Hancock, and R.G. Parton. 2008. PTRF-Cavin, a conserved cytoplasmic protein required for caveola formation and function. *Cell.* 132:113-124.

Hinners, I., and S.A. Tooze. 2003. Changing directions: clathrin-mediated transport between the Golgi and endosomes. *Journal of cell science.* 116:763-771.

Hinshaw, J.E., and S.L. Schmid. 1995. Dynamin self-assembles into rings suggesting a mechanism for coated vesicle budding. *Nature.* 374:190-192.

Hirschmann, D.T., C.A. Kasper, and M. Spiess. 2015. Quantitative analysis of transferrin cycling by automated fluorescence microscopy. *Methods Mol Biol.* 1270:365-378.

Hirst, J., G.H. Borner, R. Antrobus, A.A. Peden, N.A. Hodson, D.A. Sahlender, and M.S. Robinson. 2012a. Distinct and Overlapping Roles for AP-1 and GGAs Revealed by the "Knocksideways" System. *Curr Biol.*

Hirst, J., G.H. Borner, M. Harbour, and M.S. Robinson. 2005. The aftiphilin/p200/gamma-synergin complex. *Mol Biol Cell.* 16:2554-2565.

Hirst, J., J.R. Edgar, G.H. Borner, S. Li, D.A. Sahlender, R. Antrobus, and M.S. Robinson. 2015. Contributions of epsinR and gadkin to clathrin-mediated intracellular trafficking. *Mol Biol Cell.* 26:3085-3103.

Hirst, J., C. Irving, and G.H. Borner. 2012b. Adaptor Protein Complexes AP-4 and AP-5: New Players in Endosomal Trafficking and Progressive Spastic Paraplegia. *Traffic.*

Hirst, J., S.E. Miller, M.J. Taylor, G.F. von Mollard, and M.S. Robinson. 2004. EpsinR is an adaptor for the SNARE protein Vti1b. *Mol Biol Cell.* 15:5593-5602.

Hirst, J., A. Motley, K. Harasaki, S.Y. Peak Chew, and M.S. Robinson. 2003. EpsinR: an ENTH domain-containing protein that interacts with AP-1. *Mol Biol Cell.* 14:625-641.

Hirst, J., D.A. Sahlender, M. Choma, R. Sinka, M.E. Harbour, M. Parkinson, and M.S. Robinson. 2009. Spatial and functional relationship of GGAs and AP-1 in Drosophila and HeLa cells. *Traffic.* 10:1696-1710.

Hirst, J., A. Schlacht, J.P. Norcott, D. Traynor, G. Bloomfield, R. Antrobus, R.R. Kay, J.B. Dacks, and M.S. Robinson. 2014. Characterization of TSET, an ancient and widespread membrane trafficking complex. *Elife.* 3:e02866.

Hoffhines, A.J., E. Damoc, K.G. Bridges, J.A. Leary, and K.L. Moore. 2006. Detection and purification of tyrosine-sulfated proteins using a novel anti-sulfotyrosine monoclonal antibody. *J Biol Chem*. 281:37877-37887.

Hollopeter, G., J.J. Lange, Y. Zhang, T.N. Vu, M. Gu, M. Ailion, E.J. Lambie, B.D. Slaughter, J.R. Unruh, L. Florens, and E.M. Jorgensen. 2014. The membrane-associated proteins FCHo and SGIP are allosteric activators of the AP2 clathrin adaptor complex. *Elife*. 3.

Hong, W. 2005. SNAREs and traffic. *Biochim Biophys Acta*. 1744:493-517.

Honke, K., and N. Kotani. 2011. The enzyme-mediated activation of radical source reaction: a new approach to identify partners of a given molecule in membrane microdomains. *J Neurochem*. 116:690-695.

Hopkins, C.R., K. Miller, and J.M. Beardmore. 1985. Receptor-mediated endocytosis of transferrin and epidermal growth factor receptors: a comparison of constitutive and ligand-induced uptake. *J Cell Sci Suppl*. 3:173-186.

Horazdovsky, B.F., B.A. Davies, M.N. Seaman, S.A. McLaughlin, S. Yoon, and S.D. Emr. 1997. A sorting nexin-1 homologue, Vps5p, forms a complex with Vps17p and is required for recycling the vacuolar protein-sorting receptor. *Mol Biol Cell*. 8:1529-1541.

Hosoi, H., M.B. Dilling, T. Shikata, L.N. Liu, L. Shu, R.A. Ashmun, G.S. Germain, R.T. Abraham, and P.J. Houghton. 1999. Rapamycin causes poorly reversible inhibition of mTOR and induces p53-independent apoptosis in human rhabdomyosarcoma cells. *Cancer Res*. 59:886-894.

Howes, M.T., M. Kirkham, J. Riches, K. Cortese, P.J. Walser, F. Simpson, M.M. Hill, A. Jones, R. Lundmark, M.R. Lindsay, D.J. Hernandez-Deviez, G. Hadzic, A. McCluskey, R. Bashir, L. Liu, P. Pilch, H. McMahon, P.J. Robinson, J.F. Hancock, S. Mayor, and R.G. Parton. 2010a. Clathrin-independent carriers form a high capacity endocytic sorting system at the leading edge of migrating cells. *The Journal of cell biology*. 190:675-691.

Howes, M.T., S. Mayor, and R.G. Parton. 2010b. Molecules, mechanisms, and cellular roles of clathrin-independent endocytosis. *Current opinion in cell biology*. 22:519-527.

Hughes, K.R., and A.P. Waters. 2017. Rapid inducible protein displacement in Plasmodiumin vivo and in vitro using knocksideways technology. *Wellcome Open Res*. 2:18.

Humphries, D.E., and J.E. Silbert. 1988. Chlorate: a reversible inhibitor of proteoglycan sulfation. *Biochem Biophys Res Commun*. 154:365-371.

Humphries, W.H.t., C.J. Szymanski, and C.K. Payne. 2011. Endo-lysosomal vesicles positive for Rab7 and LAMP1 are terminal vesicles for the transport of dextran. *PLoS One*. 6:e26626.

Hung, V., S.S. Lam, N.D. Udeshi, T. Svinkina, G. Guzman, V.K. Mootha, S.A. Carr, and A.Y. Ting. 2017. Proteomic mapping of cytosol-facing outer mitochondrial and ER membranes in living human cells by proximity biotinylation. *Elife*. 6.

Hung, V., N.D. Udeshi, S.S. Lam, K.H. Loh, K.J. Cox, K. Pedram, S.A. Carr, and A.Y. Ting. 2016. Spatially resolved proteomic mapping in living cells with the engineered peroxidase APEX2. *Nat Protoc*. 11:456-475.

Hung, V., P. Zou, H.W. Rhee, N.D. Udeshi, V. Cracan, T. Svinkina, S.A. Carr, V.K. Mootha, and A.Y. Ting. 2014. Proteomic mapping of the human mitochondrial intermembrane space in live cells via ratiometric APEX tagging. *Mol Cell*. 55:332-341.

Hunziker, W., J.A. Whitney, and I. Mellman. 1992. Brefeldin A and the endocytic pathway. Possible implications for membrane traffic and sorting. *FEBS Lett*. 307:93-96.

Huotari, J., and A. Helenius. 2011. Endosome maturation. *EMBO J*. 30:3481-3500.

Hurley, J.H., and S.D. Emr. 2006. The ESCRT complexes: structure and mechanism of a membrane-trafficking network. *Annu Rev Biophys Biomol Struct*. 35:277-298.

Huser, S., G. Suri, P. Crottet, and M. Spiess. 2012. Interaction of amphiphysins with AP-1 clathrin adaptors at the membrane. *The Biochemical journal*.

Huttner, W.B. 1988. Tyrosine sulfation and the secretory pathway. *Annu Rev Physiol*. 50:363-376.

Hwang, J., and P.J. Espenshade. 2016. Proximity-dependent biotin labelling in yeast using the engineered ascorbate peroxidase APEX2. *Biochem J*. 473:2463-2469.

I

Iacopetta, B.J., and E.H. Morgan. 1983. The kinetics of transferrin endocytosis and iron uptake from transferrin in rabbit reticulocytes. *J Biol Chem*. 258:9108-9115.

Iida, H., and Y. Shibata. 1989. Delivery of lectin-labeled membrane to the trans-Golgi network and secretory granules in cultured atrial myocytes. *J Histochem Cytochem*. 37:1885-1892.

Interlandi, G., S.K. Wetzel, G. Settanni, A. Pluckthun, and A. Caflisch. 2008. Characterization and further stabilization of designed ankyrin repeat proteins by combining molecular dynamics simulations and experiments. *J Mol Biol*. 375:837-854.

Ishizaki, R., H.W. Shin, H. Mitsuhashi, and K. Nakayama. 2008. Redundant roles of BIG2 and BIG1, guanine-nucleotide exchange factors for ADP-ribosylation factors in membrane traffic between the trans-Golgi network and endosomes. *Mol Biol Cell*. 19:2650-2660.

Itabe, H., T. Yamaguchi, S. Nimura, and N. Sasabe. 2017. Perilipins: a diversity of intracellular lipid droplet proteins. *Lipids Health Dis*. 16:83.

Ittig, S.J., C. Schmutz, C.A. Kasper, M. Amstutz, A. Schmidt, L. Sauteur, M.A. Vigano, S.H. Low, M. Affolter, G.R. Cornelis, E.A. Nigg, and C. Arrieumerlou. 2015. A bacterial type III secretion-based protein delivery tool for broad applications in cell biology. *J Cell Biol*. 211:913-931.

J

Jedrychowski, M.P., C.A. Gartner, S.P. Gygi, L. Zhou, J. Herz, K.V. Kandror, and P.F. Pilch. 2010. Proteomic analysis of GLUT4 storage vesicles reveals LRP1 to be an important vesicle component and target of insulin signaling. *J Biol Chem*. 285:104-114.

Jin, M., G.G. Sahagian, Jr., and M.D. Snider. 1989. Transport of surface mannose 6-phosphate receptor to the Golgi complex in cultured human cells. *J Biol Chem*. 264:7675-7680.

Johannes, L., and B. Goud. 1998. Surfing on a retrograde wave: how does Shiga toxin reach the endoplasmic reticulum? *Trends Cell Biol*. 8:158-162.

Johannes, L., and B. Goud. 2000. Facing inward from compartment shores: how many pathways were we looking for? *Traffic*. 1:119-123.

Johannes, L., R.G. Parton, P. Bassereau, and S. Mayor. 2015. Building endocytic pits without clathrin. *Nat Rev Mol Cell Biol*. 16:311-321.

Johannes, L., and V. Popoff. 2008. Tracing the retrograde route in protein trafficking. *Cell*. 135:1175-1187.

Johannes, L., D. Tenza, C. Antony, and B. Goud. 1997. Retrograde transport of KDEL-bearing B-fragment of Shiga toxin. *J Biol Chem*. 272:19554-19561.

Johannes, L., and C. Wunder. 2011. Retrograde transport: two (or more) roads diverged in an endosomal tree? *Traffic*. 12:956-962.

K

Kaiser, P.D., J. Maier, B. Traenkle, F. Emele, and U. Rothbauer. 2014. Recent progress in generating intracellular functional antibody fragments to target and trace cellular components in living cells. *Biochim Biophys Acta*. 1844:1933-1942.

Kalin, S., D.P. Buser, and M. Spiess. 2016. A fresh look at the function of Rabaptin5 on endosomes. *Small GTPases*. 7:34-37.

Kalin, S., D.T. Hirschmann, D.P. Buser, and M. Spiess. 2015. Rabaptin5 is recruited to endosomes by Rab4 and Rabex5 to regulate endosome maturation. *J Cell Sci*. 128:4126-4137.

Kehoe, J.W., and C.R. Bertozzi. 2000. Tyrosine sulfation: a modulator of extracellular protein-protein interactions. *Chem Biol*. 7:R57-61.

Kery, V., D. Elleder, and J.P. Kraus. 1995. Delta-aminolevulinate increases heme saturation and yield of human cystathionine beta-synthase expressed in Escherichia coli. *Arch Biochem Biophys*. 316:24-29.

Keyel, P.A., S.C. Watkins, and L.M. Traub. 2004. Endocytic adaptor molecules reveal an endosomal population of clathrin by total internal reflection fluorescence microscopy. *The Journal of biological chemistry*. 279:13190-13204.

Kim, D.I., S.C. Jensen, K.A. Noble, B. Kc, K.H. Roux, K. Motamedchaboki, and K.J. Roux. 2016a. An improved smaller biotin ligase for BioID proximity labeling. *Mol Biol Cell*. 27:1188-1196.

Kim, D.I., S.C. Jensen, and K.J. Roux. 2016b. Identifying Protein-Protein Associations at the Nuclear Envelope with BioID. *Methods Mol Biol*. 1411:133-146.

Kim, D.I., and K.J. Roux. 2016. Filling the Void: Proximity-Based Labeling of Proteins in Living Cells. *Trends Cell Biol*. 26:804-817.

Kirchhausen, T. 1999. Adaptors for clathrin-mediated traffic. *Annual review of cell and developmental biology*. 15:705-732.

Kirchhausen, T., D. Owen, and S.C. Harrison. 2014. Molecular structure, function, and dynamics of clathrin-mediated membrane traffic. *Cold Spring Harb Perspect Biol*. 6:a016725.

Kirchhofer, A., J. Helma, K. Schmidthals, C. Frauer, S. Cui, A. Karcher, M. Pellis, S. Muyldermans, C.S. Casas-Delucchi, M.C. Cardoso, H. Leonhardt, K.P. Hopfner, and U. Rothbauer. 2010. Modulation of protein properties in living cells using nanobodies. *Nat Struct Mol Biol*. 17:133-138.

Kirkham, M., and R.G. Parton. 2005. Clathrin-independent endocytosis: new insights into caveolae and non-caveolar lipid raft carriers. *Biochimica et biophysica acta*. 1746:349-363.

Klausner, R.D., J.G. Donaldson, and J. Lippincott-Schwartz. 1992. Brefeldin A: insights into the control of membrane traffic and organelle structure. *J Cell Biol*. 116:1071-1080.

Klokk, T.I., A.B. Lingelem, A.G. Myrann, and K. Sandvig. 2011. Role of phospholipase A(2) in retrograde transport of ricin. *Toxins (Basel)*. 3:1203-1219.

Klumperman, J. 2011. Architecture of the mammalian Golgi. *Cold Spring Harb Perspect Biol*. 3.

Klumperman, J., A. Hille, T. Veenendaal, V. Oorschot, W. Stoorvogel, K. von Figura, and H.J. Geuze. 1993. Differences in the endosomal distributions of the two mannose 6-phosphate receptors. *J Cell Biol*. 121:997-1010.

Kohl, A., H.K. Binz, P. Forrer, M.T. Stumpp, A. Pluckthun, and M.G. Grutter. 2003. Designed to be stable: crystal structure of a consensus ankyrin repeat protein. *Proc Natl Acad Sci U S A*. 100:1700-1705.

Krise, J.P., P.M. Sincock, J.G. Orsel, and S.R. Pfeffer. 2000. Quantitative analysis of TIP47-receptor cytoplasmic domain interactions: implications for endosome-to-trans Golgi network trafficking. *J Biol Chem*. 275:25188-25193.

Kroemer, G., and M. Jaattela. 2005. Lysosomes and autophagy in cell death control. *Nat Rev Cancer*. 5:886-897.

Kubala, M.H., O. Kovtun, K. Alexandrov, and B.M. Collins. 2010. Structural and thermodynamic analysis of the GFP:GFP-nanobody complex. *Protein Sci*. 19:2389-2401.

Kucera, A., O. Bakke, and C. Progida. 2016a. The multiple roles of Rab9 in the endolysosomal system. *Commun Integr Biol*. 9:e1204498.

Kucera, A., M. Borg Distefano, A. Berg-Larsen, F. Skjeldal, U. Repnik, O. Bakke, and C. Progida. 2016b. Spatiotemporal Resolution of Rab9 and CI-MPR Dynamics in the Endocytic Pathway. *Traffic*. 17:211-229.

Kumari, S., and S. Mayor. 2008. ARF1 is directly involved in dynamin-independent endocytosis. *Nature cell biology*. 10:30-41.

L

La Fontaine, S., and J.F. Mercer. 2007. Trafficking of the copper-ATPases, ATP7A and ATP7B: role in copper homeostasis. *Arch Biochem Biophys*. 463:149-167.

Lakadamyali, M., M.J. Rust, and X. Zhuang. 2006. Ligands for clathrin-mediated endocytosis are differentially sorted into distinct populations of early endosomes. *Cell*. 124:997-1009.

Lam, S.S., J.D. Martell, K.J. Kamer, T.J. Deerinck, M.H. Ellisman, V.K. Mootha, and A.Y. Ting. 2015. Directed evolution of APEX2 for electron microscopy and proximity labeling. *Nat Methods*. 12:51-54.

Lamaze, C., A. Dujeancourt, T. Baba, C.G. Lo, A. Benmerah, and A. Dautry-Varsat. 2001. Interleukin 2 receptors and detergent-resistant membrane domains define a clathrin-independent endocytic pathway. *Mol Cell*. 7:661-671.

Laulagnier, K., N.L. Schieber, T. Maritzen, V. Haucke, R.G. Parton, and J. Gruenberg. 2011. Role of AP1 and Gadkin in the traffic of secretory endo-lysosomes. *Mol Biol Cell*. 22:2068-2082.

Le Sage, V., A. Cinti, and A.J. Mouland. 2016. Proximity-Dependent Biotinylation for Identification of Interacting Proteins. *Curr Protoc Cell Biol*. 73:17 19 11-17 19 12.

Lefrancois, S., J. Zeng, A.J. Hassan, M. Canuel, and C.R. Morales. 2003. The lysosomal trafficking of sphingolipid activator proteins (SAPs) is mediated by sortilin. *EMBO J*. 22:6430-6437.

Leto, D., and A.R. Saltiel. 2012. Regulation of glucose transport by insulin: traffic control of GLUT4. *Nat Rev Mol Cell Biol*. 13:383-396.

Lewin, D.A., D. Sheff, C.E. Ooi, J.A. Whitney, E. Yamamoto, L.M. Chicione, P. Webster, J.S. Bonifacino, and I. Mellman. 1998. Cloning, expression, and localization of a novel gamma-adaptin-like molecule. *FEBS Lett*. 435:263-268.

Li, P., J. Li, L. Wang, and L.J. Di. 2017. Proximity labeling of interacting proteins: Application of BioID as a discovery tool. *Proteomics*.

Lieu, Z.Z., M.C. Derby, R.D. Teasdale, C. Hart, P. Gunn, and P.A. Gleeson. 2007. The golgin GCC88 is required for efficient retrograde transport of cargo from the early endosomes to the trans-Golgi network. *Molecular biology of the cell*. 18:4979-4991.

Lieu, Z.Z., and P.A. Gleeson. 2010. Identification of different itineraries and retromer components for endosome-to-Golgi transport of TGN38 and Shiga toxin. *Eur J Cell Biol*. 89:379-393.

Lippincott-Schwartz, J., L. Yuan, C. Tipper, M. Amherdt, L. Orci, and R.D. Klausner. 1991. Brefeldin A's effects on endosomes, lysosomes, and the TGN suggest a general mechanism for regulating organelle structure and membrane traffic. *Cell*. 67:601-616.

Livingstone, C., D.E. James, J.E. Rice, D. Hanpeter, and G.W. Gould. 1996. Compartment ablation analysis of the insulin-responsive glucose transporter (GLUT4) in 3T3-L1 adipocytes. *Biochem J*. 315 (Pt 2):487-495.

Llorente, A., A. Rapak, S.L. Schmid, B. van Deurs, and K. Sandvig. 1998. Expression of mutant dynamin inhibits toxicity and transport of endocytosed ricin to the Golgi apparatus. *J Cell Biol*. 140:553-563.

Lo, H.P., T.E. Hall, and R.G. Parton. 2016. Mechanoprotection by skeletal muscle caveolae. *Bioarchitecture*. 6:22-27.

Lo, H.P., S.J. Nixon, T.E. Hall, B.S. Cowling, C. Ferguson, G.P. Morgan, N.L. Schieber, M.A. Fernandez-Rojo, M. Bastiani, M. Floetenmeyer, N. Martel, J. Laporte, P.F. Pilch, and R.G. Parton. 2015. The caveolin-cavin system plays a conserved and critical role in mechanoprotection of skeletal muscle. *J Cell Biol*. 210:833-849.

Lobel, P., K. Fujimoto, R.D. Ye, G. Griffiths, and S. Kornfeld. 1989. Mutations in the cytoplasmic domain of the 275 kd mannose 6-phosphate receptor differentially alter lysosomal enzyme sorting and endocytosis. *Cell*. 57:787-796.

Lombardi, D., T. Soldati, M.A. Riederer, Y. Goda, M. Zerial, and S.R. Pfeffer. 1993. Rab9 functions in transport between late endosomes and the trans Golgi network. *EMBO J*. 12:677-682.

Lubben, N.B., D.A. Sahlender, A.M. Motley, P.J. Lehner, P. Benaroch, and M.S. Robinson. 2007. HIV-1 Nef-induced down-regulation of MHC class I requires AP-1 and clathrin but not PACS-1 and is impeded by AP-2. *Molecular biology of the cell*. 18:3351-3365.

Luzio, J.P., S.R. Gray, and N.A. Bright. 2010. Endosome-lysosome fusion. *Biochem Soc Trans*. 38:1413-1416.

Luzio, J.P., P.R. Pryor, and N.A. Bright. 2007. Lysosomes: fusion and function. *Nature reviews. Molecular cell biology*. 8:622-632.

M

Ma, L., P.K. Umasankar, A.G. Wrobel, A. Lymar, A.J. McCoy, S.S. Holkar, A. Jha, T. Pradhan-Sundd, S.C. Watkins, D.J. Owen, and L.M. Traub. 2016. Transient Fcho1/2Eps15/RAP-2 Nanoclusters Prime the AP-2 Clathrin Adaptor for Cargo Binding. *Dev Cell*. 37:428-443.

Mallard, F., C. Antony, D. Tenza, J. Salamero, B. Goud, and L. Johannes. 1998. Direct pathway from early/recycling endosomes to the Golgi apparatus revealed through the study of shiga toxin B-fragment transport. *J Cell Biol*. 143:973-990.

Mallard, F., and L. Johannes. 2003. Shiga toxin B-subunit as a tool to study retrograde transport. *Methods Mol Med*. 73:209-220.

Mardones, G.A., P.V. Burgos, D.A. Brooks, E. Parkinson-Lawrence, R. Mattera, and J.S. Bonifacino. 2007. The trans-Golgi network accessory protein p56 promotes long-range movement of GGA/clathrin-containing transport carriers and lysosomal enzyme sorting. *Molecular biology of the cell*. 18:3486-3501.

Maritzen, T., T. Zech, M.R. Schmidt, E. Krause, L.M. Machesky, and V. Haucke. 2012. Gadkin negatively regulates cell spreading and motility via sequestration of the actin-nucleating ARP2/3 complex. *Proc Natl Acad Sci U S A*. 109:10382-10387.

Marron-Terada, P.G., M.K. Hancock, D.J. Haskins, and N.M. Dahms. 2000. Recognition of Dictyostelium discoideum lysosomal enzymes is conferred by the amino-terminal carbohydrate binding site of the insulin-like growth factor II/mannose 6-phosphate receptor. *Biochemistry*. 39:2243-2253.

Martell, J.D., T.J. Deerinck, Y. Sancak, T.L. Poulos, V.K. Mootha, G.E. Sosinsky, M.H. Ellisman, and A.Y. Ting. 2012. Engineered ascorbate peroxidase as a genetically encoded reporter for electron microscopy. *Nat Biotechnol*. 30:1143-1148.

Massol, R.H., W. Boll, A.M. Griffin, and T. Kirchhausen. 2006. A burst of auxilin recruitment determines the onset of clathrin-coated vesicle uncoating. *Proceedings of the National Academy of Sciences of the United States of America*. 103:10265-10270.

Matsudaira, T., T. Niki, T. Taguchi, and H. Arai. 2015. Transport of the cholera toxin B-subunit from recycling endosomes to the Golgi requires clathrin and AP-1. *J Cell Sci*. 128:3131-3142.

Matsudaira, T., Y. Uchida, K. Tanabe, S. Kon, T. Watanabe, T. Taguchi, and H. Arai. 2013. SMAP2 regulates retrograde transport from recycling endosomes to the Golgi. *PLoS One*. 8:e69145.

Maxfield, F.R., and T.E. McGraw. 2004. Endocytic recycling. *Nature reviews. Molecular cell biology*. 5:121-132.

Maxfield, F.R., and D.J. Yamashiro. 1987. Endosome acidification and the pathways of receptor-mediated endocytosis. *Adv Exp Med Biol*. 225:189-198.

Mayor, S., and R.E. Pagano. 2007. Pathways of clathrin-independent endocytosis. *Nature reviews. Molecular cell biology*. 8:603-612.

Mayor, S., R.G. Parton, and J.G. Donaldson. 2014. Clathrin-independent pathways of endocytosis. *Cold Spring Harb Perspect Biol*. 6.

Mayor, S., and H. Riezman. 2004. Sorting GPI-anchored proteins. *Nature reviews. Molecular cell biology*. 5:110-120.

McGough, I.J., and P.J. Cullen. 2011. Recent advances in retromer biology. *Traffic*. 12:963-971.

McGough, I.J., and P.J. Cullen. 2013. Clathrin is not required for SNX-BAR-retromer-mediated carrier formation. *Journal of cell science*. 126:45-52.

McKenzie, J.E., B. Raisley, X. Zhou, N. Naslavsky, T. Taguchi, S. Caplan, and D. Sheff. 2012. Retromer guides STxB and CD8-M6PR from early to recycling endosomes, EHD1 guides STxB from recycling endosome to Golgi. *Traffic*. 13:1140-1159.

McMahon, H.T., and E. Boucrot. 2011. Molecular mechanism and physiological functions of clathrin-mediated endocytosis. *Nature reviews. Molecular cell biology*. 12:517-533.

Medigeshi, G.R., and P. Schu. 2003. Characterization of the in vitro retrograde transport of MPR46. *Traffic*. 4:802-811.

Mehus, A.A., R.H. Anderson, and K.J. Roux. 2016. BioID Identification of Lamin-Associated Proteins. *Methods Enzymol*. 569:3-22.

Mellman, I. 1996. Endocytosis and molecular sorting. *Annu Rev Cell Dev Biol*. 12:575-625.

Meresse, S., T. Ludwig, R. Frank, and B. Hoflack. 1990. Phosphorylation of the cytoplasmic domain of the bovine cation-independent mannose 6-phosphate receptor. Serines 2421 and 2492 are the targets of a casein kinase II associated to the Golgi-derived HAI adaptor complex. *J Biol Chem*. 265:18833-18842.

Merrifield, C.J. 2012. Fishing for clathrin-coated pit nucleators. *Nature cell biology*. 14:452-454.

Mettlen, M., D. Loerke, D. Yarar, G. Danuser, and S.L. Schmid. 2010. Cargo- and adaptor-specific mechanisms regulate clathrin-mediated endocytosis. *The Journal of cell biology*. 188:919-933.

Meyer, C., D. Zizioli, S. Lausmann, E.L. Eskelinen, J. Hamann, P. Saftig, K. von Figura, and P. Schu. 2000. mu1A-adaptin-deficient mice: lethality, loss of AP-1 binding and rerouting of mannose 6-phosphate receptors. *EMBO J*. 19:2193-2203.

Miaczynska, M., S. Christoforidis, A. Giner, A. Shevchenko, S. Uttenweiler-Joseph, B. Habermann, M. Wilm, R.G. Parton, and M. Zerial. 2004. APPL proteins link Rab5 to nuclear signal transduction via an endosomal compartment. *Cell*. 116:445-456.

Mihov, D., E. Raja, and M. Spiess. 2015. Chondroitin Sulfate Accelerates Trans-Golgi-to-Surface Transport of Proteoglycan Amyloid Precursor Protein. *Traffic*. 16:853-870.

Mills, I.G., A.T. Jones, and M.J. Clague. 1999. Regulation of endosome fusion. *Mol Membr Biol*. 16:73-79.

Mishra, S.K., P.A. Keyel, M.J. Hawryluk, N.R. Agostinelli, S.C. Watkins, and L.M. Traub. 2002. Disabled-2 exhibits the properties of a cargo-selective endocytic clathrin adaptor. *The EMBO Journal*. 21:4915-4926.

Montanaro, L., S. Sperti, and F. Stirpe. 1973. Inhibition by ricin of protein synthesis in vitro. Ribosomes as the target of the toxin. *Biochem J*. 136:677-683.

Moren, B., C. Shah, M.T. Howes, N.L. Schieber, H.T. McMahon, R.G. Parton, O. Daumke, and R. Lundmark. 2012. EHD2 regulates caveolar dynamics via ATP-driven targeting and oligomerization. *Mol Biol Cell*. 23:1316-1329.

Mukadam, A.S., and M.N. Seaman. 2015. Retromer-mediated endosomal protein sorting: The role of unstructured domains. *FEBS Lett*. 589:2620-2626.

Mullins, C., and J.S. Bonifacino. 2001. The molecular machinery for lysosome biogenesis. *Bioessays*. 23:333-343.

Muyldermans, S. 2001. Single domain camel antibodies: current status. *J Biotechnol*. 74:277-302.

Muyldermans, S. 2013. Nanobodies: natural single-domain antibodies. *Annu Rev Biochem*. 82:775-797.

Muyldermans, S., T. Atarhouch, J. Saldanha, J.A. Barbosa, and R. Hamers. 1994. Sequence and structure of VH domain from naturally occurring camel heavy chain immunoglobulins lacking light chains. *Protein Eng*. 7:1129-1135.

N

Nair, P., B.E. Schaub, and J. Rohrer. 2003. Characterization of the endosomal sorting signal of the cation-dependent mannose 6-phosphate receptor. *J Biol Chem*. 278:24753-24758.

Nakada-Tsukui, K., Y. Saito-Nakano, V. Ali, and T. Nozaki. 2005. A retromerlike complex is a novel Rab7 effector that is involved in the transport of the virulence factor cysteine protease in the enteric protozoan parasite Entamoeba histolytica. *Mol Biol Cell*. 16:5294-5303.

Navarro Negredo, P., J.R. Edgar, A.G. Wrobel, N.R. Zaccai, R. Antrobus, D.J. Owen, and M.S. Robinson. 2017. Contribution of the clathrin adaptor AP-1 subunit micro1 to acidic cluster protein sorting. *J Cell Biol*.

Nedumpully-Govindan, P., L. Li, E.G. Alexov, M.A. Blenner, and F. Ding. 2014. Structural and energetic determinants of tyrosylprotein sulfotransferase sulfation specificity. *Bioinformatics*. 30:2302-2309.

Nelson, A.L. 2010. Antibody fragments: hope and hype. *MAbs*. 2:77-83.

Nielsen, M.S., C. Gustafsen, P. Madsen, J.R. Nyengaard, G. Hermey, O. Bakke, M. Mari, P. Schu, R. Pohlmann, A. Dennes, and C.M. Petersen. 2007. Sorting by the cytoplasmic domain of the amyloid precursor protein binding receptor SorLA. *Mol Cell Biol*. 27:6842-6851.

Nielsen, M.S., P. Madsen, E.I. Christensen, A. Nykjaer, J. Gliemann, D. Kasper, R. Pohlmann, and C.M. Petersen. 2001. The sortilin cytoplasmic tail conveys Golgi-endosome transport and binds the VHS domain of the GGA2 sorting protein. *EMBO J*. 20:2180-2190.

O

Ohno, H., J. Stewart, M.C. Fournier, H. Bosshart, I. Rhee, S. Miyatake, T. Saito, A. Gallusser, T. Kirchhausen, and J.S. Bonifacino. 1995. Interaction of tyrosine-based sorting signals with clathrin-associated proteins. *Science*. 269:1872-1875.

Olsnes, S., and A. Pihl. 1972. Ricin - a potent inhibitor of protein synthesis. *FEBS Lett*. 20:327-329.

Orsel, J.G., P.M. Sincock, J.P. Krise, and S.R. Pfeffer. 2000. Recognition of the 300-kDa mannose 6-phosphate receptor cytoplasmic domain by 47-kDa tail-interacting protein. *Proc Natl Acad Sci U S A*. 97:9047-9051.

Owen, D.J., B.M. Collins, and P.R. Evans. 2004. Adaptors for clathrin coats: structure and function. *Annual review of cell and developmental biology*. 20:153-191.

Owen, D.J., and P.R. Evans. 1998. A structural explanation for the recognition of tyrosine-based endocytotic signals. *Science*. 282:1327-1332.

P

Pagano, A., P. Crottet, C. Prescianotto-Baschong, and M. Spiess. 2004. In vitro formation of recycling vesicles from endosomes requires adaptor protein-1/clathrin and is regulated by rab4 and the connector rabaptin-5. *Molecular biology of the cell*. 15:4990-5000.

Pallesen, L.T., and C.B. Vaegter. 2012. Sortilin and SorLA regulate neuronal sorting of trophic and dementia-linked proteins. *Mol Neurobiol*. 45:379-387.

Parton, R.G., and M.A. del Pozo. 2013. Caveolae as plasma membrane sensors, protectors and organizers. *Nat Rev Mol Cell Biol*. 14:98-112.

Pavelka, M., J. Neumuller, and A. Ellinger. 2008. Retrograde traffic in the biosynthetic-secretory route. *Histochem Cell Biol*. 129:277-288.

Pearse, B.M. 1975. Coated vesicles from pig brain: purification and biochemical characterization. *Journal of Molecular Biology*. 97:93-98.

Pearse, B.M. 1976. Clathrin: a unique protein associated with intracellular transfer of membrane by coated vesicles. *Proceedings of the National Academy of Sciences of the United States of America*. 73:1255-1259.

Perrin, L., S. Lacas-Gervais, J. Gilleron, F. Ceppo, F. Prodon, A. Benmerah, J.F. Tanti, and M. Cormont. 2013. Rab4b controls an early endosome sorting event by interacting with the gamma-subunit of the clathrin adaptor complex 1. *J Cell Sci*. 126:4950-4962.

Petris, M.J., and J.F. Mercer. 1999. The Menkes protein (ATP7A; MNK) cycles via the plasma membrane both in basal and elevated extracellular copper using a C-terminal di-leucine endocytic signal. *Hum Mol Genet*. 8:2107-2115.

Pfeffer, S.R. 2009. Multiple routes of protein transport from endosomes to the trans Golgi network. *FEBS Lett*. 583:3811-3816.

Pfeffer, S.R. 2012. Cargo carriers from the Golgi to the cell surface. *EMBO J.* 31:3954-3955.

Phair, R.D., and T. Misteli. 2001. Kinetic modelling approaches to in vivo imaging. *Nat Rev Mol Cell Biol.* 2:898-907.

Plaut, R.D., and N.H. Carbonetti. 2008. Retrograde transport of pertussis toxin in the mammalian cell. *Cell Microbiol.* 10:1130-1139.

Pluckthun, A. 2015. Designed ankyrin repeat proteins (DARPins): binding proteins for research, diagnostics, and therapy. *Annu Rev Pharmacol Toxicol.* 55:489-511.

Pol, A., S.P. Gross, and R.G. Parton. 2014. Review: biogenesis of the multifunctional lipid droplet: lipids, proteins, and sites. *J Cell Biol.* 204:635-646.

Polishchuk, R., and S. Lutsenko. 2013. Golgi in copper homeostasis: a view from the membrane trafficking field. *Histochem Cell Biol.* 140:285-295.

Ponnambalam, S., M. Girotti, M.L. Yaspo, C.E. Owen, A.C. Perry, T. Suganuma, T. Nilsson, M. Fried, G. Banting, and G. Warren. 1996. Primate homologues of rat TGN38: primary structure, expression and functional implications. *Journal of cell science.* 109 (Pt 3):675-685.

Ponnambalam, S., C. Rabouille, J.P. Luzio, T. Nilsson, and G. Warren. 1994. The TGN38 glycoprotein contains two non-overlapping signals that mediate localization to the trans-Golgi network. *The Journal of cell biology.* 125:253-268.

Popoff, V., G.A. Mardones, S.K. Bai, V. Chambon, D. Tenza, P.V. Burgos, A. Shi, P. Benaroch, S. Urbe, C. Lamaze, B.D. Grant, G. Raposo, and L. Johannes. 2009. Analysis of articulation between clathrin and retromer in retrograde sorting on early endosomes. *Traffic.* 10:1868-1880.

Popoff, V., G.A. Mardones, D. Tenza, R. Rojas, C. Lamaze, J.S. Bonifacino, G. Raposo, and L. Johannes. 2007a. The retromer complex and clathrin define an early endosomal retrograde exit site. *Journal of cell science.* 120:2022-2031.

Popoff, V., G.A. Mardones, D. Tenza, R. Rojas, C. Lamaze, J.S. Bonifacino, G. Raposo, and L. Johannes. 2007b. The retromer complex and clathrin define an early endosomal retrograde exit site. *J Cell Sci.* 120:2022-2031.

Port, F., M. Kuster, P. Herr, E. Furger, C. Banziger, G. Hausmann, and K. Basler. 2008. Wingless secretion promotes and requires retromer-dependent cycling of Wntless. *Nat Cell Biol.* 10:178-185.

Poteryaev, D., S. Datta, K. Ackema, M. Zerial, and A. Spang. 2010. Identification of the switch in early-to-late endosome transition. *Cell.* 141:497-508.

Progida, C., L. Cogli, F. Piro, A. De Luca, O. Bakke, and C. Bucci. 2010. Rab7b controls trafficking from endosomes to the TGN. *J Cell Sci.* 123:1480-1491.

Progida, C., M.S. Nielsen, G. Koster, C. Bucci, and O. Bakke. 2012. Dynamics of Rab7b-dependent transport of sorting receptors. *Traffic.* 13:1273-1285.

Prydz, K., A.W. Brandli, M. Bomsel, and K. Simons. 1990. Surface distribution of the mannose 6-phosphate receptors in epithelial Madin-Darby canine kidney cells. *J Biol Chem.* 265:12629-12635.

Prydz, K., S.H. Hansen, K. Sandvig, and B. van Deurs. 1992. Effects of brefeldin A on endocytosis, transcytosis and transport to the Golgi complex in polarized MDCK cells. *J Cell Biol.* 119:259-272.

Pryor, P.R., L. Jackson, S.R. Gray, M.A. Edeling, A. Thompson, C.M. Sanderson, P.R. Evans, D.J. Owen, and J.P. Luzio. 2008. Molecular basis for the sorting of the SNARE VAMP7 into endocytic clathrin-coated vesicles by the ArfGAP Hrb. *Cell.* 134:817-827.

Puertollano, R., R.C. Aguilar, I. Gorshkova, R.J. Crouch, and J.S. Bonifacino. 2001. Sorting of mannose 6-phosphate receptors mediated by the GGAs. *Science*. 292:1712-1716.

Puertollano, R., N.N. van der Wel, L.E. Greene, E. Eisenberg, P.J. Peters, and J.S. Bonifacino. 2003. Morphology and dynamics of clathrin/GGA1-coated carriers budding from the trans-Golgi network. *Molecular biology of the cell*. 14:1545-1557.

R

Rader, C. 2009. Overview on concepts and applications of Fab antibody fragments. *Curr Protoc Protein Sci*. Chapter 6:Unit 6 9.

Radhakrishna, H., and J.G. Donaldson. 1997. ADP-ribosylation factor 6 regulates a novel plasma membrane recycling pathway. *J Cell Biol*. 139:49-61.

Rajasekaran, A.K., J.S. Humphrey, M. Wagner, G. Miesenbock, A. Le Bivic, J.S. Bonifacino, and E. Rodriguez-Boulan. 1994. TGN38 recycles basolaterally in polarized Madin-Darby canine kidney cells. *Molecular biology of the cell*. 5:1093-1103.

Rapak, A., P.O. Falnes, and S. Olsnes. 1997. Retrograde transport of mutant ricin to the endoplasmic reticulum with subsequent translocation to cytosol. *Proc Natl Acad Sci U S A*. 94:3783-3788.

Rapoport, I., W. Boll, A. Yu, T. Bocking, and T. Kirchhausen. 2008. A motif in the clathrin heavy chain required for the Hsc70/auxilin uncoating reaction. *Molecular biology of the cell*. 19:405-413.

Rea, S., and D.E. James. 1997. Moving GLUT4: the biogenesis and trafficking of GLUT4 storage vesicles. *Diabetes*. 46:1667-1677.

Reddy, J.V., A.S. Burguete, K. Sridevi, I.G. Ganley, R.M. Nottingham, and S.R. Pfeffer. 2006. A functional role for the GCC185 golgin in mannose 6-phosphate receptor recycling. *Mol Biol Cell*. 17:4353-4363.

Reider, A., S.L. Barker, S.K. Mishra, Y.J. Im, L. Maldonado-Baez, J.H. Hurley, L.M. Traub, and B. Wendland. 2009. Syp1 is a conserved endocytic adaptor that contains domains involved in cargo selection and membrane tubulation. *EMBO J*. 28:3103-3116.

Renard, H.F., M. Simunovic, J. Lemiere, E. Boucrot, M.D. Garcia-Castillo, S. Arumugam, V. Chambon, C. Lamaze, C. Wunder, A.K. Kenworthy, A.A. Schmidt, H.T. McMahon, C. Sykes, P. Bassereau, and L. Johannes. 2015. Endophilin-A2 functions in membrane scission in clathrin-independent endocytosis. *Nature*. 517:493-496.

Rhee, H.W., P. Zou, N.D. Udeshi, J.D. Martell, V.K. Mootha, S.A. Carr, and A.Y. Ting. 2013. Proteomic mapping of mitochondria in living cells via spatially restricted enzymatic tagging. *Science*. 339:1328-1331.

Riederer, M.A., T. Soldati, A.D. Shapiro, J. Lin, and S.R. Pfeffer. 1994. Lysosome biogenesis requires Rab9 function and receptor recycling from endosomes to the trans-Golgi network. *J Cell Biol*. 125:573-582.

Rink, J., E. Ghigo, Y. Kalaidzidis, and M. Zerial. 2005. Rab conversion as a mechanism of progression from early to late endosomes. *Cell*. 122:735-749.

Robinson, M.S. 2004. Adaptable adaptors for coated vesicles. *Trends in cell biology*. 14:167-174.

Robinson, M.S. 2015. Forty Years of Clathrin-coated Vesicles. *Traffic*. 16:1210-1238.

Robinson, M.S., and J. Hirst. 2013. Rapid inactivation of proteins by knocksideways. *Curr Protoc Cell Biol*. 61:15 20 11-17.

Robinson, M.S., D.A. Sahlender, and S.D. Foster. 2010. Rapid inactivation of proteins by rapamycin-induced rerouting to mitochondria. *Developmental cell*. 18:324-331.

Rojas, R., S. Kametaka, C.R. Haft, and J.S. Bonifacino. 2007a. Interchangeable but essential functions of SNX1 and SNX2 in the association of retromer with endosomes and the trafficking of mannose 6-phosphate receptors. *Mol Cell Biol*. 27:1112-1124.

Rojas, R., S. Kametaka, C.R. Haft, and J.S. Bonifacino. 2007b. Interchangeable but essential functions of SNX1 and SNX2 in the association of retromer with endosomes and the trafficking of mannose 6-phosphate receptors. *Mol Cell Biol*. 27:1112-1124.

Rojas, R., T. van Vlijmen, G.A. Mardones, Y. Prabhu, A.L. Rojas, S. Mohammed, A.J. Heck, G. Raposo, P. van der Sluijs, and J.S. Bonifacino. 2008. Regulation of retromer recruitment to endosomes by sequential action of Rab5 and Rab7. *J Cell Biol*. 183:513-526.

Rosenquist, G.L., and H.B. Nicholas, Jr. 1993. Analysis of sequence requirements for protein tyrosine sulfation. *Protein Sci*. 2:215-222.

Rosorius, O., G. Mieskes, O.G. Issinger, C. Korner, B. Schmidt, K. von Figura, and T. Braulke. 1993. Characterization of phosphorylation sites in the cytoplasmic domain of the 300 kDa mannose-6-phosphate receptor. *Biochem J*. 292 (Pt 3):833-838.

Rothbauer, U., K. Zolghadr, S. Muyldermans, A. Schepers, M.C. Cardoso, and H. Leonhardt. 2008. A versatile nanotrap for biochemical and functional studies with fluorescent fusion proteins. *Mol Cell Proteomics*. 7:282-289.

Rothbauer, U., K. Zolghadr, S. Tillib, D. Nowak, L. Schermelleh, A. Gahl, N. Backmann, K. Conrath, S. Muyldermans, M.C. Cardoso, and H. Leonhardt. 2006. Targeting and tracing antigens in live cells with fluorescent nanobodies. *Nat Methods*. 3:887-889.

Roux, A., K. Uyhazi, A. Frost, and P. De Camilli. 2006. GTP-dependent twisting of dynamin implicates constriction and tension in membrane fission. *Nature*. 441:528-531.

Roux, K.J. 2013. Marked by association: techniques for proximity-dependent labeling of proteins in eukaryotic cells. *Cell Mol Life Sci*. 70:3657-3664.

Roux, K.J., D.I. Kim, and B. Burke. 2013. BioID: a screen for protein-protein interactions. *Curr Protoc Protein Sci*. 74:Unit 19 23.

Roux, K.J., D.I. Kim, M. Raida, and B. Burke. 2012. A promiscuous biotin ligase fusion protein identifies proximal and interacting proteins in mammalian cells. *J Cell Biol*. 196:801-810.

S

Saavedra, L., A. Mohamed, V. Ma, S. Kar, and E.P. de Chaves. 2007. Internalization of beta-amyloid peptide by primary neurons in the absence of apolipoprotein E. *J Biol Chem*. 282:35722-35732.

Sabharanjak, S., P. Sharma, R.G. Parton, and S. Mayor. 2002. GPI-anchored proteins are delivered to recycling endosomes via a distinct cdc42-regulated, clathrin-independent pinocytic pathway. *Developmental cell*. 2:411-423.

Safaiyan, F., S.O. Kolset, K. Prydz, E. Gottfridsson, U. Lindahl, and M. Salmivirta. 1999. Selective effects of sodium chlorate treatment on the sulfation of heparan sulfate. *J Biol Chem*. 274:36267-36273.

Saftig, P., and J. Klumperman. 2009. Lysosome biogenesis and lysosomal membrane proteins: trafficking meets function. *Nature reviews. Molecular cell biology*. 10:623-635.

Saint-Pol, A., B. Yelamos, M. Amessou, I.G. Mills, M. Dugast, D. Tenza, P. Schu, C. Antony, H.T. McMahon, C. Lamaze, and L. Johannes. 2004. Clathrin adaptor epsinR is required for retrograde sorting on early endosomal membranes. *Developmental cell*. 6:525-538.

Salazar, G., S. Zlatic, B. Craige, A.A. Peden, J. Pohl, and V. Faundez. 2009. Hermansky-Pudlak syndrome protein complexes associate with phosphatidylinositol 4-kinase type II alpha in neuronal and non-neuronal cells. *J Biol Chem*. 284:1790-1802.

Sandvig, K., O. Garred, K. Prydz, J.V. Kozlov, S.H. Hansen, and B. van Deurs. 1992. Retrograde transport of endocytosed Shiga toxin to the endoplasmic reticulum. *Nature*. 358:510-512.

Sandvig, K., S. Olsnes, J.E. Brown, O.W. Petersen, and B. van Deurs. 1989. Endocytosis from coated pits of Shiga toxin: a glycolipid-binding protein from Shigella dysenteriae 1. *J Cell Biol*. 108:1331-1343.

Sandvig, K., and B. van Deurs. 1994. Endocytosis and intracellular sorting of ricin and Shiga toxin. *FEBS Lett*. 346:99-102.

Sandvig, K., and B. van Deurs. 1996. Endocytosis, intracellular transport, and cytotoxic action of Shiga toxin and ricin. *Physiol Rev*. 76:949-966.

Sandvig, K., and B. van Deurs. 2002. Membrane traffic exploited by protein toxins. *Annu Rev Cell Dev Biol*. 18:1-24.

Sandvig, K., and B. van Deurs. 2005. Delivery into cells: lessons learned from plant and bacterial toxins. *Gene Ther*. 12:865-872.

Scheele, U., C. Kalthoff, and E. Ungewickell. 2001. Multiple interactions of auxilin 1 with clathrin and the AP-2 adaptor complex. *The Journal of biological chemistry*. 276:36131-36138.

Schilling, J., J. Schoppe, and A. Pluckthun. 2014. From DARPins to LoopDARPins: novel LoopDARPin design allows the selection of low picomolar binders in a single round of ribosome display. *J Mol Biol*. 426:691-721.

Schmidt, B., C. Kiecke-Siemsen, A. Waheed, T. Braulke, and K. von Figura. 1995. Localization of the insulin-like growth factor II binding site to amino acids 1508-1566 in repeat 11 of the mannose 6-phosphate/insulin-like growth factor II receptor. *J Biol Chem*. 270:14975-14982.

Schmidt, V., A. Subkhangulova, and T.E. Willnow. 2017. Sorting receptor SORLA: cellular mechanisms and implications for disease. *Cell Mol Life Sci*. 74:1475-1483.

Schoneberg, J., I.H. Lee, J.H. Iwasa, and J.H. Hurley. 2017. Reverse-topology membrane scission by the ESCRT proteins. *Nat Rev Mol Cell Biol*. 18:5-17.

Schweizer, A., S. Kornfeld, and J. Rohrer. 1996. Cysteine34 of the cytoplasmic tail of the cation-dependent mannose 6-phosphate receptor is reversibly palmitoylated and required for normal trafficking and lysosomal enzyme sorting. *The Journal of cell biology*. 132:577-584.

Schweizer, A., S. Kornfeld, and J. Rohrer. 1997. Proper sorting of the cation-dependent mannose 6-phosphate receptor in endosomes depends on a pair of aromatic amino acids in its cytoplasmic tail. *Proc Natl Acad Sci U S A*. 94:14471-14476.

Scott, C.C., F. Vacca, and J. Gruenberg. 2014. Endosome maturation, transport and functions. *Semin Cell Dev Biol*. 31:2-10.

Seaman, M.N. 2004. Cargo-selective endosomal sorting for retrieval to the Golgi requires retromer. *J Cell Biol*. 165:111-122.

Seaman, M.N. 2007. Identification of a novel conserved sorting motif required for retromer-mediated endosome-to-TGN retrieval. *J Cell Sci*. 120:2378-2389.

Seaman, M.N. 2012. The retromer complex - endosomal protein recycling and beyond. *J Cell Sci*. 125:4693-4702.

Seaman, M.N., M.E. Harbour, D. Tattersall, E. Read, and N. Bright. 2009. Membrane recruitment of the cargo-selective retromer subcomplex is catalysed by the small GTPase Rab7 and inhibited by the Rab-GAP TBC1D5. *J Cell Sci.* 122:2371-2382.

Seaman, M.N., E.G. Marcusson, J.L. Cereghino, and S.D. Emr. 1997. Endosome to Golgi retrieval of the vacuolar protein sorting receptor, Vps10p, requires the function of the VPS29, VPS30, and VPS35 gene products. *J Cell Biol.* 137:79-92.

Seaman, M.N., J.M. McCaffery, and S.D. Emr. 1998. A membrane coat complex essential for endosome-to-Golgi retrograde transport in yeast. *J Cell Biol.* 142:665-681.

Seifert, W., Y. Posor, P. Schu, G. Stenbeck, S. Mundlos, S. Klaassen, P. Nurnberg, V. Haucke, U. Kornak, and J. Kuhnisch. 2016. The progressive ankylosis protein ANK facilitates clathrin- and adaptor-mediated membrane traffic at the trans-Golgi network-to-endosome interface. *Hum Mol Genet.* 25:3836-3848.

Seko, Y., T. Fujimura, T. Yao, H. Taka, R. Mineki, K. Okumura, and K. Murayama. 2015. Secreted tyrosine sulfated-eIF5A mediates oxidative stress-induced apoptosis. *Sci Rep.* 5:13737.

Shi, A., L. Sun, R. Banerjee, M. Tobin, Y. Zhang, and B.D. Grant. 2009. Regulation of endosomal clathrin and retromer-mediated endosome to Golgi retrograde transport by the J-domain protein RME-8. *The EMBO Journal.* 28:3290-3302.

Shi, G., M. Azoulay, F. Dingli, C. Lamaze, D. Loew, J.C. Florent, and L. Johannes. 2012a. SNAP-tag Based Proteomics Approach for the Study of the Retrograde Route. *Traffic.*

Shi, G., M. Azoulay, F. Dingli, C. Lamaze, D. Loew, J.C. Florent, and L. Johannes. 2012b. SNAP-tag based proteomics approach for the study of the retrograde route. *Traffic.* 13:914-925.

Shi, J., and K.V. Kandror. 2005. Sortilin is essential and sufficient for the formation of Glut4 storage vesicles in 3T3-L1 adipocytes. *Dev Cell.* 9:99-108.

Shiba, Y., W. Romer, G.A. Mardones, P.V. Burgos, C. Lamaze, and L. Johannes. 2010. AGAP2 regulates retrograde transport between early endosomes and the TGN. *J Cell Sci.* 123:2381-2390.

Shimobayashi, M., and M.N. Hall. 2016. Multiple amino acid sensing inputs to mTORC1. *Cell Res.* 26:7-20.

Sigismund, S., V. Algisi, G. Nappo, A. Conte, R. Pascolutti, A. Cuomo, T. Bonaldi, E. Argenzio, L.G. Verhoef, E. Maspero, F. Bianchi, F. Capuani, A. Ciliberto, S. Polo, and P.P. Di Fiore. 2013. Threshold-controlled ubiquitination of the EGFR directs receptor fate. *EMBO J.* 32:2140-2157.

Sigismund, S., E. Argenzio, D. Tosoni, E. Cavallaro, S. Polo, and P.P. Di Fiore. 2008. Clathrin-mediated internalization is essential for sustained EGFR signaling but dispensable for degradation. *Developmental cell.* 15:209-219.

Sigismund, S., T. Woelk, C. Puri, E. Maspero, C. Tacchetti, P. Transidico, P.P. Di Fiore, and S. Polo. 2005. Clathrin-independent endocytosis of ubiquitinated cargos. *Proc Natl Acad Sci U S A.* 102:2760-2765.

Sincock, P.M., I.G. Ganley, J.P. Krise, S. Diederichs, U. Sivars, B. O'Connor, L. Ding, and S.R. Pfeffer. 2003. Self-assembly is important for TIP47 function in mannose 6-phosphate receptor transport. *Traffic.* 4:18-25.

Skrlec, K., B. Strukelj, and A. Berlec. 2015. Non-immunoglobulin scaffolds: a focus on their targets. *Trends Biotechnol.* 33:408-418.

Smith, J.S., and S. Rajagopal. 2016. The beta-Arrestins: Multifunctional Regulators of G Protein-coupled Receptors. *J Biol Chem.* 291:8969-8977.

Snider, M.D., and O.C. Rogers. 1985. Intracellular movement of cell surface receptors after endocytosis: resialylation of asialo-transferrin receptor in human erythroleukemia cells. *J Cell Biol.* 100:826-834.

Soldati, T., M.A. Riederer, and S.R. Pfeffer. 1993. Rab GDI: a solubilizing and recycling factor for rab9 protein. *Mol Biol Cell*. 4:425-434.

Sorkin, A., and M. von Zastrow. 2009. Endocytosis and signalling: intertwining molecular networks. *Nat Rev Mol Cell Biol*. 10:609-622.

Stahlschmidt, W., M.J. Robertson, P.J. Robinson, A. McCluskey, and V. Haucke. 2014. Clathrin terminal domain-ligand interactions regulate sorting of mannose 6-phosphate receptors mediated by AP-1 and GGA adaptors. *The Journal of biological chemistry*. 289:4906-4918.

Staudt, C., E. Puissant, and M. Boonen. 2016. Subcellular Trafficking of Mammalian Lysosomal Proteins: An Extended View. *Int J Mol Sci*. 18.

Steinberg, F., M. Gallon, M. Winfield, E.C. Thomas, A.J. Bell, K.J. Heesom, J.M. Tavare, and P.J. Cullen. 2013. A global analysis of SNX27-retromer assembly and cargo specificity reveals a function in glucose and metal ion transport. *Nat Cell Biol*. 15:461-471.

Stenmark, H. 2009. Rab GTPases as coordinators of vesicle traffic. *Nature reviews. Molecular cell biology*. 10:513-525.

Stenmark, H., and V.M. Olkkonen. 2001. The Rab GTPase family. *Genome Biol*. 2:REVIEWS3007.

Stenmark, H., G. Vitale, O. Ullrich, and M. Zerial. 1995. Rabaptin-5 is a direct effector of the small GTPase Rab5 in endocytic membrane fusion. *Cell*. 83:423-432.

Stettler, H., N. Beuret, C. Prescianotto-Baschong, B. Fayard, L. Taupenot, and M. Spiess. 2009. Determinants for chromogranin A sorting into the regulated secretory pathway are also sufficient to generate granule-like structures in non-endocrine cells. *Biochem J*. 418:81-91.

Stimpson, H.E., C.P. Toret, A.T. Cheng, B.S. Pauly, and D.G. Drubin. 2009. Early-arriving Syp1p and Ede1p function in endocytic site placement and formation in budding yeast. *Mol Biol Cell*. 20:4640-4651.

Stockli, J., D.J. Fazakerley, and D.E. James. 2011. GLUT4 exocytosis. *J Cell Sci*. 124:4147-4159.

Stoeber, M., I.K. Stoeck, C. Hanni, C.K. Bleck, G. Balistreri, and A. Helenius. 2012. Oligomers of the ATPase EHD2 confine caveolae to the plasma membrane through association with actin. *EMBO J*. 31:2350-2364.

Stone, M.J., S. Chuang, X. Hou, M. Shoham, and J.Z. Zhu. 2009. Tyrosine sulfation: an increasingly recognised post-translational modification of secreted proteins. *New biotechnology*. 25:299-317.

Stoorvogel, W. 1998. Analysis of the endocytic system by using horseradish peroxidase. *Trends in cell biology*. 8:503-505.

Stoorvogel, W. 2008. Analyzing endosomes in nonsectioned cells by transmission electron microscopy. *Methods Mol Biol*. 440:247-257.

Stoorvogel, W., H.J. Geuze, J.M. Griffith, A.L. Schwartz, and G.J. Strous. 1989. Relations between the intracellular pathways of the receptors for transferrin, asialoglycoprotein, and mannose 6-phosphate in human hepatoma cells. *J Cell Biol*. 108:2137-2148.

Stoorvogel, W., H.J. Geuze, J.M. Griffith, and G.J. Strous. 1988. The pathways of endocytosed transferrin and secretory protein are connected in the trans-Golgi reticulum. *J Cell Biol*. 106:1821-1829.

Stoorvogel, W., H.J. Geuze, and G.J. Strous. 1987. Sorting of endocytosed transferrin and asialoglycoprotein occurs immediately after internalization in HepG2 cells. *J Cell Biol*. 104:1261-1268.

Stoorvogel, W., G.J. Strous, H.J. Geuze, V. Oorschot, and A.L. Schwartz. 1991. Late endosomes derive from early endosomes by maturation. *Cell*. 65:417-427.

Stowell, M.H., B. Marks, P. Wigge, and H.T. McMahon. 1999. Nucleotide-dependent conformational changes in dynamin: evidence for a mechanochemical molecular spring. *Nat Cell Biol.* 1:27-32.

Strochlic, T.I., T.G. Setty, A. Sitaram, and C.G. Burd. 2007. Grd19/Snx3p functions as a cargo-specific adapter for retromer-dependent endocytic recycling. *J Cell Biol.* 177:115-125.

Sudhof, T.C., and J. Rizo. 2011. Synaptic vesicle exocytosis. *Cold Spring Harb Perspect Biol.* 3.

Sundborger, A., C. Soderblom, O. Vorontsova, E. Evergren, J.E. Hinshaw, and O. Shupliakov. 2011. An endophilin-dynamin complex promotes budding of clathrin-coated vesicles during synaptic vesicle recycling. *Journal of cell science.* 124:133-143.

Sweitzer, S.M., and J.E. Hinshaw. 1998. Dynamin undergoes a GTP-dependent conformational change causing vesiculation. *Cell.* 93:1021-1029.

T

Tabuchi, M., N. Tanaka, J. Nishida-Kitayama, H. Ohno, and F. Kishi. 2002. Alternative splicing regulates the subcellular localization of divalent metal transporter 1 isoforms. *Mol Biol Cell.* 13:4371-4387.

Tabuchi, M., I. Yanatori, Y. Kawai, and F. Kishi. 2010. Retromer-mediated direct sorting is required for proper endosomal recycling of the mammalian iron transporter DMT1. *J Cell Sci.* 123:756-766.

Taguchi, T. 2013. Emerging roles of recycling endosomes. *J Biochem.* 153:505-510.

Takatsu, H., M. Sakurai, H.W. Shin, K. Murakami, and K. Nakayama. 1998. Identification and characterization of novel clathrin adaptor-related proteins. *J Biol Chem*. 273:24693-24700.

Tam, J.H., and S.H. Pasternak. 2015. Imaging the Intracellular Trafficking of APP with Photoactivatable GFP. *J Vis Exp*:e53153.

Tam, J.H., C. Seah, and S.H. Pasternak. 2014. The Amyloid Precursor Protein is rapidly transported from the Golgi apparatus to the lysosome and where it is processed into beta-amyloid. *Mol Brain*. 7:54.

Taylor, M.J., D. Perrais, and C.J. Merrifield. 2011. A high precision survey of the molecular dynamics of mammalian clathrin-mediated endocytosis. *PLoS Biol.* 9:e1000604.

Tcatchoff, L., S. Andersson, A. Utskarpen, T.I. Klokk, S.S. Skanland, S. Pust, V. Gerke, and K. Sandvig. 2012. Annexin A1 and A2: roles in retrograde trafficking of Shiga toxin. *PLoS One*. 7:e40429.

Teasdale, R.D., and B.M. Collins. 2012. Insights into the PX (phox-homology) domain and SNX (sorting nexin) protein families: structures, functions and roles in disease. *Biochem J.* 441:39-59.

Temkin, P., B. Lauffer, S. Jager, P. Cimermancic, N.J. Krogan, and M. von Zastrow. 2011. SNX27 mediates retromer tubule entry and endosome-to-plasma membrane trafficking of signalling receptors. *Nat Cell Biol.* 13:715-721.

Theos, A.C., D. Tenza, J.A. Martina, I. Hurbain, A.A. Peden, E.V. Sviderskaya, A. Stewart, M.S. Robinson, D.C. Bennett, D.F. Cutler, J.S. Bonifacino, M.S. Marks, and G. Raposo. 2005. Functions of adaptor protein (AP)-3 and AP-1 in tyrosinase sorting from endosomes to melanosomes. *Mol Biol Cell.* 16:5356-5372.

Traub, L.M., and J.S. Bonifacino. 2013. Cargo recognition in clathrin-mediated endocytosis. *Cold Spring Harbor perspectives in biology*. 5.

Trischler, M., W. Stoorvogel, and O. Ullrich. 1999. Biochemical analysis of distinct Rab5- and Rab11-positive endosomes along the transferrin pathway. *J Cell Sci.* 112 (Pt 24):4773-4783.

Trousdale, C., and K. Kim. 2015. Retromer: Structure, function, and roles in mammalian disease. *Eur J Cell Biol*. 94:513-521.

Truttmann, M.C., Q. Wu, S. Stiegeler, J.N. Duarte, J. Ingram, and H.L. Ploegh. 2015. HypE-specific nanobodies as tools to modulate HypE-mediated target AMPylation. *J Biol Chem*. 290:9087-9100.

U

Uchida, Y., J. Hasegawa, D. Chinnapen, T. Inoue, S. Okazaki, R. Kato, S. Wakatsuki, R. Misaki, M. Koike, Y. Uchiyama, S. Iemura, T. Natsume, R. Kuwahara, T. Nakagawa, K. Nishikawa, K. Mukai, E. Miyoshi, N. Taniguchi, D. Sheff, W.I. Lencer, T. Taguchi, and H. Arai. 2011. Intracellular phosphatidylserine is essential for retrograde membrane traffic through endosomes. *Proc Natl Acad Sci U S A*. 108:15846-15851.

Umasankar, P.K., L. Ma, J.R. Thieman, A. Jha, B. Doray, S.C. Watkins, and L.M. Traub. 2014. A clathrin coat assembly role for the muniscin protein central linker revealed by TALEN-mediated gene editing. *Elife*. 3.

Ungewickell, E., H. Ungewickell, S.E. Holstein, R. Lindner, K. Prasad, W. Barouch, B. Martin, L.E. Greene, and E. Eisenberg. 1995. Role of auxilin in uncoating clathrin-coated vesicles. *Nature*. 378:632-635.

Utskarpen, A., H.H. Slagsvold, T.G. Iversen, S. Walchli, and K. Sandvig. 2006. Transport of ricin from endosomes to the Golgi apparatus is regulated by Rab6A and Rab6A'. *Traffic*. 7:663-672.

V

van Dam, E.M., T. Ten Broeke, K. Jansen, P. Spijkers, and W. Stoorvogel. 2002. Endocytosed transferrin receptors recycle via distinct dynamin and phosphatidylinositol 3-kinase-dependent pathways. *The Journal of biological chemistry*. 277:48876-48883.

van der Sluijs, P., M. Hull, P. Webster, P. Male, B. Goud, and I. Mellman. 1992. The small GTP-binding protein rab4 controls an early sorting event on the endocytic pathway. *Cell*. 70:729-740.

van Deurs, B., T.I. Tonnessen, O.W. Petersen, K. Sandvig, and S. Olsnes. 1986. Routing of internalized ricin and ricin conjugates to the Golgi complex. *J Cell Biol*. 102:37-47.

van Meel, E., and J. Klumperman. 2008. Imaging and imagination: understanding the endo-lysosomal system. *Histochem Cell Biol*. 129:253-266.

van Meel, E., and J. Klumperman. 2014. TGN exit of the cation-independent mannose 6-phosphate receptor does not require acid hydrolase binding. *Cell Logist*. 4:e954441.

van Rahden, V.A., K. Brand, J. Najm, J. Heeren, S.R. Pfeffer, T. Braulke, and K. Kutsche. 2012. The 5-phosphatase OCRL mediates retrograde transport of the mannose 6-phosphate receptor by regulating a Rac1-cofilin signalling module. *Hum Mol Genet*. 21:5019-5038.

van Weering, J.R., R.B. Sessions, C.J. Traer, D.P. Kloer, V.K. Bhatia, D. Stamou, S.R. Carlsson, J.H. Hurley, and P.J. Cullen. 2012. Molecular basis for SNX-BAR-mediated assembly of distinct endosomal sorting tubules. *EMBO J*. 31:4466-4480.

Varlamov, O., and L.D. Fricker. 1998. Intracellular trafficking of metallocarboxypeptidase D in AtT-20 cells: localization to the trans-Golgi network and recycling from the cell surface. *J Cell Sci*. 111 (Pt 7):877-885.

Visintin, M., E. Tse, H. Axelson, T.H. Rabbitts, and A. Cattaneo. 1999. Selection of antibodies for intracellular function using a two-hybrid in vivo system. *Proc Natl Acad Sci U S A*. 96:11723-11728.

W

Waguri, S., F. Dewitte, R. Le Borgne, Y. Rouille, Y. Uchiyama, J.F. Dubremetz, and B. Hoflack. 2003. Visualization of TGN to endosome trafficking through fluorescently labeled MPR and AP-1 in living cells. *Mol Biol Cell*. 14:142-155.

Wahle, T., K. Prager, N. Raffler, C. Haass, M. Famulok, and J. Walter. 2005. GGA proteins regulate retrograde transport of BACE1 from endosomes to the trans-Golgi network. *Mol Cell Neurosci*. 29:453-461.

Wakana, Y., R. Kotake, N. Oyama, M. Murate, T. Kobayashi, K. Arasaki, H. Inoue, and M. Tagaya. 2015. CARTS biogenesis requires VAP-lipid transfer protein complexes functioning at the endoplasmic reticulum-Golgi interface. *Mol Biol Cell*. 26:4686-4699.

Wakana, Y., J. van Galen, F. Meissner, M. Scarpa, R.S. Polishchuk, M. Mann, and V. Malhotra. 2012. A new class of carriers that transport selective cargo from the trans Golgi network to the cell surface. *The EMBO Journal*. 31:3976-3990.

Wakana, Y., J. Villeneuve, J. van Galen, D. Cruz-Garcia, M. Tagaya, and V. Malhotra. 2013. Kinesin-5/Eg5 is important for transport of CARTS from the trans-Golgi network to the cell surface. *The Journal of cell biology*.

Wandinger-Ness, A., and M. Zerial. 2014. Rab proteins and the compartmentalization of the endosomal system. *Cold Spring Harb Perspect Biol*. 6:a022616.

Wartosch, L., N.A. Bright, and J.P. Luzio. 2015. Lysosomes. *Curr Biol*. 25:R315-316.

Wassmer, T., N. Attar, M.V. Bujny, J. Oakley, C.J. Traer, and P.J. Cullen. 2007. A loss-of-function screen reveals SNX5 and SNX6 as potential components of the mammalian retromer. *Journal of cell science*. 120:45-54.

Watanabe, S., and E. Boucrot. 2017. Fast and ultrafast endocytosis. *Curr Opin Cell Biol*. 47:64-71.

Wauben-Penris, P.J., G.J. Strous, and H.A. van der Donk. 1988. Kinetics of transferrin endocytosis and iron uptake by intact isolated rat seminiferous tubules and Sertoli cells in culture. *Biol Reprod*. 38:853-861.

Wigge, P., K. Kohler, Y. Vallis, C.A. Doyle, D. Owen, S.P. Hunt, and H.T. McMahon. 1997. Amphiphysin heterodimers: potential role in clathrin-mediated endocytosis. *Molecular biology of the cell*. 8:2003-2015.

Wilfling, F., J.T. Haas, T.C. Walther, and R.V. Farese, Jr. 2014. Lipid droplet biogenesis. *Curr Opin Cell Biol*. 29:39-45.

Willett, R., I. Pokrovskaya, T. Kudlyk, and V. Lupashin. 2014. Multipronged interaction of the COG complex with intracellular membranes. *Cell Logist*. 4:e27888.

Willnow, T.E., and O.M. Andersen. 2013. Sorting receptor SORLA--a trafficking path to avoid Alzheimer disease. *J Cell Sci*. 126:2751-2760.

Willox, A.K., and S.J. Royle. 2012. Stonin 2 is a major adaptor protein for clathrin-mediated synaptic vesicle retrieval. *Curr Biol*. 22:1435-1439.

Wolins, N.E., B. Rubin, and D.L. Brasaemle. 2001. TIP47 associates with lipid droplets. *J Biol Chem*. 276:5101-5108.

X

Xing, Y., T. Bocking, M. Wolf, N. Grigorieff, T. Kirchhausen, and S.C. Harrison. 2010. Structure of clathrin coat with bound Hsc70 and auxilin: mechanism of Hsc70-facilitated disassembly. *The EMBO Journal*. 29:655-665.

Y

Yang, Z.R. 2009. Predicting sulfotyrosine sites using the random forest algorithm with significantly improved prediction accuracy. *BMC Bioinformatics*. 10:361.

Yu, A., J.F. Rual, K. Tamai, Y. Harada, M. Vidal, X. He, and T. Kirchhausen. 2007. Association of Dishevelled with the clathrin AP-2 adaptor is required for Frizzled endocytosis and planar cell polarity signaling. *Developmental cell*. 12:129-141.

Yu, J., J. Chia, C.A. Canning, C.M. Jones, F.A. Bard, and D.M. Virshup. 2014. WLS retrograde transport to the endoplasmic reticulum during Wnt secretion. *Dev Cell*. 29:277-291.

Yu, J.W., and M.A. Lemmon. 2001. All phox homology (PX) domains from Saccharomyces cerevisiae specifically recognize phosphatidylinositol 3-phosphate. *J Biol Chem*. 276:44179-44184.

Z

Zerial, M., and H. McBride. 2001. Rab proteins as membrane organizers. *Nat Rev Mol Cell Biol*. 2:107-117.

Zhang, P., Y. Wu, T.Y. Belenkaya, and X. Lin. 2011. SNX3 controls Wingless/Wnt secretion through regulating retromer-dependent recycling of Wntless. *Cell Res*. 21:1677-1690.

Zhen, Y., and H. Stenmark. 2015. Cellular functions of Rab GTPases at a glance. *J Cell Sci*. 128:3171-3176.

Zhou, W., B.P. Duckworth, and R.J. Geraghty. 2014. Fluorescent peptide sensors for tyrosylprotein sulfotransferase activity. *Anal Biochem*. 461:1-6.

Zimmerberg, J., and S. McLaughlin. 2004. Membrane curvature: how BAR domains bend bilayers. *Curr Biol*. 14:R250-252.

Zimmermann, M., R. Cal, E. Janett, V. Hoffmann, C.G. Bochet, E. Constable, F. Beaufils, and M.P. Wymann. 2014. Cell-permeant and photocleavable chemical inducer of dimerization. *Angew Chem Int Ed Engl*. 53:4717-4720.

Zizioli, D., E. Forlanelli, M. Guarienti, S. Nicoli, A. Fanzani, R. Bresciani, G. Borsani, A. Preti, F. Cotelli, and P. Schu. 2010. Characterization of the AP-1 mu1A and mu1B adaptins in zebrafish (Danio rerio). *Dev Dyn*. 239:2404-2412.

Zizioli, D., C. Geumann, M. Kratzke, R. Mishra, G. Borsani, D. Finazzi, E. Candiello, and P. Schu. 2017. gamma2 and gamma1AP-1 complexes: Different essential functions and regulatory mechanisms in clathrin-dependent protein sorting. *Eur J Cell Biol*. 96:356-368.

Zizioli, D., C. Meyer, G. Guhde, P. Saftig, K. von Figura, and P. Schu. 1999. Early embryonic death of mice deficient in gamma-adaptin. *J Biol Chem*. 274:5385-5390.

List of Abbreviations

A

ADP	Adenosine diphosphate
AMPA	α-amino-3-hydroxy-5-methyl-4-isoxazolepropionic acid
ANTH	AP180 N-terminal homology domain
ANK	Progressive ankylosis protein
AP-1, -2, -3, -4, -5	Adaptor protein complex-1, -2, -3, -4, -5
APP	Amyloid precursor protein
APEX	Ascorbate peroxidase
APP	Amyloid precursor protein
AR	Ankyrin repeat
ARF	ADP-ribosylation factor
ARH	Autosomal recessive hypercholesterolemia
ASGPR	Asialoglycoprotein receptor
ATP	Adenosine trisphosphate
ATP7A/B	ATPase copper transporting type A/B

B

BACE	β site APP cleavage enzyme
BAP	Biotin acceptor peptide
BAR	Bin/Amphiphysin/Rvs
β_2AR	β_2 adrenergic receptor
BCA	Bicinchoninic acid
BFA	Brefeldin A
BG	Benzylguanine
BSA	Bovine serum albumin

C

CARTS	Carriers of the TGN to the cell surface
Cas9	CRISPR-associated protein 9
CAV1/2	Caveolin-1/2
CCP	Clathrin-coated pit
CCV	Clathrin-coated vesicles
CDE	Clathrin-dependent endocytosis
CDR	Complementarity-determining regions

CDMPR	Cation-dependent mannose-6-phosphate receptor
CHC	Clathrin heavy chain
CIE	Clathrin-independent endocytosis
CIMPR	Cation-independent mannose-6-phosphate receptor
CLC	Clathrin light chain
CLIC	Clathrin-independent carriers
CLINT	clathrin interactor 1
CME	Clathrin-mediated endocytosis
CNX	Calnexin
COG	Conserved oligomeric complex
COPI and II	Coatomer protein I and II
COX IV	cytochrome C oxidase IV
CPY	Carboxypeptidase Y
CRISPR	Clustered regularly interspaced short palindromic repeats
CSC	Cargo selective complex
CRC	Cargo recognition complex

D

DAB	3,3'-Diaminobenzidine
Dab2	Disabled homolog 2
DAPI	4',6-Diamidino-2-phenylindole
DARPins	Designed ankyrin repeat proteins
DMSO	Dimethyl sulfoxide
DMT1	Divalent metal ion transporter 1
DTT	Dithiothreitol

E

EE	Early endosome
EEA1	Early endosomal antigen 1
EGF	Epidermal growth factor
EGFP	Enhanced green fluorescent protein
EGFR	Epidermal growth factor receptor
EM	Electron microscopy
ENTH	Epsin N-terminal homology domain
EPS15	Epidermal growth factor receptor (EGFR) pathway substrate 15
ER	Endoplasmic reticulum
ERGIC	ER-Golgi intermediate compartment
ESCRT	Endosomal sorting complex required for transport

F

F_{ab}	Antigen-binding fragments
FACS	Fluorescence-activated cell sorting
FCH	Fer/Cip4 homology domain
FCHO	Fer/Cip4 homology domain-only
FEME	Fast endophilin-mediated endocytosis
FIC	Filamentation induced by cAMP
FKBP12	FK506-binding protein of 12 kDa
FR	Framework regions
FRB	FKBP-rapamycin binding

G

GAK	Cyclin G-associated kinase
GalT	β-1,4-galactosyltransferase
GAPDH	Glyceraldehyde 3-phosphate dehydrogenase
GCC185	Golgi coiled-coil protein of 185 kDa
GDP	Guanosine diphosphate
GEEC	GPI-AP enriched endocytic compartments
GEF	Guanine nucleotide exchange factor
GET	Guided entry of tail-anchored proteins
GFP	Green fluorescent protein
GGA	Golgi-localized, γ-ear-containing, ARF-binding protein
GLUT	Glucose transporter
GPCR	G-protein coupled receptor
GPI-AP	Glycosylphosphatidylinositol-anchored protein
GSC	GLUT4 storage compartments
GTP	Guanosine trisphosphate

H

H1	Homologous polypeptide 1 of ASGPR
HA	Hemagglutinin
hcAb	Homodimeric heavy chain antibodies
HRB	HIV Rev-binding protein (HRB)
HRP	Horseradish peroxidase
Hsc70	Heat shock cognate 70
Hsp	Heat shock protein
Hrs	Hepatocyte growth factor-regulated tyrosine kinase substrate

K

k_{app}	Apparent rate constant
KD	Knockdown
KO	Knockout
KS	Knocksideways

I

IF	Immunofluorescence
IgG	Immunoglobulin G
IgNAR	Immunoglobulin new antigen receptor
IL-2	Interleukin-2
IL-2R	Interleukin-2 receptor
ILV	Intraluminal vesicles
IPTG	Isopropyl-β-D-thiogalactopyranosid

L

LAMP-1	Lysosome-associated membrane protein-1
LDL	Low-density lipoprotein
LDLR	Low-density lipoprotein receptor
LMP	Lysosomal membrane proteins

M

ManII	α-mannosidase II
MBP	Maltose-binding protein
MPR/M6PR	Mannose-6-phosphate receptor
MTCO2	Mitochondrially encoded cytochrome C oxidase II
MVB	Multivesicular bodies
MW	Molecular weight

N

NAE	Nuclear envelope-associated endosomes
NLS	Nuclear localization signal
NMDA	N-methyl-D-aspartate

P

PAPS	3'-Phosphoadenosine-5'-phosphosulfate
PAPST	3'-Phosphoadenosine-5'-phosphosulfate transporter
PBS	Phosphate-buffered saline
PE	Pseudomonas exotoxin A
PIC	Protease inhibitor cocktail
PIP	Phosphatidylinositol phosphate
PI(3)P	Phosphatidylinositol-3-phosphate
PI(3,5)P	Phosphatidylinositol-(3,5)-bisphosphate
PI(4)P	Phosphatidylinositol-4-phosphate
PI(4,5)P	Phosphatidylinositol-(4,5)-bisphosphate
PLIN-3	Perlipin-3
PM	Plasma membrane
PMSF	Phenylmethylsulfonyl fluoride
PP_i	Pyrophosphate
POI	Protein of interest
PTM	Posttranslational modification
PX	Phagocytic oxidase (phox) homology domain

R

Rab	Ras-related proteins in/from rat brain
RME-8	Required for receptor-mediated endocytosis 8 protein
RNAi	RNA interference
ROI	Region of interest
RT	Room temperature

S

SA	Streptavidin
SAP	Sphingolipid activator proteins
scFV	Single-chain variable fragment
SD	Standard deviation
sdAb	Single-domain antibody
SDS-PAGE	Sodium dodecyl sulfate polyacrylamide gel electrophoresis
sgRNA	Single guide RNA
shGalT	Short version of β-1,4-galactosyltransferase
SiaT	α-2,6-sialyltransferase
SNARE	Soluble N-ethylmaleimide-sensitive factor attachment receptor

SNX	Sorting nexin
SLC	Solute carrier family
SorLA	Sortilin-related receptor with LDLR class A repeats
STX	Syntaxin
STxB	Shiga toxin subunit B

T

T	Time of steady-state (total cell)
TBS	Tris buffered saline
TEN	Tubular endosomal network
TEV	Tobacco etch virus
Tf	Transferrin
TfR	Transferrin receptor
TGN	Trans-Golgi network
TIRF	Total internal reflection fluorescence
TIP47	Tail-interacting protein 47
TOR	Target of rapamycin
TPST	Tyrosylprotein sulfotransferase
TS	Tyrosine sulfation
$\tau_{1/2}$	Half-life of steady-state (total cell)

V

VHH	Variable homodimeric heavy-chain antibody
VHH_{GFP}	Anti-GFP nanobody
VHH_{mCh}	Anti-mCherry nanobody
Vps	Vacuolar protein sorting protein
vti1a	Vesicular transport through interaction with t-SNAREs homolog 1a
vti1b	Vesicular transport through interaction with t-SNAREs homolog 1b
VTN	Vesicular tubular network

W

WB	Western blotting
WGA	Wheat germ agglutinin
WLS	Wntless

Curriculum Vitae

Name: Dominik Pascal Buser
Place of birth: Basel
Date of birth: September 25, 1988
Current address: Baselmattweg 135, 4123 Allschwil
Native place: Zunzgen (BL)
Phone number: 0041 79 701 23 81
E-mail: Dominik-Pascal.Buser@unibas.ch or dominik.p.buser@gmail.com
Nationality: Swiss citizenship
Martial status: Single

Education and Training

Primary school	August 1995 to June 2000 in Lampenberg (BL)
Secondary school	August 2000 to June 2002 (Niveau E) in Oberdorf (BL) August 2002 to June 2004 (Niveau P) in Oberdorf (BL)
High school	August 2004 to December 2007 (Gymnasium) in Liestal (BL) Main subject: Economies and Laws
University	September 2008 to June 2011 in Basel, Biozentrum, University of Basel Degree: Bachelor of Science (B.Sc.) in Biology, Major in Molecular Biology
	August 2011 to January 2013 in Basel, Biozentrum, University of Basel Degree: Master of Science (M.Sc.) in Molecular Biology
	June 2013 to September 2017 in Basel, Biozentrum, University of Basel To date: PhD student in Biochemistry

Fellowships and Awards

Matura award	Matura award (Baselbieter Maturapreis 2007) for educational performance with regard to the final mark. Students are awarded if their average grade (according to the Swiss grade system) is > 5.3 (at Gymnasium Liestal)
FFE	International Fellowship for Excellence (PhD program) at the Biozentrum, University of Basel (2012). FFEs are yearly awarded to talented, qualified, ambitious and highly motivated students in Life Sciences for a period of three years (at University of Basel, Biozentrum)
Talk price	Best talk (1st) at the 7th Biozentrum PhD Retreat in Saas-Fee (2015). Title: Knock, knock, knock - Rapid inactivation of target proteins using knock-sideways (at University of Basel, Biozentrum)
Talk price	Third best talk (3rd) at the 9th Biozentrum PhD Retreat in Martigny (2017). Title: A versatile nanobody-based approach to analyze retrograde transport from the cell surface (at University of Basel, Biozentrum)

Research Experience

Aug. 2011 – Jan. 2013	Master student in the laboratory of Prof. Dr. Martin Spiess Biozentrum, University of Basel Master thesis title: Effect of glycosaminoglycan chains on protein transport and sorting
Feb. 2013 – Mar 2013	Rotational doctoral student in the laboratory of Prof. Dr. Christoph Dehio Biozentrum, University of Basel Project title: Investigation of Bartonella effector protein (Beps) conferring FIC domain-mediated AMPylation
Apr. 2013 – May 2013	Rotational doctoral student in the laboratory of Prof. Dr. Peter Scheiffele Biozentrum, University of Basel Project title: Phosphotyrosine-dependent interaction of neurexins with PDZ proteins and PTPs
June. 2013 – today	Doctoral student in the laboratory of Prof. Dr. Martin Spiess Biozentrum, University of Basel Project title: A versatile nanobody-based toolset to analyze retrograde transport from the cell surface

Posters and Talk Presentations

BZ Symposium 2013	Poster presentation. Title: Got a ticket for the TGV from the TGN? The effect of glycosaminoglycan chains on protein transport and sorting. Biozentrum Symposium 2013 at St. Chrischona
PhD Retreat 2013	Poster presentation. Title: Investigation of proteoglycan traffic in the late secretory pathway. 6th PhD Retreat in Interlaken
Conference 2014	Poster presentation. Title: Investigation of proteoglycan traffic in the late secretory pathway. BSCB conference 'The Dynamic Cell 2014' in Cambridge (UK)
PhD Retreat 2014	Poster presentation. Title: Investigation of clathrin-mediated TGN exit using knocksideways. 6th PhD Retreat in Engelberg
PhD Retreat 2015	Talk presentation. Title: Knock, knock, knock – Rapid inactivation of target proteins using knocksideways. 7th PhD Retreat in Saas-Fee
PhD Retreat 2016	Poster presentation. Title: Knocksideways-mediated inactivation of clathrin/AP-1 carriers to elucidate bidirectional traffic in the TGN-to-endosome interface. 8th PhD Retreat in Romanshorn
BZ Symposium 2017	Poster presentation. Title: A versatile nanobody-based approach to analyze retrograde transport from the cell surface. Biozentrum Symposium 2017 at Theater Basel
PhD Retreat 2017	Talk presentation. Title: A versatile nanobody-based approach to analyze retrograde transport from the cell surface. 9th PhD Retreat in Martigny

Teaching and Organization Experience

Teaching	Tutor of undergraduate Biology students (2013) (Einführung in die Biologie – Vorlesung mit Übungen). Head: Prof. Dr. Michael N. Hall
Teaching	Assistant in the organization of the Biochemistry block course week 'Nucleic acids' (2011-2014) for Bachelor students in Biology. Head: Prof. Dr. Martin Spiess.
Teaching	Assistant in the organization of the Neurobiology and Cell Biology block course week (2013) for Bachelor students in Biology. Head: Prof. Dr. Peter Scheiffele.
Teaching	Assistant and captain of the Biochemistry block course week 'Proteomics of Saccharomyces cerevisiae' (2015-2016) for Bachelor students in Biology. Head: Prof. Dr. Martin Spiess.
Organization	Member of the organization team for the 'FFE Symposium 2014' in Basel
Organization	Preparation of the schedule for the fifth floor 'Departmental Seminar' at the Biozentrum

Working Experience

Hoffmann-La Roche	January to August 2008: Division Clinical Supply, Head: Dr. Christoph Mettler
	February 2009: Division Clinical Supply, Head: Dr. Christoph Mettler
	June to July 2009: Division Clinical Supply, Head: Dr. Christoph Mettler
	February 2010: Division Clinical Supply, Head: Dr. Christoph Mettler
	August to September 2010: Division Clinical Supply, Head: Dr. Christoph Mettler
	January to February 2011: Division Clinical Supply, Head: Dr. Christoph Mettler
	July to August 2011: Division Clinical Supply, Head: Dr. Christoph Mettler

Publications

Buser D.P, Prescianotto-Baschong C, Schleicher KD, Spiess M. A versatile nanobody-based toolset to analyze retrograde transport from the cell surface. In progress.

Kalin, S., **D.P. Buser**, and M. Spiess. 2016. A fresh look at the function of Rabaptin5 on endosomes. Small GTPases. 7:34-37.

Kalin, S., D.T. Hirschmann, **D.P. Buser**, and M. Spiess. 2015. Rabaptin5 is recruited to endosomes by Rab4 and Rabex5 to regulate endosome maturation. J Cell Sci. 128:4126-4137.

Miscellaneous

Language skills	German: Native speaker English: Fluent in speaking and writing French: Basic knowledge
Computer skills	Microsoft Office or iWork programs Adobe Photoshop and Illustrator Fiji, Omero, Serial Cloner and others